Estudio de carbonatos microbiales en afloramiento como análogos de la caracterización y modelización de reservorios de hidrocarburos

Ramón Mercedes Martín

Grup de Geologia Sedimentària

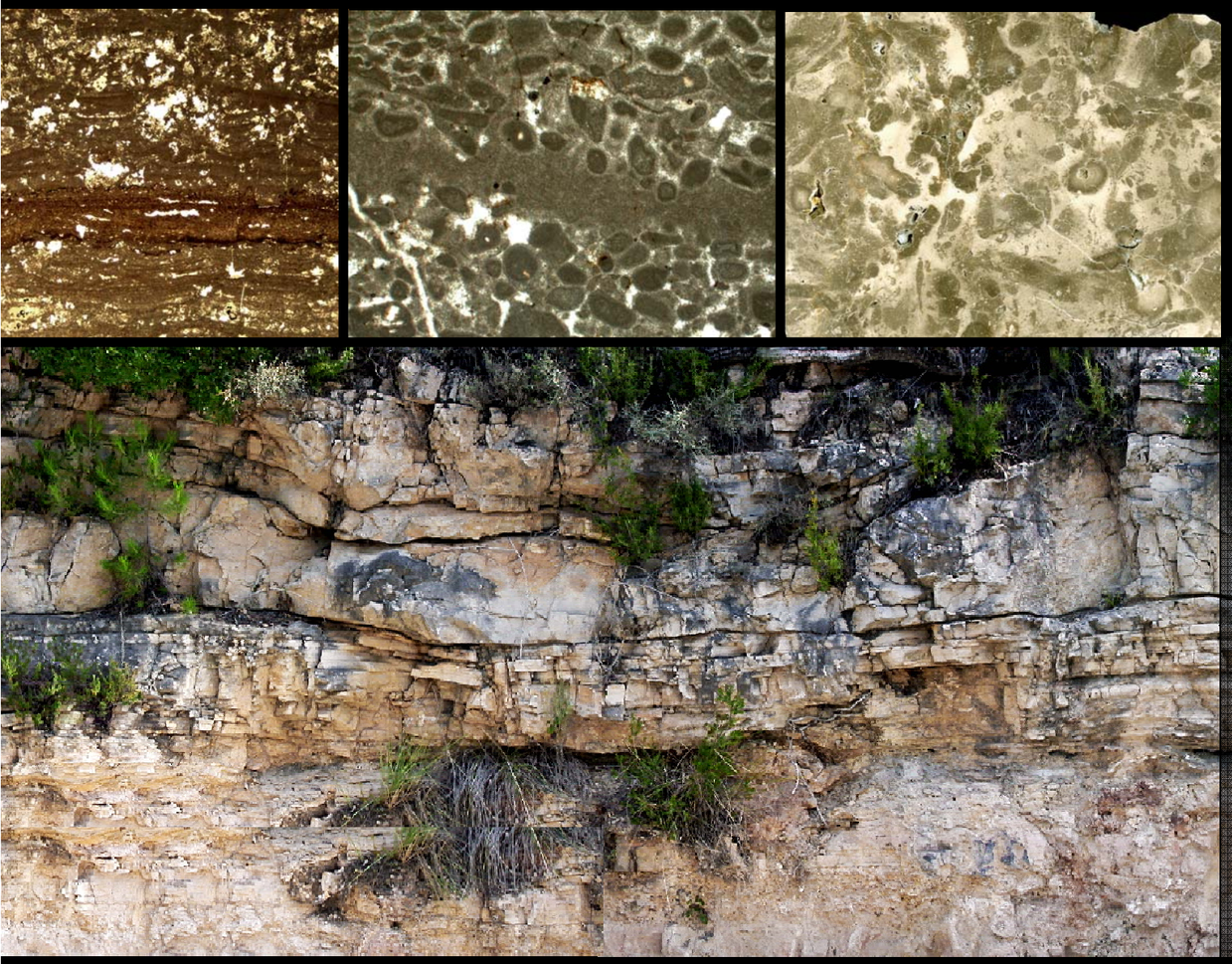

Septiembre 2013

Estudio de carbonatos microbiales en afloramiento como análogos de la caracterización y modelización de reservorios de hidrocarburos

Ramón Mercedes Martín

Universitat de Barcelona

REPSOL

Facultat de Geologia
Departament de Geoquímica, Petrologia i Prospecció Geològica
Programa de Doctorat en "Ciències de la Terra"
Universitat de Barcelona

Estudio de carbonatos microbiales en afloramiento como análogos de la caracterización y modelización de reservorios de hidrocarburos

Ramón Mercedes Martín

Tesis Doctoral dirigida por

Dr. Ramon Salas

Dra. Concha Arenas Abad

Facultat de Geologia
Departament de Geoquímica, Petrologia i Prospecció Geològica
Programa de Doctorat en “Ciències de la Terra”
Universitat de Barcelona

Estudio de carbonatos microbiales en afloramiento como análogos de la caracterización y modelización de reservorios de hidrocarburos

Ramón Mercedes Martín

Tesis Doctoral dirigida por:

Dr. Ramon Salas
Dpto. de Geoquímica, Petrologia i Prospecció Geològica
Facultat de Geologia
Universitat de Barcelona

Dra. Concha Arenas
Dpto. Ciencias de la Tierra
Área de Estratigrafía
Universidad de Zaragoza

Septiembre 2013

Facultat de Geologia
Departament de Geoquímica, Petrologia i Prospecció Geològica
Programa de Doctorat en “Ciències de la Terra”
Universitat de Barcelona

Estudio de carbonatos microbiales en afloramiento como análogos de la caracterización y modelización de reservorios de hidrocarburos

Memoria de Tesis Doctoral presentada por Ramón Mercedes Martín
para optar al Grado de Doctor en Geologia. La Tesis se ha desarrollado en el marco del Programa de Doctorat en Ciències de la Terra, bajo la dirección del Dr. Ramon Salas y la Dra. Concha Arenas

Ramón Mercedes Martín

Dirigida por:

Dr. Ramon Salas

Dra. Concha Arenas

Septiembre 2013

A mis padres, Carmen y Ramón
y a Ramon Salas

AGRADECIMIENTOS

Esta Tesis Doctoral no podría haberse realizado sin la participación y ayuda de personas e instituciones, a las que me gustaría expresar mi más sincero agradecimiento.

A Rafa Montes, mi anterior jefe, por la comprensión y empatía que me brindó para iniciar esta Tesis, a pesar de que ello suponía dejar mi anterior empleo.

A Ramon Salas, mi mentor y padre intelectual. Por haber cumplido su palabra desde el principio, por su implicación, dedicación, capacidad de gestión, proximidad humana y científica, por su amistad y su sentido del humor. *De gran vull ser com tu! Gràcies!*

A Concha Arenas, por abrirme al fascinante mundo de los microbialitos. Por su predisposición absoluta a ayudar, su enorme capacidad científica, organizativa y humana y sobretodo por su dedicación y humildad durante todo este tiempo. Gracias!

A Mateu Esteban, por su dedicación y capacidad científica que puso al servicio de este proyecto, por su sabia orientación y consejo y por haber arrojado luz en los momentos clave durante el desarrollo de este trabajo. *Gràcies!*

A REPSOL EXPLORACIÓN, por haber financiado este su primer proyecto de Tesis Doctoral con la Universitat de Barcelona. También a los proyectos de investigación I+D+i del Gobierno español (CGL-2008-04916), al Grup Consolidat de Recerca 'Geologia Sedimentària' (2009SGR-1451) y al programa Consolider-Ingenio 2010 (CSD 2006-0004) 'Topo-Iberia' por haber financiado parte de esta Tesis.

A Jordi Maria de Gibert, que nos dejó prematuramente. Ya no le podré agradecer en persona las discusiones e ideas que me aportó sobre las icnofaunas triásicas así que lo hago en estas líneas: gracias por tu asesoramiento, amistad y sentido del humor.

A JJ Pueyo, por su capacidad didáctica y por haberme ilustrado con diversas técnicas analíticas.

A Anna Travé, por la ayuda que me ha brindado siempre que la he necesitado y por haberme prestado material interesante para la realización de la Tesis. *Gràcies Anna, per la teva energia, humor i proximitat*!

A Montse y al Servei de Làmina Prima de la UB y a Jordi Illa por su tenacidad realizando las láminas delgadas, por haberme enseñado sus trucos y por su predisposición y simpatía.

A Jordi Baguena y Montse Errea, por la gestión y administración de los temas relacionados con la Beca Repsol y por su simpatía.

A mis compañeros de viaje durante mi andadura con la Tesis: Vinyet, Irene, Josep Anton, Guillem, Ander, Emili, Sergi, Yael, Sedo, Agustín, Hasdrúbal, Eloi, Telm, Juandi, Mar, Alex, Flavia, Consuelo, Ruben, Luís y en especial a Carmen, por haber compartido también alegrías, penas, ilusiones y sus *boquerones en vinagre*, también fuera de la Sala de Becarios. A todos vosotros gracias por los buenos momentos compartidos, los debates, las barbacoas y la energía positiva y ayuda que me habéis brindado durante todo este tiempo.

A todos los compañeros/as del Departament, por su simpatía y por haber compartido conmigo el día a día en la Facultat.

Many thanks also go to GVK for revising the English of the manuscripts and for his interesting discussions. *The way you do, the things you do*.

A Lluís Cabrera, por la gestión interna y externa de los temas relacionados con el convenio Repsol-UB, así como por tu confianza y proximidad siempre que he necesitado tu ayuda o consejo.

A Joan Guimerà, por su ayuda con los aspectos tectónicos y estructurales del trabajo y su predisposición a echar una mano cuando hacía falta.

A Marc Aurell, por haber ayudado a mejorar los dos primeros papers con sus críticas y visión constructivas.

A Bruno Granier y Ioan Bucur, por haberse encargado de algunas de las determinaciones micropaleontológicas (dasicladáceas y microproblematica) de muchas láminas delgadas.

Al *Paratge Natural d'Interés Natural de Poblet*, por haberme facilitado el acceso a la zona protegida de la Serra de l'Ermita, donde se efectuó trabajo de campo.

Y por último a todos mis amigos y familiares por haberme alentado y compartido conmigo esta aventura y haberme ayudado a ser mejor persona. Muchas gracias!

Índice

Summary

The Upper Muschelkalk sedimentary record of the Triassic Catalan Basin (Catalan Ranges) constitutes a major transgressive pulse of northeastern Iberia during the Ladinian. Calculated subsidence curves display two stages of rapid/decelerated total subsidence, constituting two discrete rift/post-rift pulses in the large Triassic rifting period: i) Buntsandstein - Middle Muschelkalk, and ii) Late Muschelkalk- Imon Formation (Rhaetian). The second pulse is characterized by a rapid syn-rift subsidence during the Late Muschelkalk, and a decelerated post-rift subsidence throughout the deposition of Keuper facies and Imon Formation. The Late Muschelkalk rapid syn-rift pulse of total subsidence produces gains in accommodation, which controls the development of the stromatolites and thrombolites (biostromes and mud-mounds).

The Upper Muschelkalk sedimentary record is arranged in two transgressive-regressive (T-R) sequences formed by two fault-block microbial-dominated carbonate ramps where accommodation was mainly controlled by extensional faults. A sea-level fall of at least 50 metres occurred at the end of the Early Ladinian leaving the platform subaerially exposed. As a result, a prominent karst with significant erosional incisions and profuse collapse breccia fillings was formed in the inner and middle ramp settings. The resultant subaerial unconformity bounds T-R sequences 1 and 2. T-R sequence 1 corresponds to a fault-block carbonate ramp system dominated by microbialites and oolitic shoals. T-R sequence 2 represents a fault-block carbonate ramp system mainly characterised by lagoons and shoals.

The diverse types of microbialites (stromatolites, ooidal-peloidal stromatolites and thrombolites) are widely represented in the inner and middle ramp settings, reaching a width of 45 km and an average thickness of 40 m. T-R sequence 1 contains the most noticeable microbial deposits, stromatolites in the inner ramp (up to 7 m thick) and thrombolites in the middle ramp (up to 40 m thick). T-R sequence 2 is mainly characterised by the occurrence of ooidal-peloidal stromatolites in the inner ramp and internal shoals and sheltered lagoons in the middle ramp. Microbialites exhibit a fabric-selective ancient porosity which is currently occluded by coarse calcite and quartz cements. The most common types of ancient porosity are interlaminar, vuggy and mouldic (grain dissolution and evaporite replacement).

The studied microbialites recorded a concomitant occurrence during the Lower Ladinian (Fassanian), and juxtaposition of microbial facies (stromatolites and ooidal-peloidal

stromatolites) during the Upper Ladinian (Longobardian). The simultaneous distribution of these microbialites provides insights into the growth mechanisms, diversity of microbial components, interplay of microbial and the non-microbial contribution and the paleoenvironmental constraints of their initiation and development. Despite the involvement of microbial processes in their accretion, a number of extrinsic factors such as salinity, water energy, sediment supply, type of substratum, and widespread and anomalous oceanographic conditions were instrumental in the growth of these microbialites. In addition, we discuss the possible fault-controlled hydrothermal fluid circulation which could be responsible for the corrosion, the pervasive botryoidal and fibrous marine cementation, and the development of thrombolites.

The studied carbonate ramps can be used as an analogue for ancient microbialite reservoirs in rapidly subsiding depositional areas, with a high diversity of microbial deposits formed in restricted to open marine conditions, with a wide array of ancient porosity and a well-known sequence stratigraphic context.

Resum

El registre sedimentari del Muschelkalk superior de la Conca Triàssica Catalana (Catalànids) és el resultat d'un important pols transgressiu al nord-est d'Iberia durant el Ladinià. Les corbes de subsidència total calculades mostren dues etapes de rifting ràpid-desaccelerat, les quals constitueixen dues polsacions discretes de rift-postrift dins del gran període de rifting triàssic: i) Buntsandstein - Muschelkalk mitjà, ii) facies Muschelkalk superior – Fm. Imón (Rhaètic). El segon pols es caracteritza per una subsidència ràpida sinrift durant el Muschelkalk superior, i una subsidència desaccelerada postrift al llarg de la deposició de la fàcies Keuper i la Formació Imon . El pols de subsidència total ràpida sinrift del Muschelkalk superior produeix guanys en l'acomodació, els quals controlen el desenvolupament dels estromatòlits i trombòlits (biostromes i monticles de fang microbians)

El registre sedimentari del Muschelkalk superior està ordenat en dues seqüències transgressivo-regressives (TR) formades per dues rampes carbonatades dominades per l'activitat microbiana i controlades per blocs fracturats (*fault-block microbial-dominated carbonate ramps*), en les quals l'acomodació estava controlada principalment per falles extensives. Una caiguda del nivell del mar de com a mínim 50 metres, que es va produir a finals del Ladinià, deixà la plataforma carbonàtica àmpliament exposada subaèriament. Com a resultat, es va formar un carst important amb incisions erosives significatives i abundants rebliments de bretxes de col·lapse, en les zones de rampa interna i mitjana. La discordança subaèria resultant és de caràcter regional i limita les seqüències TR 1 i TR 2 . La seqüència TR 1 correspon a un sistema de rampa carbonatada controlada per blocs fracturats dominada per microbialits i baixos (*shoals*) oolítics. La seqüència TR 2 representa també un sistema de rampa carbonatada controlada per blocs fracturats, caracteritzada principalment per llacunes (*lagoons*) i baixos (*shoals).*

Els diversos tipus de microbialits (estromatòlits, estromatòlits oolítico-peloidals i trombòlits) estan àmpliament representats en la configuració de rampa interna i mitjana, assolint un amplada de 45 quilòmetres i un gruix mitjà de 40 m. La seqüència TR 1 conté els dipòsits microbians més notables, amb els estromatòlits a la rampa interna (fins a 7 m d' espessor) i trombòlits a la rampa mitjana (fins a 40 m de gruix). La seqüència TR 2 es

caracteritza principalment per la presència d'estromatòlits oolítico-peloidals a la rampa interna i baixos interns i llacunes protegides a la rampa mitjana. Els microbialits mostren una antiga porositat fabrico-selectiva, la qual està actualment ocluida per ciments gruixuts de calcita i de quars. Els tipus més comuns d'aquesta porositat antiga són interlaminar, vacuolar (*vuggy*) i mòldica (per dissolució dels grans i el reemplaçament d'evaporites).

Els microbialits estudiats van registrar una aparició concomitant durant el Ladinià inferior (Fassanià), i la juxtaposició de fàcies microbianes (estromatòlits i estromatòlits oolítico-peloidals) durant el Ladinià superior (Longobardià). La distribució simultània d'aquests microbialits proporciona informació detallada sobre els mecanismes de creixement, la diversitat dels components microbians, la contribució dels mecanismes microbians i no microbians i les restriccions paleoambientals que varen condicionar el seu inici i desenvolupament. Tot i la participació dels processos microbians en la seva acumulació, un nombre de factors extrínsecs com ara la salinitat, l'energia de l'aigua, el subministrament de sediments, tipus de substrat, i les condicions oceanogràfiques generalitzades i anòmales van ser fonamentals en el creixement d'aquests microbialits. A més, es discuteix la circulació de fluids hidrotermals controlats per fractures com la possible causa responsable de la corrosió, la cimentació penetrativa marina botroidal i fibrosa, i el desenvolupament dels trombòlits.

Les rampes carbonàtiques estudiades es poden utilitzar com un anàleg d'antics reservoris de microbialits dipositats en àrees de subsidència ràpida, amb una alta diversitat de dipòsits microbians formats en condicions marines que poden anar de restringides fins a més obertes, amb una àmplia varietat de porositat antiga i dintre d'un context d'estratigrafia seqüèncial ben conegut.

Introducción

1.1. Tesis por compendio de artículos

La presente Tesis Doctoral se ha realizado por compendio de artículos científicos publicados en revistas indexadas en el ISI (*Institute for Scientific Information*). La confección de esta memoria se ha efectuado de acuerdo con lo dispuesto en el artículo 37 de la Normativa Reguladora del Doctorado de la Universitat de Barcelona, al amparo del Real Decreto RD 99/2011 (Aprovada por el Consell de Govern en sesión de 16 de marzo de 2012 y modificada por el Consell de Govern en fecha 9 de mayo y 19 de julio de 2012). Estos artículos, que se presentan al final de esta memoria en el apartado Anejo, se detallan a continuación:

1) Mercedes-Martín R., Salas R., Arenas C. 2013a. Microbial-dominated carbonate platforms during the Ladinian rifting: sequence stratigraphy and evolution of accommodation in a fault-controlled setting (Catalan Coastal Ranges, NE Spain). *Basin Research*, 25, 1-28.

Estado: publicado

-Ramón Mercedes:	**90%** (recolección de datos, análisis de datos, discusión de resultados, confección del manuscrito)
-Ramon Salas:	**5%** (análisis de datos, discusión de resultados)
-Concha Arenas:	**5%** (análisis de datos, discusión de resultados)

2) Mercedes-Martín R., Salas R., Arenas C. 2013b. Facies heterogeneity and depositional models of a Ladinian (Middle Triassic) microbial-dominated carbonate ramp system (Catalan Coastal Ranges, NE Spain). *Journal of Marine and Petroleum Geology*, 46, 107-128.

Estado: publicado

-Ramón Mercedes: **90%** (recolección de datos, análisis de datos, discusión de resultados, confección del manuscrito)

-Ramon Salas: **5%** (análisis de datos, discusión de resultados)

-Concha Arenas: **5%** (análisis de datos, discusión de resultados)

3) Mercedes-Martín R., Arenas C., Salas R. 2013c. Controls on microbialite diversity and occurrence in the Ladinian (Middle Triassic) of the Catalan Basin (NE Spain). *Palaeogeography, Palaeoclimatology, Palaeoecology*.

Estado: enviado y en revisión

-Ramón Mercedes: **85%** (recolección de datos, análisis de datos, discusión de resultados, confección del manuscrito)

-Concha Arenas: **10%** (análisis de datos de las facies microbianas, discusión de resultados)

-Ramon Salas: **5%** (análisis de datos sedimentarios y paleo-geográficos, discusión de resultados)

1.2. Justificación del trabajo

El presente trabajo se enmarca en el convenio entre la Universidad de Barcelona y Repsol Exploración S.A. para potenciar los estudios de doctorado en temas relacionados con la exploración de hidrocarburos. Los recientes descubrimientos de hidrocarburos en reservorios de carbonatos microbianos en los niveles presalinos del Cretácico inferior de la cuenca de Campos (Brasil) han suscitado un creciente interés por ahondar en el conocimiento de los microbialitos (factores que controlan su geometría, contribución de los procesos microbianos y no microbianos, arquitectura sedimentaria, etc).

Por este motivo y para abordar el estudio de carbonatos microbianos en afloramiento como análogos de reservorios de hidrocarburos, se seleccionó el Triásico medio (Ladiniense) de los Catalánides (facies Muschelkalk superior) debido a la

abundancia y diversidad en microbialitos (estromatolitos y trombolitos,) y a la situación análoga de desarrollarse en una etapa de régimen sinrift en ambos casos (cuenca de Campos y Cuenca Triásica Catalana). La presencia de estromatolitos y de montículos microbianos-coralinos (*mud-mounds)* ya había sido señalada en trabajos precedentes en el sector Triásico catalán (Esteban et al., 1977, Calvet et al., 1990). Sin embargo, para poder disponer de una visión completa y detallada del desarrollo de los microbialitos, se vio la necesidad de realizar un nuevo análisis estratigráfico y sedimentológico integrado y más amplio, aplicando las nuevas tendencias del análisis de cuencas y de Estratigrafía Secuencial (Catuneanu, 2009; 2011).

1.3. Objetivos

La presente Tesis Doctoral aborda la caracterización e interpretación sedimentológica de los afloramientos de carbonatos del Ladiniense de los Catalánides, entre las localidades de Pontons (Alt Penedès) y Rasquera (Ribera d'Ebre), con énfasis en las facies microbianas, como análogos de reservorios de hidrocarburos. Todo ello en el contexto de la evolución paleogeográfica de la Cuenca Triásica Catalana y, más especialmente, del desarrollo del Muschelkalk superior (Ladiniense). Para este fin, se plantearon los siguientes objetivos:

1) Disponer de un marco estratigráfico detallado que permita establecer las variaciones espaciales y temporales de las distintas facies y sus ambientes de formación.

2) Caracterizar e interpretar las facies y grupos de facies, estableciendo los procesos sedimentarios y el ambiente de depósito, haciendo hincapié en los depósitos microbianos.

3) Establecer un modelo de heterogeneidades que incluya la arquitectura sedimentaria y muestre las tendencias espaciales 2D de la porosidad.

4) Cuantificar la evolución de la acomodación durante el Ladiniense y estimar el potencial de crecimiento de las facies microbianas y de acomodación de las no microbianas en el contexto de la evolución de una cuenca sometida a una rápida subsidencia sinrift.

5) Conocer los factores que controlaron la morfología de crecimiento y la distribución espacial de los microbialitos y, en definitiva, la evolución paleogeográfica de la cuenca estudiada.

1.4. Metodología

Para la consecución de los objetivos propuestos, se llevaron a cabo dos grandes grupos de trabajos: trabajos de campo y trabajos de gabinete. La fase de trabajos de campo se inició con el levantamiento de 18 series estratigráficas a escala 1:250 entre las localidades de Pontons y Rasquera. Se confeccionaron paneles de correlación de estas columnas estratigráficas con las distintas facies identificadas utilizando la base del Keuper (Carniense) como *datum*. Los datos estratigráficos procedentes de los perfiles geológicos entre La Figuera-Montsant y entre Santa Perpetua de Gaià-Pontons, fueron proyectados en el perfil estratigráfico. Las principales fallas sinsedimentarias fueron también tenidas en cuenta en la construcción del perfil estratigráfico regional resultante. Se elaboraron, además, muchos perfiles estratigráficos detallados de cara a la descripción e interpretación de la diferentes facies reconocidas. También fueron realizadas numerosas fotografías de detalle y de paisaje con el objeto de montar fotomosaicos para la interpretación de facies, estructuras sedimentarias de gran escala y geometrías a escala sísmica.

La terminología estratigráfica empleada en este trabajo sigue los conceptos de Catuneanu et al. (2009; 2011) en lo referente a Estratigrafía Secuencial. Asímismo, se aplicaron también los conceptos propuestos por Johnson y Murphy (1984) y Embry y Johannessen (1992), sobre todo en el caso de las secuencias transgresivo-regresivas (T-R). A mayor detalle, a la hora de identificar las superficies estratigráficas y los límites entre parasecuencias y grupos de parasecuencias, fueron utilizadas las recomendaciones de Spence y Tucker (2007).

Los conceptos relativos a los modelos de rampas carbonatadas se tomaron de Burchette y Wright (1992). En cuanto a la tipología de las rampas carbonatadas, según su entorno tectónico, se empleó el trabajo de Bosence (2005). Los conceptos de bajíos internos y externos (*internal and external shoals*) fueron tomados de Colombié y Strasser (2005).

También fueron realizados análisis standard de microfacies en más de 200 láminas delgadas y 150 secciones pulidas, recolectadas durante la fase de campo. La interpretación de microfacies se hizo en base a los conceptos de Flügel (2004). Las determinaciones de porosidad modal 2D se realizaron a partir de láminas delgadas y la clasificación y terminología de Choquette y Pray (1980) para los tipos de porosidad, habiéndose realizado, además, mapas detallados de microfacies y componentes a escala microscópica.

Los fotomontajes realizados mediante fotografías panorámicas fueron interpretados en el gabinete (*line-drawings*) para identificar las geometrías de los cuerpos sedimentarios y las terminaciones de los estratos a distintas escalas.

Para cuantificar la evolución de la acomodación, fueron llevados a cabo análisis cuantitativos de la subsidencia total a partir de los datos procedentes de tres series estratigráficas correspondientes a los tres dominios estudiados. Los métodos empleados en el análisis de la subsidencia son del tipo *back-stripping* (Steckler y Watts, 1978; Sclater y Christie, 1980; Watts, 1981; Bond y Kominz, 1984). Las variables empleadas fueron: litología, edad absoluta y valores de paleobatimetrías, que fueron estimadas a partir del registro fósil, facies sedimentarias y ambientes deposicionales. La subsidencia total (descompactada) fue calculada a partir del registro estratigráfico presente en cada serie estratigráfica considerada. Las correcciones por compactación fueron llevadas a cabo empleando las relaciones porosidad-profundidad propuestas por Sclater y Christie (1980) y Schmoker y Halley (1982), para cada litología. Finalmente, la estimación cuantitativa de la acomodación, en cada sección estudiada, fue obtenida a partir de la subsidencia total calculada corregida con la paleobatimetría, siguiendo los procedimientos de Vilas et al. (2003).

A partir del perfil estratigráfico regional ladiniense se realizó una restitución palinspástica en cinco etapas del relleno sedimentario de la cuenca ladiniense utilizando técnicas geométricas.

1.5. Microbialitos: estado actual de conocimientos

El término “microbialito” procede de Burne y Moore (1987). Los microbialitos son depósitos organosedimentarios formados por la participación de comunidades microbianas bentónicas que atrapan y engloban sedimento detrítico y/o que son responsables de la precipitación mineral o la inducen. El término microbialito ha sido ampliamente utilizado para describir estromatolitos y trombolitos carbonatados y estructuras similares que se presentan con formas dómicas o columnares en aguas someras de ambientes lacustres y marinos. Así, se incluyen oncolitos, dada su estructura laminada y su origen microbiano; de hecho, pueden considerarse “estromatolitos concéntricos móviles”. En general, el término microbialito puede ser aplicado a diferentes acumulaciones autigénicas donde los microbios son localmente abundantes, como en las tufas, travertinos, espeleotemas o los depósitos generados a partir de surgencias o fumarolas (Riding, 2000; Riding, 2011).

La función de los microbios, mayormente bacterias y algas microscópicas, en relación con la formación de los microbialitos se refiere a tres hechos principales: (1) su actuación como sustratos para la nucleación o precipitación mineral; (2) el atrapamiento de partículas en suspensión; y (3) los cambios o procesos químicos ligados a la actividad fisiológica, tanto de organismos autótrofos (p. ej., cianobacterias), como heterótrofos (p. ej., bacterias sulfato-reductoras) (Chafetz y Buczinsky, 1992; Merz-Preiß y Riding, 1999; Dupraz et al., 2009; Spadafora et al., 2010).

Así, en la formación de los microbialitos, intervienen diversos componentes y procesos, ligados a la presencia de bacterias y algas pequeñas: 1) mucílagos o EPS (*extracellular polymeric substances*), segregados por los microbios, y que se acumulan en la parte externa de las células para formar una matriz adhesiva que atrapa y fija los microbios al sustrato (Riding y Awramik, 2000), 2) biofilms, que son películas bacterianas submilimétricas localizadas en los mucílagos (Riding, 2002). Rosenberg (1989) los define como “matrices heterogéneas de microorganismos unidos entre sí y sujetos al sustrato por EPS”, 3) tapices microbianos (capas milimétricas complejas formadas por cianobacterias filamentosas y diatomeas, capaces de atrapar sedimento, Riding, 2000) y 4) organomineralización *s.l.*, *sensu* Dupraz et al. (2009): precipitación de $CaCO_3$ inducida o influenciada por actividad biológica.

Por lo tanto, los depósitos de carbonatos microbianos se producen por la interacción del crecimiento y metabolismo microbiano, por la participación de los mucílagos (EPS) conjuntamente con la precipitación mineral y el atrapamiento de granos detríticos (Riding 2011). La litificación temprana de estos depósitos, que es esencial para la acreción y conservación de los carbonatos microbianos bentónicos, depende del tipo de comunidad biológica y de las condiciones ambientales (Chafetz y Buczynski, 1992; Dupraz et al., 2009). De ahí que los carbonatos microbianos sean considerados como indicadores, no sólo de los cambios en las comunidades microbianas sino también de los cambios en la química atmosférica y de la saturación oceánica, los cuales han influenciado en el metabolismo microbiano y el estado de saturación del agua marina (Riding y Liang, 2005, Riding, 2011).

Los microbios ocupan un espectro muy amplio de ambientes, incluyendo aguas que poseen una química y composición muy diversa, siendo su implicación en la sedimentación igualmente variada (Riding, 2011). Muchos microbialitos tienen una composición carbonatada, mayormente calcítica, pero también existen de aragonito o dolomita (Feldman y Mckenzie, 1997; Sanz-Montero et al., 2008; Anadón et al., 2013; García del Cura et al., 2013) y también se registran ejemplos constituidos por sílice, fosfato, hierro, manganeso y sulfato (Reolid y Nieto, 2010; Rossi et al. 2010). Los

carbonatos microbianos actuales son abundantes en ambientes donde la precipitación es mayormente inorgánica. En estos casos, las bacterias ejercen en general un débil control sobre el proceso de calcificación. Un ejemplo de este fenómeno lo constituyen las surgencias de aguas calientes o fumarolas donde el rápido enfriamiento y la fuerte degasificación de las aguas son los mecanismos de precipitación mineral más comunes. En estos casos la contribución global de los microbios es escasa, influenciando más en las texturas que en los procesos. Por el contrario, cuando las aguas están menos saturadas en minerales, la actividad microbiana puede jugar un papel predominante en la precipitación de sedimento (Riding, 2011).

Por otro lado, muchos investigadores han demostrado que los procesos metabólicos realizados por las bacterias, así como la consiguiente descomposición de la materia orgánica, causan cambios físico-químicos en su microambiente, los cuales favorecen la precipitación de carbonato cálcico (Pentecost, 1985; Castanier et al., 1989; Buczynski y Chafetz, 1991; Chafetz y Buczynski, 1992; Knorre y Krumbein, 2000). Diversos experimentos indican que las bacterias están involucradas en la precipitación de aragonito y calcita, exhibiendo diversas morfologías que parecen estar vinculadas a procesos microbianos (Castanier et al., 1989). El tamaño de cristales individuales, esferas y bastoncillos oscilan entre 1 y 4 μm, mientras que los agregados cristalinos se encuentran entre 5 y 100 μm (Flügel, 2004). Morfologías cristalinas similares en tamaño han sido observadas en cultivos de laboratorio y en sedimentos carbonatados modernos. Muchas bacterias, exceptuando las fotosintéticas (cianobacterias), son indiferentes a la presencia de luz, con lo que pueden estar presentes tanto en ambientes someros como en ambientes submareales profundos, habitats crípticos o en cuencas restringidas profundas. Asímismo, la contribución microbiana en la formación de *mud-mounds* ha sido postulada por numerosos autores (por ejemplo, Pratt, 1982; Lees and Miller, 1985; Monty, 1995).

1.5.1. Tipología y criterios de clasificación

Los microbialitos pueden llegar a formar extensas y/o potentes unidades rocosas. El conjunto de atributos macroestructurales, generalmente observables en afloramiento, permite subdividir a los microbialitos en 4 tipos principales: *estromatolitos, trombolitos, dendrolitos* y *leiolitos* (Fig. 1.1). Por su parte, las tobas y travertinos tienen sólo un origen parcialmente microbiano (Riding, 2000), si bien en los ambientes tobáceos puede formarse cualquier tipo de microbialito.

Estromatolitos. Gerdes et al. (1985) los definen como "rocas laminadas cuyo origen está relacionado claramente con la actividad de comunidades microbianas, las cuales por su morfología, fisiología y ordenación en el tiempo y en el espacio interaccionan con el medio físico para producir un modelo laminado, que se conserva en el estructura final de la roca". Riding (1991) los define como depósitos microbianos bentónicos laminados. Los estromatolitos carbonatados varían notablemente de composición, siendo la calidad de su laminación muy variable. La laminación está ligada al crecimiento biológico estacional, a la sedimentación periódica o ambas situaciones. Su formación está relacionada con los siguientes procesos: precipitación inducida por microbios, precipitación inorgánica y atrapamiento de granos. Los 4 subtipos principales son: tapices microbianos litificados aglutinados finos y gruesos (*fine grained* y *coarse agglutinated*), costras esparíticas, y la combinación de ambas: estromatolitos híbridos (*hybrid stromatolites*) (Riding, 2011) (Fig. 1.1, 1.2).

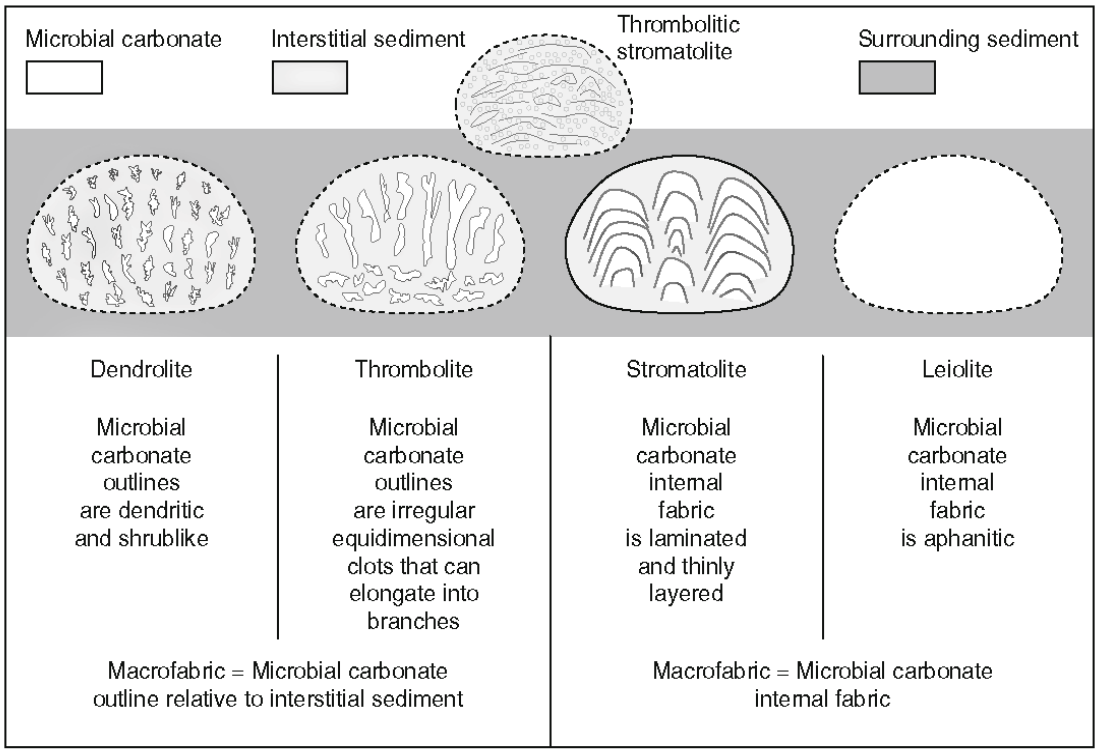

Fig 1.1. Diferentes tipos de microbialitos definidos a partir de sus macrotexturas: leiolites (afanítica), estromatolito (laminado), trombolito (*clotted*), dendrolito (dendrítica). Los ejemplos muestran domos formados por carbonato microbiano y su sedimento intersticial y se encuentran rodeados por sedimento asociado. Según Riding (2011).

Trombolitos. El término fue propuesto por Aitken (1967) para los depósitos microbianos con “estructuras criptoalgales relacionadas con estromatolitos pero con ausencia de laminación y caracterizados por una textura macroscópica moteada o

grumosa (*clotted*)". Los grumos (*clots*) difieren en color y morfología en comparación con los componentes adyacentes, dando lugar a una textura heterogénea de parches. Kennard y James (1986) llamaron *mesoclots* a los componentes de los trombolitos, los cuales son típicamente de colores oscuros y poseen una textura microcristalina (Fig. 1.1, 1.2). Exhiben una gran variedad de formas (subredondeadas, ameboides, arborescentes, digitadas, etc) y se presentan aislados, interconectados o amalgamados. El uso de los términos *clot* y *mesoclot* ha sido amplio y en muchas ocasiones ha dado lugar a confusión (Shapiro, 2000), con lo que es comprensible definir los trombolitos como "microbialitos no laminados" (Aitken, 1967; Pratt, 1982). Desde el punto de vista genético, los *clots* se interpretan como la combinación de: 1) una irregular y compleja aglutinación microbiana; calcificación *in-situ* de comunidades bacteriales dominantemente cocoidales; 2) incrustación esquelética; y 3) procesos erosivos, aunque también puede ser el resultado de calcificación de bacterias

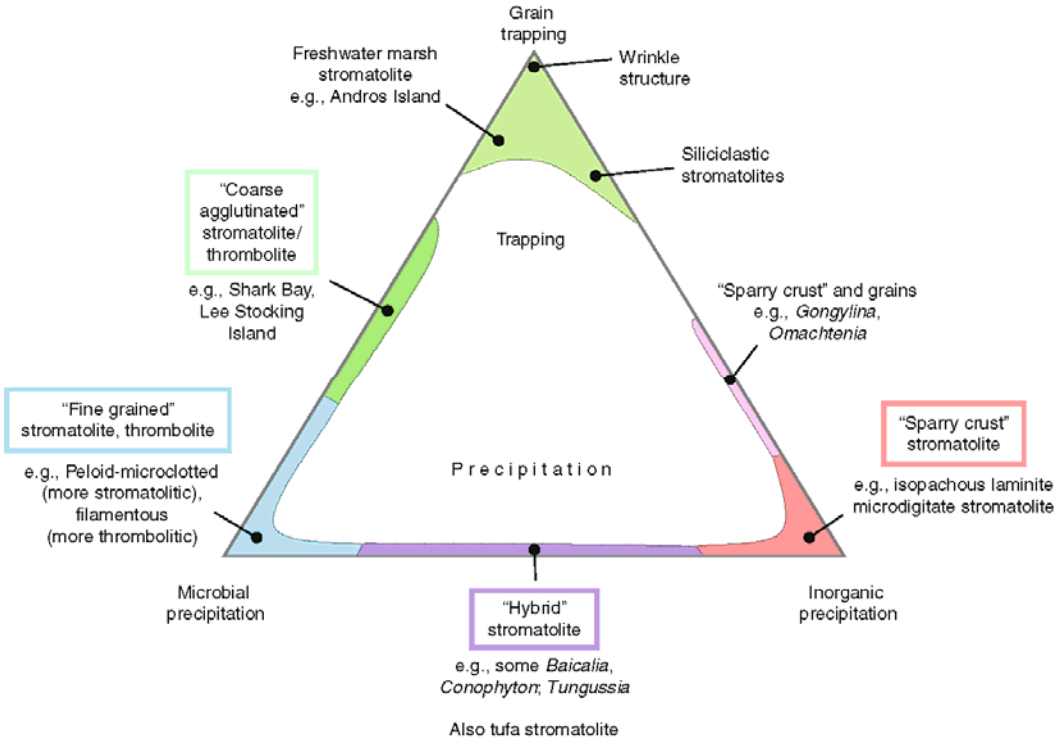

Fig 1.2. Estromatolitos y trombolitos relacionados con sus procesos formativos: atrapamiento de granos, precipitación inorgánica y precipitación inducida por microbios. Según Riding (2011).

filamentosas (Burne y Moore, 1987). Riding (2011) distingue 2 grandes subtipos de trombolitos: trombolitos de microbios calcificados y trombolitos aglutinados.

Dendrolitos. Estos microbialitos forman extensas columnas y domos que pueden estar vagamente laminados y suelen presentar estructuras dendríticas, tanto verticales como recostadas (Riding, 1991). Los dendrolitos están formados por microfósiles porostromados (calcimicrobios, como *Epiphyton*). La rápida calcificación y cementación temprana entre los microfósiles arbustivos da lugar a la formación de un armazón orgánico que proporciona un sustrato duro para la fijación de metazoos (por ejemplo, archaeociátidos y estromatopóridos). Los dendrolitos carecen de laminación, aunque se encuentran generalmente estratificados, reflejando irregularidades en su acreción. Estos organismos son muy abundantes en el Cámbrico inferior, Ordovícico inferior, Devónico superior y Carbonífero inferior (Flügel, 2004) (Fig. 1.1).

Leiolitos. Son microbialitos que poseen una macrotextura afanítica, a menudo con ausencia clara de laminación, "*clots*" o fábricas dendríticas (Riding, 2000) (Fig. 1.1). El término se acuñó a partir de ejemplos del Mioceno superior del SE de España (Braga et al., 1995) donde los leiolitos forman grandes domos en asociación con trombolitos y estromatolitos. La formación de leiolitos está favorecida por el aporte uniforme de sedimento bien clasificado en superfícies colonizadas por microbios (Flügel, 2004).

1.5.2. Reservorios de hidrocarburos en microbialitos. El caso de los materiales presal de la cuenca de Campos (Brasil)

Los reservorios de hidrocarburos asociados con carbonatos microbianos, como el Jurásico superior del Golfo de México (Mancini et al., 2004), el Carbonífero de Kazakhstan (Collins et al., 2006) o el reciente descubrimiento del Cretácico inferior de la cuenca de Campos en Brasil (Luis Dias, 2005) han reavivado intensa investigación sobre los microbialitos debido a su excelente potencial. Algunos aspectos clave que se estudian actualmente son: los procesos de formación de los carbonatos influenciados por microbios, los factores que condicionan la morfología externa de los depósitos, así como aquellos condicionantes que hacen que los microbialitos se conviertan en importantes reservorios de hidrocarburos (Awramik y Buchheim, 2012). Este conocimiento puede ser muy útil en la predicción de las heterogeneidades de grandes cuerpos microbialíticos desarrollados en cuencas sedimentarias bien estudiadas.

En este sentido, comprender los patrones sedimentarios del relleno de cuencas extensivas "rift" tempranas en las que se desarrollaron microbialitos, como Campos Basin, Brasil (Dorobek et at., 2012) o Namibe Basin, Angola (Sharp et al., 2013) es

fundamental para conocer las heterogeneidades a escala de reservorio. Recientemente, Harris et al., (2013) valoraron los estilos de sedimentación carbonatada en varias cuencas de tipo rift en las que los microbialitos y tufas son predominantes.

1.5.3. Significado de los microbialitos del Triásico medio del Tetis occidental

Tras la desaparición de los arrecifes de metazoos provocada por la extinción Permo-Triásica (Erwin, 1994; Senowbari-Daryan, 2001), los biostromos y arrecifes microbianos proliferaron durante el Triásico inferior en el Tetis occidental (Lehrmann, 1999; Flügel y Senowbari-Daryan, 2001; Pruss y Bottjer, 2005) convirtiéndose en una importante factoría de carbonatos (Fig. 1.3). Durante el Triásico medio, en los Alpes (región de Dolomitas) se desarrollaron plataformas carbonatadas aisladas dominadas por sedimentos microbianos y cementos sindeposicionales (Blendinger, 1994; 1996; Keim y Schlager, 2001). Los márgenes de las plataformas ladinienses, con mayor

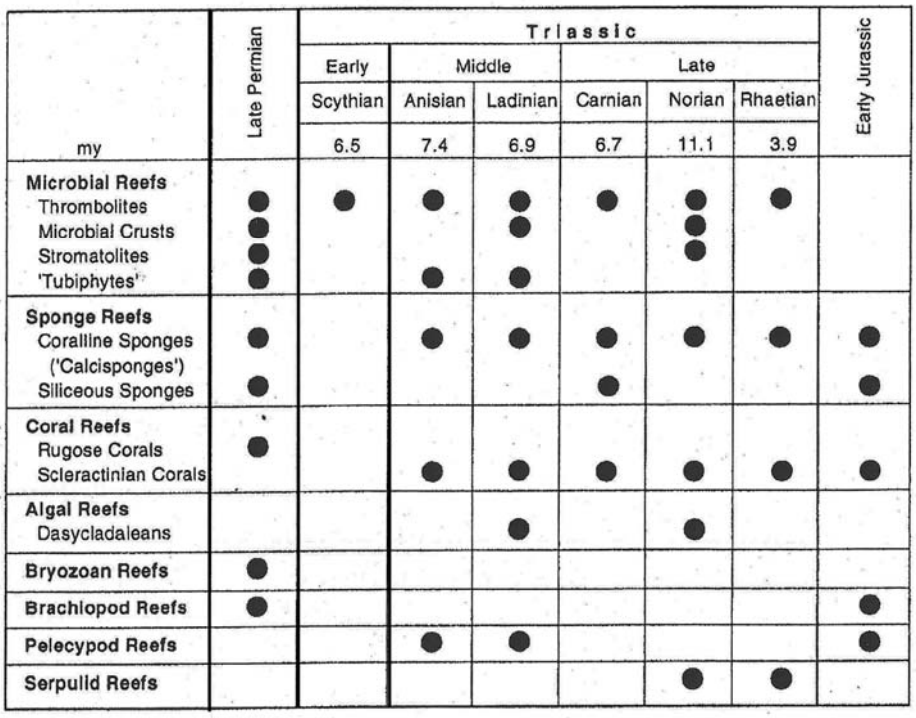

Fig. 1.3. Principales tipos de organismos formadores de arrecifes durante el Triásico. Nótese la diversidad de organismos durante el Pérmico superior y la escasez de arrecifes de metazoos durante el Triásico inferior. Los arrecifes microbianos aumentan su diversidad a partir del Anisiense (Triásico medio). Nótese que el piso Scytiense se corresponde actualmente con el Olenekiense (Gradstein et al., 2004). Según Flügel y Senowbari-Daryan (2001)

diversidad taxonómica que los anisienses (Russo et al., 1998), fueron colonizados por cianobacterias, esponjas incrustantes, *Tubiphytes*, y albergaron abundantes cementos que excedían en volumen sobre los componentes esqueléticos. En el caso del Triásico medio de Latemar (Dolomitas), cuyo modelo de plataforma sería del tipo *flat-topped, steep-fronted* (Marangon et al., 2011) (Fig. 1.4), la producción de carbonato se produjo mayoritariamente a lo largo de los márgenes y el talud y siendo del tipo *mud-mound* (factoría M, Schlager, 2000).

Los componentes primordiales son microbialitos (costras micríticas peloidales moteadas, estromatolitos y *Tubiphytes*) y cementos (Harris, 1993; Emmerich et al., 2005; Marangon et al., 2011). Por lo tanto, muchas de las plataformas que se desarrollaron en Dolomitas pueden ser consideradas como plataformas del tipo *mud-mound* y estar dominadas por microbialitos (Brandner et al., 1991; Harris, 1993; Blendinger, 1994, 1996). De este modo, los sedimentos microbianos formaron

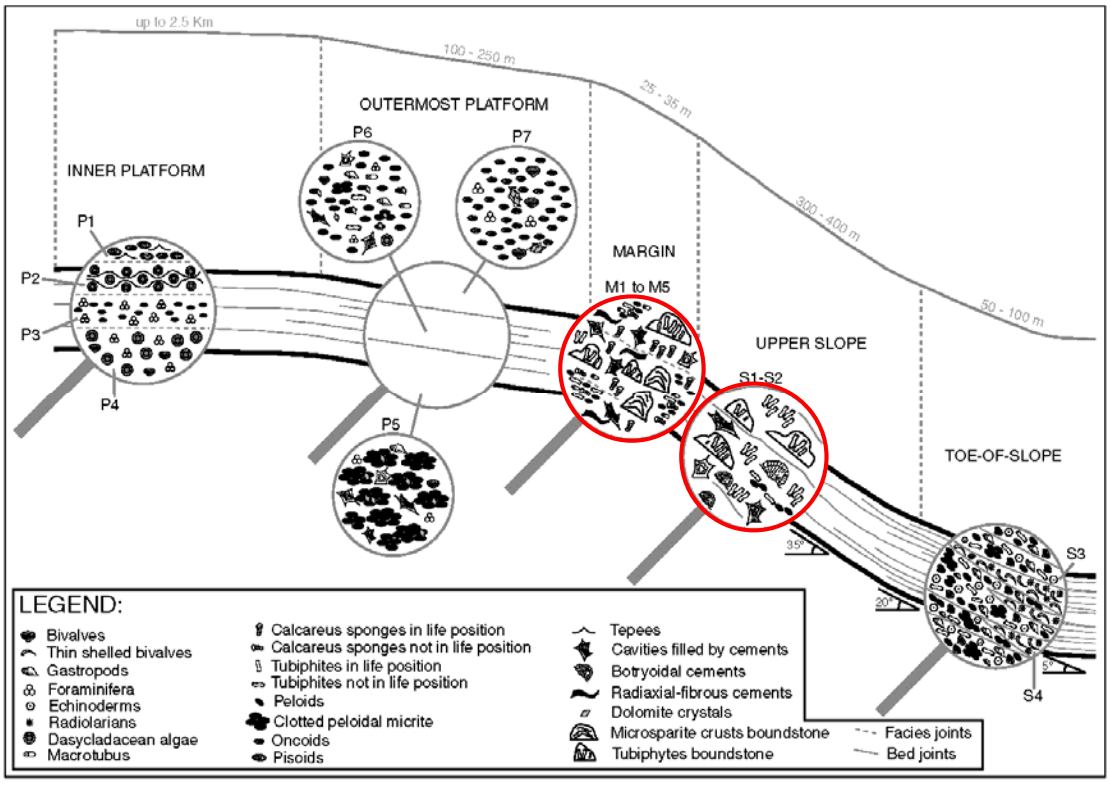

Fig 1.4. Perfil sedimentario de la plataforma carbonatada de Latemar, interpretada como una *flat-topped, steep-fronted platform.* La producción microbiana y de cementos sinsedimentarios se produce mayoritariamente entre la parte más externa de la plataforma y el talud superior (círculos rojos). Según Marangón et al. (2011).

biostromos y montículos carbonatados durante el intervalo de extinción del Triásico inferior (Olenekiense (antiguamente Scytiense) – Anisiense) en el Tetis occidental. (Fig. 1.3). En ausencia de competidores, los arrecifes y comunidades microbianas

proliferaron ampliamente; estas últimas desempeñaron una función primordial en la rigidez y estabilidad de las estructuras arrecifales (Flügel y Senowbari-Daryan, 2001).

La abundancia y diversidad de microbialitos durante el Triásico medio en el Tetis occidental convierte al Ladiniense en uno de los periodos más interesantes para el estudio de estos organismos y de los mecanismos que intervinieron en su origen, desarrollo y coexistencia.

Marco geológico y estratigráfico

2.1. Localización geográfica y geológica

El área sujeta a estudio se encuentra localizada en los Catalánides (Cordillera Costero Catalana) situados en el NE de Iberia (Fig. 2.1). La Cordillera Costero Catalana se desarrolló por inversión de los rifts mesozoicos durante los eventos de compresión alpina Cenozoica (Salas et al., 2001). Los afloramientos triásicos pertenecientes a la Cordillera Costero Catalana se extienden a lo largo de una superficie aproximada de 300 x 200 Km con una orientación NE-SO (Fig. 2.1A). La cuenca se abría hacia el mar del Neotetis (SE), de modo que las facies marinas pasaban a facies continentales hacia las partes más occidentales y septentrionales de la Meseta Castellana (Calvet et al., 1990).

2.2. Estratigrafía del Triásico de los Catalánides. El Muschelkalk superior

La sedimentación triásica tuvo lugar en cuencas extensivas controladas por fallas que se desarrollaron durante el Pérmico superior y el Triásico y registraron las denominadas “Facies Germánicas”. Estas facies, muy características de la parte meridional de las cuencas europeas y del Tetis occidental (Virgili et al., 1983), comprenden tres grandes tramos: una parte inferior, o facies Buntsandstein, una parte intermedia, o facies Musckelkalk, y una parte superior, o facies Keuper. La facies

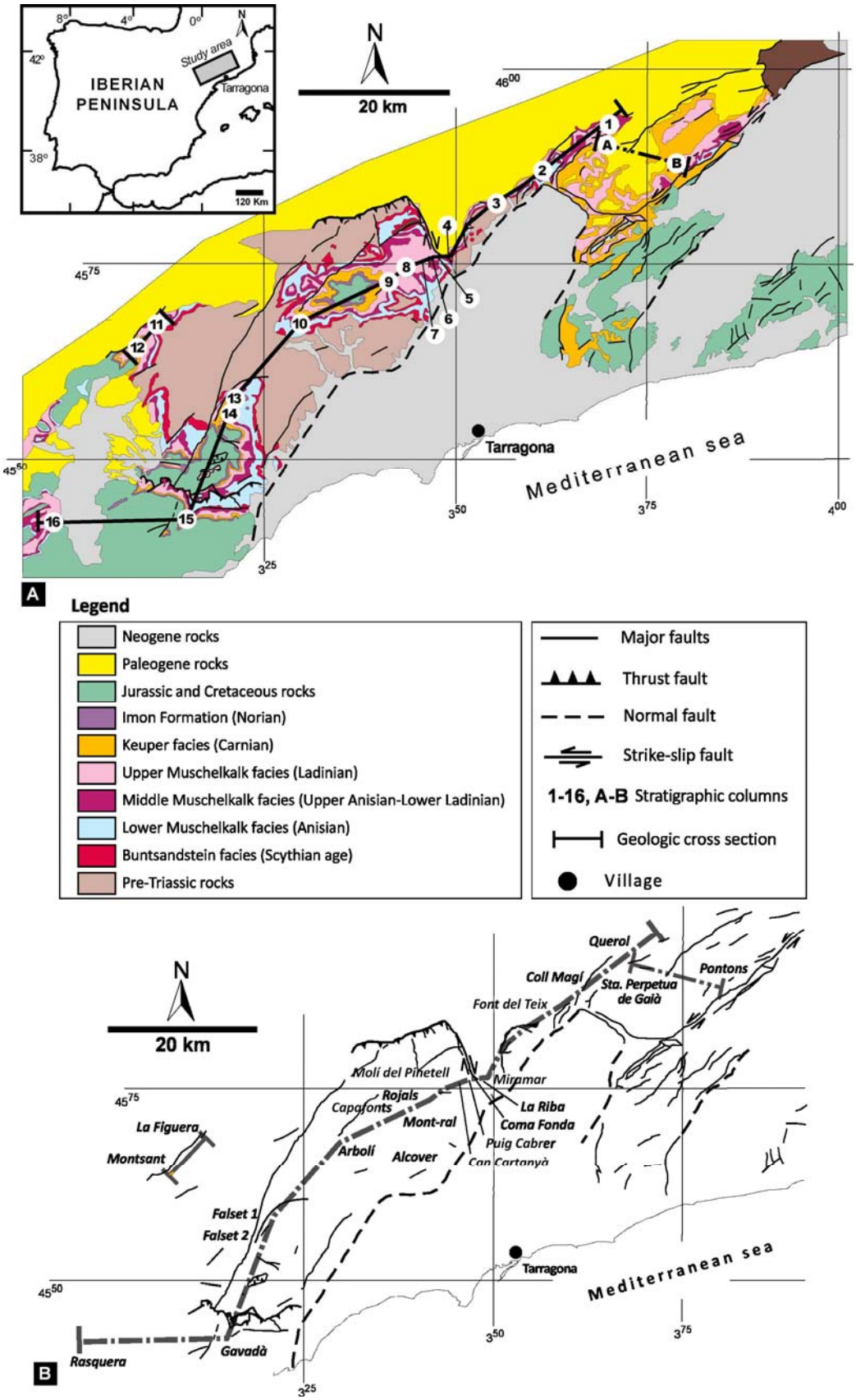

Fig. 2.1. Localización de la zona de estudio y áreas colindantes. A) Mapa geológico de la Cuenca Catalana mostrando los principales tipos de rocas así como la estructura alpina (modificado del Institut Geològic de Catalunya, 2012). Los números (1-16) y las letras (A-B) indican la situación de las columnas estratigráficas. C) Principales localidades mencionadas en el texto. Ver leyenda para más detalles. Tomado de Mercedes-Martín et al (2013a).

Buntsandstein comprende sedimentos continentales terrígenos y *red beds*. La facies Musckelkalk, consta de carbonatos, evaporitas y *red-beds*. Por último la facies Keuper consiste en sedimentos de *sabkha* (Virgili et al., 1983).

La facies Muschelkalk (Anisiense hasta Ladiniense, Triásico medio) se divide a su vez en dos unidades carbonatadas marinas separadas por una unidad siliciclástica-evaporítica. La primera unidad carbonatada (Anisiense) se corresponde con la llamada facies Muschelkalk inferior, que fue ampliamente reconocida en la Cuenca Triásica Catalana (Marzo, 1980; Virgili et al., 1983; Calvet y Ramón, 1987; Calvet et al., 1990). La segunda unidad carbonatada (Ladiniense), correspondiente a la facies Muschelkalk superior, es la más extensa y potente y se encuentra muy bien representada en la Cuenca Triásica Catalana. Esta unidad se divide en dos secuencias, según Calvet y Tucker (1995).

El espesor del Muschelkalk superior varía entre unos 100m en la región más septentrional de la zona de estudio, hasta unos 140m en la parte más meridional (Fig. 2.2). El registro sedimentario del Muschelkalk superior de la Cuenca Triásica Catalana fue subdividido por Calvet et al., (1987) en tres dominios paleogeográficos, que de NE a SO son: el dominio de Gaià, el dominio de Prades y el dominio de Baix-Ebre-Priorat

El Muschelkalk superior está integrado por diversas unidades litostratigráficas en los dominios antes mencionados (Calvet y Ramón, 1987). Estos autores reconocieron 4 unidades en el dominio de Gaià, las cuales son, de base a techo (Fig. 2.2):

1) Calizas y/o dolomías oolíticas de Rojals,
2) Calizas bioturbadas y dolomías de Benifallet,
3) Estromatolitos de Querol,
4) Dolomías margosas, margas y brechas de Capafonts.

En el dominio de Prades, el Muschelkalk superior está constituido por 5 unidades, que de base a techo son:

1) Calizas y/o dolomías oolíticas de Rojals,
2) Calizas bioturbadas y dolomías de Benifallet,
3) Arrecifes (“Mud-mounds”) de La Riba,
4) Dolomías tableadas de Alcover,
5) Dolomías margosas, margas y brechas de Capafonts.

Por su parte, en el dominio de Baix-Ebre-Priorat, el Muschelkalk superior está formado por 5 unidades, que de base a techo son:

1) Calizas y/o dolomías oolíticas de Rojals,

2) Calizas bioturbadas y dolomías de Benifallet,

3) Calizas y/o dolomías y margas con *Daonella* de Rasquera (Calvet y Tucker, 1988),

4) Calizas y/o dolomías y margas con amontes de Tivissa,

5) Dolomías margosas, margas y brechas de Capafonts. Las unidades estratigráficamente más bajas (Rojals y Benifallet) y la más alta (Capafonts) están presentes en todos los dominios sedimentarios.

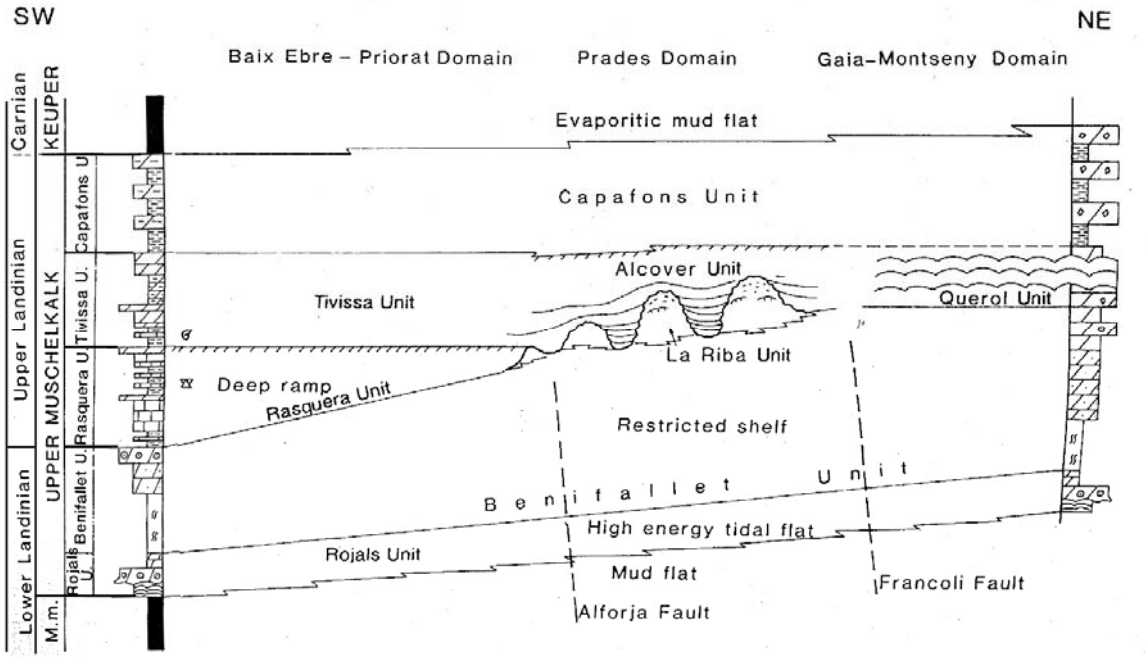

Fig 2.2. Correlación de unidades litostratigráficas entre Pontons (NE) y Rasquera (SW) de las facies Muschelkalk superior en la Cuenca Triásica Catalana. Según Calvet et al. (1990).

Calvet et al., (1990) realizaron el primer análisis secuencial del Triásico medio de la Cuenca Catalana, dividiendo sus depósitos en 2 secuencias deposicionales (SD). La SD1 incluía la parte más alta del Buntsandstein y el Muschelkalk inferior, mientras que la SD2 comprendía el Muschelkalk medio y el superior (Fig. 2.3). Sin embargo, años después, Calvet y Tucker (1995) modificaron ligeramente el esquema secuencial propuesto con anterioridad. Fue entonces cuando Calvet y Tucker (1995) sugirieron

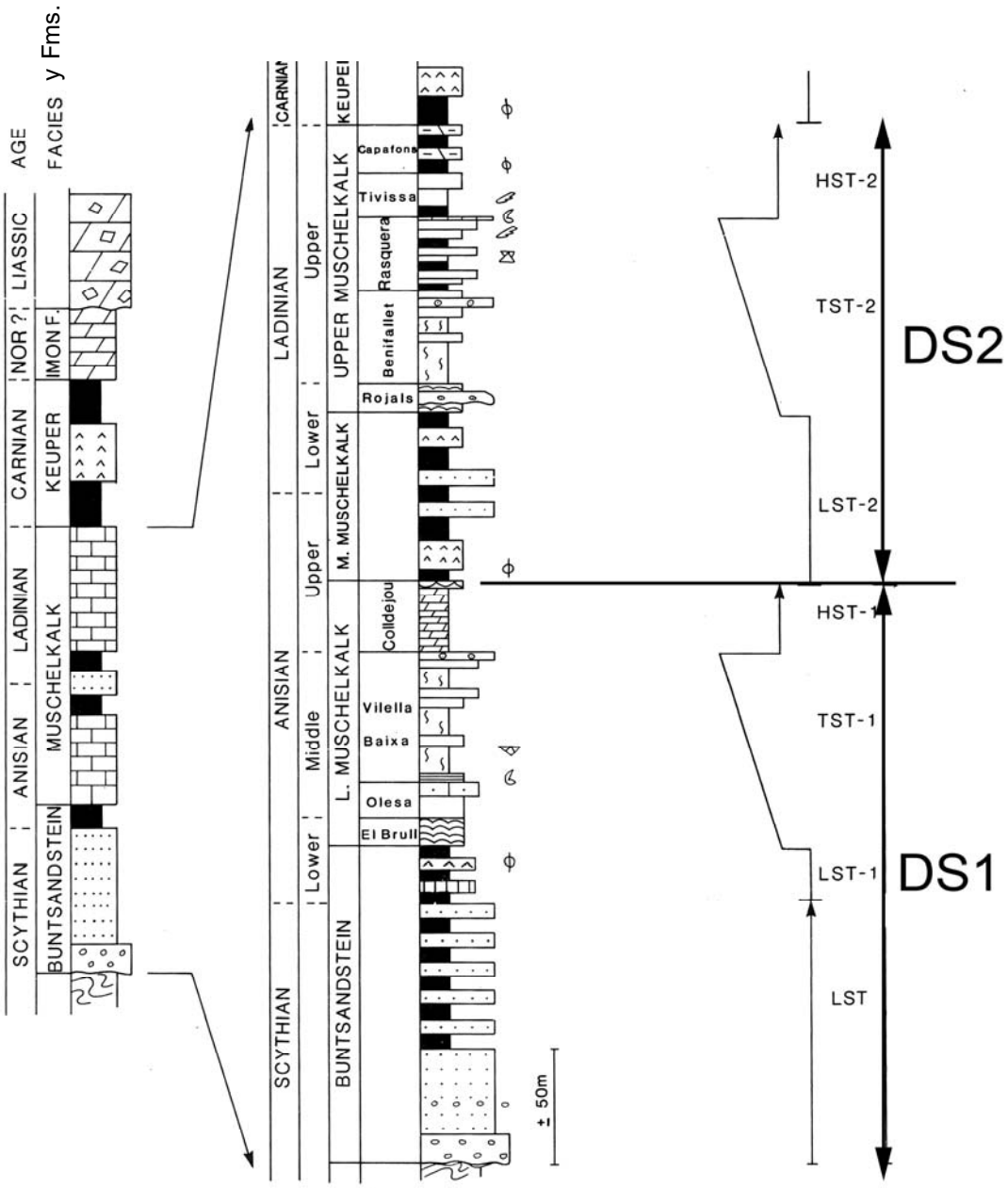

Fig 2.3. Columna sintética de los materiales triásicos de la Cuenca Catalana. Se muestran las unidades litostratigráficas, facies, secuencias deposicionales (DS) y cortejos sedimentarios definidos para el periodo Triásico inferior (facies Buntsandstein)- Triásico medio (facies Muschelkalk). Actualmente el Scytiense se corresponde con el Olenekiense (Gradstein et al., 2004). Según Calvet et al. (1990).

que el Muschelkalk medio y el superior (de edad Ladiniense) fuesen divididos en dos secuencias: L1 y L2. De este modo, las evaporitas y margas del Muschelkalk medio y la unidad de Rojals (calizas y dolomías mareales oolíticas de alta anergía) se consideraron como el *Lowstand Systems Tract* (LST1) de la primera secuencia deposicional L1 (Fig. 2.4). Por su parte, el *Transgressive Systems Tract* (TST1) estaba constituido por la unidad Benifallet (calizas y dolomías lagoonales bioturbadas).

Además, el *Highstand Systems Tract* (HST1) de esta secuencia en el dominio de Prades estaba compuesto por la unidad de *mud-mounds* de La Riba, indicando la presencia de un límite de secuencia en este punto de la sucesión sedimentaria (Fig. 2.4). De hecho, la parte alta de la unidad de La Riba se interpretó como "una superficie paleocárstica resultado de una caída relativa del nivel del mar, que determinó el final del crecimiento de los *mud-mounds*". Esta superficie representaba el LST2 de la segunda secuencia L2 (Calvet y Tucker, 1995) en el dominio de Prades. La parte inferior de la unidad Alcover se consideró como el LST2 tardío o bien el TST2. La unidad Capafonts poseía un carácter regresivo constituyendo el HST2 (Fig. 2.4).

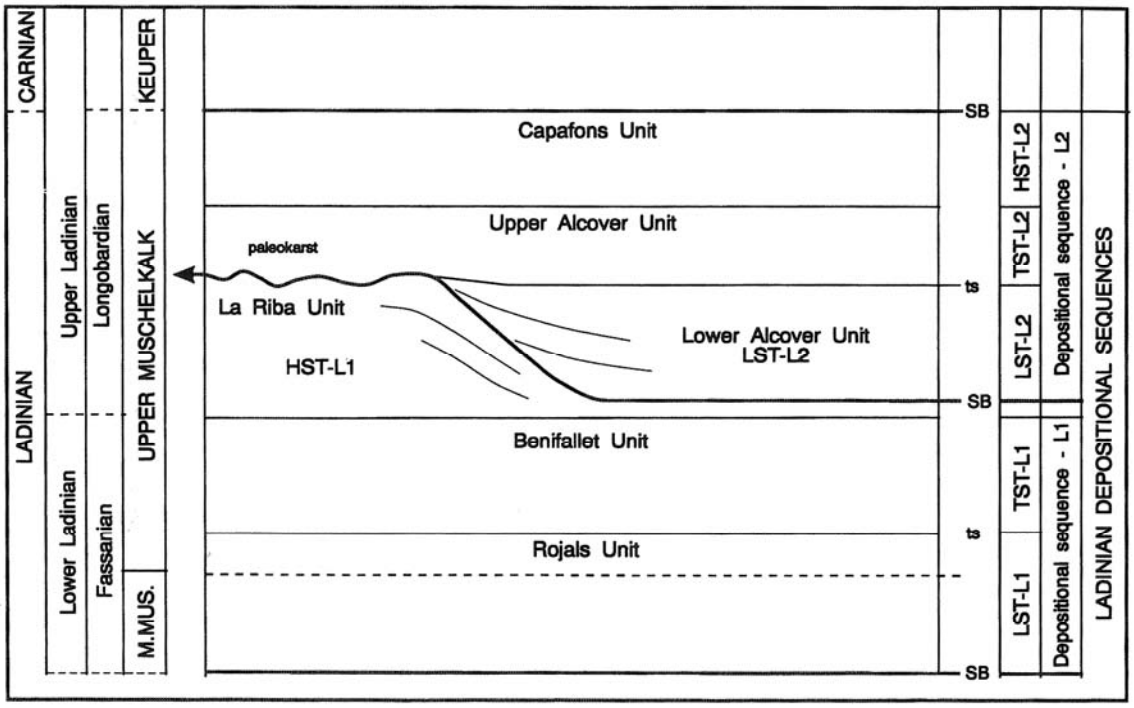

Fig 2.4. Interpretación secuencial de los materiales carbonatados del Ladiniense (Triásico medio) de la Cuenca Catalana. Nótese que esta interpretación reconoce dos secuencias deposicionales (L1 y L2) para el intervalo comprendido entre el Ladiniense inferior y el superior (facies Muschelkalk medio y Muschelkalk superior). La discordancia subaérea con paleocarst es el límite de secuencia (SB) entre L1 y L2. Según Calvet y Tucker (1995).

Calvet et al. (1990) sugirieron que las unidades de Rojals y Benifallet eran probablemente de edad Ladiniense inferior. La unidad de Rasquera sería Ladiniense superior, debido a la presencia del bivalvo *Daonella lommeli* (Virgili, 1958; Marquez, 1983), de los conodontos *Sephardiella mungoensis* y *Pseudofurnishius murcianus* (March, 1986), y de los ammonoideos *Protachyceras steinmann*, *Protachyceras hispanicum, Hungarites pradoi* (Virgili, 1958). Por su parte, la unidad Capafonts, con la

presencia de los palinomorfos *Camerosporites secatus, Praecirculina granifer* y *Duplicisporites granulates* (Solé et al., 1987) indicaría una edad Ladiniense superior.

2.3. Evolución tectonosedimentaria del Triásico

Los sistemas de *grabens* de la etapa Pérmico superior-Triásico medio de Iberia estaban estrechamente relacionados con la rápida propagación hacia el S del rift oceánico del N Europa-Groenlandia. Esto resultó en la formación de un sistema de *grabens* y *horsts*, algunos de ellos superimpuestos a fracturas Permo-Carboníferas (Ziegler, 1982; 1988). Durante la apertura y propagación del Neotetis occidental, Iberia fue afectada de forma repetida por una tectónica extensiva dando lugar a varias etapas de rifting intracontinentales durante el Mesozoico (Salas et al., 2001).

Según Calvet et al., (1990), el relleno de la Cuenca Triásica Catalana tuvo lugar en dos fases caracterizadas por dos estadios de extensión seguidos de dos fases de subsidencia regional. De este modo, consideraron al intervalo de facies Buntsandstein como un periodo sinrift, y al del Muschelkalk inferior como un periodo postrift, y posteriormente el Muschelkalk medio como un estadio sinrift seguido por el Muschelkalk superior como un estadio postrift (Fig. 2.5). Posteriormente, la evolución de Iberia durante el Pérmico superior-Mesozoico fue dividida en 3 grandes estadios de rift y postrift (Salas y Casas, 1993; Ramos et al., 1996; Salas et al., 2001). Uno de esos ciclos de rifting correspondió al Pérmico superior-Triásico, el cual afectó ampliamente a la parte más oriental de la placa Ibérica.

Más recientemente, Vargas et al. (2009), subdividieron el ciclo de rifting Pérmico superior-Triásico de Salas y Casas (1993) en varios estadios menores de rift y postrift, gracias al empleo de técnicas analíticas más precisas (Fig. 2.6). Así, Vargas et al. (2009) identificaron en la Cordillera Ibérica hasta 4 fases de rifting seguidas de una fase generalizada postrift, mientras que el basamento Triásico de la Cuenca del Ebro presenta 3 fases sinrift y 2 fases postrift. Por lo que respecta a la Cordillera Ibérica, el primer estadio de subsidencia rápida sinrift tuvo lugar en el Autuniense (Pérmico inferior) y después, durante el Thüringiense (Pérmico superior) tuvo lugar una segunda fase sinrift. La tercera fase de rifting aconteció entre el Olenekiense (facies Buntsandstein) y el Ladiniense (facies Musckelkalk superior). Durante el Carniense (facies Keuper) y Noriense, se produjo una fase generalizada de subsidencia térmica postrift. La cuarta y última fase de subsidencia rápida sinrift acaeció durante el Rhaetiense (Triásico superior) y persistió hasta el inicio del Jurásico inferior (Fm. Cortes de Tajuña, Salas et al., 2001) Paralelamente, el basamento Triásico de la

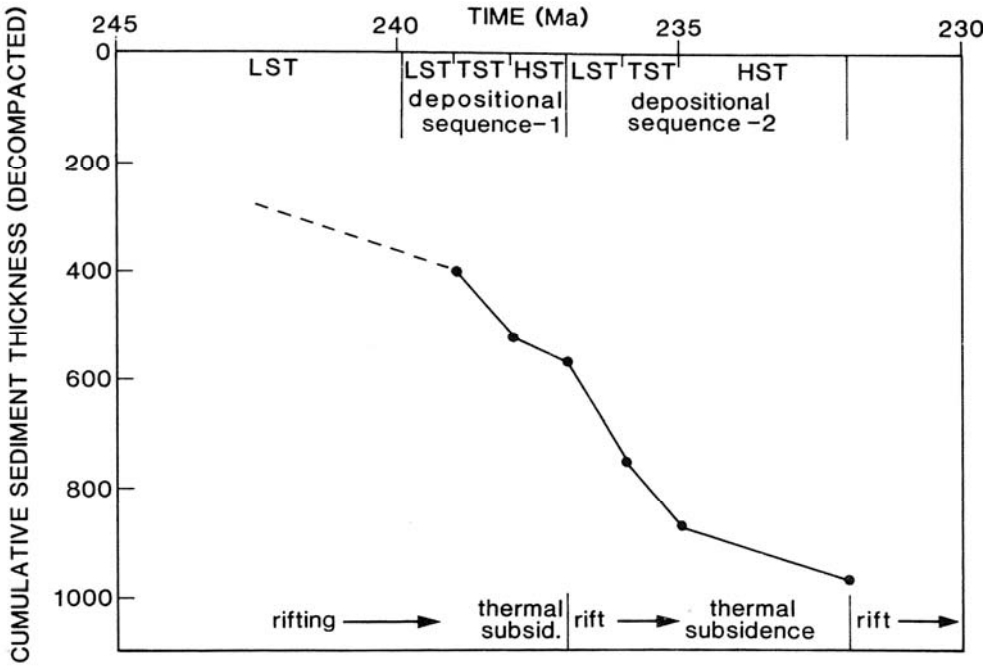

Fig 2.5. Curva de subsidencia total descompactada para el Triásico de la Cuenca Catalana integrada con los datos secuenciales de Calvet et al. (1990). Se aprecian dos grandes fases rift-postrift. La primera constituida por las facies Buntsandstein-Muschelkalk inferior y la segunda formada por las facies Muschelkalk medio-Muschelkalk. Según Calvet et al. (1990).

Cuenca del Ebro experimentó un patrón de subsidencia diferencial durante el Triásico. Esta región presentó una etapa inicial de rápida subsidencia durante el Triásico inferior-medio (Olenekiense-Ladiniense). En algunas áreas, una corta etapa de post-rift

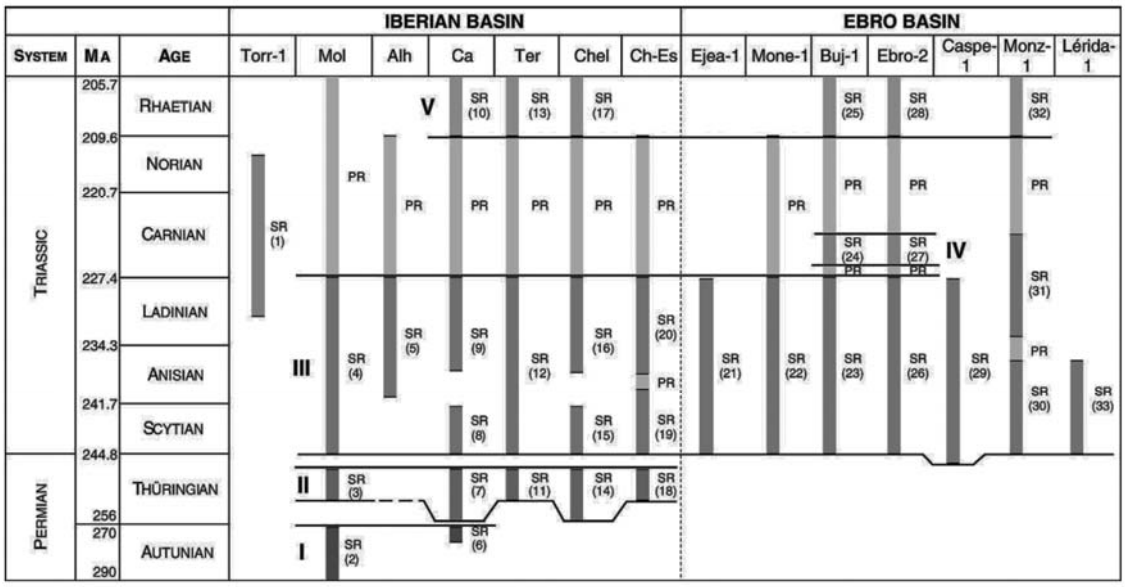

Fig 2.6. Correlación de las fases sinrift y postrift procedentes de varios sondeos en las Cuenca Ibérica y del Ebro para el intervalo Pérmico-Triásico. Nótese la existencia de una fase sinrift generalizada durante el intervalo Scytiense-Ladiniense y otro postrift entre el Carniense y la base del Rhaetiense. Según Vargas et al. (2009).

quedó registrada en el comienzo del Carniense. Una segunda etapa sinrift tuvo lugar en el Carniense medio y una subsiguiente de postrift entre el Carniense superior y el Noriense. La tercera etapa de rápida subsidencia sinrift comenzó en el Rhaetiense inferior y duró hasta el Jurásico inferior (Vargas et al., 2009) (Fig. 2.6).

De este modo, y según varios autores, la evolución de la subsidencia durante el Triásico indica que el Ladiniense fue un periodo de subsidencia sinrift generalizada y rápida en la parte oriental de la placa Ibérica, en donde se depositaron extensos depósitos de carbonatos, muchos de ellos de carácter microbiano. En la sección 3.5, se expone el modelo de subsidencia que fue obtenido a partir de datos propios y que viene a corroborar el patrón obtenido por los autores anteriores en los Catalánides.

Resultados

3.1. Facies, análisis e interpretación

Fueron reconocidas 17 tipos de facies, correspondientes a ambientes de rampa interna hasta rampa externa, los cuales se han interpretado usando criterios de litología, textura deposicional, componentes bioclásticos y no bioclásticos, características sedimentarias (p. ej., geometría y estructuras sedimentarias) y contexto estratigráfico.

Las facies fueron definidas de manera que cada una representa un ambiente sedimentario específico, dependiendo de las condiciones hidrodinámicas, tipo de sedimento producido y paleogeografía (Mercedes-Martín et al., 2013a). La distribución y continuidad de facies ha permitido reconocer los siguientes ambientes: cuenca (*basin*), bajíos externos (*external shoals*), *lagoons* protegidos (*sheltered lagoon*), bajíos internos (*internal shoals*), llanuras mareales (*tidal flats*) y playas barrera (*barrier-bank beaches*), de manera que los ambientes de mar abierto se disponen en dirección hacia el SO.

Los diferentes tipos de facies aparecen en la Tabla 1, y en las Figuras 3.1, 3.2, 3.3. Un panel de correlación de facies se muestra en la Fig. 3.4. Dichas facies fueron agrupadas en tres grandes categorías: 1) facies de grano grueso, 2) facies de grano fino, y 3) microbialitos y facies asociadas.

3.1.1. Facies de grano grueso

Fueron identificadas 6 tipos de facies carbonatadas de grano grueso en el Ladiniense de la zona estudiada: i-ii) *grainstones* oolíticos y *grainstones* bioclásticos con laminación cruzada (facies F1 y F2), iii) *wackestones* y *packstones* peloidales y bioclásticos (facies F3), iv) *floatstones* y *grainstones* oncolíticos, oolíticos y peloidales (facies F4), v) *wackestones* y *packstones* bioturbados intercalados con *grainstones* (facies F5), vi) *wackestones* y *floatstones* de moluscos intercalados con *packstones* de equinodermos (facies F6) (Mercedes-Martín et al., 2013a) (ver Tabla 1, Fig. 3.1, 3.4).

En general, las facies de grano grueso constituyen depósitos métricos a decamétricos (hasta 8 metros de espesor) de calizas *wackstones* a *grainstones* (localmente *floatstones*) dolomitizadas, de color gris claro a marronoso. Presentan estratificación cruzada de bajo ángulo con laminación paralela, *herringbone*, laminación ripple y *wavy*, aunque pueden presentar estratificación masiva y nodular. Otros elementos presentes son sigmoides y cuerpos canaliformes con depósitos de *lag* en sus bases, las cuales pueden ser erosivas o irregulares. Los componentes más frecuentes son: ooides, peloides, oncoides y microoncoides, intraclastos, cortoides, fragmentos y especímenes enteros de bivalvos, gasterópodos, espinas y placas de equínidos, crinoideos, foraminíferos. Los componentes secundarios son cantos negros, fragmentos de ostreidos, conodontos, *lumps*, foraminíferos planctónicos, microproblematica y algas dasicladáceas (Fig. 3.1 A-G)

Estas facies, que caracterizan los ambientes de depósito de rampa interna y media, se desarrollaron en ambientes marinos submareales someros, bajo moderada a alta energía y por encima del nivel de olas de buen tiempo. Los subambientes más comunes son las áreas de playas barrera, arenas carbonatadas de *shoreface*, bajíos internos y externos (*sensu* Colombié y Strasser, 2005) y *lagoons* protegidos.

3.1.2. Facies de grano fino

Un total de 3 facies carbonatadas de grano fino fueron descritas en el Ladiniense: i) *mudstones* a *wackestones* intensamente bioturbados (facies F7), ii) *mudstones* a *packstones* bioclásticos bioturbados intercalados con margas (facies F8), iii) dolomicrita-*dolomudstones* finamente laminados (facies F9) (Mercedes-Martín et al., 2013a). (ver Tabla 1, Fig. 3.1H, 3.2A-C, 3.4).

Las facies de grano fino se disponen como una alternancia de paquetes de estratos centimétricos a decimétricos (hasta 6 m de grosor), masivos a nodulosos, de

dolomudstones a *dolowackestones* bioturbados, con intervalos decimétricos de margas arcillosas bioturbadas o localmente niveles centimétricos de dolomías de grano fino, finamente laminadas. Los estratos carbonatados presentan bases irregulares y erosivas y estratificación masiva y nodular. Incluyen intervalos arenosos en los que son comunes las laminaciones plano paralelas, *wavy* y ripple. Las barras de marea y depósitos canalizados están formados por la acreción lateral de cuerpos lenticulares de grano fino. Las capas calizas tienen bioturbación, siendo comunes las icnofaunas de pequeños *Planolites* y *Thalassinoides*. En algunos lugares, son abundantes las comunidades de macroinvetebrados de cuerpo blando y también de vertebrados. Pueden ser localizados esqueletos muy bien preservados de organismos nectónicos y planctónicos, especialmente de peces, reptiles, artrópodos, equinodermos, moluscos, braquiópodos, insectos y plantas terrestres en determinados niveles (Via et al., 1977, Cartaña, 1994, Fregenal-Martínez, et al., 1995).

Los componentes más característicos son los fragmentos de bivalvos (*Daonella* y *Posidonia*), espinas de equínidos, peloides y granos de cuarzo. Los componentes secundarios de esta facies son fragmentos de gasterópodos, cefalópodos, braquiópodos, ostreidos, crinoides, ostrácodos, briozoos, foraminíferos bentónicos y microproblematica (*Tubiphytes*), oncoides, *lumps* e intraclastos.

Estas facies se formaron en diferentes ambientes sedimentarios que van desde la rampa interna (aguas marinas someras, con flujos hidráulicos moderados a altos) hasta la rampa externa (aguas marinas profundas de baja energía). Los subambientes más característicos incluyen *lagoons* protegidos intermareales a submareales e hipersalinos, llanuras mareales bioturbadas (por encima del nivel de olas de buen tiempo), o cuencas marinas restringidas (por debajo del nivel de olas de buen tiempo) (Mercedes-Martín et al., 2013a).

3.1.3. Microbialitos y facies asociadas

Se han reconocido los siguientes tipos de *boundstones* y facies carbonatadas: i) estromatolitos planares y dómicos (facies F10), ii) estromatolitos oolítico-peloidales (facies F11), iii) trombolitos microbianos-peloidales (facies F12), iv) *boundstones* de calcimicrobios con bioclastos (facies F13), v) *boundstones-rudstones* de corales-microbios (facies F14), vi) *packstones* laminados de oncoides y peloides (facies F15), vii) *packstones* a *rudstones* de dasicladáceas, peloides y bioclastos (facies F16), vii) brechas de talud dolomitizadas (facies F17). (Tabla 1, Fig. 3.2D-H, 3.3A-H, 3.4).

Los estromatolitos (facies F10 y F11) configuran dos tipos de geometrías: estratiformes con disposición interna tabular (biostromos tipo 1), y estratiformes formados por cuerpos dómicos (biostromos tipo 2). Localmente, los biostromos de tipo 2 se desarrollan por encima de los de tipo 1. Los dos tipos forman depósitos de al menos 20Km de extensión lateral, alcanzando un grosor de varios metros (hasta 5 m). Los trombolitos (facies F12) se presentan o bien como biostromos con relieve plano (biostromos trombolíticos de tipo 1), o como biohermos adyacentes con relieve de montículo (*mud-mounds* trombolíticos de tipo 2). (Fig. 3.2D, E, F)

Los estromatolitos planares y dómicos (facies F10) consisten en una alternancia de láminas de dolomicrita y doloesparita. Se formaron en ambientes marinos poco profundos de la rampa interna-media, en subambientes de llanura intermareal hipersalina en condiciones de moderada energía. La ausencia o baja diversidad de macrofauna y la presencia de texturas fenestrales de reemplazamiento de evaporitas indican que estos depósitos se formaron en ambientes áridos con salinidad superior a la normal. Las condiciones de hipersalinidad pudieron haber favorecido el desarrollo de las comunidades microbianas e inhibir la proliferación de invertebrados marinos (Mercedes-Martín, et al., 2013c).

Los estromatolitos oolítico-peloidales (facies F11) consisten en intervalos milimétricos a centimétricos de *grainstones* de ooides y peloides que alternan con intervalos micríticos milimétricos. Las geometrías estratiformes y hemielípticas de bajo relieve son las más comunes en estos depósitos. Estos biostromos pueden alcanzar un grosor de 3 m en afloramiento y pueden tener una extensión lateral de como mínimo 40 Km. Estos depósitos se desarrollaron en ambientes marinos poco profundos (intermareales a submareales), sometidos a condiciones de moderada a alta energía, por encima del nivel de olas de buen tiempo. El ambiente deposicional correspondería a un *fore-shoal* interno ubicado en la rampa interna (según Colombié y Strasser, 2005) (Fig. 3.2E-F)

Los trombolitos microbianos-peloidales (facies F12) son microbialitos no laminados que se organizan en cuerpos de espesor métrico, masivos a nodulares y que pueden incorporar esporádicos niveles estromatolíticos. La textura predominante de estos microbialitos está formada por un *mudstone-wackestone* masivo peloidal, aunque *packstones* y *grainstones* están localmente presentes. La textura macroscópica interna típica es moteada (*clotted*) y masiva peloidal. Pueden tener expresión sísmica en afloramiento debido a que su espesor puede alcanzar los 40 m, y una extensión lateral de 45 km. Estos depósitos se formaron por debajo del nivel de olas de buen tiempo, sometidos a condiciones de baja a moderada energía, en ambientes submareales y de rampa externa (Fig. 3.2G-H).

Los *boundstones* de calcimicrobios y bioclastos (facies F13) están formados por biostromos laminados de origen microbiano, que pueden ser masivos y que afloran exclusivamente por encima de las facies F16. La facies F13 está constituida por cuerpos estratiformes y tabulares de microbialitos laminados, con láminas planas a ligeramente onduladas. Pueden llegar a tener hasta 6 m de espesor y 20 Km de extensión lateral. Los intervalos arenosos presentan laminación paralela y ripple. Los componentes más frecuentes son calcimicrobios, microproblematica, y fragmentos de bivalvos. Los techos de las láminas presentan ocasionalmente superficies endurecidas (*hardgrounds*) e incrustaciones de Fe/Mn (Fig. 3.3A)

Los *boundstones-rudstones* de corales-microbios (facies F14) consisten en depósitos de tipo *wackestone* a *packstone* de bioclastos que contienen capas dolomitizadas de *boundstones* de corales aislados-microbios y localmente estromatolitos y esponjas. Estos depósitos alcanzan un espesor métrico y presentan estratificación masiva a nodular. Las partes altas de estos depósitos contienen más abundancia de estromatolitos y esponjas (hasta 15 cm de grosor) coexistiendo con los corales aislados. El ambiente deposicional de esta facies sería submareal somero, en zonas bien conectadas con mar abierto y sometido a condiciones de moderada a alta energía (Fig. 3.3B, C)

Los *packstones* laminados de oncoides y peloides (facies F15) consisten en depósitos que alcanzan hasta 4 m de espesor y como mínimo 100 Km de extensión lateral, exhibiendo una estratificación masiva. Los componentes son oncoides, peloides, intraclastos, pseudomorfos de evaporitas, fragmentos de bivalvos y equínidos. Estos cuerpos se organizan en depósitos tabulares y estratiformes (Fig. 3.3D)

Los *packstones* a *rudstones* de dasicladáceas, bioclastos y peloides (facies F16) están organizados en capas de espesor métrico y estratificación masiva a nodular. Presentan estratificación cruzada de bajo ángulo y laminación paralela y ripple, así como evidencias de superficies endurecidas y bioturbación. Los principales componentes son fragmentos de bivalvos, gasterópodos, foraminíferos, serpúlidos, restos de algas dasicladáceas (*Diplopora*?), espinas de equinodermos, tubos de anélidos, microproblematica, micrita micropeloidal, peloides, intraclastos y cuarzo. El ambiente deposicional inferido se correspondería con un *back-reef* con sedimentación carbonatada restringida (Fig. 3.3F, G).

Las brechas de talud dolomitizadas (facies F17) están asociadas a los techos de las unidades trombolíticas (facies F12). Esta facies está formada por clastos polimícticos con matriz dolomitizada de grano fino a grueso. Los clastos suelen estar incrustados por organismos microproblematica (*Tubiphytes* sp). (Fig. 3.3H) Estos

depósitos se formaron en los flancos de los *boundstones* microbianos en la rampa media y externa. Los materiales arrecifales y los organismos que constituyen los depósitos microbianos de mar abierto, fueron erosionados a pie del talud, por debajo del nivel de olas de buen tiempo. Por tanto se interpretan como depósitos submareales de baja energía.

3.2. Tipos de microbialitos y facies microbianas

El análisis e interpretación de las distintas facies microbialíticas ha sido uno de los objetivos fundamentales en este trabajo, por lo que en este apartado se presentan los principales resultados que atañen a esta facies. Tres tipos de facies microbianas pueden ser reconocidas en el Ladinense de la Cuenca Triásica Catalana: estromatolitos *sensu stricto s.s*, estromatolitos oolítico-peloidales y trombolitos (facies F10, F11 y F12, respectivamente, según Mercedes-Martín et al., 2013a, c) (Tabla 2, 3 y 4, Panel 1, 2; Figs. 3.5 a 3.12)

3.2.1. Estromatolitos *sensu stricto s.s.*

Las estructuras estromatolíticas más frecuentes son las tabulares (estratiformes, tipo 1), mientras que las estructuras abombadas (dómicas, tipo 2) son menos abundantes (Tabla 2).

Estromatolitos estratiformes - tipo 1. Están compuestos por intervalos tabulares laminados con morfologías onduladas a planas, verticalmente apilados y con espesores que oscilan entre varios milímetros hasta 50 cm. En algunos casos, los biostromos contienen pequeños cuerpos aislados con morfologías dómicas (de hasta 20 cm de ancho) o con relieves positivos de perfil cónico (de hasta 5 cm de ancho). Estos biostromos poseen varios metros de espesor (hasta 5 metros) y tienen una extensión lateral de hasta 30 Km (Figs. 3.8 A-C) En algunas áreas, se disponen sobre ellos domos estromatolíticos de mayor entidad (estromatolitos de tipo 2).

A escala mesoscópica, las láminas son continuas, lisas, planas y ocasionalmente onduladas. Menos comúnmente, se aprecian láminas convexas, generalmente cónicas. Típicamente, la laminación consiste en una alternancia de capas de dolomicrita y de doloesparita de color oscuro y claro (Fig. 3.9). Las capas de doloesparítica ocre claro son normalmente más gruesas que las capas dolomicríticas, gris oscuro, y onduladas. Ambos tipos de capas están a su vez compuestas de varias

láminas. El modo de acreción de las láminas da lugar a un apilamiento observado en los cuerpos tabulares.

Estromatolitos dómicos - tipo 2. Estos estromatolitos están caracterizados por grandes cuerpos dómicos usualmente agrupados formando depósitos extensos. Estas formas están desarrolladas por encima de los estromatolitos de tipo 1. Los domos están poco espaciados y normalmente conectados lateralmente. Las estructuras son de unos 2m de alto y 6m de ancho, aumentando el tamaño hacia el techo. La extensión lateral es al menos de 20 Km. (Fig. 3.6, 3.8A y D).

Las láminas son comúnmente onduladas a ligeramente arrugadas en la parte inferior, mientras que adquieren formas planas y onduladas en la parte superior (Fig. 3.9B). En ambas partes la continuidad de las láminas es alta. La textura y patrón de la laminación a escala mesoscópica es similar a las de los estromatolitos de tipo 1, con una alternancia de capas claras y oscuras. Algunos cuerpos estromatolíticos pueden incluir capas centimétricas de intraclastos y estructuras de *tepee* de escala decimétrica. Evidencias de microcarst y superficies endurecidas (*hardgrounds*) se observan dentro de los microbialitos, así como abundantes texturas fenestrales. Los cristales de pseudomorfos de evaporitas son abundantes en las intercalaciones dolomíticas de grano fino.

Características microscópicas

Ambos tipos de estromatolitos (tipo 1 y 2) poseen una microestructura y textura similar (Fig. 3.9). Las capas claras y oscuras están formadas por láminas claras y oscuras; el espesor y tonalidad de cada tipo de lámina determina el tono más claro u oscuro de las capas en que se encuentran. Las láminas claras consisten en dolomicrita peloidal, microdoloesparita y doloesparita. Estas láminas tienen un grosor que oscila entre 500 y 1500µm y un perfil plano a ligeramente ondulado, generalmente con bases netas y pasando gradualmente hacia techo a láminas oscuras. En algunos casos, las láminas claras desarrollan estructuras dómicas compuestas de filamentos dolomicríticos subperpendiculares a los domos. Las láminas oscuras están compuestas de dolomicrita densa, mayormente peloidal y *clotted*.

Las láminas sencillas varían de 100 a 250µm en grosor y poseen perfiles ondulados a dómicos. Las parejas de láminas claras y oscuras se designan como parejas de tipo A. Se han observado filamentos micríticos aislados subperpendiculares a las láminas oscuras, así como restos de calcimicrobios (*Cayeuxia* sp., y otras formas) que están enraizados en estas láminas y se extienden hasta alcanzar las láminas claras suprayacentes. Los restos filamentosos recuerdan a cianobacterias.

3.2.2. Estromatolitos oolítico-peloidales

Estos estromatolitos consisten en capas de *grainstones* oolítico-peloidales alternando con intervalos dolomicríticos. Las geometrías más comunes son las estratiformes y las estructuras hemielípticas de bajo relieve. Se pueden llegar a formar grandes biostromos mediante el apilamiento sucesivo de intervalos laminados planos. Estos estromatolitos alcanzan los 3 m de espesor y un mínimo de 40 Km de extensión lateral (Tabla 3, Fig. 3.6, 3.8E, F, Fig. 3.10).

La estructura interna consiste en capas de *grainstones* (lisas, planas o ligeramente onduladas) que alternan con capas micríticas (tabulares a onduladas). Las capas de *grainstones* oolíticos tienen un grosor que oscila entre varios milímetros a 5 cm, mientras que los intervalos micríticos varían entre varias μm y 2 cm de espesor (Fig. 3.10). El espesor de las capas micríticas se usó como criterio para designar a 2 tipos de parejas *grainstone*-micrita: parejas de tipo B y parejas de tipo C. Las parejas de tipo B, las láminas micríticas alcanzan varias μm de grosor, mientras que las parejas de tipo C están formadas por láminas micríticas que exceden un grosor de 100 μm. Las parejas de tipo C son más abundantes que las de tipo B (Tabla 3).

Intervalos de grainstone

Las capas de *grainstones* (hasta 5 cm de grosor) están formadas por ooides oscuros, subesféricos, redondeados a subredondeados y bien clasificados (hasta 0,3 mm de diámetro). Se encuentran comúnmente micritizados, sin estructura o con textura microcristalina. Los peloides (hasta 0,8 mm de diámetro) son los segundos componentes más frecuentes. Son redondeados a subangulares y de grano fino. Muchos peloides provienen de ooides, bioclastos o pelets fecales micritizados y recristalizados, dando lugar a una estructura microcristalina de tono marrón. Se aprecian *lumps* (hasta 5,6 mm de diámetro) y menos comúnmente *grapestones* (hasta 7,2 mm de diámetro). Estos granos compuestos son redondeados, elípticos y esféricos y contienen envueltas lisas y microcristalinas; se encuentran cementos doloesparíticos uniendo los granos individuales (Fig. 3.10).

Intervalos dolomicríticos

Los intervalos micríticos y de grano fino (de 10μm a 2 cm de espesor) están compuestos por láminas de dolomicrítica peloidal a masiva de color marrón oscuro a claro. Las láminas son comúnmente paralelas, planas y con una continuidad lateral variable. Algunas presentan evidencias de microerosión y las cavidades resultantes quedan rellenadas de pequeños ooides, dando lugar a perfiles ondulados. También

están presentes grietas de desecación, e incluso se aprecian niveles de bioturbación provocados por actividad de metazoos (Fig. 3.10).

Restos microbianos

Estos microbialitos contienen abundantes restos microbianos que proporcionan evidencias de que la actividad microbiana jugó un papel importante en su formación. Los restos filamentosos son más frecuentes en los intervalos dolomicríticos y están comúnmente enraizados en las láminas dolomicríticas peloidales-masivas oscuras, desarrollando una compleja red de filamentos microbianos subparalelos a subperpendiculares a la laminación. Por su parte, los intervalos de *grainstones* están formados por abundantes granos agregados (*lumps* y *grapestones*) cuyas capas envolventes pueden haber tenido un origen mediado por microbios a pesar que sus restos no hayan sido encontrados propiamente.

3.2.3. Trombolitos

Los trombolitos consisten en extensos cuerpos dolomíticos, de espesor métrico a decamétrico, masivos a nodulares y esencialmente no laminados, si bien pueden incluir esporádicos niveles de estromatolitos de tipo 1. Estas sucesiones trombolíticas son comúnmente de espesor decimétrico y típicamente consisten en cuerpos sedimentarios continuos y de texturas uniformes, alcanzando un espesor máximo de 40 m. (Panel 2, Fig. 3.5, 3.7, 3.8G y H, 3.11, 3.12).

Se observan dos tipos de trombolitos: biostromos de relieves planos (tipo 1, estratiformes) y biohermos con relieves positivos (tipo 2, *mud-mound*). Estos dos tipos afloran en el dominio de Prades y Baix-Ebre-Priorat y alcanzan una extensión lateral de mínima de 45 Km. Ocasionalmente se observan algunos cuerpos dómicos aislados (de hasta 4 m de grosor) (Tabla 4).

Características microscópicas

Los trombolitos están compuestos de una textura grumosa o moteada (*clotted*, Aitken, 1967; Burne y Moore, 1987) y se distinguen los siguientes componentes texturales (Mercedes-Martín et al. 2013c).

Mesoclots micríticos densos (Dmm, dense micritic mesoclots). Los *mesoclots* (*sensu* Kennard y James, 1986) representan los constituyentes microbianos por excelencia del armazón trombolítico (Fig. 3.11, 3.12). Los *mesoclots* están constituidos

por masas microcristalinas densas masivas y oscuras, generalmente redondeadas, ameboides o arborescentes de hasta 4 cm de diámetro. Microscópicamente, estas masas están formadas por varios elementos: i) capas/ películas dolomicríticas peloidales a micropeloidales (biofilms calcificados de Riding, 2002), ii) microfósiles calcificados (p. ej., calcimicrobios como *Garwoodia* y *Cayeuxia*, microproblematica como *Tubiphytes*, *Koivaella*? *Isnella*? *Archaeolithoporella*?), iii) cuerpos micropeloidales dispersos y aislados de origen microbiano (p. ej., bacterias cocoidales y racimos micropeloidales), iv) ocasionalmente esponjas aisladas (*Solenolmia manon manon*). Algunas Dmm presentan cavidades de corrosión más abundantes en la parte inferior de los cuerpos trombolíticos.

Matriz micrítica (Mm, micritic matrix). La matriz micrítica presente entre los *mesoclots* consiste en un *mudstone* de color gris a marrón, homogéneo y sin estructura y menos comúnmente un *wackestone* de intraclastos (milimétricos a submilimétricos). Algunos granos de cuarzo y peloides se encuentran ocasionalmente embebidos en la matriz. Estas masas micríticas representan sedimento interno original desprovisto de señales de bioturbación por organismos (Fig. 3.11).

Masas intraclásticas y peloidales (Ipm intraclastic and peloidal masses). Las cavidades existentes entre el armazón están rellenas de un *wackestone* de intraclastos y peloides (Fig. 3.11, 3.12). Los peloides son redondeados a subangulosos (hasta 0,4 mm de diámetro), y los intraclastos son redondeados a angulares, con baja esfericidad y hasta 1,5 mm de longitud. Se reconocen foraminíferos bentónicos, gasterópodos, braquiópodos y bivalvos. Ocasionalmente algunos intraclastos consisten en elementos microbianos retrabajados. Estas masas intraclásticas y peloidales están presentes en las cavidades entre los Dmm, mostrando un relleno episódico.

Cementos botroidales y fibrosos (Bfc, botryoidal amd fibrous cements). Algunas muestras contienen abundantes cementos botroidales y fibrosos marinos tempranos que se disponen rellenando cavidades y constituyen hasta el 40% del volumen de las láminas delgadas estudiadas (Fig. 3.12). Estos cementos están íntimamente ligados a Dmm. En algunos casos, los *biofilms* incrustan los bordes de estos cementos. En otros casos, múltiples generaciones de cementos ocluyen los espacios porosos existentes entre los componentes microbianos. Porcentualmente en volumen, los cementos son los componentes más significativos de las partes altas de los trombolitos. Algunas muestras contienen restos de cementos autigénicos de barita dentro de la matriz dolomítica.

TYPE OF FACIES	FACIES ASSEMBLAGE	DESCRIPTION	MAIN CONSTITUENTS	SECONDARY CONSTITUENTS	SEDIMENTARY FEATURES	DEPOSITIONAL ENVIRONMENTS
Coarse-grained grainstone facies associations	F1	Oolitic grainstone	Ooids	Bivalves, peloids (locally)	Low-angle cross bedding, plane parallel and herringbone stratification; hummocky cross stratification (locally); herringbone and wavy lamination; climbing ripples (locally); massive bedding (locally); tidal bundles, tidal channels; basal lag deposits (locally); erosive bases	Marine shallow subtidal shoals, moderate to high energy conditions. Above fair-weather wave base. Inner-middle ramp
	F2	Cross-bedded skeletal grainstone	Ooids, unidentified bioclasts	Ostracods, gastropods, foraminifera, peloids, intraclasts, litoclasts; cortoids (locally)	Undulous and low-angle cross bedding, plane parallel and herringbone stratification; herringbone, ripple, plane parallel and wavy lamination; climbing ripples (locally); massive bedding (locally); tidal bundles, tidal bars, tidal channels; basal lag deposits (locally); microbial laminations (rare); erosive bases	Marine shallow subtidal beach-barrier island; high energy conditions. Above fair-weather wave base. Internal shoals. Inner ramp
	F3	Peloidal and skeletal wackestone to packstone	Peloids, fragments of bivalves and echinoids	Microoncoids, fragments of gastropods, crinoids; intraclasts	Massive or nodular bedding; herringbone, plane parallel, ripple and wavy lamination; hummocky cross stratification (locally); unidentified burrows, hardgrounds and borings (locally); erosive bases	Marine shallow-water, moderate to high energy conditions. Intertidal to subtidal. Above fair-weather wave base. Beach-barrier island? to shoreface carbonate sands
	F4	Oncolitic-oolitic-peloidal floatstone and grainstone	Oncoids, ooids, peloids,intraclasts, fragments of bivalves and echinoids	Fragments of ostreids, echinoids, gastropods, dasyclad algae; cortoids and aggregates (locally)	Massive or nodular bedding; Plane parallel to low-angle cross-bedding stratification; Erosive bases; Unidentified burrows and root plants; plane parallel, herringbone, wavy and ripple lamination; tidal bundles and tidal channels; basal lag deposits (locally); hardgrounds and Fe/Mn encrustations	Marine shallow-water, moderate to high energy conditions. Subtidal. Above fair-weather wave base. Sheltered lagoon.
	F5	Bioturbated wackestone and packstone with grainstone	Oncoids, ooids, fragments and whole skeletons of bivalves and echinoids	Black pebble intraclasts; planctonic foraminifera; conodonts	Massive, nodular and undulous bedding. Plane parallel lamination (rare). Unidentified burrows and ichnofauna	Below fair-weather wave base, moderate energy conditions. Subtidal. Middle ramp
	F6	Wackestone to floatstone of mollusks interbedded with packstone of echinoderms	Oncoids and microoncoids, fragments of crinoids, bivalves and echinoids	Fragments of gastropods; peloids; Microproblematica; foraminifera	Low-angle cross bedding, ripple, plane-parallel and wavy lamination; massive bedding (locally); tidal bundles; basal lag deposits (locally); unidentified escaping burrows; erosive bases	Marine shallow-water, moderate to high energy conditions. Above fair-weather wave base. Subtidal. Middle ramp
Muddy facies associations	F7	Strongly burrowed skeletal mudstone to wackestone	Fragments of bivalves and echinoids, quartz grains	Fragments of gastropods, peloids, carbonatic intraclasts	Massive or nodular bedding, *Planolites* ichnofauna; *Thalassinoides* ichnofauna (locally); plane parallel, ripple and wavy lamination (locally); tidal channels and tidal bars; tidal bundles (locally), hummocky cross stratification (rare); conglomerate lag deposits (locally); slump-scars and carbonate breccias (rarely)	Marine shallow-water, moderate to high energy conditions. Above fair-weather wave base. Hypersaline intertidal to subtidal sheltered lagoons and tidal flats
	F8	Burrowed skeletal mudstone to packstone interbedded with marls	Peloids , fragments of bivalves and echinoids	Fragments of gastropods, intraclasts, *Tubiphytes*, foraminifera; cephalopods, crinoids, brachiopods, ostreids, bryozoans and ostracods (rare); oncoids, aggregates (rare); quartz grains (locally)	Massive or nodular bedding; plane parallel, wavy and ripple lamination (occassionally); unidentified burrows; *Planolites* ichnofauna; *Thalassinoides* ichnofauna (locally); erosive bases; channelized deposits (calciturbidites?) and slumps (locally); hardgrounds and Fe/Mn mineralizations	Below storm wave base, moderate to low energy conditions. Deep subtidal. Outer ramp.
	F9	Thin-bedded laminated dolomicrite-dolomudstone	Fragments and whole skeletons of mollusks and macroinvertebrates	Small fragments of bivalves and other unidentified skeletal components	Event-bedding stratification; plane parallel ard ripple lamination (locally); Deep water ichnofauna; unidentified burrows and borings; gas-bubble casts; evaporite moulds; hardgrounds and Fe/Mn encustrations (locally)	Below fair-weather wave base, low energy restricted conditions. Subtidal. Middle-outer ramp

TABLA 1. Clasificación de facies e interpretación de ambientes sedimentarios del área estudiada.

TYPE OF FACIES	FACIES ASSEMBLAGE	DESCRIPTION	MAIN CONSTITUENTS	SECONDARY CONSTITUENTS	SEDIMENTARY FEATURES	DEPOSITIONAL ENVIRONMENTS
Microbialites and related facies associations	F10	Planar and domal stromatolites	Microbial laminations (domal and planar in shape)	Flat-pebble intraclasts (locally)	Microbial laminations (plane parallel and domal), birdeyes and fenestral fabrics, teppe structures, karst related structures, hardgrounds, pseudomorphs after evaporite minerals	Marine shallow-water, moderate energy conditions. Hypersaline intertidal to supratidal flats. Inner ramp
	F11	Ooidal-peloidal stromatolites	Microbial laminations (domal and planar in shape), ooids, peloids	Aggregates, flat-pebble intraclasts; Bahamite peloids (locally); Quarz grains	Microbial laminations (planar paralel and domal), birdeyes and fenestral fabrics; teppe structures; plane parallel, herringbone, wavy and ripple lamination (locally); microhardgrounds, borings; tidal channels (rare)	Marine shallow-water, moderate to high energy conditions. Intertidal to subtidal. Above fair-weather wave base. Internal fore-shoals. Inner ramp
	F12	Microbial-peloidal thrombolites	Peloids, micropeloids, Microproblematica (*Garwoodia, Tubiphytes, Cayeuxia*)	Intraclasts, bivalves, oncoids, quarz grains, foraminifera	Massive or nodular bedding; erosive bases (locally); microbial laminations	Below fair-weather wave base, low to moderate energy conditions. Subtidal. Outer ramp.
	F13	Calcimicrobial boundstone with bioclasts	Calcimicrobes, fragments of bivalves, gastropods	Fe/ Mn encrustrations and hardgrounds (locally)	Massive bedding; plane parallel and ripple lamination (locally); Microbial laminations (domal and planar in shape); Birdeyes and fenestral fabrics	Marine shallow-water, moderate to high energy conditions. Above fair-weather wave base. Intertidal. Middle ramp
	F14	Coral-microbial boundstone to rudstone	Scleractinian corals, worm tubes, sponges?, peloids, organomicrites	Intraclasts, fragments of bivalves; foraminifera, serpulids, Microproblematica *(Garwoodia, Girvanella?, Tubiphytes),*	Massive bedding, hardgrounds, unidentified burrows (locally)	Marine shallow-water, moderate to high energy conditions. Above fair-weather wave base. Subtidal. Middle ramp
	F15	Laminated packstone of oncoids and peloids	Oncoids, peloids,intraclasts, fragments of bivalves and echinoids	Peloidal micrite and filamentous microbial remains	Massive bedding; microbial laminations (planar paralel and domal), birdeyes and fenestral fabrics; ripple and plane parallel lamination (locally); Calcite pseudomorphs after evaporite minerals	Marine shallow-water, moderate energy conditions. Intertidal to supratidal flats. Inner-middle ramp
	F16	Packstone to rudstone of dasyclads, bioclasts and peloids	Intraclasts, peloids, fragments of Dasyclad algae, *Tubiphytes*	Fragments of bivalves, gastropods, echinoids; foraminifera, Microproblematica; Microbial boundstones and skeletal stromatolites (locally)	Massive bedding to low angle cross-bedding, plane-paralel and ripple lamination. Hardgrounds and Fe/Mn encrustrations (locally); Erosive bases	Marine shallow-water, moderate to high energy conditions. Above fair-weather wave base. Subtidal. Middle ramp
	F17	Foreslope dolomitic breccias	Carbonate clasts	Microproblematica encrusters	Massive to coarsely bedding. Poor to moderate sorting; polymictic composition; heterometric; clast-supported and mud-supported (locally); subangular to subrounded clasts.	Below fair-weather wave base to hemipelagic, low energy conditions. Subtidal. Outer ramp

TABLA 1 (continuación). Clasificación de facies e interpretación de ambientes sedimentarios del área estudiada.

MICROBIALITE TYPE	MICROBIALITE SUBTYPE	GEOMETRY AND DIMENSIONS	TEXTURE AND LAMINATION	MICROBIAL REMAINS
Stromatolites s.s.	Type 1: Stratiform	Tabular, rarely dome-shaped Thickness: up to 5 m Width: - Lateral extent: at least 30 Km Rare small dome-shaped bodies (up to 15 cm high and 20 cm wide) and low synoptic relief bodies with a conical profile (up to 2 cm high and 5 cm wide)	Alternation of thicker dark and thinner light dolomicrite and dolosparite layers (Type A couplets) Light laminae: peloidal dolomicrite, microdolospar and dolospar (500 to 1500 µm thick) Dark laminae: dense dolomicrite, mostly peloidal, clotted and cloudy (100 to 250 µm thick) Composite intervals composed of several dark laminae (2 to 4 mm thick)	Light laminae: Domed structures (convex-upward bodies) with filamentous dolomicrite bodies subperpendicular to the domes Isolated fan-like, filament-bearing dolomicrite bodies subperpendicular to the lamination Dark laminae: Subperpendicular, isolated micrite filamentous bodies Calcimicrobial bodies (*Cayeuxia*-like forms)
	Type 2: Domal	Head-shaped, domed buildups commonly linked laterally Thickness: up to 2 m Width: 6 m Lateral extent: at least 20 Km Rare small, isolated spaced intermingled domes (up to 10 cm high and 15 cm wide)		

TABLA 2. Características de las facies de estromatolitos s.s. (facies F10)

MICROBIALITE TYPE	GEOMETRY AND DIMENSIONS	TEXTURE AND LAMINATION	MICROBIAL REMAINS
Ooidal-peloidal stromatolites	Stratiform and low-relief hemielliptical buildups. Thickness: up to 3 m Width: - Lateral extent: at least 40 Km	Alternation of oolitic grainstone layers with micrite layers (both dolomitised) *Oolitic layers*: smooth, planar to slightly wavy (sub-millimeter to a 5 cm thick) *Micritic layers*: tabular to wavy (few μm to 2 cm thick) Type B couplets: micritic layers with several μm thick Type C couplets: micritic layers exceeding 1mm thick	<u>Oolitic layers</u>: Aggregate grains (lumps and grapestones) with microbially mediated laminated coatings <u>Micritic layers:</u> Microbial filaments rooted in dark, massive to peloidal dolomicrite laminae Small and spiraliform filaments → bouquets Thicker and rectilinear → isolated and disperse

TABLA 3. Características de las facies de estromatolitos oolítico-peloidales (facies F11)

MICROBIALITE TYPE	MICROBIALITE SUBTYPE	GEOMETRY AND DIMENSIONS	TEXTURE AND MICROBIAL REMAINS
Thrombolites	Type 1: Stratiform	Extensive flat-relief biostromes Thickness: average of 40 m Width: - Lateral extent: at least 45 Km	<u>Dense micritic mesoclots</u> (Dmm): dark-coloured, massive and dense microcrystalline masses. 1) Micropeloidal to peloidal cloudy dolomicritic veneers (biofilms) 2) Calcified microfossils (*Garwoodia*, *Cayeuxia*-like porostromate calcimicrobes, *Tubiphytes, Koivaella?, Isnella?* or *Tubiphytes*-like, 3) Isolated and dispersed micropeloidal bodies (e.g. coccoid bacteria bushes and micropeloidal clusters) 4) Isolated sponges (*Solenolmia manon manon)* <u>Micritic matrix</u> (Mm): homogeneous and structureless light mudstone. <u>Intraclastic-peloidal masses</u> (Ipm): Interframework cavities filled with intraclastic and peloidal wackestone. <u>Botryoidal and fibrous cements</u> (Bfc): cavity-filling early marine cements (botryoidal and fibrous).
	Type 2: Mud mound	Head-shaped, domed buildups commonly linked laterally Thickness: average of 40 m Width: 50-100m Lateral extent: at least 45 Km	

TABLA 4. Características de las facies de trombolitos (facies F12)

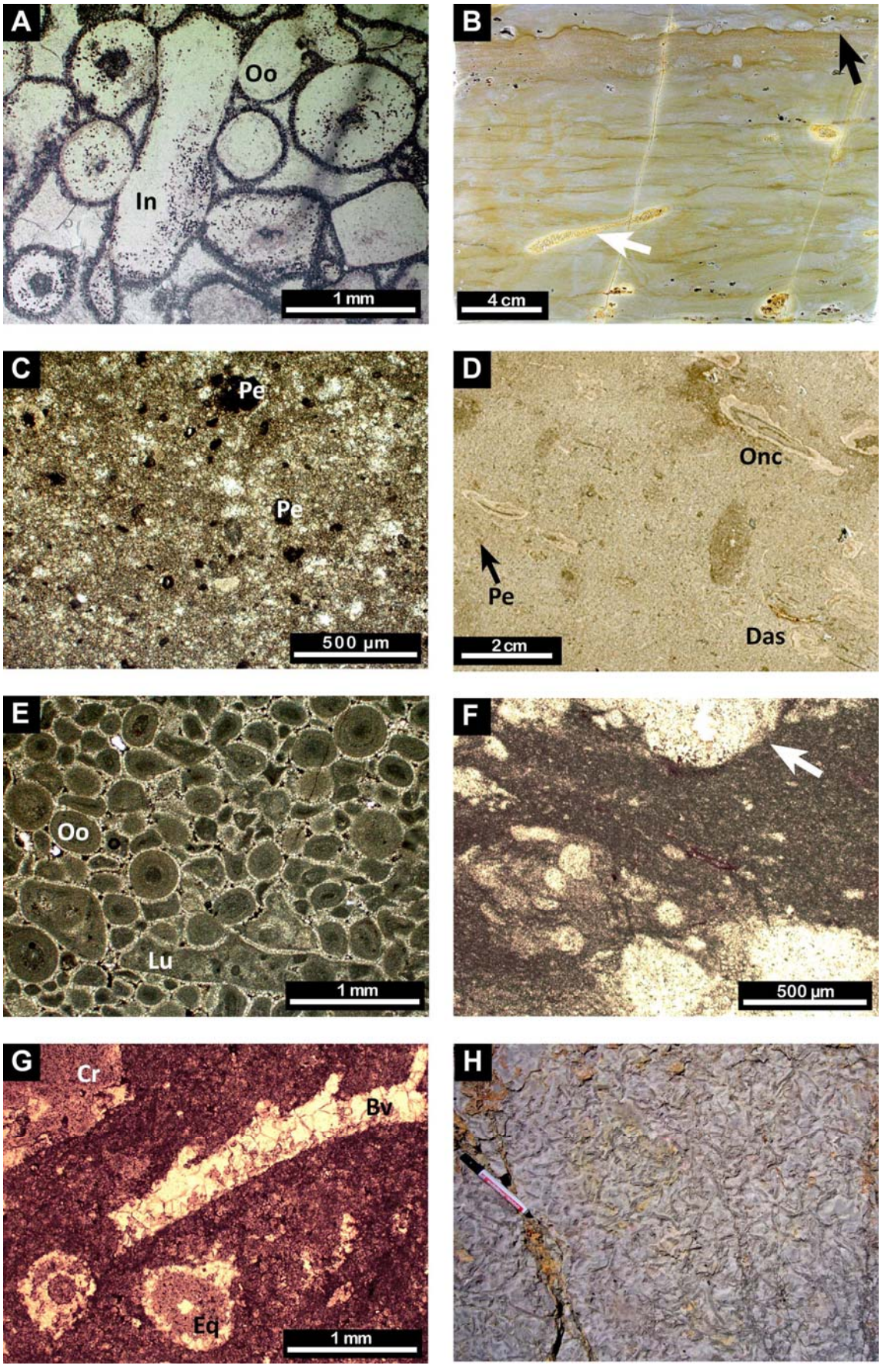
A
Oo
In
1 mm
B
4 cm
C
Pe
Pe
500 µm
D
Onc
Pe
Das
2 cm
E
Oo
Lu
1 mm
F
500 µm
G
Cr
Bv
Eq
1 mm
H

Fig. 3.1. Microfotografías y fotografías de afloramiento de las facies reconocidas. A) *Grainstones* oolítico (Oo), intraclastos (In) (Facies F1, Tabla 1). B) Sección pulida de un *grainstones* bioclásticos con estratificación cruzada. Se observan laminación cruzada de bajo ángulo con laminación ripple y trazas de bioturbación (flecha blanca). Pequeña superficie endurecida (flecha negra) (Facies F2, Tabla 1). C) *Wackestones-packstones* bioclástico y peloidal con matriz dolomitizada y pequeños peloides (Pe) (Facies F3, Tabla 1). D) *Floatstones-grainstones* oncolítico-oolítico-peloidal, mostrando abundantes oncoides (Onc), esqueletos de dasicladáceas elongados revestidos (Das), y peloides (Pe) (Facies F4, Tabla 1). E) Sección pulida de un *grainstones* oolítico bien clasificado (Oo), granos revestidos (*lumps*, Lu) (Facies F4, Tabla 1). F) *Wackestones-packstones* bioturbado interestratificado con *grainstones*. Posee una matriz de *wackestones* con pequeños peloides, bivalvos y icnofauna indeterminada (flecha blanca) (facies F5, Tabla 1). G) *Wackestones* a *floatstones* de moluscos interestratificados con *packstones* de equinodermos. Se observa una matriz de *wackstones* con grandes esqueletos de bivalvos (Bv), fragmentos de crinoideos (Cr) y espinas de equínidos (Eq) (Facies F6, Tabla 1). H) Fotografía de afloramiento del *mudstone-wackestone* bioclástico intensamente bioturbado, mostrando las texturas de bioturbación producidas por Planolites sp.y otros icnofósiles de cuerpo blando. Lápiz = 15 cm (Facies F7, Tabla 1). Tomado de Mercedes-Martín et al. (2013a). ←

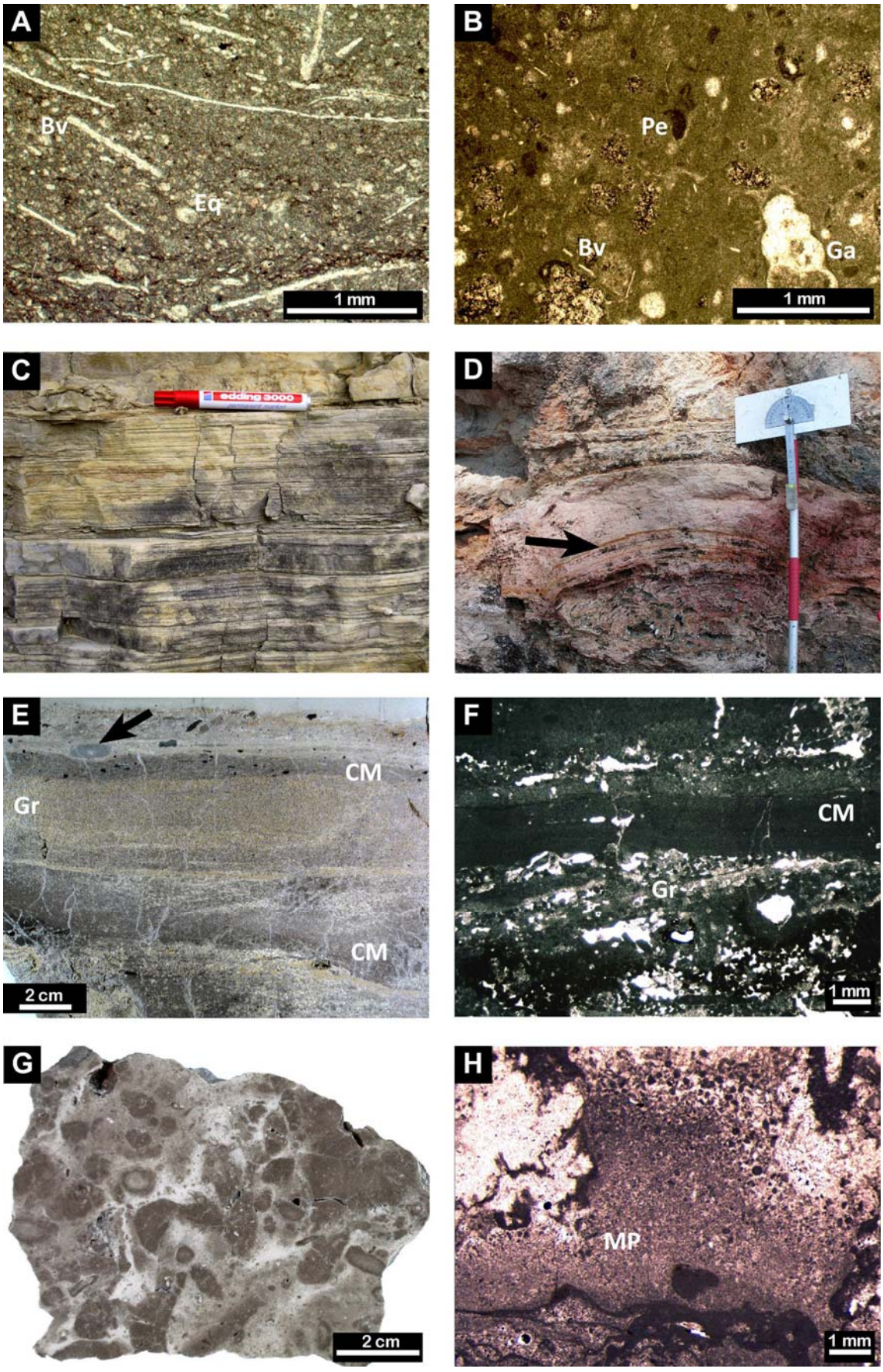
A
Bv
Eq
1 mm
B
Pe
Bv
Ga
1 mm
C
edding 3000
D
E
CM
Gr
CM
2 cm
F
CM
Gr
1 mm
G
2 cm
H
MP
1 mm

Fig. 3.2. Microfotografías y fotografías de afloramiento de las facies reconocidas. A) *Mudstones-wackestones* bioclásticos intensamente bioturbados con fragmentos de bivalvos alargados (Bv) y espinas de equínidos (Eq)(Facies F7, Tabla 1). B) *Mudstones-packestones* bioclásticos bioturbados interestratificados con margas. Peloides (Pe), fragmentos de bivalvos (Bv), equínidos y gasterópodos (Ga) están presentes en la matriz fangosa (Facies F8, Tabla 1). C) Fotografía de afloramiento de las dolomicritas-*dolomudstones* finamente laminadas mostrando una tosca laminación plano-paralela. La laminación ripple ha sido usualmente observada (arriba izquierda). Marcador = 15 cm (Facies F9, Tabla 1). D) Afloramiento de un domo de 80 cm de espesor mostrando la facies de estromatolitos dómicos y planares. Véase la textura fenestral a lo largo de las láminas macroscópicas (flecha negra) (Facies F10, Tablas 1 y 2). E) Sección pulida de los estromatolitos oolítico-peloidales mostrando la alternancia macroscópica de láminas. Las capas de *grainstone* (Gr) muestran una porosidad móldica y vuggy antigua. Algunas capas intraclásticas (flechas negras) tapizan las capas micríticas *clotted* (CM) (Facies F11, Tablas 1 y 2). F) Alternancia de capas micríticas masivas a *clotted* (CM) con intervalos planos o ligaremente ondulados de *grainstones* oolítico-peloidales (Gr) (Facies F11, Tablas 1 y 2). G) Sección pulida de los trombolitos microbianos-peloidales mostrando los *mesoclots* con textura macroscópica oscura, redondeada a alargada y rodeada de cavidades internas que están rellenas con micrita *clotted* densa (Facies F12, Tablas 1 y 2). H) Cavidades rellenas de *mudstones-wackestones* con texturas micríticas *clotted*, peloides y micropeloides (MP) (Facies F12, Tablas 1 y 2). Tomado de Mercedes-Martín et al. (2013a).←

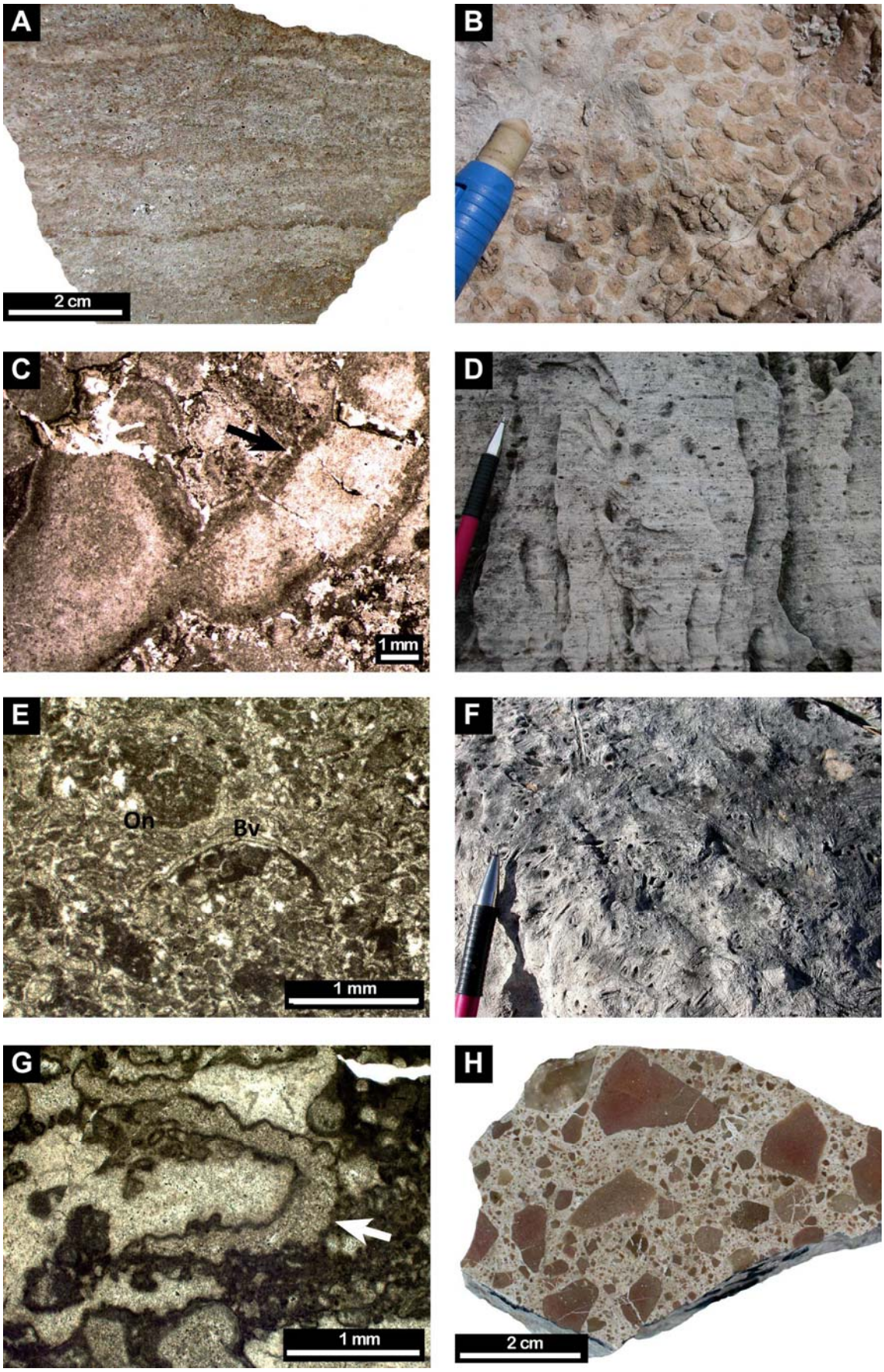
A
2 cm
B
C
1 mm
D
E
On
Bv
1 mm
F
G
1 mm
H
2 cm

Fig. 3.3. Microfotografías y fotografías de afloramiento de las facies reconocidas. A) Sección pulida de los *boundstones* de calcimicrobios con bioclastos, localmente con incrustaciones de Fe/Mn y superficies endurecidas (láminas oscuras). Las texturas fenestrales y *birdeyes* son comunes a lo largo de las láminas macroscópicas (Facies F13, Tabla 1). B) Fotografía de afloramiento del *boundstones-rudstones* de corales y microbios, mostrando una pequeña colonia de corales con coralitos redondeados y embebidos en una matriz fangosa (porción de escala = 3 cm) (Facies F14, Tabla 1). C) *Wackestones-packstones* dolomitizados con corales escleractínidos ramosos (flecha negra) (Facies F14, Tabla 1). D) Fotografía de afloramiento de los *packstones* laminados de oncoides y peloides con texturas laminadas en paralelo y abundante porosidad vacuolar (Facies F15, Tabla 1). E) *Packstones* con bivalvos (Bv) y oncoides (On) rodeados de organomicritas con texturas peloidales y *clotted* (Facies F15, Tabla 1). F) Fotografía de afloramiento de *packstones* a *rudstones* de dasicladáceas, bioclastos y peloides exhibiendo la acumulación de tallos alargados de algas dasicladáceas (escala= 7 cm) (Facies F16, Tabla 1). G) Secciones longitudinales de algas dasicladáceas (flecha blanca) incrustadas por *Tubiphytes* sp. (facies F16, Tabla 1). H) Sección pulida de las brechas matriz-soportadas de talud dolomitizadas, caracterizadas por cantos pobremente a moderadamente seleccionados, derivados de los flancos de los trombolitos (Facies F17, Tabla 1) Tomado de Mercedes-Martín et al. (2013a). ←

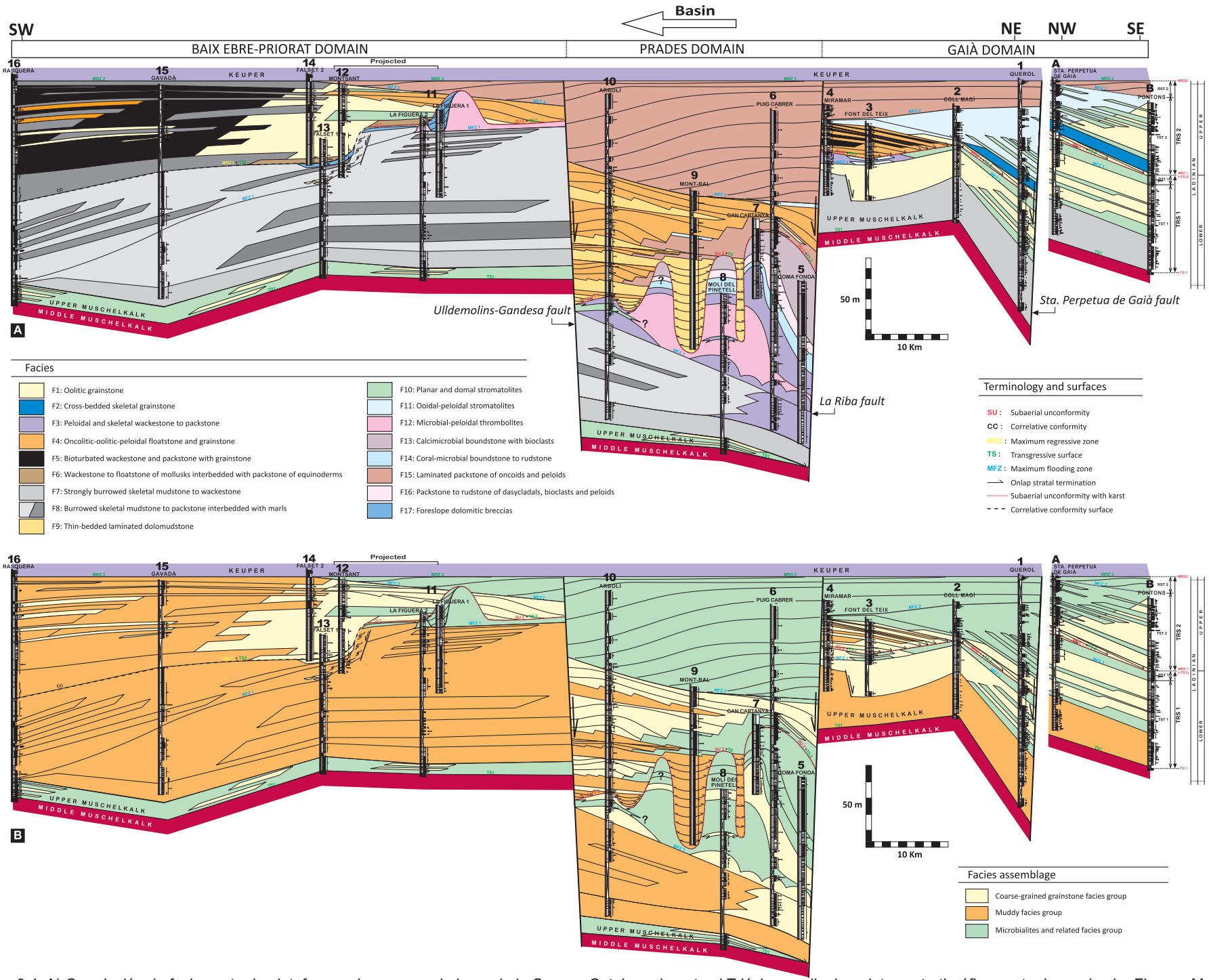

Fig. 3.4. A) Correlación de facies entre la plataforma y la cuenca a lo largo de la Cuenca Catalana durante el Triásico medio. Los datos estratigráficos entre las series La Figuera-Montsant y entre Sta. Perpetua de Gaià y Pontons están proyectados en el mismo perfil geológico. Ver Fig. 2.1 para localización de las series estratigráficas. Nótese que la escala vertical ha sido exagerada. B) El mismo perfil geológico mostrando los tres tipos de asociaciones de facies. Mercedes-Martín et al., (2013b)

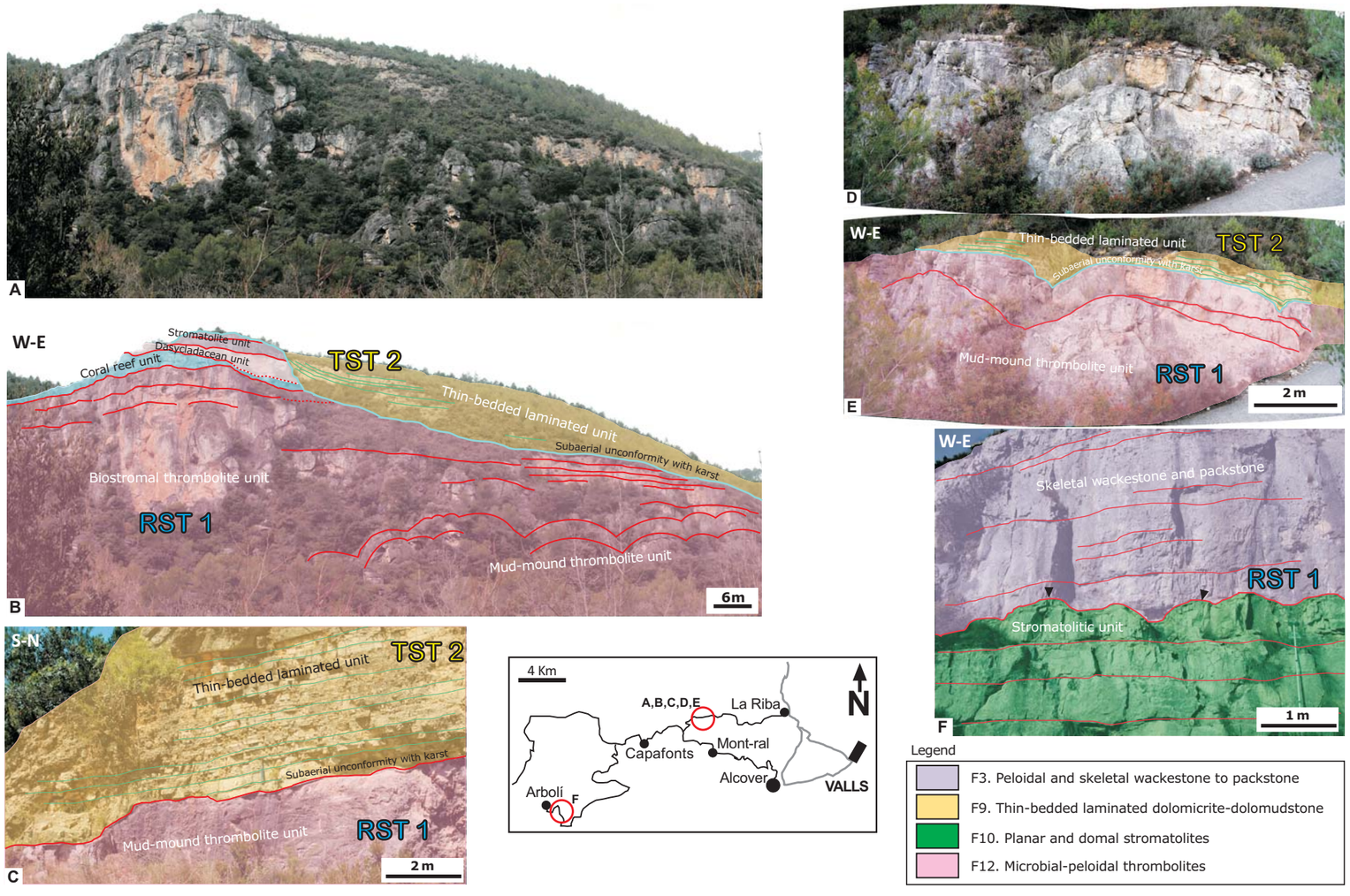

Fig. 3.5. Afloramientos de microbialitos mostrando sus geometrías, relaciones de facies e interpretación secuencial en el dominio de Prades. A) Fotomosaico tomado cerca de la serie de Molí del Pinetell (La Riba). B) Line-drawings e interpretación secuencial donde se muestra el límite entre la T-R1 y 2 (linia color turquesa) y sus respectivas facies. Nótese que la unidad trombolítica biostromal muestra una geometría tabular alrededor de los flancos. Una unidad trombolítica métrica del tipo mud-mound aflora en la base de algunos biostromos. C) Line-drawings e interpretación secuencial del límite entre la T-R1 y 2 cerca de la serie de Molí del Pinetell. Esta superfície está caracterizada por un paleocarst. D) La unidad trombolítica del tipo mud-mound representa la base de unidad trombolítica biostromal en B. E) Line-drawings e interpretación secuencial de la fotografía previa mostrando las facies y el límite entre la T-R1 y 2. F) Line-drawings e interpretación secuencial de los depósitos microbiales más someros y occidentales en la serie de Arbolí. Nótense los domos estromatolíticos aflorando en esta áera (flechas negras).

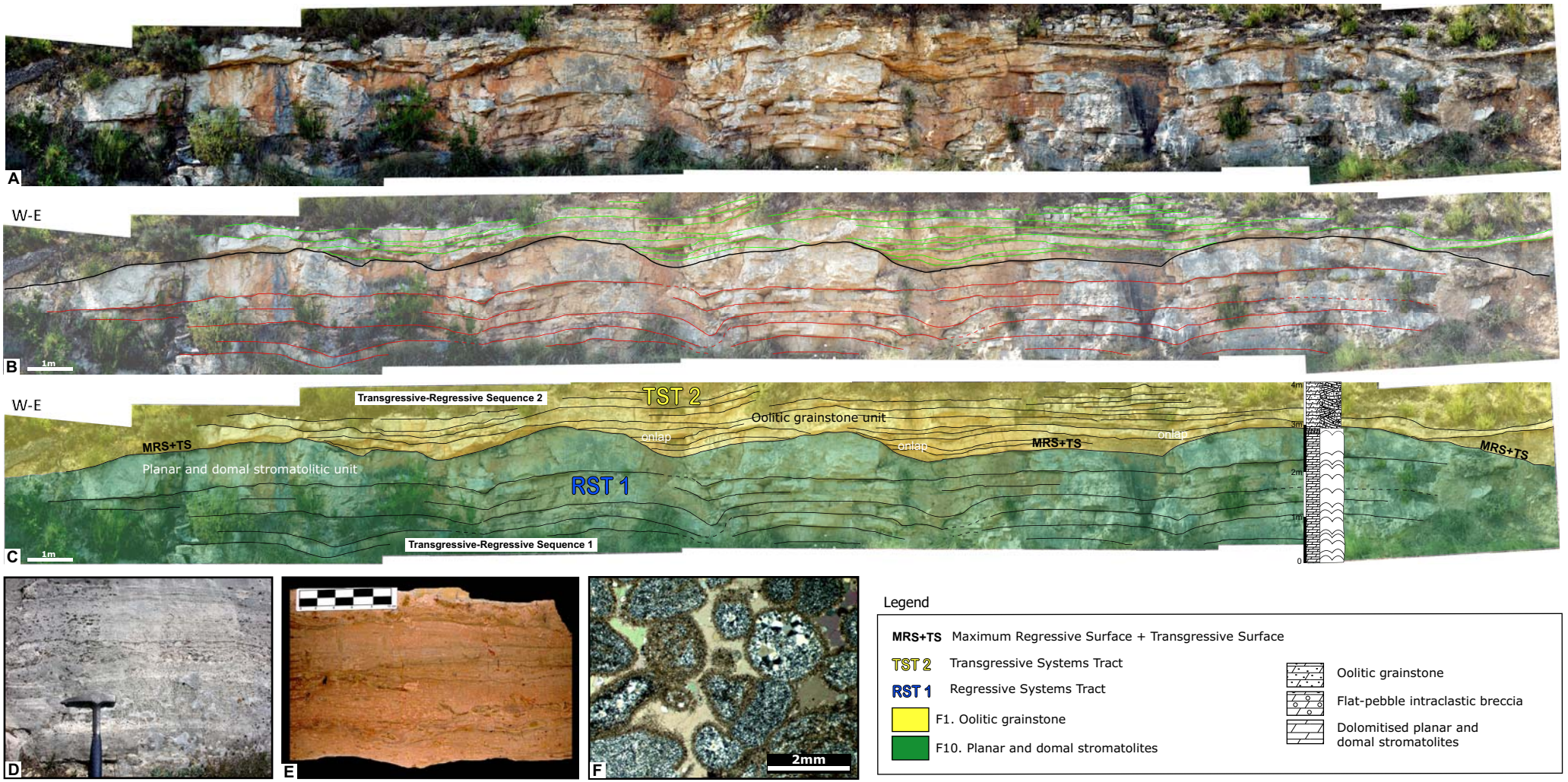

Panel 1. A) Facies de estromatolitos planares y dómicos (F10) superpuestos por grainstones oolíticos (F1) en el dominio de Gaià, sección Querol. B) Interpretación de line-drawings mostrando el límite (linea negra) entre las secuencias T-R 1 y 2. C) Interpretación secuencial exhibiendo las principales superficies estratigráficas, facies y una serie estratigráfica sintética (parte derecha). Ver leyenda para más detalles. Nótese la terminación en onlap de la facies F1 por encima de las geometrías dómicas que caracterizan las partes altas de la facies F10. D) Fotografía de afloramiento mostrando ejemplos tabulares y laminados que se registran en la base de la facies F10. F) Grainstone oolítico (facies F1) formado por ooides silicificados.

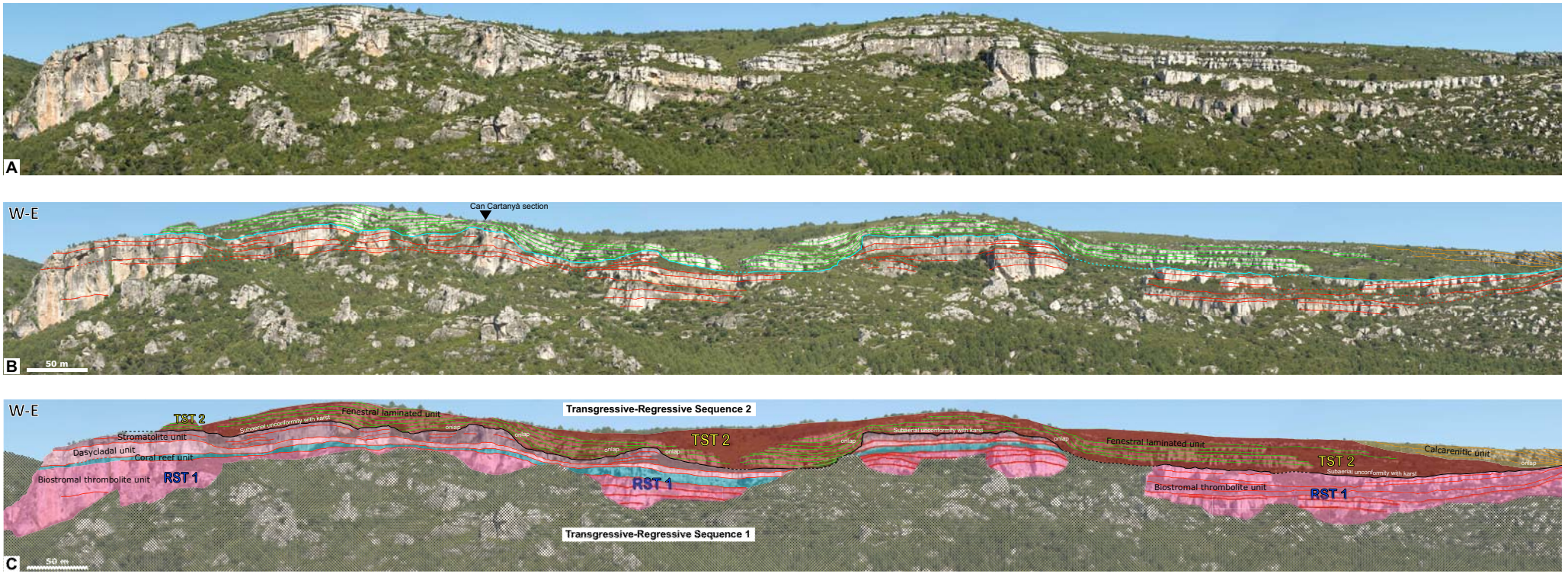

Legend

- F4. Oncolitic-oolitic-peloidal floatstone and grainstone
- F12. Microbial-peloidal thrombolites
- F13. Calmicrobial boundstone with bioclasts
- F14. Coral-microbial boundstone to rudstone
- F15. Laminated packstone of oncoids and peloids
- F16. Packstone to rudstone of dasyclads, bioclasts and peloids
- TST 2 Transgressive Systems Tract
- RST 1 Regressive Systems Tract
- Covered

Panel 2. A) Geometrías de incisión afectando a las facies F12 y geometrías progradantes (facies F15 y 16) que downlapan el techo de la unidad trombolítica del tipo mud-mound (facies F12, parte derecha) en el dominio de Prades, a lo largo del rio Brugent, localidad La Riba. B) Interpretación de line-drawings del fotomosaico previo mostrando el límite entre la T-R 1 y 2 (línia azul turquesa). C) Interpretación secuencial del fotomosaico previo, mostrando las principales superficies estratigráficas, facies y geometrías de los cuerpos sedimentarios. Nótese la terminación en onlap de las facies F4 por encima de la discordancia subarérea con carst (línia negra).

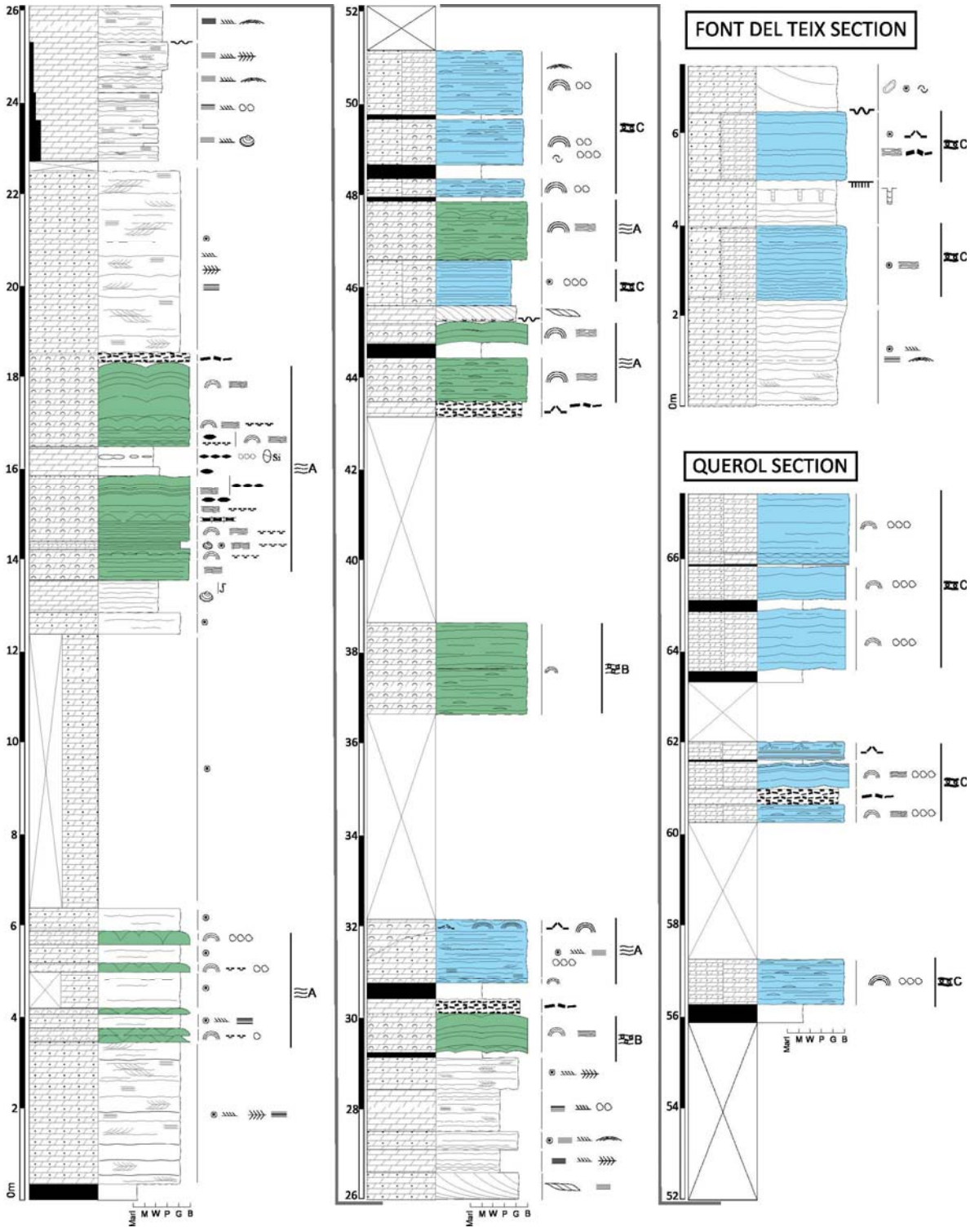

Fig. 3.6. Series estratigráficas de Querol y Font del Teix (consultar la Fig. 3.7 para detalles de la leyenda). Los intervalos con estromatolitos s.s. (facies F10) se han coloreado en verde. Los estromatolitos oolítico-peloidales (facies F11) en azul. Tomado de Mercedes-Martín et al. (2013c).

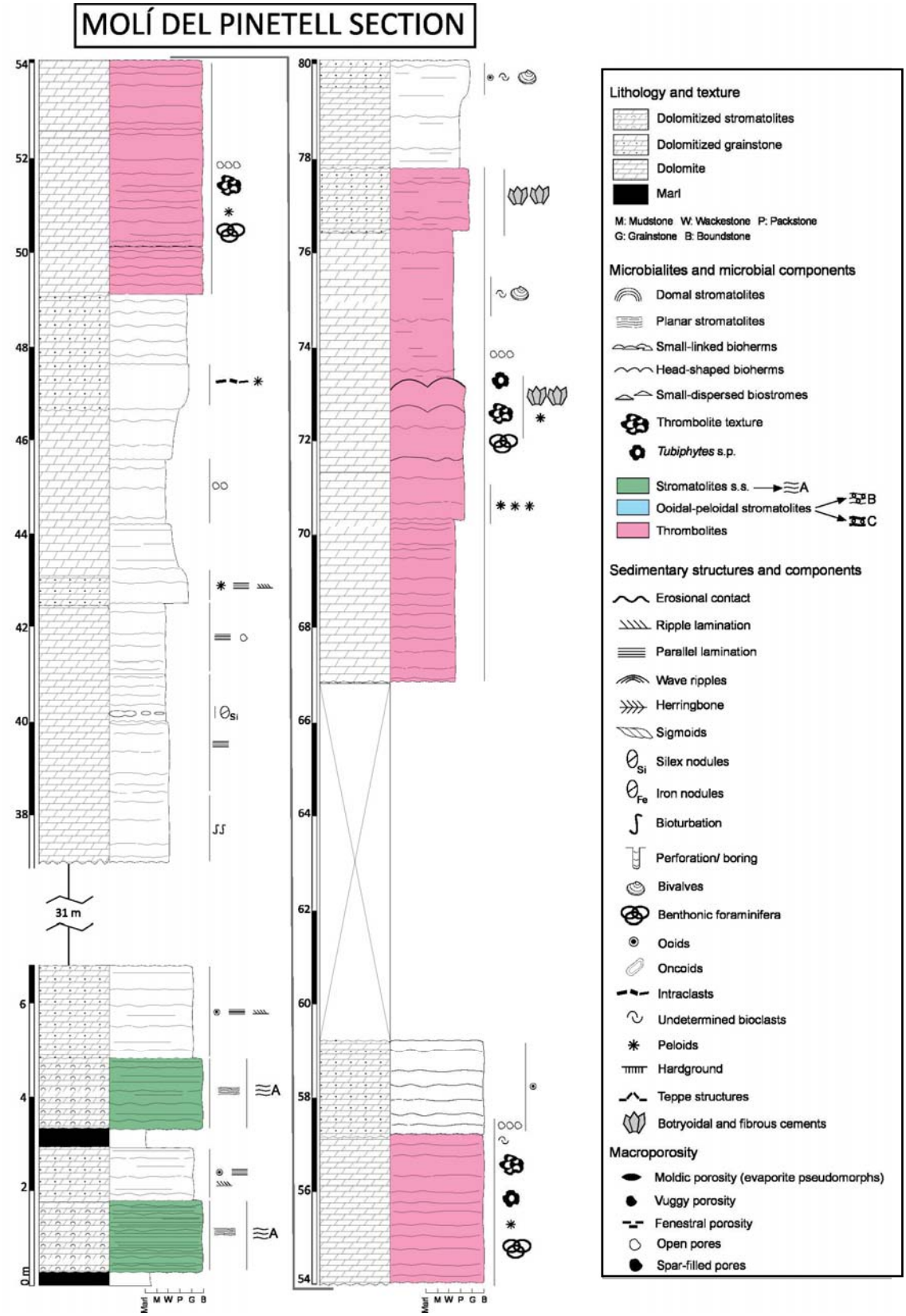

Fig. 3.7. Serie estratigráfica de Molí del Pinetell. Los estromatolitos s.s. (facies F10) se han coloreado en verde. Los trombolitos (facies F12) en color rosado. Nótese un incremento de los cementos botroidales y fibrosos hacia techo de las unidades trombolíticas. Tomado de Mercedes-Martín et al. (2013c).

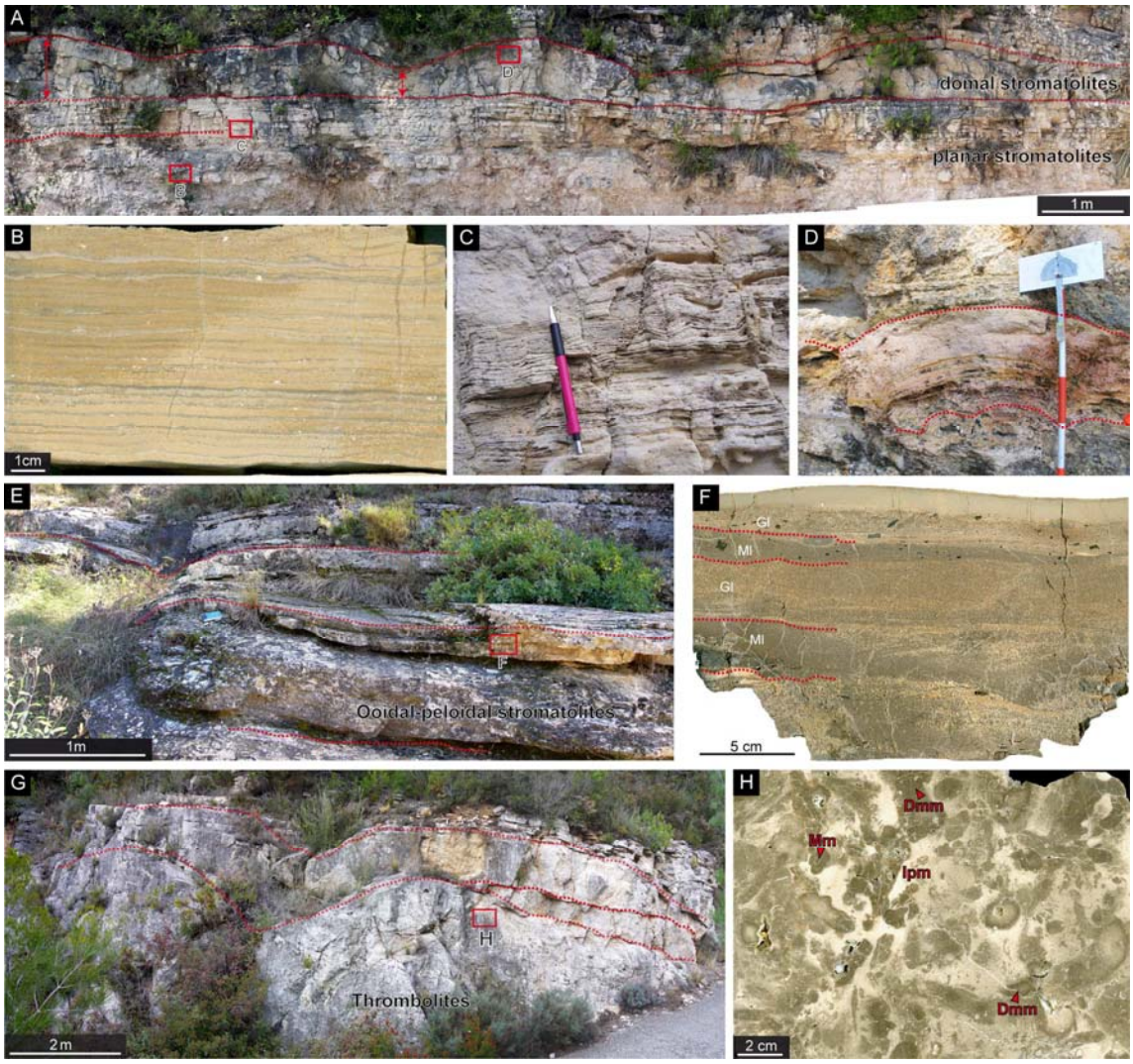

Fig 3.8. Fotografías de afloramiento y secciones pulidas de los microbialitos. A) Fotomosaico de los estromatolitos s.s. mostrando la yuxtaposición de las morfologías de Tipo 1 (formas planares) y de Tipo 2 (formas dómicas). B) Sección pulida de estromatolitos planares mostrando una alternancia de capas dolomíticas claras y oscuras, planas y continuas. C) Pequeño domo estromatolítico constituido por capas continuas y macroporosidad fenestral. E) Fotografía de los estromatolitos oolítico-peloidales caracterizados por estructuras hemielípticas de bajo relieve. F) Detalle de sección pulida del afloramiento de E, mostrando una alternancia de intervalos de *grainstone* (GI) con intervalos micríticos (MI). Nótese la presencia de algunos intraclastos en el techo. G) Fotografía de los trombolitos en la sección de Molí del Pinetell. Nótese la geometría de *mound*. H) Detalle de sección pulida del afloramiento en G, exhibiendo las texturas *clotted* características de los trombolitos (Ipm: masas intraclásticas y peloidales; Mm: matriz micrítica y Dmm: *mesoclots* micríticos densos). Tomado de Mercedes-Martín et al. (2013c). Lápiz = 15 cm.

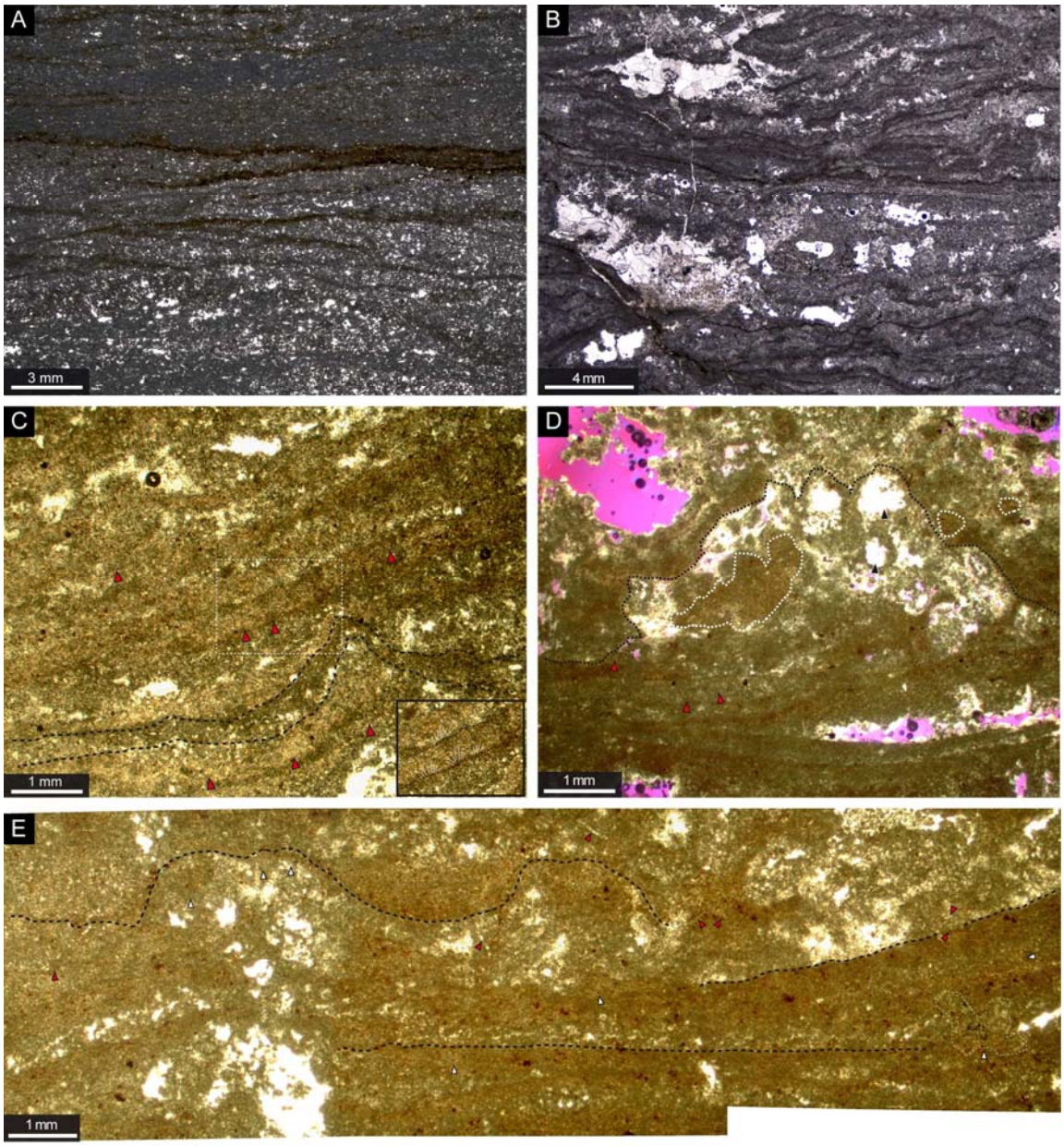

ig. 3.9. Microfotografías de los estromatolitos s.s. mostrando las parejas de Tipo A. A) Alternancia de láminas dolomicríticas oscuras y claras. Nótese el apilamiento paralelo de las láminas, las cuales son típicamente onduladas. B) Alternancia de láminas dolomicríticas oscuras y claras con perfiles ondulados y arrugados. Nótese la presencia de pequeños domos (parte izquierda), así como una porosidad fenestral y vacuolar antigua ocluida con doloesparita. C) Detalle de un domo formado por la alternancia de láminas. Las láminas claras incluyen pequeñas estructuras dómicas (cuerpos convexos hacia arriba) las cuales contienen filamentos subperpendiculares a los domos (flechas rojas). D) Detalle de un domo constituido por calcimicrobios (similares a *Cayeuxia,* en círculos blancos) y su porosidad móldica ocluida asociada (flechas negras). Nótese los cuerpos filamentosos (flechas rojas) embebidos en láminas claras, así como los poros interlaminares (parte inferior) correspondientes a tapices microbianos degradados. E) Fotomosaico representando dos pequeños domos constituidos por restos de filamentos microbianos (flechas rojas) y calcimicrobios arbustivos (flechas y círculo blanco). Los poros rosas se deben a los efectos de la meteorización y a la realización de las láminas delgadas. Tomado de Mercedes-Martín et al. (2013c).

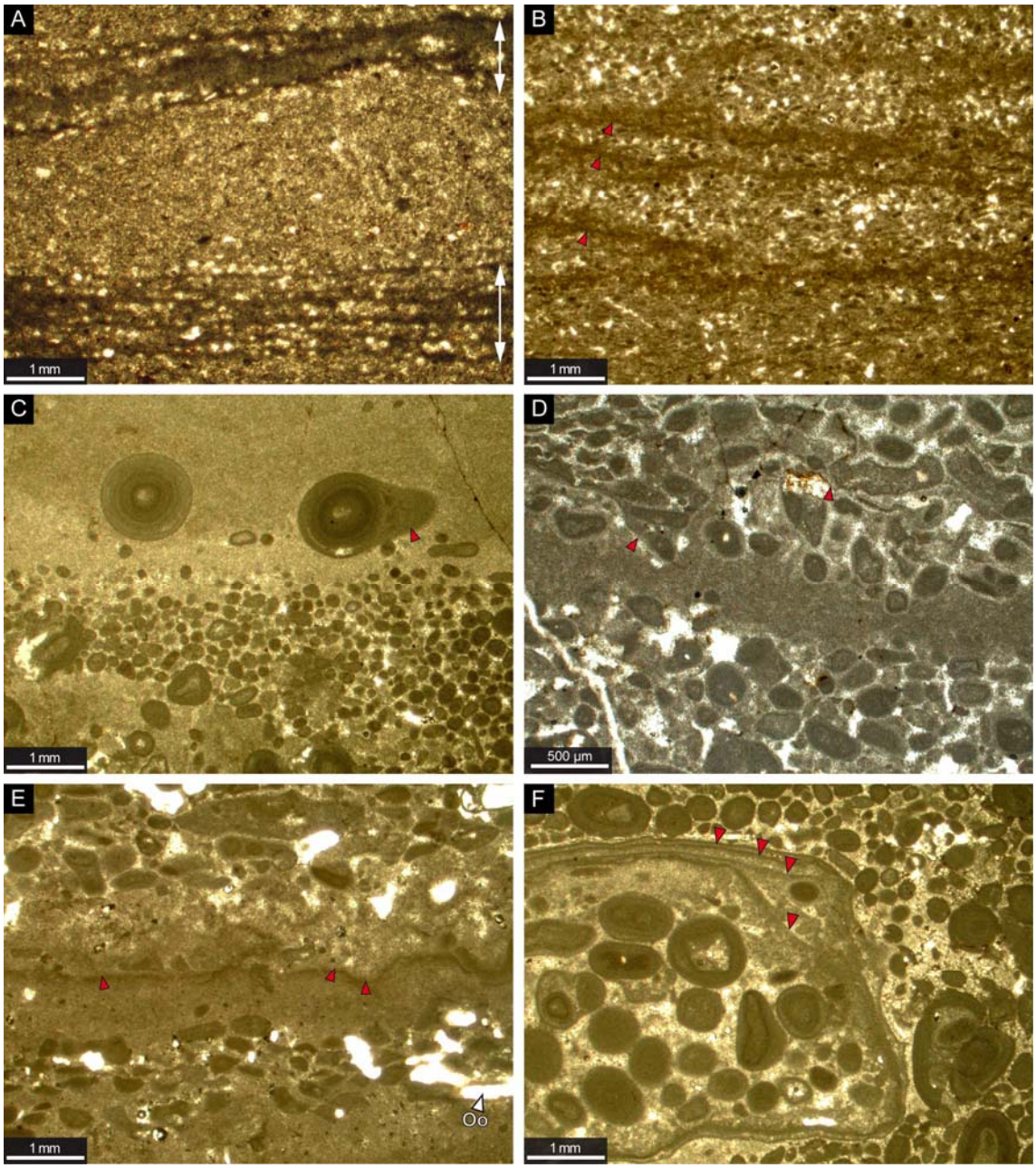

Fig. 3.10. Microfotografías de los estromatolitos s.s. y estromatolitos oolítico-peloidales. A) Intervalos compuestos en los estromatolitos s.s. (parejas Tipo A), consistentes en varias láminas oscuras (flechas) de mm de espesor alternando con láminas claras de dolomicrita peloidal. B) Parejas de Tipo B en estromatolitos oolítico-peloidales. Las flechas marcan la alternancia de capas regulares de *grainstone* con capas micríticas onduladas a tabulares, de varios µm de espesor. C) Parejas de Tipo C en estromatolitos oolítico-peloidales. Algunos ooides se encuentran incorporados en las capas micríticas y desarrollan cortezas micríticas (flecha roja). D) Parejas de Tipo C en estromatolitos oolítico-peloidales. Algunos intervalos micríticos muestran evidencias de erosión y relleno de ooides (flechas), así como delgadas costras ferruginosas en el techo. Nótese que los granos compuestos están micritizados. E) Restos de filamentos microbianos (flechas) comúnmente enraizados en las láminas dolomicríticas oscuras peloidales a masivas. La porosidad oomóldica (Oo) es frecuente. Algunos *grapestones* son observados en el techo. F) Los granos agregados de los estromatolitos oolítico-peloidales están formados por una alternancia de delgadas láminas dolomicríticas oscuras y de láminas dolomicríticas peloidales a micropeloidales claras (flechas). Los granos suelen estar micritizados. Tomado de Mercedes-Martín et al. (2013c).

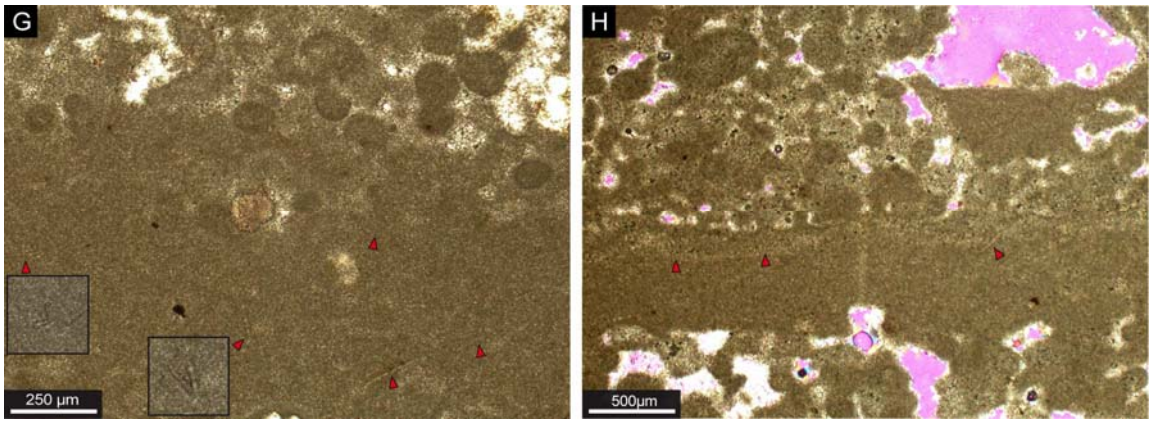

Fig 3.10 (continuación). Restos de filamentos microbianos (flechas) han sido observados en los intervalos dolomicríticos de los estromatolitos oolítico-peloidales. Estos filamentos se encuentran adheridos a las láminas oscuras, dolomicríticas peloidales a masivas. H) Los filamentos microbianos suparalelos a subperpendiculares (flechas) de las capas micríticas desarrollan una retícula caótica y compleja. Los poros rosas se deben a los efectos de la meteorización y a la realización de las láminas delgadas. Tomado de Mercedes-Martín et al. (2013c).

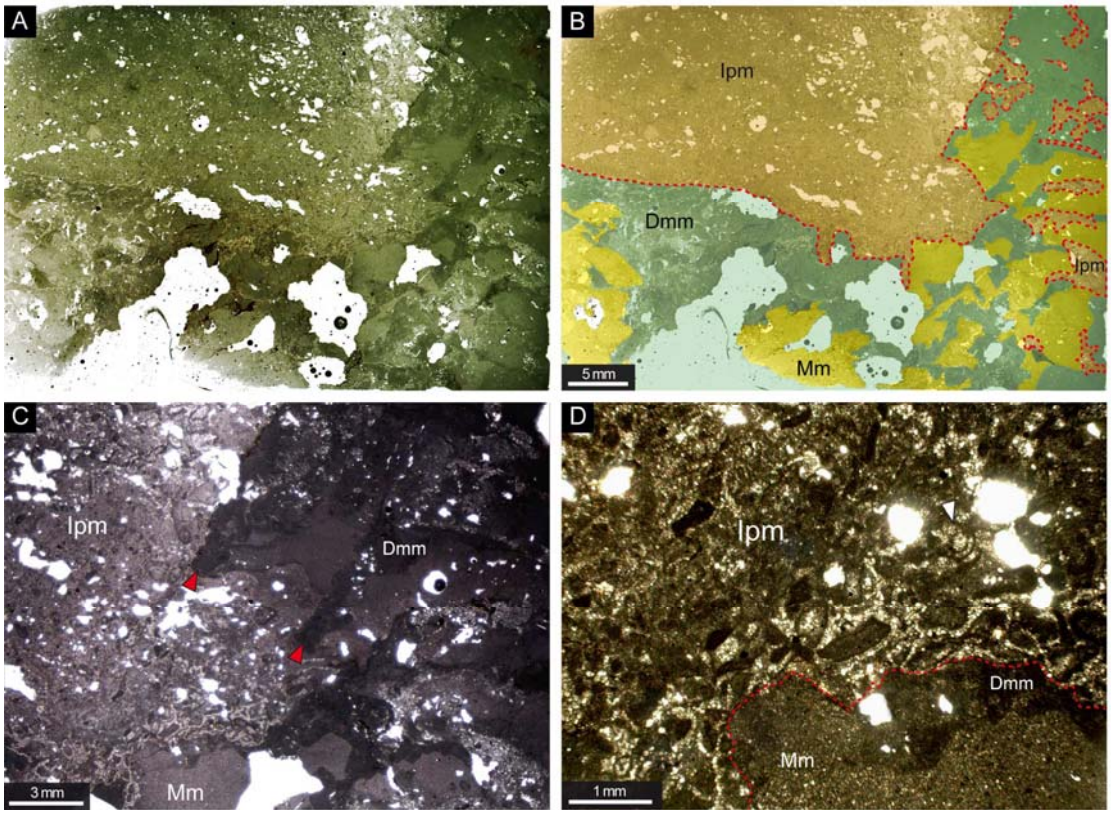

Fig. 3.11. Microfotografías de trombolitos. Ipm = Masas intraclásticas y peloidales; Dmm = *Mesoclots* micríticos densos; Mm = matriz micrítica. A) Textura trombolítica en lámina delgada. B) *Mapping* de los componentes identificados en la lámina delgada en A. Nótese que Ipm se encuentra rellenando las cavidades internas generadas por procesos de corrosión (línea discontinua). Dmm está compuesto por masas microcristalinas densas, masivas y oscuras con formas arborescentes, redondeadas y ameboides. Mm está compuesto por un *mudstone* claro sin estructura que representa el sedimento interno. C) Detalle de la lámina delgada previa. Nótese que Dmm (flechas rojas) está compuesto por masas dolomicríticas peloidales a micropeloidales. Se observa una delgada capa intraclástica en la base del relleno de Ipm. D) Detalle de la lámina delgada previa. Nótese la microdoloesparita a doloesparita neomórfica reemplazando la matriz dolomicrítica alrededor de los intraclastos (centro fotografía). La superfície de corrosión (línea discontinua) afecta a Mm y a Dmm. Los poros rosas se deben a los efectos de la meteorización y a la realización de las láminas delgadas. Tomado de Mercedes-Martín et al. (2013c).

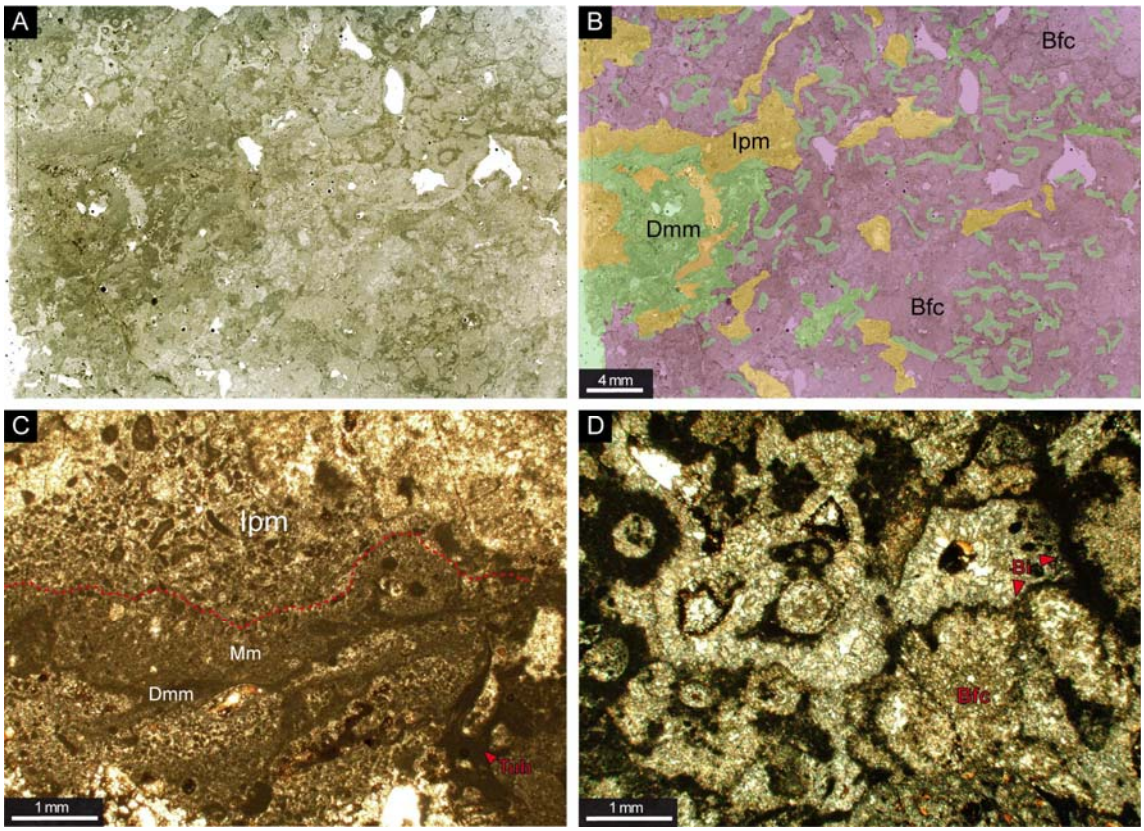

Fig. 3.12. Microfotografías de trombolitos. Ipm = Masas intraclásticas y peloidales; Dmm = *Mesoclots* micríticos densos; Mm = matriz micrítica; Bfc = cementos botroidales y fibrosos; Tub = *Tubiphytes*. A) Textura trombolítica en lámina delgada. B) *Mapping* de los componentes identificados en la lámina delgada en A. Nótese que Bfc es el componente más abundante. C) Dmm aparece en forma de costras dolomicríticas, peloidales a micropeloidales. Las cavidades internas están rellenadas posteriormente con Mm y Ipm. Nótese la presencia de *Tubiphytes* sp. D) Bfc mostrando cementos botroidales incrustados por *biofilms* (Bi) los cuales crecieron sincrónicamente. Los poros se deben a los efectos de la meteorización y a la realización de las láminas delgadas. Tomado de Mercedes-Martín et al. (2013c).

3.3. Estratigrafía secuencial

La calidad y continuidad de los afloramientos estudiados ha permitido reconocer los modelos de apilamiento agradantes, progradantes y retrogradantes de las sucesiones estratigráficas, y en bastantes ocasiones, las geometrías deposicionales de los cuerpos sedimentarios. Asimismo, gracias al reconocimiento de las superficies estratigráficas y de los modelos de apilamiento se pudieron identificar dos grandes secuencias de depósito transgresivo-regresivas (T-R 1 y T-R 2) en el Ladiniense de la Cuenca Triásica Catalana (Mercedes-Martín et al., 2013a) (Fig. 3.13, 3.14). La definición de estas secuencias T-R se basa en los criterios de Embry y Johannessen (1992).

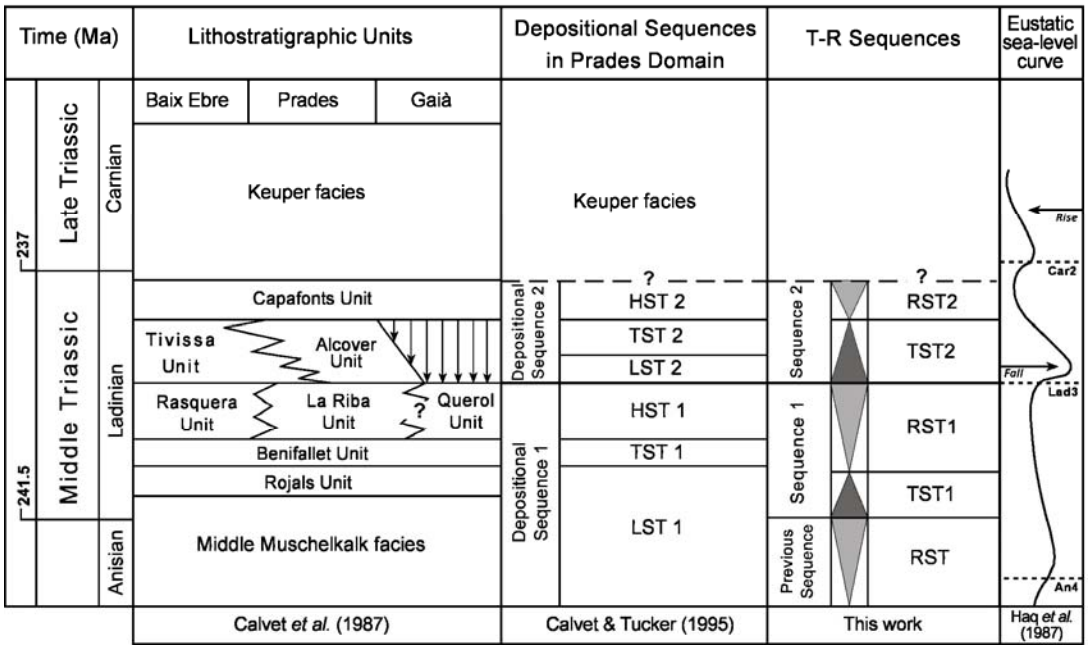

Fig. 3.13. Armazón litostratigráfico de la Cuenca Catalana durante parte del Triásico medio, según los dominios paleogeográficos (modificado de Calvet et al., 1987). Secuencias deposicionales definidas para el dominio de Prades (modificado de Calvet y Tucker, 1995). Secuencias transgresivo-regresivas (T-R) propuestas por Mercedes-Martín et al. (2013a). Curva eustática procedente d Haq et al. (1987) y edades absolutas de Gradstein et al. (2012). Tomado de Mercedes-Martín et al. (2013a).

Las superficies estratigráficas reconocidas han sido: límite basal secuencia T-R1, TS1, MFZ1, límite secuencias T-R1 y 2 (SU), MRZ1, MFZ2 y MRZ2 (Fig. 3.14).

El límite inferior de la secuencia T-R 1 está representado por una superficie transgresiva (TS1) que puede ser correlacionada entre Rasquera y Pontons separando los depósitos regresivos del Muschelkalk medio, de los depósitos marinos someros del Muschelkalk superior. El Muschelkalk medio está integrado por materiales

siliciclásticos y evaporitas que datan del Anisiense-Ladiniense inferior basal. La mencionada TS está fosilizada por tres tipos de facies: 1) estromatolitos dómicos y planares, 2) *grainstone* oolítico y 3) *dolomudstone* finamente laminado a masivo. Esta superficie puede ser identificada en el dominio de Prades y en el de Baix-Ebre-Priorat.

La zona de máxima inundación (MFZ1) marca el final de la transgresión, y puede ser identificada a través del cambio de modelo de apilamiento (*thickening-upwards parasequences* → *single shallowing-upwards parasequences*, en la secuencia T-R1, o bien *deepening phase* → *static shallow-water phase*, en la secuencia T-R 2, según Spence y Tucker, 2007). En la secuencia T-R1 este cambio de patrón de apilamiento se puede observar fácilmente en la parte interna de la rampa (dominio de Gaià) a través de un marcado cambio de facies, pasando de *grainstones* oolíticos (submareales) a estromatolitos dómicos y planares (intermareales). Fueron reconocidas superficies condensadas con superficies endurecidas y bajas tasas de sedimentación (*starvation*) a techo de los bajíos oolíticos en las partes más externas de la rampa interna (sección Miramar, Fig. 3.14). La MFZ2 correspondiente a la secuencia T-R 2 se identifica a través de un claro paso de condiciones transgresivas (*shoals* marinos) a condiciones regresivas (estromatolitos perimareales) en todo el dominio de Gaià.

La MRZ de la secuencia T-R1 (MRZ1) se ha podido trazar en la parte interna de la rampa (dominio de Gaià) entre las secciones Coll Magí y Sta. Perpetua de Gaià. La MRZ1 se identifica a través de un cambio en el tipo de apilamiento estratal (*single shallowing-upwards parasequences* → *thinning-upwards parasequences* según Spence y Tucker, 2007) mientras que la MRZ2 se identifica por un cambio entre los materiales perimareales y las llanuras evaporíticas/sabkhas del Keuper. Algunos depósitos transgresivos (sección de Sta Perpetua de Gaià) onlapan la MRZ1, proporcionando evidencias de la presencia de playas (facies de *grainstones* oolíticos con estratificación cruzada) que retrogradan por encima de los depósitos regresivos previos (facies de estromatolitos dómicos y planares).

La discordancia subaérea (SU) del límite entre las secuencias T-R 1 y 2 es una superficie que se puede reconocer a escala regional, especialmente entre los dominios de Gaià y Prades (Fig. 3.14). Esta discordancia está asociada a una significativa caída del nivel del mar, representando el límite entre las secuencias T-R1 y T-R 2. Está acompañada de disolución y carstificación de los estromatolitos de la rampa interna y de los biostromos microbianos y *mud-mounds* de la rampa media, pertenecientes a la secuencia T-R1. En la sección de Arbolí, la SU se solapa con la TS1, entre el Cortejo Regresivo 1 (*Regressive System Tract 1*, RST1) y el Cortejo Transgresivo 2 (*Transgressive System Tract 2*, TST2) generando una superficie compuesta formada

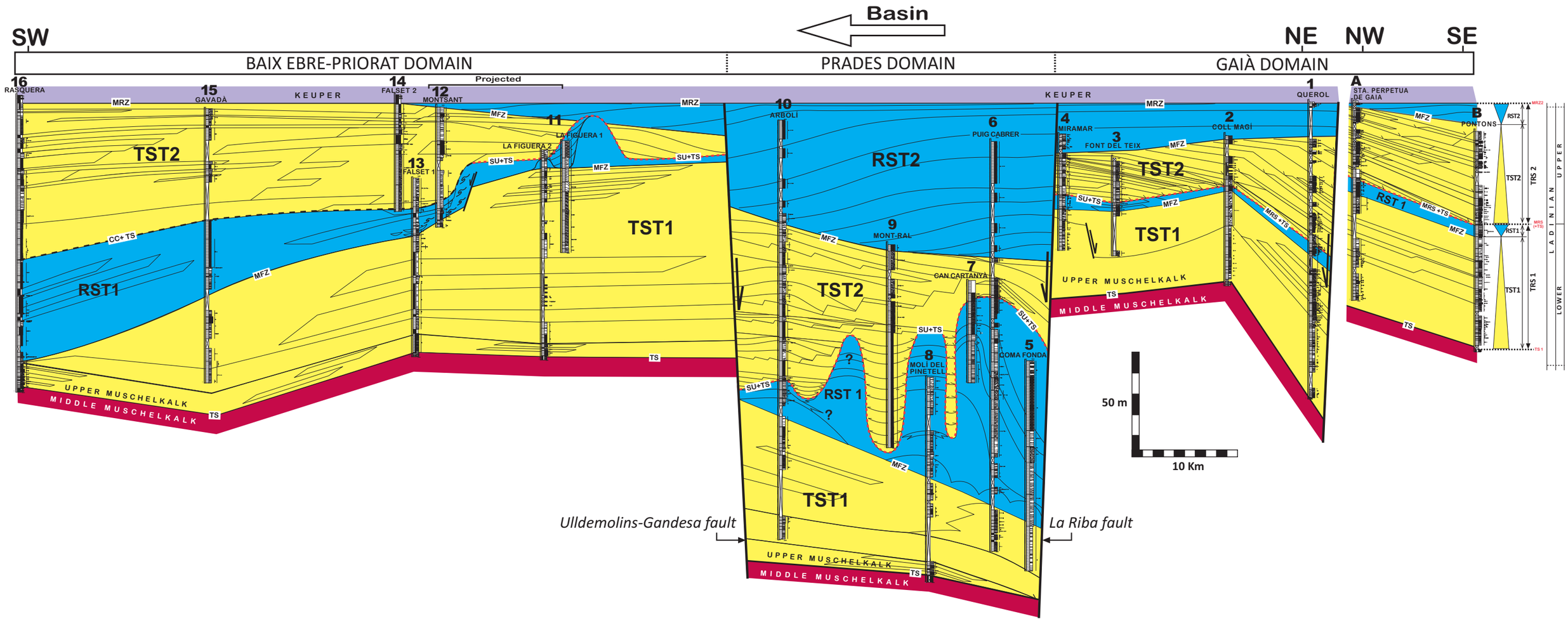

Colour squeme	T-R Sequences	Systems Tracts and Surfaces	Tipology of Surfaces
	Keuper facies	TST: Transgressive Systems Tract	CC/SU
	RST2	RST: Regressive Systems Tract	MRZ
	TST2	CC: Correlative conformity	MRS/TS
	RST1	SU: Subaerial unconformity	MFZ
	TST1	MRS/Z: Maximum Regressive Surface/ Zone	TS
	Middle Muschelkalk facies	TS: Transgressive Surface	
		MFZ: Maximum Flooding Zone	

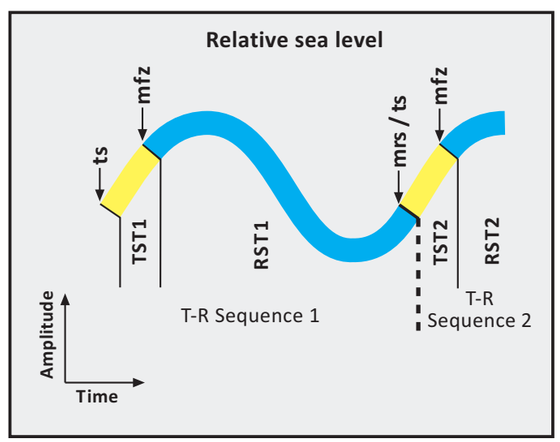

Fig. 3.14. Interpretación de Estratigrafía secuencial a lo largo del perfil de correlación de facies de la Fig. 3.4. Véase la leyenda para más detalles. Se han utilizado las secuencias T-R de Embry y Johannessen (1992). Tomado de Mercedes-Martín et al. (2013a).

por superficies endurecidas y niveles ferruginosos que tapizan la superficie carstificada.

3.4. La caída del nivel del mar durante el Ladiniense

Con el depósito de los materiales regresivos (RST1) de la secuencia T-R 1, el nivel del mar comenzó a descender como refleja la sedimentación de la MRZ1. Como resultado, los materiales de dichos depósitos regresivos, formados por carbonatos microbianos (estromatolitos y *mud-mounds*), quedaron expuestos y ampliamente carstificados, con lo que la factoría de carbonatos microbianos que predominaba en aquel momento cesó (Fig. 3.15). La caída del nivel del mar se estima que fue alrededor de 50 metros. La discordancia subaérea observable entre las secciones de Coll Magí y La Figuera lleva asociadas cavidades de disolución cársticas, brechas de colapso y estructuras en V (*V-structures*) reconocidas ampliamente a lo largo de la cuenca.

Asímismo importantes incisiones erosivas decamétricas (*incised valleys*, valles incisos) se formaron en relación a la caída del nivel de base debida al descenso del nivel del mar en el dominio de Prades. No obstante, no se han podido reconocer evidencias de exposición subaérea con carst en las unidades de estromatolitos de Querol y Pontons (dominio de Gaià) (Fig. 3.15). Este hecho se debe a la subsidencia diferencial de los distintos dominios paleogeográficos junto al posible basculamiento hacia el NE del bloque de Gaià, que permitió que parte de este bloque permaneciese sumergido (Fig. 3.18C). Sin embargo, la parte oeste de este dominio (cerca de la sección de Miramar) permaneció emergida, con lo que resultó subaereamente expuesta y carstificada.

3.5. Evolución de la acomodación y subsidencia

Con la intención de estimar la evolución de la acomodación a lo largo de la cuenca estudiada y para cada secuencia T-R identificada, se elaboró un modelo que tiene en cuenta los espesores obtenidos en cada una de las series estratigráficas. Para este fin, los espesores de las series estratigráficas se proyectaron usando las zonas de máxima inundación (MFZ) como *datum* (Fig. 3.16). Este método es útil porque es independiente del tipo de factoría de carbonatos y de la tasa de sedimentación.

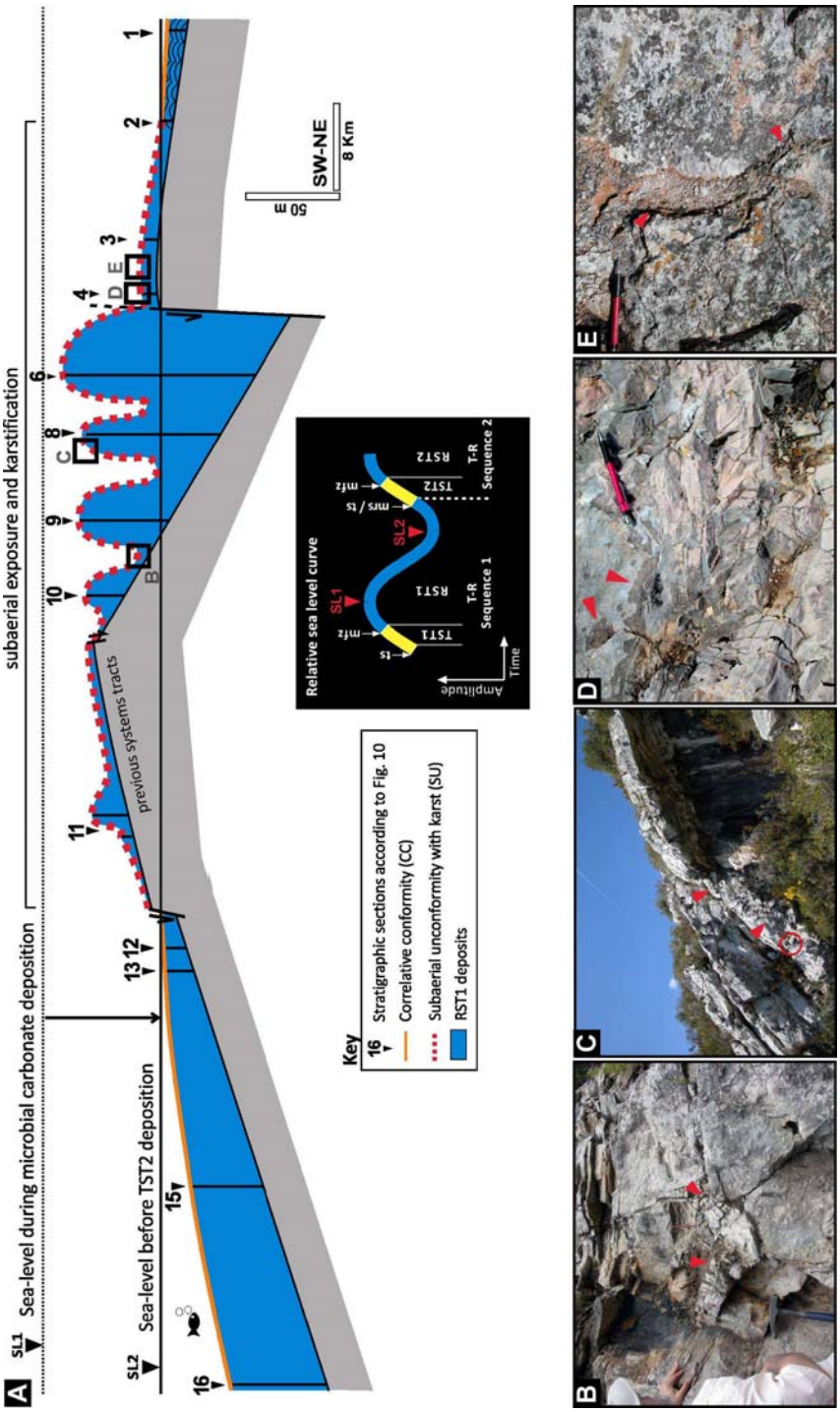

Fig. 3.15. Perfil escalonado de la rampa carbonatada correspondiente a la T-R1, entre Pontons y Rasquera. A) Evolución del nivel del mar entre el comienzo de la caída del nivel del mar (SL1) y el final de la regresión (SL2). Nótese que la significativa caída del nivel del mar generó una extensa área de exposición subarérea que afectó a los dominos de la rampa interna a externa. Los números equivalen a las series estratigráficas de la Fig. 3.4**.** B, C, D y E) Ejemplos de carst asociados a la exposición subarérea, en el límite entre las secuencias T-R 1 y 2. B) Estructuras en V (*v-structures*) a techo de la unidad trombolítica *mud-mound* (flechas rojas). C) Packbrechas mosaico-cementadas (*cemented mosaic packbreccias*, flechas rojas) por encima de los flancos de los *mud-mounds*. Martillo = 32 cm. D) Rellenos de floatbrechas de escombros particulados (*particulate rubble packbreccias,* flechas rojas) presentes en la parte occidental del dominio de Gaià (serie Miramar). Tomado de Mercedes-Martín et al. (2013a). Lápiz = 15 cm

Los resultados muestran una representación gráfica del espacio neto disponible para la sedimentación. El registro sedimentario del TST1 de la secuencia T-R1 no muestra cambios significativos en el espacio de acomodación a lo largo de la cuenca. Las menores acomodaciones fueron registradas cerca de las secciones de Puigcabrer y Molí del Pinetell (dominio de Prades), y también en la sección de Rasquera (dominio de Baix-Ebre-Priorat), sugiriendo que los depocentros estaban mayoritariamente ubicados en los dominios de Prades y Gaià. Por lo tanto, durante el TST1 hubo una evolución uniforme de la acomodación (Fig. 3.16).

Durante el RST1 de la secuencia T-R1 la configuración de la cuenca cambió notablemente. Un importante depocentro, con altos valores de acomodación, se desarrolló en el dominio de Prades entre las secciones de Coma Fonda y Arbolí, mientras que los dominios de Gaià y Baix-Ebre-Priorat experimentaron un menor espacio de acomodación. Una estructura de *semi-graben* controlado por fallas explicaría la heterogeneidad observada en el dominio de Prades. De hecho, la participación de la falla maestra de La Riba, entre Miramar y Coma Fonda, generó una marcada heterogeneidad que repercutió en un incremento notable de la acomodación en esta área. Al mismo tiempo, el dominio de Baix-Ebre-Priorat registró menores variaciones en el espacio de acomodación. Un pequeño cambio en acomodación fue observado entre las secciones de La Figuera y Montsant, proporcionando evidencia sobre la existencia de una fractura en esta región (Fig. 3.16).

Durante el TST2 de la secuencia T-R2, una marcada compartimentalización tuvo lugar en la cuenca, de modo que ésta quedó subdividida en tres dominios sedimentarios coincidentes con los dominios de Gaià, Prades y Baix-Ebre-Priorat. Estas áreas quedaron delimitadas las unas de las otras por dos sistemas de fallas: La Riba y Montsant. Un incremento generalizado de la acomodación se detectó en estas áreas durante el TST2, el cual fue desencadenado por la subsidencia controlada por esas fallas.

La sedimentación del RST2 de la secuencia T-R2 está marcada por una amplia reducción de la acomodación en el dominio de Baix-Ebre-Priorat. La tasa de acomodación en el dominio de Gaià quedó reducida en comparación con el TST2.

Por otra parte, se han realizado cálculos de subsidencia total para tres secciones estratigráficas seleccionadas de las áreas de Pontons, Puigcabrer y Rasquera correspondientes con los tres dominios sedimentarios de la Cuenca Triásica Catalana. Estas tres curvas de subsidencia total, con las respectivas correcciones paleobatimétricas, representan una buena aproximación a la cuantificación de la evolución de la acomodación durante el Triásico en el área de estudio. En líneas generales, las tres curvas de subsidencia total muestran un patrón muy similar a lo

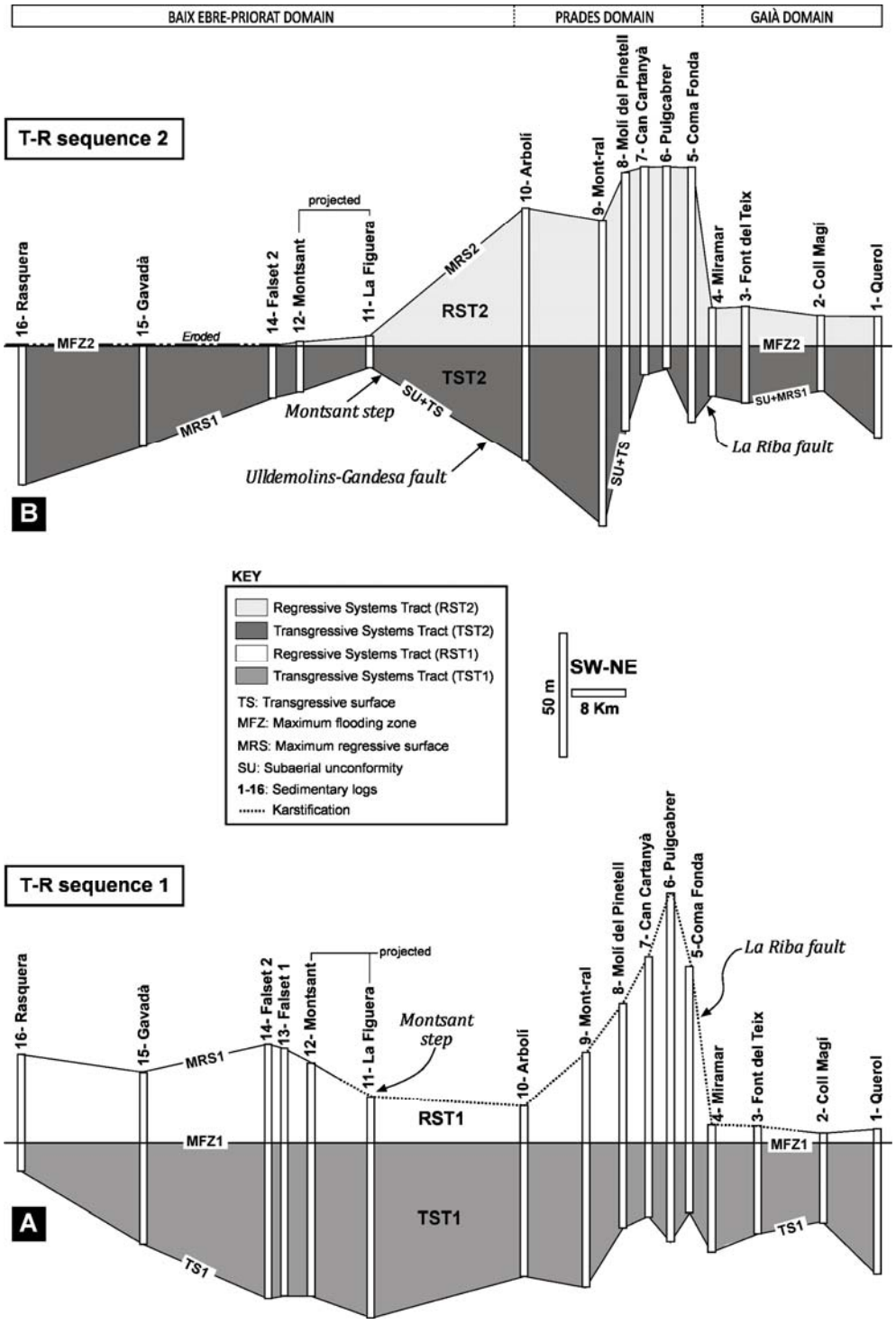

Fig. 3.16. Correlación de espesores estratigráficos entre Querol y Rasquera, considerando la zona de máxima inundación (MFZ) de cada secuencia T-R como *datum*. Las variaciones de acomodación a lo largo de la cuenca se muestran gráficamente. Ver la leyenda para más detalles. A) Variación de la acomodación en la secuencia T-R1. Las principales características son la homogeneidad del registro sedimentario durante el TST1 y el incremento de los espesores en el dominio de Prades durante el RST1. B) Variación de la acomodación de la secuencia T-R2. La heterogénea distribución del registro sedimentario durante el TST2 revela un incremento de la acomodación en los dominios de Prades y Baix Ebre-Priorat. Durante el RST2, el dominio de Prades actuó como un importante depocentro a tenor de los espesores estratigráficos observados en esa área. Tomado de Mercedes-Martín et al. (2013a).

largo del tiempo. En todas las secciones, las curvas muestran un episodio inicial de subsidencia decelerada representada por los sedimentos de la facies Buntsandstein (Olenekiense, 244,8-240,2 Ma). Una fase posterior, caracterizada por un episodio de rápida subsidencia durante el Muschelkalk inferior (Anisiense superior, 240,2-237,1 Ma) se observó en todas las secciones estratigráficas. El intervalo del Muschelkalk medio está representado por un estadio de subsidencia decelerada (237,1-233 Ma). Durante la sedimentación del Muschelkalk superior (Ladiniense, 233-227,4 Ma) la subsidencia total alcanzó 470 m. Este periodo está caracterizado por una reanudación de la subsidencia rápida, la cual fue especialmente elevada en el dominio de Prades.

En este dominio, el desarrollo de un *semi-graben* controlado por fallas está ligado a esta etapa de subsidencia rápida que controló el depósito de las facies del Muschelkalk superior. Sin embargo, durante el Carniense y el Noriense (233-209,6 Ma), facies Keuper, una significativa deceleración de la subsidencia se registró en todas las secciones y dominios analizados. Finalmente, durante el Rhaetiense (209,6-205,7 Ma) tuvo lugar el evento de subsidencia con mayor deceleración en la Cuenca Triásica Catalana, dando lugar al depósito de carbonatos marinos someros de la Fm. Imón (Arnal et al., 2002).

Todas las curvas muestran una tendencia similar con dos partes bien diferenciadas de subsidencia total rápida/decelerada (R/D) representando dos pulsos discretos rift/postrift a lo largo del estadio de rifting que aconteció durante todo el Triásico (Fig. 3.17). El primer pulso (R/D1) se define por una subsidencia sinrift rápida entre 244,8 y 237,1 Ma incluyendo las facies Buntsandstein y el Muschelkalk inferior y una subsidencia postrift decelerada, que incluye los depósitos del Muschelkalk medio (237,1 – 233 Ma). El segundo pulso (R/D2) está también caracterizado por una subsidencia sinrift rápida desde 233 a 227,4 Ma, correspondiente con el depósito de las facies Muschelkalk superior, y por una etapa de subsidencia postrift decelerada desde 227,4 a 205,7 Ma, coincidiendo con la facies Keuper y Fm. Imon.

Los rápidos pulsos de subsidencia total sinrift se corresponden con los principales periodos extensivos con actividad de fallas y reactivación de bloques basculados, procesos que produjeron ganancias de acomodación. Los pulsos lentos de subsidencia postrift indican periodos locales de reequilibrio térmico, por enfriamiento lento de la corteza previamente calentada durante las fases de fractura anteriores (McKenzie, 1978; Salas et al., 2001), que ocasionaron pérdidas de acomodación. Los resultados obtenidos en este trabajo están en consonancia con los modernos análisis cuantitativos de subsidencia llevamos a cabo por Vargas (2002) y Vargas et al. (2009) para los depósitos Triásicos de las regiones de la

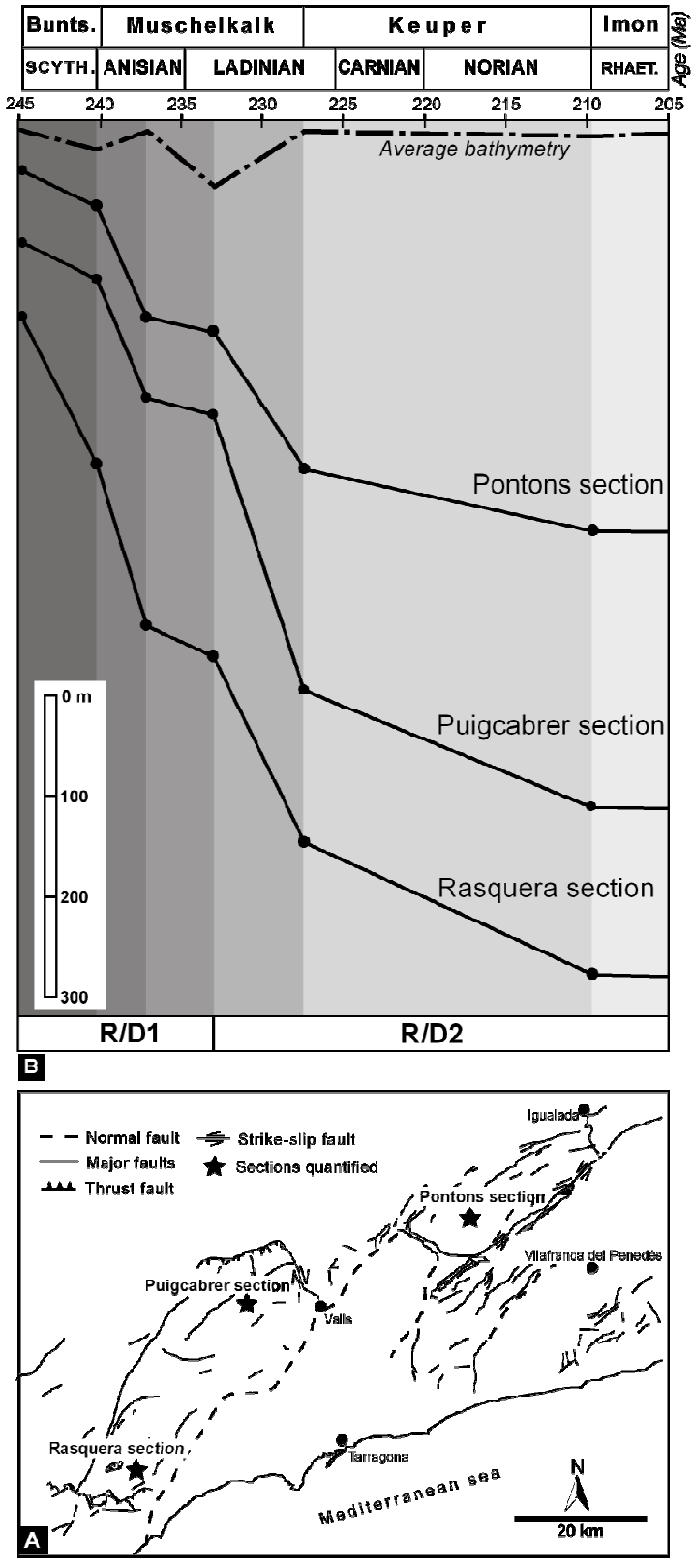

Fig. 3.17. A) Mapa tectónico esquemático de la Cuenca Catalana mostrando la ubicación de las principales series estratigráficas empleadas para los análisis de subsidencia cuantitativos. B) Curvas de subsidencia total descompactadas y corregidas por paleobatimetría representando la acomodación total. La curva de paleobatimetría media ha quedado reflejada en la parte alta. Edades absolutas de Gradstein et al. (1994). R/D1 y R/D2: estadios de subsidencia total rápida/ decelerada. Tomado de Mercedes-Martín et al. (2013a).

Cuenca Ibérica y Cuenca del Ebro. Tres fases sinrift y dos estadios postrift fueron identificados en la Cuenca del Ebro. En la parte oriental de la Cuenca del Ebro, la subsidencia del zócalo Triásico en los sondeos Monzón-1 y Lérida-1 (Vargas et al., 2009) presenta una gran similitud con la del Triásico de la Cuenca Catalana. En estos sondeos, fueron registrados hasta dos periodos de subsidencia rápida (Olenekiense-Anisiense medio y Anisiense superior-Carniense inferior), y también fueron descritos dos estadios de subsidencia decelerada (Anisiense medio-Anisiense superior y Carniense medio-Noriense superior) (Vargas et al., 2009).

Calvet et al. (1990) también calcularon las tasas de sedimentación usando curvas de subsidencia descompactadas (subsidencia total) para el periodo Triásico (Fig. 2.5). Sin embargo, según estos autores, tuvieron lugar dos fases de extensión, cada una de ellas seguida de un estadio de subsidencia regional. La primera fase permitió el depósito de las facies Buntsandstein (sinrift) y Muschelkalk inferior (postrift). La segunda fase permitió la sedimentación del Muschelkalk medio (sinrift) y del Muschelkalk superior (postrift). Esta interpretación sugería que las facies clásticas se sedimentaron durante periodos sinrift, mientras que las carbonatadas lo hicieron durante etapas postrift (subsidencia regional). No obstante, hay que señalar que la curva de subsidencia de Calvet et al. (1990) puso de manifiesto la existencia de un pequeño segmento de subsidencia rápida en el comienzo de las etapas de sedimentación carbonatada, Muschelkalk inferior y superior.

3.6. Arquitectura estratigráfica

La distribución de facies en el tiempo y el espacio, es decir la arquitectura estratigráfica, está controlada por la evolución geotectónica de la cuenca sedimentaria, el tipo y tasa de producción de carbonato y el lugar preferencial de depósito.

La evolución de la arquitectura estratigráfica ha sido dividida en cinco estadios sucesivos. Cada estadio está caracterizado por la presencia de facies concretas en cada dominio sedimentario dentro de la rampa (zona interna, media y externa) por el resultado de la caída del nivel del mar del Ladiniense superior. La Figura 3.18 representa el modelo conceptual 3D (2D dimensional+1D temporal) que muestra los cinco estadios evolutivos de la arquitectura estratigráfica durante el Ladiniense (Mercedes-Martín et al. 2013b)

3.6.1. Primer estadio transgresivo (TST1)

El primer estadio transgresivo se corresponde con la primera transgresión ladiniense por encima de las facies clásticas y capas rojas (*red beds*) del Muschelkalk medio, denominado TST1 (Fig.3.18A)

Durante el primer pulso de este estadio, extensos depósitos se acumularon en la rampa interna, la cual estaba localizada entre Miramar y Rasquera. Estos depósitos se formaron en llanuras mareales carbonatadas compuestas de abundantes estromatolitos planares (facies F10) los cuales se hallaban adyacentes a bajíos oolíticos de pequeña envergadura (facies F1). En este momento, no se registraron ambientes de rampa media o externa en la zona de estudio.

El segundo pulso de este estadio estaba caracterizado por el desarrollo de extensos ambientes de llanuras submareales fangosas, entre Miramar y Rasquera (rampa media y externa), y de *lagoons* submareales-intermareales protegidos, entre Miramar y Pontons (rampa interna). En estos ambientes se formaron facies de *mudstones* y *wackestones* bioclásticos intensamente bioturbados (facies F7), y separados por pequeños bancos formados por *wackestones* y *packtones* bioclásticos y peloidales.

El último pulso del primer estadio transgresivo estuvo dominado por la sedimentación de extensos bajíos oolíticos submareales (facies F1) en la rampa interna (Miramar a Pontons) y por ambientes submareales profundos caracterizados por *mudstones* y *packstones* bioturbados con margas intercaladas (facies F8) en la rampa externa (Miramar a Rasquera). El desarrollo coetáneo de la falla de La Riba jugó un papel muy importante en la disposición de ambientes durante este estadio transgresivo, distribución de facies y espesores de cuerpos sedimentarios.

3.6.2. Amplio desarrollo de los sistemas microbianos (RST1)

Las parasecuencias del RST1 mostraron una tendencia somerizante y unos patrones de apilamiento agradantes y progradantes. Durante el RST1, los carbonatos microbianos fueron las factorías de carbonatos más comunes a lo largo de los ambientes de rampa interna a media-externa: estromatolitos dómicos y planares (facies F10) se desarrollaron en condiciones hipersalinas en la rampa interna, mientras que importantes depósitos de biostromos microbianos y *mud-mounds* (facies F12) se formaron en condiciones de mar abierto a restringidas en la rampa media-externa. La subsidencia sinrift inducida por fallas favoreció la compartimentalización del dominio de Prades generando un importante depocentro en esta región Fig. 3.18B. Como

resultado, se registró una gran heterogeneidad en los espesores en este dominio. Una gran diversidad de facies (*boundstones* de calcimicrobios, facies F13; *boundstones* de corales y microbios; facies F14 y *packstones* y *rudstones* de dasicladáceas; facies F16) tapizaron localmente los biostromos microbianos y los *mud-mounds*. Además, se encuentran depósitos de talud progradantes adjacentes a los flancos de los biostromos y *mud-mounds*, los cuales indicaban la presencia de un considerable depocentro en la parte oriental del dominio de Prades, como consecuencia de la participación de la falla de La Riba. Por otro lado, en la parte más occidental del dominio de Prades se registraron extensivos cinturones de facies con geometrías tabulares y un apilamiento agradante. Durante este estadio, el ambiente de rampa externa estaba situado en el dominio de Baix Ebre-Priorat. Alrededor de la sección de Montsant, un escarpe con buzamiento hacia el SO se desarrolló coetáneamente con el depósito de *mudstones* y *packstones* bioturbados (facies F6) el cual se extendió hacia cuenca.

3.6.3. Caída del nivel del mar

Una caída del nivel del mar de al menos 50 m, mantuvo el dominio de Gaià y de Prades expuesto subaéreamente y sometido a carstificación. El resultado fue una superficie incidida que representa una discontinuidad (Fig.3.18C). En este momento, varias áreas en los dominios de Gaià, Prades y Baix Ebre-Priorat se convirtieron en importantes depocentros para el depósito de carbonatos, mientras que en otros predominó la disolución y desmantelamiento de los carbonatos previos. No existen evidencias de exposición subaérea en la parte meridional del dominio de Gaià, lo que sugiere que los bloques estaban basculados hacia el NE (Mercedes-Martín et al. 2013a).

3.6.4. Amplio desarrollo de *lagoons* protegidos y bajíos (TST2)

Durante el TST2, los *wackestones* y *packstones* bioturbados (facies F5) se acumularon como facies de mar abierto, en un ambiente de rampa externa proximal (Falset y Rasquera). Por su parte, el ambiente de rampa media estaba constituido por bajíos externos (Falset a Montsant) que dieron lugar a grandes espesores de *grainstones* (facies F1) y extensos *lagoons* protegidos (Montsant a Coll Magí) Estos depósitos conforman parasecuencias grano y estrato decrecientes. Además, los ambientes de rampa interna y media (dominio de Gaià, desde Coll Magí a Pontons),

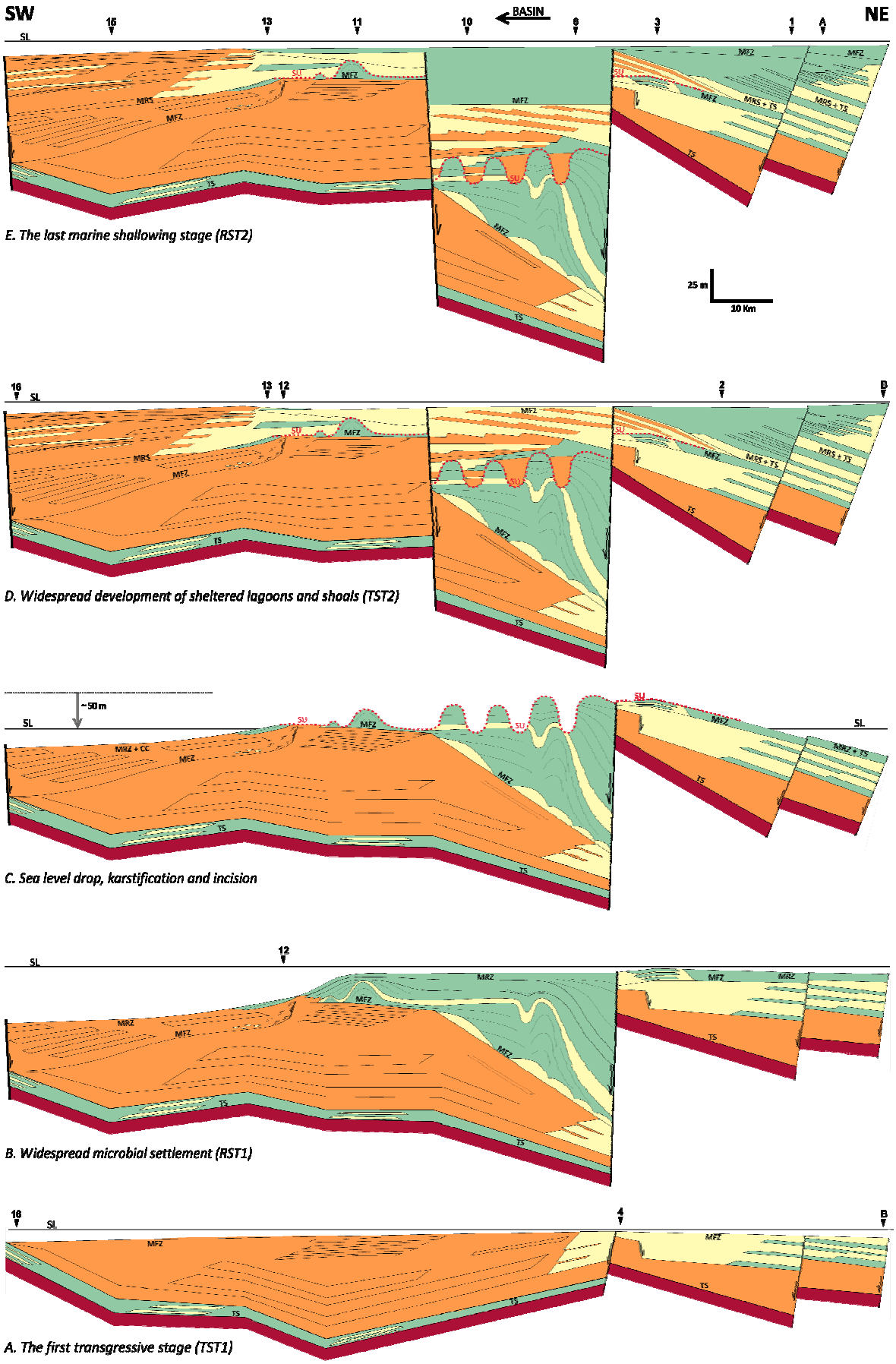
SW
NE
BASIN
SL
MFZ
MRS
TS
SU
MRS + TS
25 m
10 Km
~50 m
MRZ + CC
MRZ
E. The last marine shallowing stage (RST2)
D. Widespread development of sheltered lagoons and shoals (TST2)
C. Sea level drop, karstification and incision
B. Widespread microbial settlement (RST1)
A. The first transgressive stage (TST1)

formados por facies de *floatstones* y *grainstones* oncolíticos y oolíticos (facies F4). estaban formados por bajíos internos dominados en este momento por calcarenitas con laminación cruzada y *grainstones* oolíticos (facies F1 y F2) así como también por *fore-shoals* internos, los cuales estaban caracterizados por amplios cinturones de estromatolitos oolítico-peloidales (facies F11) (Fig. 3.18D)

3.6.5. El último estadio somerizante marino (RST2)

Los depósitos de este periodo (RST2) estuvieron ampliamente representados en el dominio de Prades y Gaià. Importantes y heterogéneos espesores de *packstones* laminados de oncoides (facies F15) rellenaron la cuenca desde Pontons a Montsant (Fig.3.18E). Estos materiales se depositaron en un ambiente de rampa interna en forma de llanuras supramareales e intermareales, dando lugar a parasecuencias agradantes y progradantes. La falla de Ulldemolins-Gandesa y La Riba desempeñaron un papel predominante en la configuración de este depocentro sedimentario donde se acumularon depósitos someros.

3.7. Modelos deposicionales

El complejo sinrift de plataformas carbonatadas del Ladiniense de la Cuenca Triásica Catalana estaba constituido por dos tipos de rampas carbonatadas (sistema de rampa inferior y superior) correspondientes a las secuencias T-R 1 y T-R2 (Mercedes-Martín et al., 2013b). El reconocimiento preciso de las fracturas extensivas regionales sinsedimentarias y su delimitación espacial y temporal ha resultado ser un factor esencial para la reconstrucción de los modelos deposicionales así como para

Fig. 3.18. Evolución de la arquitectura sedimentaria durante el Ladiniense de la Cuenca Triásica Catalana. A) El primer estadio transgresivo (TST1) dio lugar a una rampa carbonatada homoclinal y posteriormente a una rampa carbonatada de bloques fracturados dominada por oleaje. B) El RST1 correspondió a un evento de proliferación microbiana de estromatolitos y trombolitos durante un periodo de remarcable subsidencia sinrift. Durante este periodo se desarrolló una rampa carbonatada de bloques fracturados dominada por microbios. C) Una considerable caída del nivel del mar de al menos 50 m. generó una incisión erosiva y carstificación de la plataforma. D) Durante el TST2 se desarrollan *lagoons* protegidos y bajíos dando lugar a una rampa carbonatada de bloques fracturados dominada por bancos-barrera. E) El último pulso regresivo (RST2) correspondió a un periodo de deposición extensiva de carbonatos perimareales y el desarrollo de rampa de aguas somera. Los números representan las secciones estratigráficas. Tomado de Mercedes-Martín et al. (2013b).←

delimitar los valores de subsidencia-acomodación de cada dominio (Fig. 3.18, 3.19). El modelo de rampa inferior, correspondiente a la secuencia T-R1 (Ladiniense inferior) ha sido interpretado como una rampa controlada por bloques fracturados (*fault-block ramp*). El estadio TST1 estuvo definido por dos pulsos sedimentarios y un RST1 formado por un pulso sedimentario. El primer estadio del TST1 estuvo mayor-mente caracterizado por un evento de colonización de carbonatos microbianos por encima del intervalo siliciclástico y evaporítico de la facies Muschelkalk medio, dando lugar a un perfil sedimentario de rampa homoclinal (*homoclinal ramp*). El segundo estadio del TST1 estuvo formado por facies fangosas, especialmente la rampa media y externa y por depósitos tabulares de facies

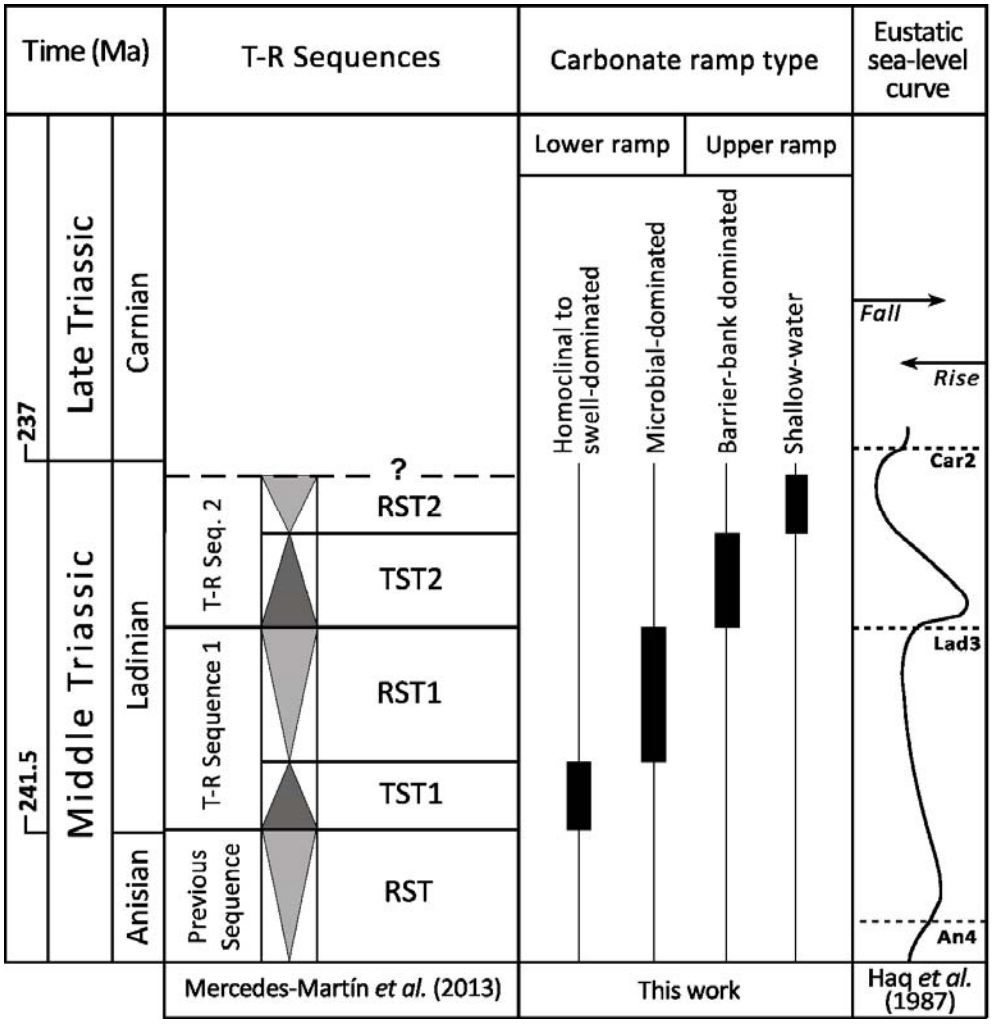

Fig. 3.19. Tipos de rampas carbonatadas desarrolladas en la Cuenca Triásica Catalana (Triásico medio) y su armazón de estratigrafía secuencial. Las edades absolutas fueron tiomadas de Gradstein et al., (2012) y la curva eustática de Haq et al., (1987). Tomado de Mercedes-Martín et al. (2013b)

de grano grueso en la rampa interna. Para este segundo estadio del TST1 se ha inferido un perfil deposicional del tipo rampa de bloques fracturados dominada por oleaje (*swell-dominated fault-block ramp*) (Fig.3.19)

La actividad de fallas sinsedimentarias en el dominio de Gaià causada por la falla de La Riba, modificaron la fisiografía de la cuenca creando áreas subsidentes que generaron ambientes sedimentarios específicos durante el TST1. El RST1 contenía los depósitos microbianos más prominentes, como estromatolitos en la rampa interna (hasta 10 m de espesor) y trombolitos en la rampa media (hasta 40 m de espesor). Durante este estadio, el dominio de Prades se convirtió en una importante área subsidente donde potentes espesores de unidades trombolíticas (*mud-mound* y biostromos microbianos) se acumularon gracias al aumento del espacio de acomodación generado por la falla de La Riba. Además, el dominio de Gaià experimentó unas ganancias menores de acomodación lo cual permitió que en la rampa interna se desarrollasen al mismo tiempo estromatolitos planares y dómicos. El modelo deposicional para este estadio correspondía a una rampa de bloques fracturados dominada dominada por microbios (*microbial-dominated fault-block ramp*) (Fig.3.19).

El modelo de rampa superior, correspondiente a la secuencia T-R2 (Ladiniense superior) también representa una rampa de bloques fracturados (*fault-block ramp*) controlada por las fallas de Ulldemolins-Gandesa y La Riba. El TST2 estuvo caracterizado por un amplio desarrollo de *lagoons* protegidos y bajíos internos y externos, mostrando una gran continuidad de facies (más de 140 Km a lo largo de la cuenca), desde la rampa interna a la media-externa. La actividad prolongada de las fallas de Ulldemolins-Gandesa y La Riba permitió al dominio de Prades mantener su carácter subsidente y acomodar decenas de metros de depósitos carbonatados. *Grainstones* y *floatstones* oncolíticos-oolíticos se formaron en los *lagoons* protegidos de estos emplazamientos. Además, enormes estromatolitos oolíticos se depositaron en la rampa interna en ambientes de *fore-shoals* internos. En el dominio de Gaià se registraron espesores variables como consecuencia de la actuación de la falla de Sta. Perpetua de Gaià. El modelo deposicional corresponde a una rampa de bloques fracturados dominada por bancos barrera (*barrier-bank dominated fault-block ramp*). El RST2 estuvo exclusivamente formado por *packstones* laminados de oncoides y peloides que fueron depositados en extensas llanuras perimareales ocupando más de 100Km de la rampa interna y media. Durante este estadio, las fallas de Ulldemolins-Gandesa y La Riba estuvieron activas, generando una considerable cantidad de espacio de acomodación que fue rellenado por depósitos somerizantes. El modelo

sedimentario correspondería con una rampa de bloques fracturados de agua somera (*shallow-water fault-block ramp*). (Fig.3.19).

3.8. Distribución 2D de la porosidad en los microbialitos

Las muestras de microbialitos, pertenecientes a las facies F10, F11, F12 y F15, se analizaron para conocer el tipo de porosidad y sus porcentajes modales. En láminas delgadas la porosidad antigua aparece ocluida por cementos esparíticos de calcita y menos frecuentemente por cemento s de cuarzo. Gran parte de la porosidad presente en las muestras (más del 20%) tiene un origen reciente debido al afloramiento o a la manipulación mecánica de las muestras. Esta porosidad no se tuvo en cuenta para las estimaciones. Los valores de porosidad cementada se estimaron mediante la observación y contaje de los poros ocluidos con el microscopio petrográfico (Fig. 3.20, 3.21, Tabla 5).

El TST1 registró una abundante presencia de estromatolitos (facies F10) a lo largo de toda la plataforma. Este cortejo sedimentario representó el evento microbiano más extendido y homogéneo, que dio lugar a microbialitos estratiformes (tipo 1), los cuales contienen porosidades modales de hasta el 10%. El RST1 estuvo constituido por mayores espesores de microbialitos y un espectro de morfologías más amplio: estromatolitos (facies F10) en el dominio de Gaià y trombolitos (facies F12) en el dominio de Prades. La media de porosidad modal oscila entre el 5 y el 20%.

Durante el TST2, los estromatolitos oolítico-peloidales (facies F11) en el dominio de Gaià y los depósitos microbianos correspondientes a las facies F15 en el dominio de Prades, presentan una porosidad que oscila entre el 10 y el 15%. Durante el RST2 se formaron los mayores espesores de carbonatos microbianos (facies F15) que estuvieron distribuidos a lo largo de todos los dominios sedimentarios. La porosidad modal puede alcanzar hasta el 15% (Mercedes-Martín et al., 2013b).

3.8.1. Porosidad en los estromatolitos dómicos y planares (facies F10)

Este tipo de estromatolitos generó una porosidad interlaminar y vacuolar (*vuggy*). La primera pudo evolucionar a la segunda por procesos de disolución tardíos. Los valores de porosidad modal llegan hasta el 10%. Estos poros consisten en cavidades alargadas aisladas de tamaños milimétricos (entre 1 y 3 mm), distribuidas de forma paralela a la laminación estromatolítica. Algunos horizontes con abundante porosidad

pueden estar rodeados de zonas carbonatadas con total ausencia de macroporosidad (Fig. 3.20, Tabla 5).

Esta porosidad se interpreta, en algunos casos, como los lugares que ocuparon los tapices microbianos en donde algunos cuerpos bacterianos (p. ej. de tamaño milimétrico como *Cayeuxia*) más tarde se degradaron y fueron rellenados por cementos de calcita y microesparita.

Por otro lado, la porosidad vacuolar (*vuggy*), consiste en cavidades subesféricas, irregularmente alargadas y de tamaños milimétricos (entre 5 y 10mm) desarrolladas en disposición subparalela a la laminación y ocasionalmente cortándola. Los procesos de disolución pudieron empezar en cavidades interlaminares y posteriormente ser ocluidas por cemento calcítico *blocky*.

3.8.2. Porosidad en los estromatolitos oolítico-peloidales (facies F11)

La porosidad de estos microbialitos incluye los tipos vacuolar y móldica. Ambos tipos consisten en poros y cavidades de tamaños milimétricos a submilimétricos. La porosidad vacuolar alcanza unos valores modales de 15%, mientras que la porosidad móldica puede alcanzar el 20% (Fig. 3.21, Tabla 5). La porosidad vacuolar consiste en cavidades milimétricas (de hasta 5 mm de ancho) de formas irregulares, dendríticas y subangulares desarrolladas preferencialmente en los niveles de *grainstones*. Este fenómeno sugiere que los procesos de disolución tuvieron lugar antes de la cementación de dichas cavidades.

La porosidad móldica está ampliamente distribuida en los horizontes de *grainstones* de oolitos y peloides. Esta porosidad fábrica-selectiva afecta a ooides, oncoides, peloides y otros litoclastos generando una conectividad entre los poros de baja a moderada (con diámetros de hasta 1mm). La porosidad móldica no está actualmente cerrada por cementos calcíticos, aunque a menudo presente cementos calcíticos *rim* relictos, sugiriendo la existencia de procesos de disolución tardíos.

3.8.3. Porosidad en los trombolitos (facies F12)

Los trombolitos contienen usualmente porosidad vacuolar (*vuggy*) la cual se encuentra rellena de cementos calcíticos o de cristales euhedrales de cuarzo. Esta porosidad móldica es secundaria debido a que su origen se produjo a través del reemplazamiento de dolomía por minerales evaporíticos (anhidrita o yeso) tal y como advirtieron Tucker y Marshall (2004). Dependiendo de la eficacia del reemplazo mineral, algunas vacuolas se encuentran parcialmente abiertas y pueden resultar

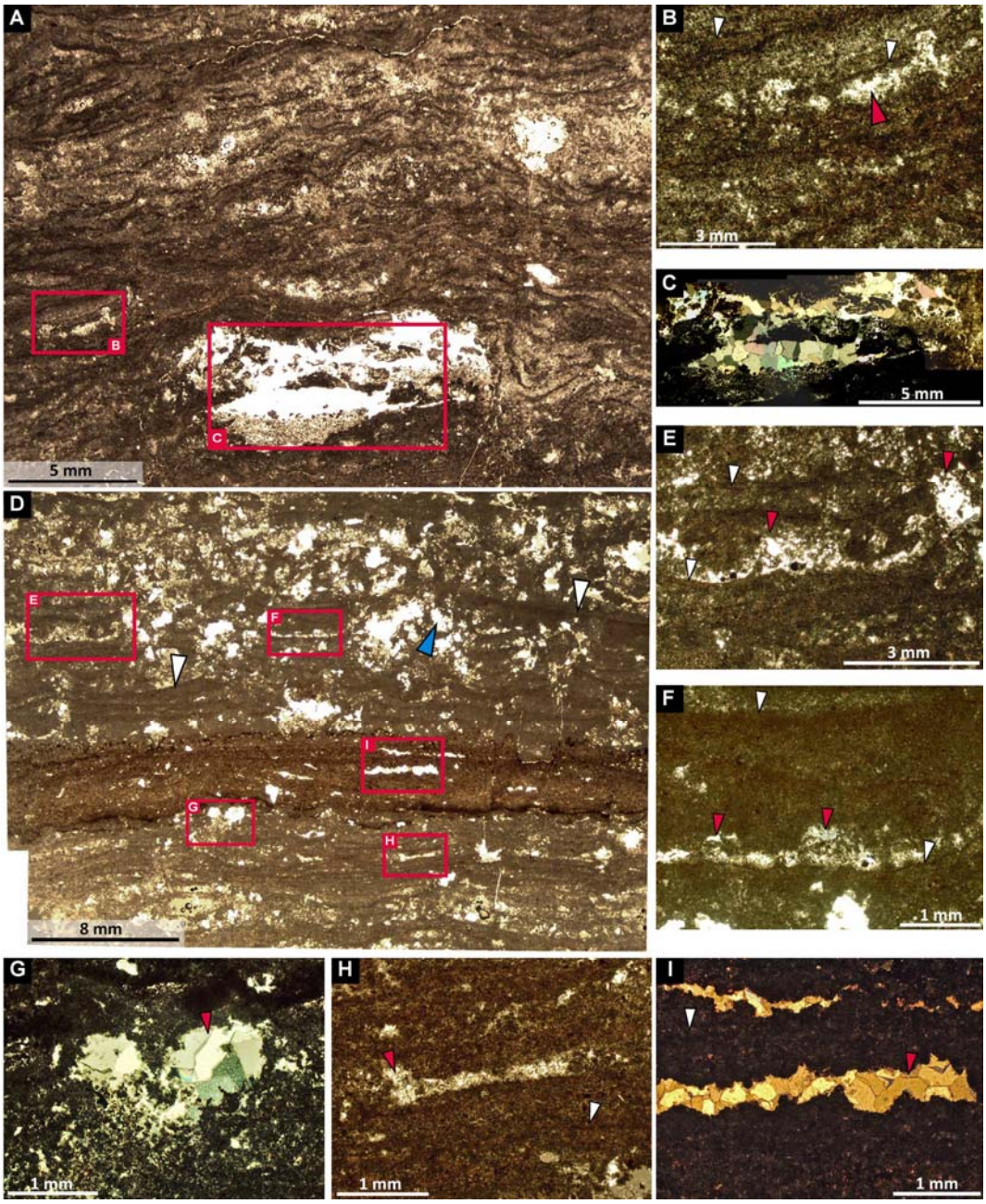

Fig. 3.20. Microfotografías exhibiendo ejemplos de porosidad antigua ocluida por cementos de calcita en los estromatolitos planares y dómicos (facies F10). A) Textura laminada mostrando diferentes tipos de poros y cavidades. Nótense las láminas microbianas onduladas y continuas. B) Poros interlaminares cementados (flecha roja) siguiendo la laminación microbiana (flecha blanca). Luz polarizada. C) Porosidad vacuolar rellenada de cementos calcíticos de tipo *blocky* y granular. Luz polarizada. D) Laminaciones microbianas exhibiendo algunos ejemplos de porosidades. Nótense las láminas subparalelas (flechas blancas). E) Poros interlaminares dentro de la textura laminada (flechas blancas) mostrando una morfología convexa asociada con antiguos emplazamientos de crecimiento microbiano (flechas rojas). Luz polarizada. F) Algunos poros interlaminares rellenos de esparita (flechas rojas) estuvieron aparentemente ocupados por calcimicrobios y tapices microbianos, los cuales definen una textura laminar (flechas blancas). Luz polarizada. G) Poros interlaminares cementados (flecha roja) se desarrollaron debajo de las láminas onduladas. (H, I) Poros interlaminares elongados (flecha roja) se desarrollaron paralelos a la laminación (flecha blanca) y fueron rellenados posteriormente con cementos calcíticos *blocky*. Luz polarizada. Tomado de Mercedes-Martín et al. (2013b).

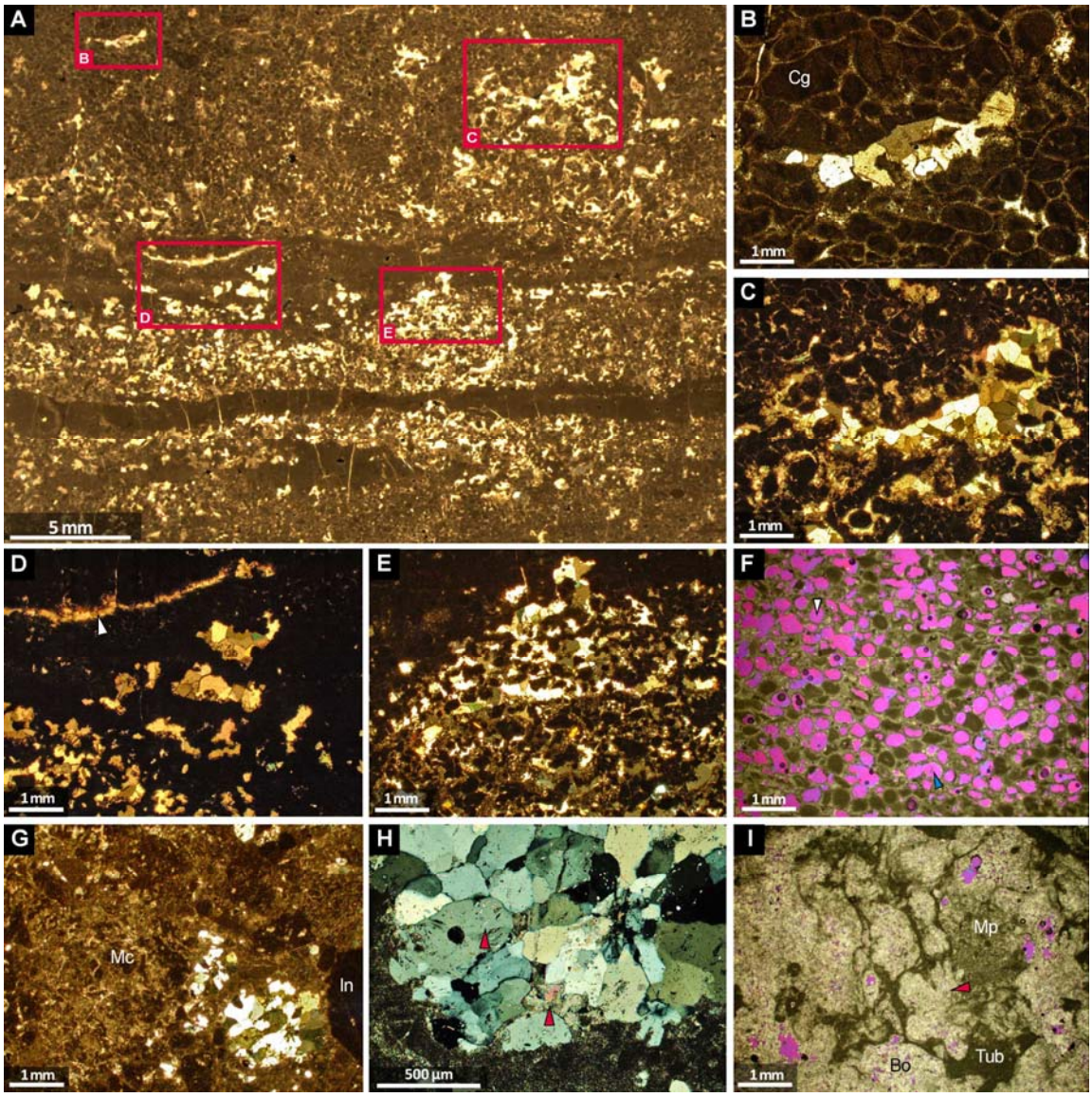

Fig. 3.21. Microfotografías exhibiendo ejemplos de porosidad antigua ocluida por cementos *blocky* de calcita en los estromatolitos oolítico-peloidales (facies F11) y en trombolitos (facies F12). A) Lámina delgada mostrando la alternancia de capas de *grainstone* y capas de *mudstone* en las facies F11. Luz polarizada. B) Porosidad vacuolar ocluida por cementos calcíticos esparíticos. Nótense los cementos alrededor de los granos agregados (Cg). Luz polarizada. C) Porosidad vacuolar en los intervalos de *grainstones*. D) Porosidad vacuolar desarrollada dentro de los intervalos de *mudstones* y rellenada por cementos esparíticos. Nótense las cavidades fenestrales subparalelas y elongadas (flecha blanca). Luz polarizada. E) Porosidad vacuolar en los intervalos de *grainstone*. Una porosidad inicial intergranular mejorada por un lixiviado (*leaching*) selectivo puede haber originado la porosidad vacuolar, la cual se encuentra ocluida por cementos esparíticos. Luz polarizada. F) Porosidad móldica abundante (flechas blancas) afectando a ooides y peloides. Nótese la porosidad vacuolar interconectada que se genera a partir de una porosidad móldica previa. G) Trombolitos formados por costras de Microproblematica (Mc) e intraclastos (In), mostrando porosidad ocluida (masas blancas). H) Cavidad en trombolito cementada por cuarzo con presencia de minúsculas inclusiones de anhidrita (flechas rojas). I) Trombolito con abundante presencia de cementos botroidales (Bo) rodeados de costras de *Tubiphytes* (Tub) y masas micropeloidales (Mp). El color rosa indica la porosidad reciente. Tomado de Mercedes-Martín et al. (2013b).

Facies	Dimensions	Structure	Morphotypes	Depositional environment and constraints	Systems Tracts	Porosity types/ values
F10 Planar and domal stromatolites	at least 20 km wide at least 7 m thick	laminated	Type 1 Biostromes (stratiform) Type 2 Biostromes (head-shaped)	Restricted to hypersaline Attached to coarse-grained substrates Associated to marine flooding surfaces Moderate energy conditions	TST1 RST1 TST2	Interlaminar voids Ancient vuggy up to 10%
F11 Ooidal-peloidal stromatolites	at least 40 km wide at least 3 m thick	laminated	Stratiform geometries Low-relief hemi-elliptical	Semi-restricted to open-marine Attached to coarse-grained substrates Associated to transgressive surfaces Moderate to high energy conditions	TST2	Ancient vuggy up to 15% Mouldic (grain dissolution) up to 20%
F12 Microbial-peloidal thrombolites	at least 45 km wide at least 40 m thick	thrombolitic	Type 1 Biostromal thrombolites Type 2 Mud-mound thrombolites	Semi-restricted to open-marine Attached to coarse-grained substrates Associated to marine flooding surfaces Low to moderate energy conditions	RST1	Mouldic (evaporite replacement) up to 10%
F15 Laminated packstone of oncoids and peloids	at least 100 km wide at least 70 m thick	laminated	Flat laminated and locally domal	Open marine Attached to coarse-grained substrates Associated to maximum flooding surfaces Low energy conditions	RST2	Mouldic (evaporite replacement) up to 15 %

TABLA 5. Atributos deposicionales y de reservorio de las facies microbialíticas. Los valores de porosidad están referidos a porosidad antigua ocluida por cementos calcíticos.

lugares de generación de porosidad. Los valores de porosidad modal alcanzan un máximo de 10% (Fig. 3.21G-I, Tabla 5).

Además, algunas vacuolas se desarrollaron dentro de cementos y después de procesos de dolomitización ligados a circulación de agua marina (Tucker y Marshall, 2004). Aunque las facies trombolíticas pueden desarrollar porosidad móldica, esta facies son comúnmente no porosas. El motivo es que sus componentes (masas micríticas micropeloidal y peloidales generadas *in-situ*) están rodeados por cementos fibrosos tempranos y botroidales que rellenaban la porosidad que dejaban las fábricas microbianas.

3.8.4. Porosidad en los *packstones* laminados de oncoides y peloides (facies F15)

La porosidad en esta facies posee una distribución homogénea de poros milimétricos mostrando un aspecto externo en forma de coliflor. Los valores de porosidad modal son de hasta el 15%. Esta porosidad móldica consiste en cavidades subelípticas a alargadas de pequeño tamaño (hasta 3 mm) que representan pseudomorfos de minerales evaporíticos (anhidrita). Estos poros están ocluidos por cementos calcíticos granulares a *blocky* distribuidos en niveles específicos dentro de esta facies (Fig. 3.22, Tabla 5).

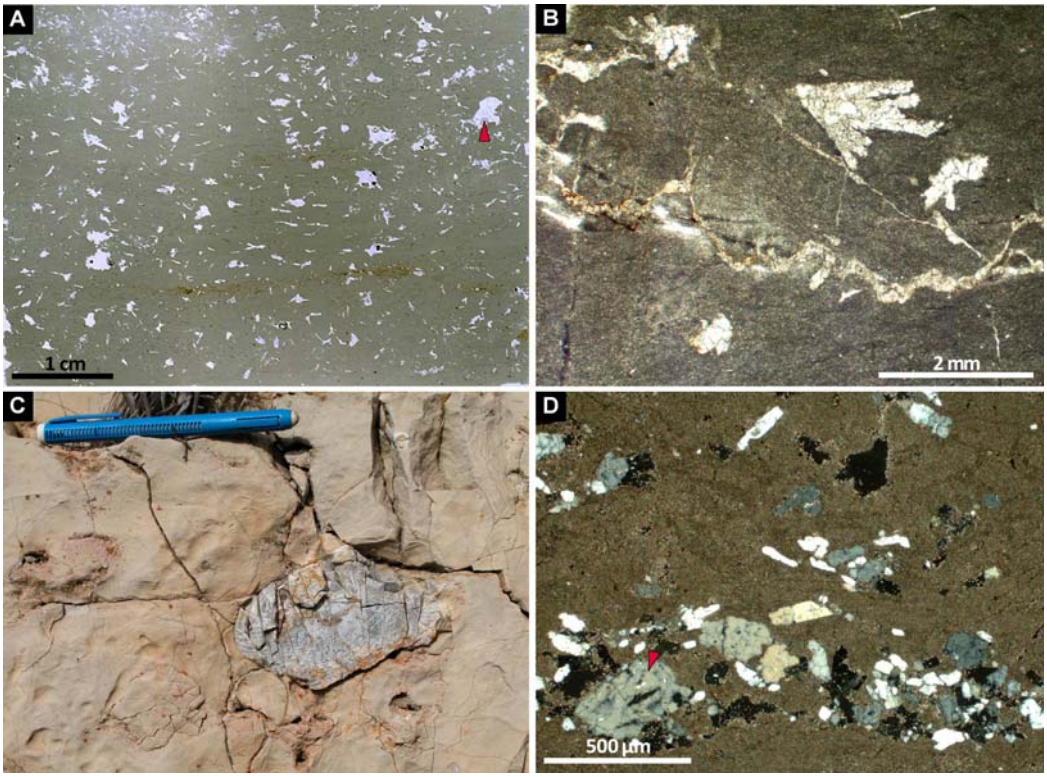

Fig. 3.22. *Véase la página siguiente*→

Fig. 3.22. (*Viene de la página anterior*) Fotografías mostrando ejemplos de porosidad antigua en las facies de *packstones* laminados con oncoides y peloides (facies F15). A) Textura interna de las facies F15. B) Porosidad móldica dentro de pseudomorfos de cristales evaporíticos actualmente rellenados con cementos calcíticos *blocky*. C) Fotografía de afloramiento de masas silicificadas subesféricas interpretadas como un reemplazamiento tardío de nódulos evaporíticos. D) Porosidad móldica rellenada con cementos granulares de cuarzo con presencia de minúsculas inclusiones de anhidrita (flecha roja). Luz polarizada. Marcador = 15 cm. Tomado de Mercedes-Martín et al. (2013b).

Discusión

4.1. Cambios del nivel del mar durante el Ladiniense

La significativa caída del nivel del mar registrada en el techo del RST1 de la secuencia T-R1 está bien documentada en otras cuencas triásicas del Tetis, como en los Alpes, Cuenca de París, Mar del Norte, Mar de Barents o Cuenca Alemana (Gianolla y Jacquin, 1998). Según estos autores, una nueva calibración de las interpretaciones de la estratigrafía secuencial triásica en el dominio del mar del Tetis y Boreal ha resultado en el reconocimiento de cuatro ciclos T-R de segundo orden a lo largo de Europa occidental. El techo del segundo ciclo T-R (R2 de Gianolla y Jacquin, 1998) corresponde a un máximo regresivo que registra una importante discordancia regional de edad Ladiniense superior (Biddle, 1984; Brandner, 1984; Haq et al., 1987). Estas discordancias están comúnmente asociadas con superficies visibles de carst, grandes acumulaciones de megabrechas y la truncación erosional de los taludes y márgenes de plataforma, así como incisiones erosivas.

Goggin y Jacquin (1998) distinguieron la secuencia K1, de edad Ladiniense superior-Carniense inferior en la cuenca intraplaca de París. El límite de secuencia K1 se identificó como una discordancia erosiva mostrando truncación erosional de los depósitos arenosos previos. Un basculamiento regional tuvo lugar en la porción occidental de la cuenca a lo largo del límite de secuencia K1.

En los Alpes meridionales occidentales, Gaetani et al. (1998) también reconocieron la secuencia más alta del Ladiniense en la plataforma carbonatada de

Esino, cuyo límite de secuencia basal está localmente definido como un evento de carstificación penetrativa (máximo de 80m; Jadoul y Frisia, 1988; Feist-Burkhardt et al., 2008) en la plataforma interna. Las porciones más distales de la cuenca presentan depósitos de megabrechas.

En los Alpes meridionales (N de Italia), igualmente, Gianolla et al. (1998, 2011) observaron que la discordancia del Ladiniense superior correspondió con una significativa superficie de carst localizada en el techo de las unidades Sciliar Dolomite 3, Esino Limestones 3 y San Salvatore Dolomite 3. Por otro lado, en las cuencas occidentales de las Dolomitas, el límite de secuencia coincidió con una prominente superficie erosional submarina en la base de "Marmolada Conglomerate". La significativa discordancia subaérea situada a techo del ciclo transgresivo-regresivo (T-R) del Ladiniense se reconoció también en otras regiones del mundo, como en la Cuenca de Sverdrup en el Archipiélago Ártico Canadiense (Embry, 1988).

4.2. Heterogeneidades y modelos deposicionales en el Ladiniense del Tetis

El estudio de la arquitectura de facies ha permitido conocer mejor algunos de los puntos clave que afectaron a la dinámica de crecimiento de las rampas carbonatadas del Ladiniense de la Cuenca Triásica Catalana. El régimen tectónico extensivo controla las plataformas carbonatadas, en lo relativo a la distribución, morfología 2D, así como las secuencias deposicionales y las características estratigráficas de gran escala (Bosence, 2005). A pesar de la compartimentalización de la Cuenca Triásica Catalana acaecida durante el Ladiniense, las irregularidades de la paleotopografía previa y sinsedimentaria fueron compensadas por significativas tasas de producción de carbonatos. Como resultado, la geometría de los cuerpos sedimentarios y la continuidad de los cinturones de facies sugieren un perfil sedimentario del tipo rampa con algunos escalones (*fault-block ramp*, Mercedes-Martín, 2013a,b). Un buen ejemplo de esta tendencia fue observada durante el RST1 en el dominio de Prades, donde una marcada diferencia de espesores se registró entre el bloque hundido (Coma Fonda) y el bloque levantado (Miramar) a través de la falla de La Riba. Esto indica que la tasa de subsidencia, que dio lugar al incremento del espacio de acomodación, fue igualada por la tasa de crecimiento de los cuerpos microbianos (facies F12 a F16). En otras palabras, el espacio disponible para depósito fue rápidamente rellenado por las facies F12 a F16, las cuales estaban predominantemente caracterizadas por componentes microbianos, dando lugar a un perfil deposicional del tipo rampa controlada por bloques fracturados (*fault-block ramp*). La evidencia que corrobora este perfil

deposicional de tipo rampa es la ausencia de márgenes de plataforma asociados con escarpes y la ausencia de facies de talud bien definidas con relación a las fallas activas. Sin embargo, en otros casos, como en la proximidad de Montsant, el basculamiento de bloques asociados a fallas sinsedimentarias dio lugar a depósitos de *debris flow* y de *slumps* indicando la existencia de pequeños escarpes. En el surco intracuenca ubicado en el dominio de Prades, entre las fallas de La Riba y Ulldemolins-Gandesa el relleno sedimentario estaba caracterizado por la presencia de facies de rampa media y la ausencia de facies de cuenca o rampa externa. De ese modo, este surco no se ha podido considerar como una cuenca intraplaforma (*intrashelf basin*) (Fig. 4.1).

Por el contrario, la relación entre la creación de espacio de acomodación y la producción de carbonatos fue notablemente diferente en otras cuencas del Triásico medio de la región del Tetis. Así, en Latemar, la plataforma carbonatada del Anisiense superior de la región del O de Dolomitas, es un ejemplo de plataforma aislada por bloques de falla poligonales, que creció durante un episodio de muy elevada subsidencia (Preto et al., 2011). La plataforma interna muestra ciclos de facies perimareales bien laminadas, somerizantes y con apilamientos agradantes. Mientras que el talud estuvo dominado por procesos gravitacionales, y compuesto por megabrechas, turbiditas y *slumps,* mostrando apilamientos progradantes (Marangón et al., 2011). La plataforma Ladiniense de Marmolada, la cual es considerada como una plataforma carbonatada aislada y limitada por fallas sinsedimentarias, sufrió una fuerte agradación que generó un notable contraste de facies entre los depósitos laminados de la plataforma y los depósitos de talud. Estos taludes estaban formados por clinoformas de megabrechas carbonatadas interestratificadas con sedimentos pelágicos de cuenca (Blendinger, 1986). En los ejemplos italianos, la tasa de desplazamiento de las fallas excedió la tasa de sedimentación de carbonatos dando lugar a una asimetría tectónica que resultó en un marcado contraste de espesores de facies. Esta tasa de sedimentación carbonática favoreció el desarrollo de pequeñas plataformas carbonatadas aisladas en los altos estructurales y de cuencas intraplataforma (*intrashelf basins*) en las depresiones. Este tipo de situaciones no han sido constatadas en la Cuenca Triásica Catalana

Además, la plataforma de Latemar (Harris, 1993; Marangon et a., 2011) estuvo formada por abundantes *boundstones* dominados por microbios y cementos tempranos, preferencialmente localizados en el margen de plataforma y talud (estimaciones areales de: 750 m de ancho y 875 m de espesor). Similarmente, la

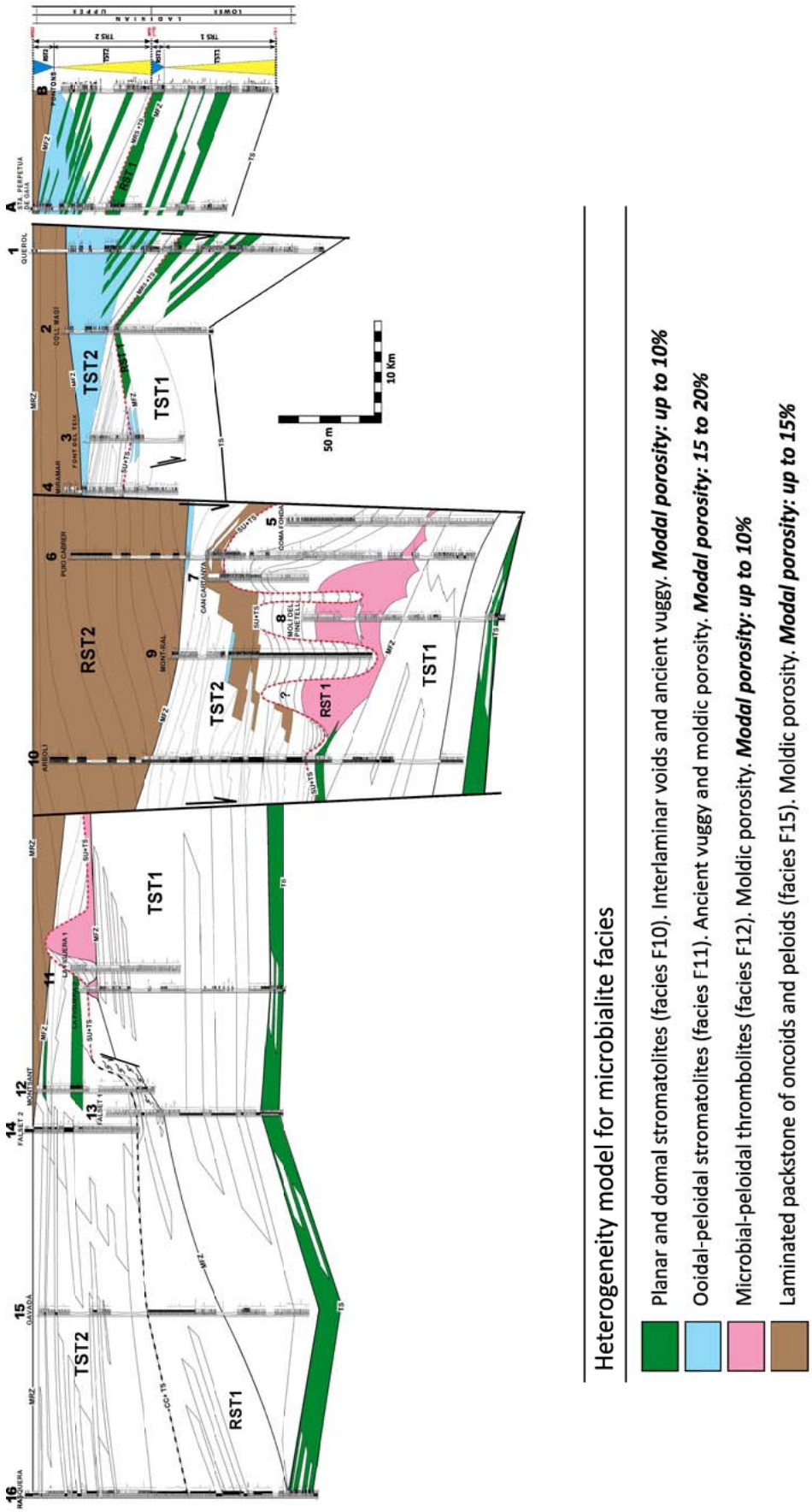
TST2
TST1
RST2
RST1
RST 1
50 m
10 Km
Heterogeneity model for microbialite facies
Planar and domal stromatolites (facies F10). Interlaminar voids and ancient vuggy. Modal porosity: up to 10%
Ooidal-peloidal stromatolites (facies F11). Ancient vuggy and moldic porosity. Modal porosity: 15 to 20%
Microbial-peloidal thrombolites (facies F12). Moldic porosity. Modal porosity: up to 10%
Laminated packstone of oncoids and peloids (facies F15). Moldic porosity. Modal porosity: up to 15%

plataforma carbonatada aislada de Tengiz, del Carbonífero inferior (Weber et al., 2003; Collins et al., 2006) estuvo constituida por abundantes *boundstones* microbianos y abundantes cementos localizados en la transición entre la plataforma externa y talud superior y también el talud medio y superior (estimaciones areales de: 416 m de ancho y 250 m de espesor). Estos ejemplos muestran que la distribución areal de microbialitos en plataformas aisladas ha estado generalmente limitada al margen de plataforma y talud presentando estrechos cinturones progradantes.

Sin embargo, las rampas controladas por bloques fracturados (*fault-block ramps*) del Ladiniense de la Cuenca Triásica Catalana estuvieron caracterizadas por cinturones de depósitos microbianos continuos de geometrías tabulares y estratiformes de una gran continuidad lateral (estimaciones areales de 45 Km de ancho y 40m de espesor en trombolitos, y hasta 30 Km de ancho y 7 m de espesor en estromatolitos) (Fig. 4.1).

4.3. Controles en el crecimiento de los microbialitos

4.3.1. Estromatolitos s.s. (facies F10)

Estos depósitos se formaron básicamente durante el RST1 y el TST2 en ambientes intermareales a submareales someros de la rampa interna, donde alcanzaron sus mayores espesores y tamaños. Estos depósitos se nuclearon en un sustrato constituido por *packstones* bioclásticos, *grainstones* oolíticos o brechas intraclásticas sugiriendo que el tipo de sustrato jugó un papel destacado en su iniciación, como ocurre en los estromatolitos de las Bahamas (Reid et al., 1995), en el Great Bank of Guizhou (Lehrmann, 1999) o en Shark Bay (Jahnert y Collins, 2012).

El análisis estratigráfico ha revelado que los depósitos estromatolíticos de mayor espesor crecieron predominantemente en la zona intermareal de un ambiente protegido por bajíos (*backshoals*). En este ambiente, la influencia de las corrientes de marea y olas fue limitada y el aporte de sedimento grueso aparentemente nulo o limitado. Además, la presencia coetánea de condiciones restringidas (alta evaporación e hipersalinidad) pudo haber inhibido los depredadores y la competición de los

Fig. 4.1. Modelo de heterogeneidades incluyendo la arquitectura de facies y la distribución de porosidad en las facies microbialíticas de las rampas carbonatadas ladinienses. Tomado de Mercedes-Martín et al (2013b) ←

invertebrados marinos, teniendo en cuenta su escasa representación (Garrett, 1970; Browne et al., 2000), contribuyendo al desarrollo de estos microbialitos en la rampa interna (Mercedes-Martín et al., 2013a,c).

La transición observada entre el Tipo 1 (estromatolitos planares) y el Tipo 2 (estromatolitos dómicos) a lo largo del tiempo se explica mejor por el incremento del espacio de acomodación favorecido por fallas sinrift (Mercedes-Martín et al., 2013a,c) que por una variación de los constructores microbianos (Sumner, 2000; Harwood y Sumner, 2011) o por un cambio de condiciones intermareales (somero) a submareales (profundo) (Arenas y Pomar, 2011).

Andres y Reid (2006) y Eckman et al., (2008) sugirieron que la macromorfología de los estromatolitos de Highborne Cay (Bahamas) estaba primariamente controlada por el espacio de acomodación, las condiciones hidrodinámicas y los patrones sedimentarios. Según estos autores, la distribución y morfología de los estromatolitos, estuvo controlada por el tipo de sedimento y la movilidad de los granos. Por su parte, Jahnert y Collins (2011, 2012) sugirieron que la morfología general de los depósitos microbianos estaba relacionada con la interacción entre el aporte de sedimento, topografía y gradiente del sustrato.

La microestrutura y textura de los microbialitos ha sido considerada de origen microbiano (p. ej., bacterial, mayormente cianobacterias). La alternancia de láminas dolomicríticas gris oscuro con láminas doloesparíticas/dolomicroesparíticas ocre claro se explica por la combinación de diferentes procesos.

Las capas gruesas y de colores claros se formaron mediante procesos de atrapamiento e incorporación de granos finos de sedimento (*trapping and binding*) por comunidades microbianas, que además favorecían la precipitación de $CaCO_3$. La precipitación de calcita mediada por la actividad metabólica microbiana indujo la litificación de las láminas de acuerdo con la consideración de varios autores (Burne y Moore, 1987; Pentecost, 1991; Chafetz y Buczynski, 1992).

Las capas más finas y de colores oscuros se formaron como resultado de actividad bacterial (son los denominados tapices microbianos o *algal mats*), que se produce principalmente durante periodos de interrupción sedimentaria (o menor aporte sedimentario) y predominancia de acreción microbiana (Chafetz y Buczynski, 1992; Reid et al., 1995; Reid et al., 2000). Este tipo de laminación puede reflejar la participación de diversos procesos influenciados por el medio y que hayan afectado a los patrones microbianos. La ausencia de sedimentos de grano grueso en las láminas y el hecho que éstas estén con frecuencia parcialmente dolomitizadas, hace difícil valorar el grado de contribución de los diferentes procesos microbianos. Aunque la degasificación física de CO_2 puede ser la responsable de la precipitación de carbonato

en algunos ambientes deposicionales (p. ej., aguas someras y agitadas), la abundancia y diversidad de filamentos microbianos calcificados junto con la presencia de numerosos calcimicrobios, sugiere que la precipitación microbiana de carbonato pudo contribuir significativamente en la litificación temprana de estos microbialitos (Visscher et al., 2000; Dupraz y Visscher, 2005).

4.3.2. Estromatolitos oolítico-peloidales (facies F11)

Estos microbialitos se formaron durante el RST1 y TST2. En contraste con los estromatolitos s.s., los estromatolitos oolítico-peloidales crecieron bajo condiciones variables de energía hidráulica y en lugares donde el aporte de sedimentos (aloquímicos) condicionó su formación. Paralelamente, durante periodos de alta energía, ooides y peloides se acumularon bajo la influencia de corrientes de marea y oleaje. Paralelamente, durante periodos de menor energía hidráulica, el cese del depósito de ooides y peloides favoreció la formación de intervalos micríticos y micropeloidales. La asociación de estos microbialitos con laminación *wavy*, ripple y *herringbone* es consistente con una sedimentación producida en un ambiente submareal sometido a flujos de energía hidráulica intermitentes. La formación de granos agregados o compuestos (*grapestones*) tuvo lugar bajo la influencia de microbios, los cuales pueden haber sido muy efectivos en la incorporación y cementación de ooides unidos por “algas” o foraminíferos incrustantes en ambientes marinos (Winland y Matthews, 1974). Según estos autores, la formación de estos granos estuvo favorecida por una elevada tasa de circulación de agua, turbulencia y bajas tasas de sedimentación. Purdy (1963) subrayó la influencia biogénica en el origen de cementos intergranulares y posteriormente, Macintyre et al., (2000) interpretaron los granos agregados como ejemplos de granos fusionados por efecto de la actividad de cianobacterias endolíticas.

Además, en los ejemplos de este trabajo, la abundancia de granos redondeados de composición dolomicrítica y sin estructura (*bahamite peloids*) en los intervalos de *grainstone* sugiere que tuvo lugar micritización causada por actividad biológica. En la isla de Andros, Monty (1967) registró la transformación de granos a una textura criptocristalina provocada por fenómenos de perforación “algal”. De igual manera, los estromatolitos de Exuma Cay (Bahamas) presentan evidencias de microperforaciones y micritizaciones en las capas oolíticas producidas por cianobacterias (Reid et al., 1995; Macintyre et al., 2000) siendo sus efectos observables incluso por debajo de las superficies microperforadas. La presencia de *bahamite peloids* también ha sido documentada en los estromatolitos del Turoniense superior del norte de la Cordillera

Ibérica (Rodríguez-Martínez et al., 2011), cuya formación ha sido atribuida a los procesos antes mencionados.

En los estromatolitos oolítico-peloidales del Triásico, predominan los procesos de micritización y fusión de granos, indicando que los microbios participaron activamente en la formación de estos depósitos. El amplio desarrollo de capas dolomicríticas, la abundante presencia de filamentos microbianos y las texturas dolomicríticas peloidales son compatibles con una precipitación de carbonato influenciada por microbios. Durante los periodos de escasa tasa de sedimentación, las capas micríticas quedaron colonizadas por organismos perforantes y endolíticos (esponjas y macrofauna bentónica) dando lugar a perforaciones milimétricas. De igual modo en las capas oolíticas, el atrapamiento e incorporación de granos (ooides y *grapestones*) por cianobacterias y EPS (*extracellular polymeric substances*) tuvo lugar durante los periodos de sedimentación activa.

4.3.3. Trombolitos (facies F12)

Estos microbialitos se formaron exclusivamente durante el RST1 y ocuparon los ambientes de rampa media y externa. Las geometrías de los depósitos trombolíticos (biostromos y biohermos) estuvo controlada por la creación de espacio de acomodación debido a la actuación de la falla de La Riba (Mercedes-Martín et al., 2013a). En el dominio de Prades, los trombolitos generalmente se nuclean en un sustrato de *wackestones* y *packstones* bioclásticos y peloidales, mientras que en el dominio de Baix Ebre-Priorat, crecieron encima de niveles formados por *mudstones* y *packstones* bioclásticos y bioturbados. El crecimiento trombolítico estuvo condicionado por la naturaleza de los *mesoclots*, la presencia de componentes microbianos específicos, el tipo de sedimento que formó la matriz, así como los procesos de relleno de cavidades.

La forma y la distribución de los Dmm (Mesoclots micríticos densos) muestran que los fenómenos de acreción fueron los mecanismos de crecimiento más frecuentes, formando un armazón rígido y continuo por encima de los componentes preexistentes (sedimento o cementos). No hay evidencias que sugieran la existencia de mecanismos de atrapamiento e incorporación de granos aloquímicos dentro de los *mesoclots*. De hecho, el armazón de los trombolitos (Dmm) se debe a la calcificación de diferentes tipos de microorganismos (calcimicrobios, cianobacterias y comunidades microbianas dominadas por cocoides). Tal y como sugirió Webb (1987), la incrustación, rotura y transporte de esos componentes puede haber sido el mecanismo que estuviese involucrado en la dispersión y recolonización durante periodos de mayor energía de

flujo. La presencia de niveles grano decrecientes y de algunos bioclastos en Mm (matriz micrítica) y Ipm (Masas intraclásticas y peloidales) apunta a una depósito a partir de decantación de sedimento que rellena cavidades preexistentes. A pesar de la existencia de procesos de retrabajamiento y granoselección de aloquímicos entre cavidades, la litificación temprana de las estructuras *clotted* y de los diversos cuerpos microbianos fue el mecanismo clave en la formación de los trombolitos.

La acumulación de sedimento interno (aloquímicos, como intraclastos, peloides, bioclastos: Ipm) ha sido registrada también en otros arrecifes trombolíticos (Kennard y James, 1986; Webb, 1987; Kahle, 2001; Pratt y Haidl, 2008). Estos componentes pudieron originarse por procesos bioquímicos o fisico-químicos, desintegración de organismos o la combinación de cualquiera de estos procesos (Kahle, 2001). Como consecuencia, el transporte y retrabajamiento de estos componentes dentro de las cavidades depende de la existencia de un cierto flujo energético. Por esta razón, un ambiente submareal somero, influenciado por periodos de tormentas y corrientes estaría asociado con la formación de los trombolitos ladinienses.

Paralelamente, el desarrollo de cementos marinos jugó un papel crucial en el crecimiento y cohesión de los trombolitos. De hecho, la presencia de abundante cemento botroidal primario rellenando cavidades o incluso rodeando los principales componentes (calcimicrobios, costras microbianas, filamentos crípticos y formas similares a *Tubiphytes*) sugiere que la cementación tuvo lugar simultáneamente con el crecimiento microbiano (Aitken y Narbonne, 1989; Kah y Grotzinger, 1992; Chow y George, 2004). Además, la diversidad morfológica de gran escala que presentan los trombolitos (Tipo 1 y de Tipo 2, Mercedes-Martín et al., 2013a) apunta a que estos microbialitos fueron capaces de crecer rápidamente para amoldarse a las cambiantes condiciones ambientales, principalmente debido al incremento del espacio de acomodación y de la lámina de agua.

Calvet y Tucker (1995) situaron los trombolitos en los montículos trombolíticos (*mud-mounds*). Estos autores pusieron de manifiesto que dichos montículos presentaban una zonación vertical, así, por encima de las facies trombolíticas se registró un complejo carbonatado terminal compuesto por arrecifes arrecifales coralinas de aguas someras (facies F14 de Mercedes-Martín et al., 2013a). Asímismo, Tucker et al., (1995) reconocieron cementos marinos botroidales y fibrosos asociados a las facies coralinas y cuyo origen se produjo en una fase diagenética temprana, por bombeo de agua marina a través de dichos materiales. Estas facies coralinas están a su vez fosilizadas por unidades de gravas carbonatadas y *rudstones* de algas dasicladáceas.

La textura *mesoclotted* de los trombolitos estudiados comprende diferentes tipos de productos microbianos reconocidos por sus texturas. La naturaleza microbiana de los *mesoclots* se manifiesta por sus distintas formas de crecimiento, mostrando estructuras de acreción, de atrapamiento y de incrustación. Así, los componentes microbianos que contribuyeron a la acreción de los trombolitos serían: *biofilms* calcificados, calcimicrobios, formas bacteriales filamentosas y cocoidales, o la yuxtaposición de cualquiera de ellas.

Diversos tipos de *biofilms* calcificados han sido descritos en los trombolitos ladinienses y están a menudo asociados con el grupo de microproblematica *Tubiphytes* (ver Senowbari-Daryan, 2013) y con las formas crípticas de *Archaeolithoporella*. Este último organismo formaba revestimientos y costras finas acompañadas de cementos sindeposicionales marinos fibrosos y botroidales durante el Paleozoico (Sano et al., 1990; Shen et al., 2012). De igual manera, los fenómenos de incrustación realizados por los organismos microproblematica desempeñaron un papel esencial en la acreción de los trombolitos ladinienses. Los microproblematica y los cementos sindeposicionales actuaron como estabilizadores del armazón. En el caso de los calcimicrobios, se encuentran menos representados en los trombolitos ladinienses (*Cayeuxia, Garwoodia*, microbios porostromados), aunque favorecieron la construcción del microbialito.

Además, se observan agregados esféricos en forma de racimo constituidos por dolomicrita *clotted* y peloides (grosor de 80 a 100 µm) que flotan dentro de un cemento marino doloesparítico a microdoloesparítico. Aunque el origen de estos agregados puede ser múltiple, la distribución, morfología en racimo y el hecho que se encuentran rodeados de cemento sugiere que fueron el producto de la degradación *in situ* de colonias bacteriales cocoidales durante una etapa de diagénesis temprana (Chafetz, 1986; Riding y Tomás, 2006).

La presencia de cementos autigénicos de barita en los trombolitos puede indicar la presencia de fluidos hidrotermales, los cuales pueden también haber favorecido la formación de los componentes microbianos y de los cementos marinos botroidales y fibrosos. Las mineralizaciones del tipo MVT (*Mississippi Valley Type*) son conocidas desde la antigüedad en la región de estudio, a través de la explotación minera a pequeña escala de depósitos de sulfuros de plomo-zinc. Por tanto, debería tenerse en consideración algún mecanismo físico-químico que pudiera explicar cómo los fluidos hidrotermales pudieron favorecer la formación de cementos y texturas microbianas en de los montículos trombolíticos (*mud-mounds*). Dichos fluidos se propagarían a través de las zonas de falla con surgencias de aguas hidrotermales, como apuntó Monty (1985). Además, las características que presentan algunas cavidades internas de los

trombolitos pueden ser consideradas como originadas por procesos de corrosión producida por fluidos hidrotermales en el sentido de Esteban et al. (2009).

4.4. Controles en la distribución y concurrencia de los microbialitos

El estudio de la distribución espacial y temporal de facies sugiere que los microbialitos presentes en el RST1 y TST2 crecieron contemporáneamente en diferentes subambientes dentro de la rampa o incluso en ambientes similares o iguales, desarrollándose en zonas estratigráficas equivalentes en el tiempo (Fig. 4.2, A y B).

4.4.1. Concurrencia de estromatolitos s.s., estromatolitos oolítico-peloidales y trombolitos en el RST1

La coetánea presencia de estos microbialitos tuvo lugar dentro del RST1. Algunos factores ambientales jugaron un rol fundamental en el desarrollo de determinados microbialitos y otros factores actuaron de forma combinada para favorecer su coexistencia (Fig. 4.2A).

La biomasa microbiana prospera como consecuencia de la hipersalinidad, a menudo relacionada con las altas tasas de evaporación y presencia de aguas restringidas, factores que eliminan a muchos competidores (Browne et al., 2000) y aseguran una baja diversidad de especies eucariotas (Shark Bay, Australia: Playford y Cockbain, 1976; Jahnert y Collins, 2012). Similarmente, estas condiciones prevalecieron y favorecieron la proliferación de los estromatolitos s.s. que se desarrollaron en una bahía restringida hipersalina en la rampa interna.

Paralelamente, el movimiento de sedimento ha sido considerado como un factor crítico que restringe o elimina a las comunidades bióticas responsables de la disrupción de los tapices microbianos en algunos lugares de Bahamas (Steneck et al., 1993; Reid et al., 1995; Golubic y Browne, 1996). De igual modo, los estromatolitos oolítico-peloidales del RST1 se desarrollaron bajo condiciones submareales someras proliferando durante periodos intermitentes de alta movilidad de sedimento y de predominio de la calcificación microbiana. Además, las comunidades microbianas favorecieron la rápida litificación sindeposicional, de modo que fueron probablemente las responsables de la acreción de los estromatolitos oolítico-peloidales. La interacción de factores biológicos y oceanográficos puede haber favorecido la precipitación carbonatada, como se ha sugerido para los estromatolitos

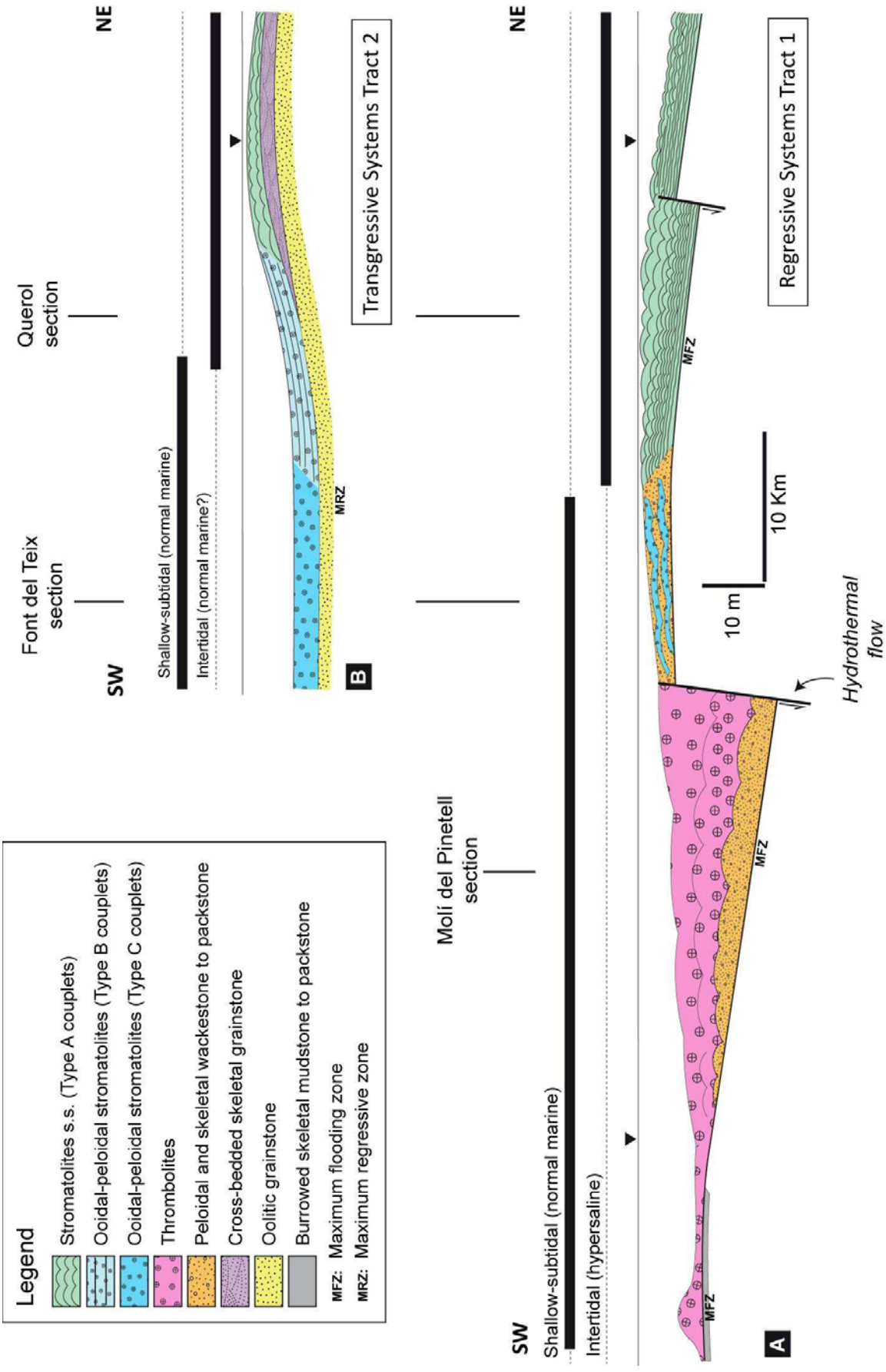
Legend
Stromatolites s.s. (Type A couplets)
Ooidal-peloidal stromatolites (Type B couplets)
Ooidal-peloidal stromatolites (Type C couplets)
Thrombolites
Peloidal and skeletal wackestone to packstone
Cross-bedded skeletal grainstone
Oolitic grainstone
Burrowed skeletal mudstone to packstone
MFZ: Maximum flooding zone
MRZ: Maximum regressive zone
Font del Teix section
SW
NE
Shallow-subtidal (normal marine)
Intertidal (normal marine?)
MRZ
B
Transgressive Systems Tract 2
Querol section
Molí del Pinetell section
Shallow-subtidal (normal marine)
Intertidal (hypersaline)
MFZ
MFZ
MFZ
10 m
10 Km
Hydrothermal flow
A
Regressive Systems Tract 1

de Bahamas (Whittle et al., 1993). Finalmente, los trombolitos crecieron en ambientes submareales someros dentro de la zona fótica (como sugiere la presencia de calcimicrobios). Las microtexturas muestran una fuerte heterogeneidad y sugieren la presencia de diferentes comunidades (calcimicrobios, cianobacterias cocoides, esponjas), así como cementos marinos).

La proliferación de los trombolitos se explica por la interacción de diversos mecanismos biológicos y físico-químicos los cuales pueden haber actuado secuencialmente o al mismo tiempo. No obstante, es necesario un estudio más preciso para comprender la evolución vertical, la variabilidad textural y los procesos de corrosión-cementación en las facies trombolíticas.

Paralelamente, el tipo de sustrato ha sido considerado como un factor importante en el inicio y desarrollo de los trombolitos (Kennard, 1994; Lehrmann, 1999; Emmerich et al., 2005) y estromatolitos (Reid et al., 1995; 2003; Andres y Reid, 2006). De hecho, todos los microbialitos ladinienses se nuclearon encima de un sustrato estabilizado y consolidado compuesto por depósitos oolítico-peloidales o bioclásticos.

Por otro lado, muchos tipos de microbios o microorganismos bentónicos (bacterias cocoidales y filamentosas, entre otras) colonizan frecuentemente los ambientes marinos someros, pero son limitados o están ausentes en lugares donde predomina una intensa bioturbación (Browne et al., 2000). De este modo, la competición ejercida por metazoos (fauna que se alimenta de los microbios) ha sido interpretada como un factor importante responsable de la reducción de la biomasa microbiana, cohesión y continuidad de los tapices (Garrett, 1970; Neumann et al., 1970; Macintyre et al., 1996; Riding y Liang, 2005). De hecho, la parte más baja del Ladiniense de la Cuenca Triásica Catalana está caracterizada por un empobrecimiento de las macrofaunas de invertebrados y un abundancia y baja diversidad de asociaciones de ichnofósiles (facies F7 de Mercedes-Martín et al., 2013a) reflejando un periodo de condiciones marinas restringidas (Jordi M. Gibert, com. pers.). Estas condiciones fueron decisivas en la reducción de los competidores microbianos y en el

Fig. 4.2. Perfil deposicional microbiano exhibiendo la presencia de microbialitos dentro de un contexto secuencial. A) Perfil inferido para el RST1 mostrando la presencia coetánea de estromatolitos s.s., estromatolitos oolítico-peloidales y trombolitos ocupando diferentes ambientes deposicionales dentro de la rampa dominada por bloques fracturados. Nótese que los trombolitos se desarrollan únicamente en el bloque hundido de la falla de La Riba y cuya formación puede estar relacionada con fluidos hidrotermales. Por otro lado, los estromatolitos s.s.y los estromatolitos oolítico-peloidales se desarrollaron en el bloque levantado. B) Perfil inferido para el TST2 mostrando la concurrencia de estromatolitos s.s., estromatolitos oolítico-peloidales. Nótese que estos microbialitos se desarrollaron sólo en la rampa interna de la rampa. Tomado de Mercedes-Martín et al. (2013c). ←

incremento de la producción microbiana durante todo el Ladiniense. Como resultado, la coetánea concurrencia de diversos microbialitos pudo ser debida, al menos en parte, a un evento oceanográfico adverso o a la existencia de condiciones biogeoquímicas concretas las cuales redujeron sustancialmente los organismos que se alimentaban de microbios.

4.4.2. Juxtaposición de estromatolitos s.s. y estromatolitos oolítico-peloidales en el TST2

Durante el TST2, los estromatolitos s.s. y los estromatolitos oolítico-peloidales consiguieron crecer en mutua asociación en el mismo ambiente deposicional de la parte interna de los bajíos externos (*inner fore-shoal*) dando lugar progresivamente a un conjunto de microbialitos que eran más aptos para atrapar e incorporar sedimento en sus tapices. En este sentido, se observa una zonación vertical (yuxtaposición) de diferentes tipos de parejas de láminas (capas tipo A→B→C) la cual revela que los principales procesos microbianos fueron cambiando con el tiempo.

Los parejas del Tipo A, se desarrollaron inicialmente en microbialitos donde la acreción se producía por precipitación de calcita mayormente inducida por actividad microbiana. En las parejas del Tipo B, los procesos de atrapamiento e incorporación de sedimento, así como micritización y fusión de granos fueron los procesos responsables de su formación. Finalmente, las parejas del Tipo C se formaron en las etapas tardías de la colonización microbiana y en las que abundaban los procesos de micritización, fusión de granos, perforaciones por organismos endolíticos, formación de *grapestones* y cementación temprana.

Las variaciones observadas entre las distintas parejas de láminas atestiguan cambios ambientales y condiciones específicas de la dinámica sedimentaria como principal causa implicada en su formación. Los microbialitos caracterizados por las parejas del Tipo A se formaron en la zona intermareal superior; las parejas del Tipo B están asociadas a la zona intermareal inferior-submareal somera, mientras que las parejas del Tipo C están formadas bajo condiciones submareales someras. Las variaciones del nivel del mar de cuarto orden condicionaron la profundidad de la lámina de agua (influencia submareal o intermareal), el grado de energía hidráulica de olas y corrientes de marea, el tipo de sedimento disponible y la tasa de sedimentación. Por tanto, estos factores controlaron los procesos microbianos y sus texturas y en definitiva la tipología de microbialitos.

Algunos autores (Harwood y Sumner, 2011) atribuyen la superposición de distintos tipos texturales (p. ej., trombolítica y estromatolítica) al crecimiento simultáneo de comunidades microbianas morfológicamente diferentes antes que a un cambio de la dinámica sedimentaria local, como ocurre en el caso de la yuxtaposición de texturas *clotted* con texturas del tipo *grainstone* en el caso del Neoproterozoico de California (Harwood y Sumner, 2011). Estos autores registraron los denominados "microbialitos compuestos", cuyas estructuras *clotted* (trombolíticas) y laminadas (estromatolíticas) se entremezclaron a escala subcentimétrica en el mismo ambiente perimareal. En este caso, la predominancia de *clots* microbianos asociados con láminas irregulares y discontinuas, así como texturas *clotted* interestratificadas con texturas laminadas da consistencia al origen antes mencionado.

Sin embargo, la presencia intermitente de sedimentos de grano grueso (ooides, peloides y *grapestones*) en los microbialitos ladinienses sugiere que su origen está más íntimamente ligado a factores extrínsecos (pequeños cambios en el espacio de acomodación o aporte sedimentario), aunque un cambio vertical de las comunidades microbianas podría ser tenido en consideración.

4.4.3. Comparación con ejemplos fósiles y actuales

Los estromatolitos s.s. del Ladiniense son similares a los conocidos ejemplos de Hamelin Pool en Australia. La bahía hipersalina de Shark Bay (Logan y Cebulski, 1970; Logan et al., 1974; Jahnet y Collins, 2012) contiene unidades estromatolíticas sometidas a salinidades anormales como consecuencia de la alta evaporación y la presencia de barreras físicas que impiden la circulación de agua (Faure Sill). Sin embargo, existe una diferencia entre las morfologías observadas en Hamelin Pool y en la Cuenca Triásica Catalana. Mientras que en Shark Bay los estromatolitos más comunes desarrollados en ambientes submareales someros e intermareales poseen formas columnares, los estromatolitos s.s. ladinienses presentan formas tabulares (Tipo 1) predominando sobre las dómicas (Tipo 2). Sin embargo, en Shark Bay, las formas dómicas y tabulares están preferencialmente localizadas en las zonas de promontorios (con gradientes de 4m/ 100m) antes que en zonas de bahías (gradientes de 30-50cm/ 1000m). Esto refleja que los gradientes de sustrato elevados favorecen el crecimiento de depósitos microbianos dómicos de grandes relieves antes que depósitos de pavimentos microbianos tabulares (Jahnert y Collins, 2012).

Por otro lado, las formas ladinienses presentan una notable similitud con los estromatolitos de Santa Pola (Mioceno), formados en ambientes someros y mayoritariamente intermareales (Feldmann y McKenzie, 1997). Estromatolitos

columnares y dómicos de enorme tamaño se desarrollaron en posiciones adyacentes a estromatolitos tabulares y estratiformes en áreas con escasa deposición de arena, en ambientes de poca energía, y durante los periodos de nivel de mar alto. Estos estromatolitos dolomíticos fueron interpretados como originados en ambientes de alta salinidad.

En el caso del Mioceno de Mallorca, Arenas y Pomar (2010) atribuyeron el cambio de estromatolitos estratiformes/pequeños domos a formas con grandes domos a un incremento del espacio de acomodación y cambios batimétricos. Por otro lado, los microbialitos intermareales de Shark Bay incluyen texturas *clotted* trombolíticas (tapices postulares, Logan et al., 1974; Jahnert y Collins, 2012) y también estructuras laminadas (tapices planos, Logan et al., 1974). En ambos casos, la presencia de peloides de tamaño arena, fragmentos bioclásticos y cuarzo detrítico facilitó que los estromatolitos crecieran por atrapamiento e incorporación de partículas y la construcción de texturas fenestrales groseras por la precipitación de cementos (Logan et al., 1974).

Estas texturas son diferentes de las registradas en los estromatolitos s.s. ladinienses debido a que las formas triásicas se encontraban alejadas de las zonas con aportes sedimentarios bioclásticos y en consecuencia se encontraban menos afectadas por las intensas corrientes de marea y oleaje. Por lo tanto, los procesos de atrapamiento e incorporación de partículas finas junto con la calcificación microbiana fueron responsables de la laminación bien definida que se observa en los estromatolitos ladinienses.

Los estromatolitos oolítico-peloidales muestran grandes similitudes con algunos ejemplos marinos recientes. Los estromatolitos con parejas de Tipo B son similares a los ejemplos de Bahamas (Reid et al., 1995; 2000; Feldmann y McKenzie, 1998; Macintyre et al., 2000). Ambos tipos están compuestos por ooides y peloides bien seleccionados y capas litificadas muy finas correspondientes a horizontes micríticos. En el Ladiniense, la evidencia de micritización y raros granos fusionados cementados y truncados en sus extremos sugiere una alta similitud petrográfica con los actuales. Aunque no se observaron filamentos microbianos específicos en los ejemplos ladinienses, también existe una notable ausencia de estos elementos en los microbialitos de Bahamas, probablemente debido a su origen submareal (Reid et al., 1995).

Los procesos de microperforaciones y relleno de microcavidades así como truncación y fusión de granos han sido descritos en laminitas microbianas oolíticas en el Mioceno de Mallorca (Arenas y Pomar, 2010). Los estromatolitos oolítico-peloidales ladinienses son también muy parecidos a los del Mioceno de Mallorca en lo que se

refiere su morfología externa (Arenas y Pomar, 2010) con morfologías dominantemente tabulares en vez de columnares o domos aislados, como se registran en los equivalentes de las Bahamas (Dravis, 1983; Dill et al., 1986; Andres and Reid, 2006).

Por otro lado, los estromatolitos caracterizados por parejas de Tipo C son similares a los descritos por Chow y George (2004) en el Fameniense de Canning Basin (Australia). En este caso, los intervalos laminados y *clotted* fenestrales (de origen microbiano) están intercalados con intervalos laminados y granoclasificados (acumulación de ooides e intraclastos). Según Chow y George (2004), una compleja interacción entre la calcificación microbiana, cementación, atrapamiento e incorporación de sedimento se combinaron juntamente con factores ambientales produciendo la yuxtaposición de estas microfábricas en el mismo microbialito.

De forma análoga, los estromatolitos del Turoniense superior del norte de la Cuenca Ibérica registraron una heterogeneidad textural similar en los niveles superiores donde capas de texturas peloidales y *clotted* estaban interlaminadas con capas constituidas por *bahamite peloids*. En este trabajo, los *bahamite peloids* son interpretados como granos modificados por procesos biológicos.

Por otro lado, los arrecifes trombolíticos de las Dolomitas (Bosellini, 1986) estaban compuestos por costras biogénicas y microbianas (Harris, 1993; 1994) las cuales contribuyeron a aumentar la rigidez y estabilidad de las estructuras arrecifales (Flügel y Senowbari-Daryan, 2001). En Latemar (Dolomitas), la asociación de *bindstones* de *Tubiphytes* fue la más significativa asociación faunística y se encontraba localizada en la cresta arrecifal, mientras que los trombolitos formados por *Tubiphytes multisiphonatus* fueron más abundantes en las zonas de *back-reef sensu* Emmerich et al., (2005) o en las zonas de margen a transición de talud *sensu* Marangón et al., (2011). De forma similar, en la plataforma de Marmolada, Blendinger, (1986) registró la presencia de *Tubiphytes* y microbios porostromados en las facies arrecifales. En los Alpes (Austria), *Tubiphytes* y sphinctozoos fueron los organismos constructores de arrecifes más abundantes del Ladiniense al Carniense, en zonas de talud superior y márgenes de plataforma.

Aunque el término “trombolito” no ha sido ampliamente utilizado en algunas de las cuencas ladinienses de las Dolomitas o los Alpes, sus componentes (microbios, incrustadores y cementos sindeposicionales) actuaron como constructores del armazón jugando un rol fundamental en los procesos de litificación (Blendinger, 1994; Russo et al., 2000; Senowbari-Daryan, 2013).

4.5. Influencia hidrotermal en la formación de componentes microbianos y no-microbianos

Una de las características más llamativas de los trombolitos del Ladiniense del Tetis occidental es la abundancia de cementos marinos de morfologías botroidales y fibrosas. En líneas generales, el Triásico medio de las Dolomitas correspondió a un periodo con desarrollo de plataformas de carbonatos que crecieron bajo unas condiciones de subsidencia muy alta dando lugar la formación preferencial de plataformas carbonatadas aisladas o de tipo "atolón" (Bosellini, 1984; Blendinger, 1994; Preto et al., 2012). Estos sistemas están caracterizados por transiciones de plataforma sin protuberancias y taludes dominados por microbialitos y cementos marinos tempranos (Blendinger, 1986; 1994; Harris, 1993, 1994; Marangon et al., 2011). La plataforma Marmolada contiene una media de 20% de cementos marinos tempranos (radiaxial fibroso e isópaco) según Russo et al. (2000), o el 37% según Blendinger (1994); el macizo Sella está compuesto por una media de 37% de cementos marinos tempranos (fibrosos en forma de botroides, Keim y Schlager, 2001) y la plataforma de Latemar está formada por una media de 34% de cementos (fibrosos radiaxial y botroidales, Marangon et al., 2011). No obstante, aun teniendo en cuenta las limitaciones que suponen el uso de estas cifras, se han podido realizar algunas interpretaciones.

En los ejemplos previos, los cementos marinos tempranos son en % de volumen el componente más abundante junto con las fábricas microbialíticas (texturas estromatolíticas, trombolíticas y *biofilms*). Los trombolitos del Ladiniense de la Cuenca Triásica Catalana no son una excepción a esta regla. A pesar de que sus perfiles deposicionales coincidieron con rampas carbonatadas del tipo *fault-block*, éstas estaban compuestas como mínimo por un 40% de cementos fibrosos y botroidales y también de microbialitos, como ocurrió en sus equivalentes italianos y alpinos. Además, existe un amplio acuerdo en atribuir estos cementos a una fase diagenética marina temprana, así como en considerar que su composición original era aragonito (Blendinger, 1994; Harris, 1993, 1994; Tucker y Marshall, 2004; Seeling et al., 2005; Marangon et al., 2011). Sin embargo, la génesis de estos cementos se encuentra todavía muy debatida.

En este sentido, Van der Kooij et al., (2010) proporcionaron una interesante revisión de los factores que controlan la cementación marina masiva en ambientes de talud profundos. Aparte de los factores discutidos en trabajos previos (Grotzinger y Knoll, 1995; Webb, 1996; Seeling et al., 2005) también deberían tenerse en cuenta otros factores fisico-químicos, como es la influencia de fluidos hidrotermales originados

por anomalías térmicas que pudieron estar asociadas a la actividad magmática y volcánica.

De hecho, durante el Triásico medio y superior, se registró actividad volcánica durante la fase de rifting triásico en la Cuenca Catalana (Calvet et al., 1990; Salas y Casas, 1993) y también en la región de las Dolomitas (Doglioni, 1987). Asimismo, un mecanismo común de precipitación carbonatada se produce a través de la degasificación de aguas carbonatadas que fluyen de fuentes hidrotermales o surgencias de aguas calientes (Chafetz y Folk, 1984; Renaut y Jones, 2000). Además, los cementos botroidales asociados a los carbonatados de fuentes frías son muy frecuentes en muchos casos del registro fósil (Campbell et al., 2002; Canet et al., 2003; Gómez-Pérez, 2003).

Otro mecanismo más simple y eficaz de producir aguas hidrotermales es el conocido como de 'flujo topográfico' (*Gravity flow*) a partir de aguas meteóricas, que favorecidas por un gradiente topográfico significativo penetrarían hasta profundidades considerables a través de zonas fracturadas. Estas aguas calentadas en profundidad, de acuerdo con el grado geotérmico regional, ascenderían rápidamente por otras zonas fracturadas, de manera que no podrían ser reequilibradas térmicamente, dando lugar a fuentes o surgencias de tipo hidrotermal. Sea cual fuera el mecanismo térmico, una circulación hidrotermal más o menos prolongada en el tiempo pudo ser plausible y persistente favorecida por los procesos de fracturación sinsedimentaria, los cuales propiciaron la circulación de fluidos.

Este escenario es compatible con el contexto tectonosedimentario regional del Triásico medio (Ladiniense) de la Cuenca Triásica Catalana. Además, debe considerarse especialmente el hecho de que esta cementación masiva está comúnmente asociada con la falla de La Riba, lo cual daría fuerza a la hipótesis de los fluidos hidrotermales circulando por fallas. Estos fluidos más calientes fueron capaces de generar corrosión y los cementos marinos de morfologías botroidales y fibrosas. Es decir, las fracturas sinsedimentarias importantes, con su zona de influencia espacial, habrían jugado un importante papel en la circulación de aguas hidrotermales y la distribución de zonas de anomalías térmicas durante la sedimentación Ladiniense.

Por otra parte, la presencia de cementos autigénicos de barita en trombolitos y las mineralizaciones de tipo MVT (*Mississippi Valley Type*) de depósitos de sulfuros de plomo-zinc (galena y esfalerita) son también una prueba más de la circulación de fluidos hidrotermales en la cuenca ladiniense. En cambio, ni los estromatolitos s.s. (facies F10) ni los estromatolitos oolítico-peloidales (facies F11) presentan ninguna evidencia de este tipo de cementación.

Llegados a este punto, cabe formular algunas preguntas: ¿qué influencia tiene la contribución microbiana y no microbiana en la formación de los trombolitos? , ¿Jugaron las bacterias un papel predominante en la precipitación mineral?, ¿Estaban las bacterias meramente recubiertas de precipitados esencialmente abióticos? , ¿Son tan diferentes los procesos y productos microbianos y no microbianos en los ambientes lacustres y marinos? o ¿Pudo el hidrotermalismo favorecer los procesos de desarrollo microbiano en los trombolitos ladinienses de la Cuenca Triásica Catalana?

Varios ejemplos marinos registran la precipitación (inorgánica?) de grandes hemisferoides de botroides de aragonito creciendo coetáneamente con texturas microbianas en fuentes frías y surgencias hidrotermales (Savard et a., 1996; Peckman et al., 1999; Aharon, 2000; Peckman et a., 2001). Además, existe la percepción generalizada de que los precipitados mediados por microbios pueden posteriormente servir como lugares de nucleación de cristales inorgánicos que crecen en medios supersaturados (Renaut y Jones, 2000; Gómez-Pérez, 2003).

Las controversias sobre la contribución biótica o abiótica en los precipitados carbonatados presentes en travertinos o surgencias calientes no es nueva (Chafetz y Folk, 1984; Ford y Pedley, 1996; Renaut y Jones, 2000). Similarmente, la presencia de cementación masiva asociada a microbialitos en ambientes marinos necesita mayor investigación. Los procesos hidrotermales ligados a la presencia de anomalías térmicas y asociados a la fracturación son comunes en ambientes lacustres (Chafetz y Folk, 1984; Renaut y Jones, 2000).

Sin embargo, también podrían haber ejercido una significativa influencia sobre la producción microbiana y no microbiana de los ambientes marinos. Llegados hasta aquí y teniendo en cuenta todo lo dicho, se habría de considerar también la influencia bastante probable de la circulación de aguas hidrotermales a través de zonas de falla y su papel en el desarrollo de los trombolitos ladinienses de la Cuenca Triásica Catalana.

4.6. Rocas madres y reservorios de hidrocarburos en microbialitos

En los materiales ladinienses de la cuenca del Maestrazgo fueron registrados indicios de hidrocarburos en las *black-shales* depositadas en ambientes de cuenca, concretamente en el sondeo Bovalar 1 (Salas et al., 2001). Los datos geoquímicos y de Rock Eval de esta roca madre potencial son (A. Permanyer com. Pers): a) equivalente de vitrinita a partir de steranos: 0,85% Ro, b) pirolisis Tmax: 440ºC, y c) temperatura de enterramiento: 138ºC. Según el modelo térmico (Fig. 4.2) construido

para el pozo Bovalar 1 (R. Salas, com. Pers.) la facies de *black-shales* del Muschelkalk superior entró en ventana del petróleo a 150 Ma (Titónico) y posteriormente en ventana del gas a 100 Ma (Albiense), llegándose a enterrar hasta los 3100 m de profundidad. Actualmente las *black-shales* han suministrado restos de hidrocarburos por procesos de extracción. No se tiene noticia de reservorios de estos hidrocarburos en rocas cretácicas. Sin embargo, está probado geoquímicamente que los hidrocarburos generados a partir de la Fm. Ascla (Kimmeridgiense superior-Titónico) fueron la roca madre de los crudos del Campo de Amposta (Permanyer y Salas, 2005; Salas y Permanyer, 2003).

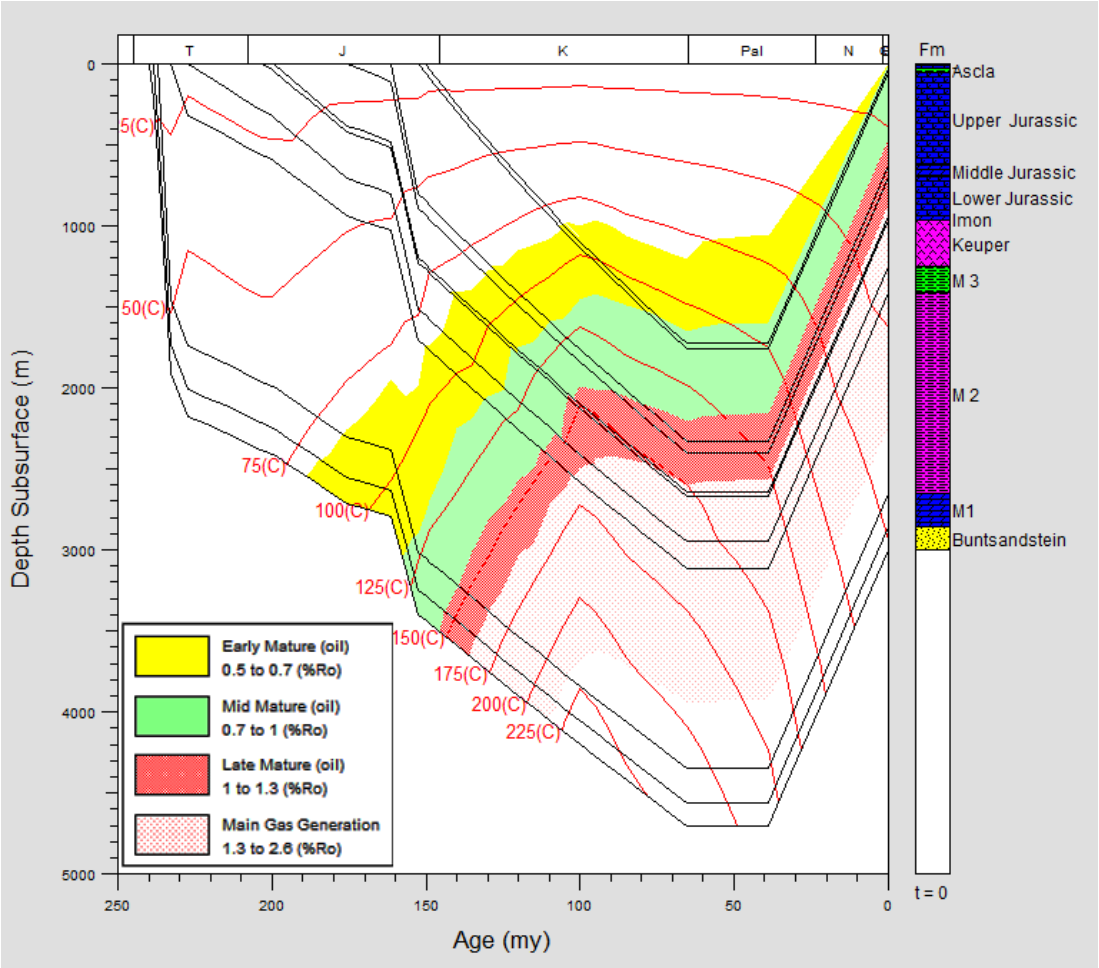

Fig. 4.3. Modelo térmico (R. Salas, com Per.) construido para el pozo Bovalar 1). Las rocas madre del Muschelkalk superior (*black-shales*) entraron en ventana del petróleo a 150 Ma (Titónico) y posteriormente en ventana del gas a 100 Ma (Albiense).

Recientemente los microbialitos han monopolizado la atención de investigadores y empresas petrolíferas a raíz del creciente interés en los procesos de biomineralización y en sus productos (Dupraz et al., 2009), así como en el posible comportamiento de sus sucesiones como reservorios de hidrocarburos (Parcell, 2002;

Adams et al., 2005; Collins et al., 2006; Ahr, 2009; Awramik y Buchheim, 2012). La caracterización de los tipos de poros en carbonatos microbianos es crucial para la correcta evaluación de sus propiedades petrofísicas y de su potencial como reservorios (Rezende et al., 2012; Tonietto et at., 2012). Las texturas microbianas muestran una considerable heterogeneidad y complejidad, reflejando la variedad de procesos biológicos que intervienen en la formación de los microbialitos (Ahr, 2008; 2009).

En el caso de los trombolitos de la Fm. Smackover del Jurásico superior (Mancini et al., 2004), la calidad de reservorio y la distribución dentro de los montículos microbianos estuvo ampliamente controlada por la distribución de las texturas microbianas y sus morfologías de crecimiento (Parcell, 2002). Aunque los parámetros deposicionales fueron clave en la calidad del reservorio, los procesos diagenéticos (diagénesis marina temprana y de enterramiento, Benson, 1985) ejercieron una influencia significativa en su calidad. La porosidad en los trombolitos de la Fm. Smackover es del tipo *shelter* y fenestral y sobre ella se superpone una porosidad secundaria intercristalina y vacuolar en dolomías (Mancini et al., 2004).

En el caso de la Cuenca Triásica Catalana, los microbialitos ladinienses mostraron una marcada porosidad antigua ligada a su textura y al ambiente deposicional. Esta porosidad ha sido afectada por diversos estadios diagenéticos (diagénesis marina, exposición subaérea, dolomitización y reemplazamiento tardío de sulfatos; Tucker y Marshall, 2004).

Las facies microbianas F10 presentan una porosidad fenestral aparentemente asociada con la degradación de tapices microbianos y calcimicrobios durante una fase de diagénesis temprana. La facies F11, muestra una textura de granos bien clasificados con abundante porosidad móldica relacionada a ambientes de alta energía. Además, la facies F12 contiene una porosidad vacuolar secundaria muy marcada que afecta a las fábricas dolomíticas, así como una porosidad móldica asociada a evaporitas. La facies F15 desarrolló una porosidad móldica producida durante el reemplazamiento de dolomita por minerales evaporíticos.

Además, como señalaron Tucker y Marshall (2004), la porosidad móldica caracterizada por cavidades de pseudomorfos de evaporitas fue común en las facies F12. Estos autores registraron numerosas vacuolas en las facies trombolíticas, parcialmente rellenadas con cementos calcíticos, cuarcíticos y *chert*, con evidencias de minúsculas inclusiones de anhidrita. El origen de estas vacuolas ha sido atribuido a la disolución local de parches de yeso/ anhidrita que reemplazó a la dolomita. La evidencia del reemplazamiento por sulfatos también fue registrado en las facies F15 y localmente en las facies F10. Tal y como apuntaron Tucker y Marshall (2004), este

reemplazamiento pudo haber sido contemporáneo con el depósito de las facies F9, cuando la cuenca estaba sometida a momentos de hipersalinidad periódica o condiciones anóxicas, o incluso durante una fase de enterramiento somero poco después del depósito de las facies evaporíticas del Keuper (Carniense).

Otra similitud entre los microbialitos del Ladiniense en la Cuenca Triásica Catalana y los trombolitos de la Fm. Smackover (Oxfordiense) es que ambos se encuentran dolomitizados. La dolomitización resultó en la creación de una porosidad vacuolar e intercristalina en dolomita que mejoró la interconectividad del reservorio en todos los tipos de trombolitos oxfordienses (Mancini et al., 2004). La dolomitización de los trombolitos de la Fm. Smackover ha sido asociada a un fenómeno de diagénesis temprana debido a la interacción de la paleotopografía, fluctuaciones del nivel del mar, circulación restringida de los océanos debido a barreras físicas y a un clima árido (Benson y Mancini, 1999).

De forma similar, los trombolitos ladinienses (facies F12) han sido afectados por una disolución de calcita-cementación de dolomita (Tucker y Marshall, 2004), la cual dio lugar a cementos esparíticos y fibrosos con fábrica *drusy* que conservan las texturas dolomíticas primarias. Según Tucker y Marshall (2004) este proceso sugiere una dolomitización temprana antes que el sedimento se hubiese estabilizado a calcita. Además, estos autores sugieren que las vacuolas de las facies arrecifales (facies F14) fueron generadas después de la dolomitización de los cementos marinos botroidales. De hecho, las facies trombolíticas registraron vacuolas tempranas posteriores a la dolomitización y cementos botroidales marinos dentro de la matriz micrítica *clotted* y también tapizados por costras microbianas formadas por *Tubiphytes*.

Por lo tanto, la dolomitización temprana pudo haber incrementado la porosidad original de los trombolitos ladinienses (facies F12), aumentando la conectividad y la calidad de reservorio. Por otro lado, los microbialitos ladinienses pueden haber experimentado un incremento de la porosidad durante o después la fase diagenética tardía de reemplazamiento de sulfatos por cementos de cuarzo y calcita.

Entender las heterogeneidades de facies depende ampliamente de la arquitectura de facies, la cual está vinculada con la evolución de la cuenca, fluctuaciones del nivel del mar y sus condicionantes paleoambientales, y también de la distribución de su porosidad, la cual está influenciada por la naturaleza de los fluidos que la rellenan y de la evolución diagenética (Rezende et at., 2012; Terra et al., 2012; Tonietto et al., 2012). Este conocimiento tiene implicaciones decisivas en lo referente al modelado y caracterización de reservorios en carbonatos microbianos.

En el caso de la Cuenca Triásica Catalana, se han podido ubicar los microbialitos en un contexto preciso de estratigrafía secuencial, y se han caracterizado

sus depósitos como unidades de reservorio empleando los valores de porosidad modal y sus respectivas arquitecturas sedimentarias (Mercedes-Martín et al., 2013a, b).

Conclusiones

5.1. Modelos deposicionales y Estratigrafía Secuencial

El registro estratigráfico del Ladiniense de la Cuenca Triásica Catalana muestra una gran diversidad de asociaciones de facies carbonatadas cuya distribución está esencialmente controlada por una subsidencia sinrift inducida por fallas, la cual también afectó a los materiales del Triásico medio de la cuenca Ibérica y del Ebro. El análisis estratigráfico y sedimentológico detallado ha permitido subdividir el registro sedimentario en 2 secuencias transgresivo-regresivas (T-R). Estas secuencias reflejan una ciclicidad de tercer orden estando caracterizadas por patrones de apilamiento específicos. Los modelos deposicionales de ambas secuencias pueden ser interpretados como rampas carbonatadas controladas por bloques fracturados (*fault-block ramps*), con ángulos deposicionales reducidos y una amplia continuidad lateral de facies.

La secuencia T-R1 (Ladiniense inferior) contiene los depósitos microbianos más significativos, esto es, estromatolitos en la rampa interna (hasta 7 m de espesor) y trombolitos en la rampa media (una media de 40 m de espesor). El TST1 se corresponde con una rampa carbonatada dominada por oleaje (*swell-dominated fault-block carbonate ramp*) y el RST1 se corresponde con una rampa carbonatada dominada por microbios (*microbial-dominated fault-block carbonate ramp)*. Por su parte, la secuencia T-R2 (Ladiniense superior) está constituida por estromatolitos oolíticos en la rampa interna y *shoals* internos y lagoons protegidos en la rampa

media. El TST2 se corresponde con una rampa carbonatada dominada por bancos-barrera (*barrier-bank dominated fault-block carbonate ramp*), mientras que el RST2 representa a una rampa carbonatada somera (*shallow-water fault-block carbonate ramp*).

Una caída del nivel del mar de al menos 50 m tuvo lugar en la parte más alta del Ladiniense inferior, dejando la plataforma bajo los efectos de una exposición subaérea. Como resultado, se formó un prominente carst con evidencias de incisiones erosivas y rellenos de brechas de colapso en las zonas de la rampa interna y media. La discordancia subaérea resultante limita las dos secuencias T-R. Esta discordancia también ha sido reconocida en numerosas cuencas del Tetis occidental y del Archipiélago Ártico Canadiense.

5.2. Subsidencia y acomodación

La rápida subsidencia sinrift fue el principal factor que controló el espacio de acomodación y los estilos deposicionales de las secuencias T-R. Diferentes barreras paleogeográficas se desarrollaron coetáneamente a las fracturas sinsedimentarias, dando lugar a cambios laterales y verticales de facies específicos. Algunas de esas barreras físicas se infieren de los siguientes hechos: 1) un cambio lateral de facies abrupto entre las facies fangosas y las facies de grano grueso (p. ej., la transición del dominio de Prades al dominio de Gaià en el TST1); 2) la abundancia de trombolitos (en el dominio de Prades prosperaron biostromos y montículos microbianos (*mud-mounds*) durante el RST1); 3) la proliferación de estromatolitos (p. ej., los estromatolitos planares y dómicos del RST1 crecieron en una bahía hipersalina protegida de los efectos de olas y corrientes); y 4) el desarrollo de bajíos (*shoals*) externos y plataformas internas protegidas (*lagoons*) en el TST2. La configuración escalonada heredada del RST1 proporcionó la paleotopografía adecuada sobre la que se distribuyeron los diferentes ambientes sedimentarios.

5.3. Arquitectura sedimentaria y calidad de reservorio en los microbialitos

Los microbialitos se desarrollaron mayoritariamente durante los periodos regresivos de tercer orden (RST1 y RST2) y fueron los principales constituyentes en volumen en todos los dominios sedimentarios. Sus depósitos muestran una marcada extensión lateral siendo esencialmente cuerpos tabulares (hasta 45 Km de extensión

lateral y 40 m de espesor en trombolitos, y hasta 30 Km de extensión lateral y 7 m de espesor en estromatolitos). Además, las facies microbianas fueron proporcionalmente más abundantes en las porciones de la rampa interna y media. A su vez, las facies fangosas y de grano grueso fueron más predominantes y extensivas durante los periodos transgresivos de tercer orden (TST1 y TST2) y volumetricamente más abundantes en las porciones de la rampa media y externa.

Las facies microbianas desarrollaron una variada porosidad ligada a la textura deposicional. La facies F10 tiene hasta un 10% de porosidad modal (fenestral). La facies F11 muestra hasta un 20% (móldica por disolución de granos). La facies F10 y F11 presentan hasta un 15% de porosidad secundaria antigua del tipo vacuolar (*vuggy*) rellenada por cementos calcíticos de tipo mosaico *blocky*. La facies F12 y F15 desarrollaron hasta un 15% de porosidad móldica por reemplazamiento de evaporitas. Porosidad y arquitectura hacen que los microbialitos del Ladiniense de la Cuenca Triásica Catalana sean candidatos apropiados para la modelización de reservorios de hidrocarburos y valiosos como análogos. Estos análogos pueden ser utilizados mayoritariamente en cuencas con regimenes de subsidencia rápida sinrift, en las que se desarrollen rampas carbonatadas del tipo *fault-block* y que estén caracterizadas por la abundancia de estromatolitos y trombolitos.

5.4. Procesos de formación de los microbialitos

Se han reconocido tres tipos de microbialitos: 1) estromatolitos *sensu stricto*, 2) estromatolitos oolíticos-peloidales y 3) trombolitos. Los estromatolitos s.s. se formaron por la combinación de procesos de atrapamiento e incorporación de partículas de tamaño limo, así como por precipitación de $CaCO_3$ mediada por microbios. Los estromatolitos oolíticos-peloidales están compuestos por capas de textura *grainstone* formadas por procesos de atrapamiento e incorporación de granos simples y agregados, con fusión de granos y micritización, así como capas de textura *mudstone* dominadas por restos o evidencias microbianas, así como por vestigios de procesos endolíticos y perforaciones. Los trombolitos se desarrollaron a través de procesos de acreción, incorporación de granos e incrustaciones mediadas por la actividad microbiana, así como por procesos de cementación penetrativa, mediados por fenómenos físico-químicos.

Los estromatolitos s.s. se depositaron en un ambiente intermareal, en una bahía hipersalina-llanura mareal, presentando similitudes con los de Shark Bay (Australia). Los estromatolitos oolíticos-peloidales se acumularon en un *fore-shoal* interno somero,

sometido a condiciones de energía moderada a alta, por encima del nivel de oleaje de buen tiempo. Estos microbialitos presentan una notable similitud con los actuales de Bahamas. Los trombolitos se depositaron por debajo del nivel de oleaje de buen tiempo, en ambientes submareales someros, sometidos a condiciones de energía baja a moderada y probablemente en la zona fótica. Los atributos texturales y faunísticos son similares a los que aparecen en las cuencas coetáneas como en Dolomitas (Italia-Alpes).

El crecimiento de los estromatolitos s.s. estuvo condicionado por la limitada presencia de fuerte oleaje y corrientes de marea junto con el aporte restringido de sedimento de grano grueso. Las condiciones hipersalinas favorecieron su desarrollo, mientras que el incremento de acomodación explicaría la transición de mega- y macromorfologías (de formas planares a formas dómicas a lo largo del tiempo). El crecimiento de los estromatolitos oolítico-peloidales estuvo influenciado por la combinación de periodos de alta energía (alto aporte de sedimento y procesos de atrapamiento e incorporación de granos) con periodos de baja energía (bajo aporte de sedimento y procesos de precipitación microbiana) caracterizados por altas tasas de cementación y rápida litificación. El crecimiento de los trombolitos estuvo controlado por procesos de incrustación y acreción. La distribución y arquitectura de los cementos fibrosos y botroidales sinsedimentarios jugó un rol fundamental el crecimiento vertical y cohesión de los trombolitos. Las surgencias submarinas de aguas hidrotermales a través de zonas de fractura (i.e. falla de La Riba) pudieron haber favorecido el desarrollo y la ubicación de los cuerpos trombolíticos en zonas adyacentes.

La concurrencia de los tres tipos de microbialitos en el RST1 puede ser explicado por la existencia de condiciones oceanográficas inusuales (hipersalinidad, anoxia generalizada?) las cuales produjeron una reducción sustancial de los depredadores de microbios. La yuxtaposición de estromatolitos s.s. y estromatolitos oolítico-peloidales durante el TST2 de la secuencia T-R2 estuvo gobernada por una ciclicidad de cuarto orden, condicionando factores como la batimetría, la energía hidráulica, el tipo de sedimento y las tasas de acumulación, los cuales controlaron el tipo de procesos y comunidades microbianas.

En definitiva, los resultados de este estudio revelan que: a) diferentes tipos de comunidades y procesos microbianos coexistieron y actuaron conjuntamente en el mismo subambiente, b) algunos de estos procesos microbianos y no microbianos pueden operar con independencia del ambiente sedimentario, y c) los procesos microbianos y no microbianos pueden haber actuado simultáneamente para construir el armazón microbialítico.

5.5. Naturaleza de los cementos sinsedimentarios

Los cementos marinos fibrosos y botroidales, texturas de corrosión y estructuras microbianas jugaron un papel fundamental en el desarrollo de los trombolitos. La abundancia de estos componentes puede ser explicada por la influencia de surgencias submarinas hidrotermales de fluidos controlados por fallas sinsedimentarias. Estos fluidos supersaturados, podrían también haber inducido la nucleación inorgánica de cementos alrededor de precipitados previos provocados por microbios (*biofilms*). Las texturas y componentes observadas en la Cuenca Triásica Catalana son muy similares a las registradas en la región de las Dolomitas, (Italia), sugiriendo que procesos similares pueden haber tenido lugar simultáneamente en durante el Ladiniense del Tetis occidental.

Bibliografía

Adams, E. W., Grotzinger, J. P., Watters, W. A., Schröder, S., McCormick, D. S. and Al-Siyabi, A. (2005). Digital characterization of thrombolite-stromatolite reef distribution in a carbonate ramp system (terminal Proterozoic, Nama Group, Namibia). *AAPG Bulletin*, 89, 1293-1318.

Aharon, P., 2000. Microbial processes and products fueled by hydrocarbons at submarine seeps. In: Riding, R., Awramik, S. M. (Eds.). *Microbial sediments*. Springer-Verlag, Heilderberg.

Ahr, W. M. 2008. *Geology of carbonate reservoirs: the identification, description, and characterization of hydrocarbon reservoirs in carbonate rocks*. John Wiley & Sons, 277p.

Ahr, W. M. 2009. Microbial carbonates as hydrocarbon reservoirs. *AAPG Search and Discovery Article. AAPG Annual Convention and Exhibition*, Denver, Colorado.

Aitken, J. D., 1967. Classification and environmental significance of crytalgal limestones and dolomites, with illustrations from the Cambrian and Ordovician of south western Alberta. *Jour. Sed. Petrol.*, 37, 1163-1178.

Aitken, J. D., Narbonne, G. M., 1989. Two occurrences of Precambrian thrombolites from the Mackenzie Mountains, Northwestern Canada. *Palaios*, 4, 384-388.

Anadón, P., Canet, C., Friedrich, W. L. 2013. Aragonite stromatolitic buildups from Santorini (Aegean Sea, Greece): Geochemical and palaeontological constraints of the caldera

palaeoenvironment prior to the Minoan eruption (ca 3600 yr bp). *Sedimentology*, 60, 1128-1155.

Andres, M. S., Reid, R. P., 2006. Growth morphologies of modern marine stromatolites: a case study from Highborne Cay, Bahamas. *Sedimen. Geol.*, 185, 319-328.

Arenas, C., Pomar, L., 2010. Microbial deposits in upper Miocene carbonates, Mallorca, Spain. *Palaeogeo., Palaeoclimat., Palaeoecol.*, 297, 465-485.

Arnal, I., Calvet, F., Márquez, L., Márquez-Aliaga, A., Solé de Porta, N. 2002. The epeiric carbonate platform (Imón and Isábena Formations) of the Upper Triassic from the Northeastern Iberian Peninsula. *Act. Geol. Hispan.*, 37, 299-328.

Awramik, S. M., Buchheim, H. P., 2012. The quest for microbialite analogs to the South Atlantic Pre-Salt carbonate hydrocarbon reservoirs of Africa and South America. *HGS International Dinner Meeting talk*. URL: http://www.hgs.org/node/4875

Benson, D. J. 1985. Diagenetic controls on reservoir development and quality, Smackover Formation of southwest Alabama. *Gulf Coast Association of Geological Societies Transactions*, 35, 317-326.

Benson, D. J., Mancini, E. A. 1999. Diagenetic influence on reservoir development and quality in the Smackover updip basement ridge play, southwest Alabama. *Gulf Coast Association of Geological Societies Transactions*, 49, 96-101.

Biddle, K. T. 1984. Triassic sea level changes and the Ladinian-Carnian stage boundary. *Nature*, 308, 631-633.

Blendinger, W., 1986. Isolated stationary carbonate platforms: the Middle Triassic (Ladinian) of the Marmolada area, Dolomites, Italy. *Sedimentology* 33, 159-183.

Blendinger, W., 1994. The carbonate factory of Middle Triassic buildups in the Dolomites, Italy: a quantitative analysis. *Sedimentology*, 41, 1147-1159.

Bond, G. C., Kominz, M. A. 1984. Construction of tectonic subsidence curves for the early Paleozoic miogeocline, southern Canadian Rocky Mountains: Implications for subsidence mechanisms, age of break-up, and crustal thinning. *Geol. Soc. Amer. Bull.,* 95, 155-173.

Bosellini, A., 1984. Progradation geometries of carbonate platforms: examplesfrom the Triassic of the Dolomites, Northen Italy. *Sedimentology*, 31, 1-24.

Bosence, D. 2005. A genetic classification of carbonate platforms based on their basinal and tectonic settings in the Cenozoic. *Sedimentary Geology*, 175, 46-72.

Braga, J.C., Martín, J.M. and Riding, R. 1995. Controls on microbial dome fabric development along a carbonate-siliclastic shelf-basin transect, Miocene, SE Spain. *Palaios*, 10, 347 – 361.

Brandner, R. 1984. Meeresspiegelschwankungen und tektonik in der Trias der NW-Tethys. *Jarb. Geolog. Bunder.*, 126, 435-475.

Brandner, R., Flügel, E., Senowbari-Daryan, B.1991. Microfacies of carbonate slope boulders: indicator of the source area (Middle Triassic: Mahlknecht Cliff, Western Dolomites). *Facies*, 25, 279-296.

Browne, K. M., Golubic, S., Seong-Joo, L., 2000. Shallow marine microbial carbonate deposits. In: Riding, R., Awramik, S. M. (Eds.). *Microbial sediments*. Springer-Verlag, Heilderberg.

Buczynski, C., Chafetz, H. S. 1991. Habit of bacterially induced precipitates of calcium carbonate and the influence of medium viscosity on mineralogy. *J. Sedimentary Research*, 61, 226-233.

Burchette, T. P. & Wright, V. P. 1992. Carbonate ramp depositional systems. *Sedimentary Geology*, 79, 3-57.

Burne, R.V. and Moore, L. S. 1987. Microbialites; organosedimentary deposits of benthic microbial communities. *Palaios*, 2, 241-254.

Calvet, F., Ramon, X., 1987. Estratigrafía, sedimentología y diagenesis del Muschelkalk inferior de los Catalánides. *Cuad. Geol. Iber.*, 11, 141-169.

Calvet, F., Tucker, M. E., 1995. Mud-mound with reefal caps in the upper Muschelkalk (Triassic), eastern Spain. *Spec. Publs. Int. Assoc. Sediment*. 23, 311-333.

Calvet, F., Tucker, M. E., Henton, J. M., 1990. Middle Triassic carbonate ramp systems in the Catalan Basin, northeast Spain: facies, systems tracts, sequences and controls. *Spec. Publs. Int. Assoc. Sediment*. 9, 79-108.

Calvet, F., Tucker, M. E.1988. Outer ramp cycles in the Upper Muschelkalk of the Catalan Basin, northeast Spain. *Sedimen. Geol.*, 57, 185-198.

Campbell, K.A., Farmer, J.D., Des Marais D., 2002. Ancient hydrocarbon seeps from the Mesozoic convergent margin of California; carbonate geochemistry, fluids and palaeoenvironments. *Geofluids*, 2, 63–94.

Canet, C., Prol-Ledesma, R. M., Melgarejo, J-C., Reyes, A., 2003. Methane-related carbonates formed at submarine hydrothermal springs: a new setting for microbially-derived carbonates?. *Marine Geology*, 199, 245-261.

Cartaña, J. 1994. Noves aportacions paleontològiques al Muschelkalk superior de les Muntanyes de Prades: el cas del Pinetell. *Quaderns de Vilaniu*, 25, 67-93.

Castanier, S., Maurin, A., Perthuisot, J.-P. 1989. Production microbienne expérimentale de corpuscules carbonatés sphéroidaux à structure fibro-radiaire. Réflexions sur la définition des ooïdes *Bull. Soc. Géol. France.*, 5, 589–595.

Catuneanu, O., Abreu, V., Bhattacharya, J.P., Blum, M. D., Dalrymple, R.W., Eriksson, P. G., Fielding, C. R., Fisher, W. L., Galloway, W. E., Gibling, M. R., Giles, K. A., Holbrook, J. M., Jordan, R., Kendall, C. G. St. C., Macurda, B., Martinsen, O. J., Miall, A. D., Neal, J. E., Nummedal, D., Pomar, L., Posamentier, H.W., Pratt, B. R., Sarg, J.F., Shanley, K.W., Steel, R. J., Strasser, A., Tucker, M. E., Winker, C., 2009. Towards the standardization of sequence stratigraphy. Earth-Science Reviews, 92, 1–33.

Catuneanu, O., Galloway, E., Kendall, G. St. C., Miall, A. D., Posamentier, H. W., Strasser, A. & Tucker, M. E. 2011. Sequence stratigraphy: methodology and nomenclature. *Newsletter Stratigraphy*, 44, 173-275.

Chafetz, H. S., Buczynski, C.,1992. Bacterially induced lithification of microbial mats. *Palaios*, 7, 277-293.

Chafetz, H. S., 1986. Marine peloids: a product of bacterially induced precipitation of calcite. *J. Sedim. Petrol.*, 56, 812-817.

Chafetz, H. S., Folk, R. L., 1984. Travertines: depositional morphology and bacterially constructed constituents. *J. Sed. Research*, 54, 289-316.

Choquette, P. W. & Pray, L. 1980. Geological nomemclature and classification of porosity in sedimentary carbonates. *AAPG Bulletin*, 54, 207-250.

Chow, N., George, A. D., 2004. Tepee-shaped agglutinated microbialites: an example from a Famenian carbonate platform on the Lennard Shelf, northen Canning Basin, Western Australia. *Sedimentology*, 51, 253-265.

Collins, J. F., Kenter, J. A. M., Harris, P. M., Kuanysheva, G., Fischer, D. J., Steffen, K. L. 2006. Facies and reservoir-quality variations in the Late Visean to Bashkirian outer platform, rim, and flank of the Tengiz buildup, Precaspian Basin, Kazakhstan. In Harris, P. M., Weber, L. J. (Eds.). Giant hydrocarbon reservoirs of the world: from rocks to reservoir characterization and modelling. *AAPG Memoir*, 88/ *SEPM Special Publication*, pp. 55-95.

Colombié, C. & Strasser, A. 2005. Facies, cycles, and controls on the evolution of a keep-up carbonate platform (Kimmeridgian, Swiss Jura). *Sedimentology*, 52, 1207-1227.

Dill, R. F., Shinn, E. A., Jones, A. T., Kelly, K., Steinen, R. P., 1986. Giant subtidal stromatolites forming in normal salinity water. *Nature*, 324, 55-58.

Doglioni, C. 1987. Tectonics of the Dolomites. *J. Struct. Geol*., 9, 181-193.

Dorobek, S., Piccoli, L., Coffey, B., Adams, A., 2012. Carbonate rock-forming processes in the Pre-Salt “sag” successions of Campos Basin, off-shore Brazil: evidence for seasonal, dominantly abiotic carbonate precipitation, substrate controls, and broader geologic implications. *AAPG Search and Discovery Article. AAPG Hedberg Conference, Microbial Carbonate Reservoir Charaterization*, Houston, Texas.

Dravis, J. J, 1983. Hardened subtidal stromatolites, Bahamas. *Science*, 219, 385-386.

Dupraz, C. and Visscher, P.T. 2005. Microbial lithification in marine stromatolites and hypersaline mats. *Trends Microbiol*., 13, 429–438.

Dupraz, C., Reid, P. R, Braissant, O., Decho, A. W, Norman, R. S., Visscher, P. T., 2009. Processes of carbonate precipitation in modern microbial mats. *Earth-Science Reviews*, 96, 141-162.

Eckman, J.E., Andres, M.S., Marinelli, R.L., Bowlin, E., Reid, R.P., Aspden, R.J., Paterson, D. M., 2008. Wave and sediment dynamics along a shallow subtidal sandy beach inhabited by modern stromatolites. *Geobiology* 6, 21–32.

Embry, A. F. & Johannessen, E. P.1992. T-R sequence stratigraphy, facies analysis and reservoir distribution in the uppermost Triassic-Lower Jurassic succession, Western Sverdrup Basin, Arctic Canada. In: Vorren, T. O., Bergsager, E., Dahl-Stamnes, O. A.,

Holter, E., Johansen, B., Lie, E., Lund, T. B. (Eds). Arctic Geology and Petroleum Potential. Special Publication, 2. *Norwegian Petroleum Society*, pp. 121-146.

Embry, A. F. 1988. Triassic sea-level changes: evidence from the Canadian Arctic Archipelago. In: Wilgus, C. K. Hastings, B. S. Kendall, C.G. St. C. , Posamentier, H. W., Ross, C. A., Van Wagoner, J. C. (Eds). Sea-Level Changes - An Integrated Approach. *Soc. Sedim. Geolo. Spec. Public*., 42, 2.

Emmerich, A., Zamparelli, V., Bechstädt, T. & Zühlke, R. 2005. The reefal margin and slope of a Middle Triassic carbonate platform: the Latemar (Dolomites, Italy). *Facies*, 50, 573-614.

Erwin, D.H. 1994. The Permo-Triassic extinction. *Nature*, 367, 231–236.

Esteban, M., Budai, T., Juhász, E., Lapointe, P., 2009. Alteration of Triassic carbonates in the Buda Mountains – a hydrothermal model. *Central European Geology*, 52, 1-29.

Esteban, M., Calzada, S. Y Via, L. 1977. Ambiente deposicional de los yacimientos fosilíferos del Muschelkalk superior de Alcover-Montral. *Cuad. Geol. Ibérica*, 4, 189-200.

Feldmann, M., McKenzie, J. A., 1997. Messinian stromatolite-thrombolite associations, Santa Pola, SE Spain: an analogue for the Paleozoic? *Sedimentology*, 44, 893-914.

Flügel, E, Senowbari-Daryan, B., 2001. Triassic reefs of the Tethys. In: Stanley, G. (Ed.). The history and sedimentology of ancient reef systems. *Topics in Geobiology*, 17, 217-249.

Flügel, E., 2004. *Microfacies of carbonate rocks. Analysis, interpretation and application*. Springer-Verlag Berlin Heildelberg.

Ford, T. D., Pedley, H. M., 1996. A review of tufa and travertine deposits of the world. *Earth-Science Reviews*, 41, 117-175.

Fregenal-Martínez, M, Meléndez, N., Martínez-Delcòs, X. 1995. Montsec and Montral- Alcover, Two Konservat-Lagerstätten, Catalonia, Spain. Field trip guide book-II. Inter. Sympo. Litho. Limes. *Institut d'Estudis Ilerdencs*, 12-29. Lleida

Gaetani, M., Gnaccolini, M., Jadoul, F., Garzanti, E.1998. Multiorder sequence stratigraphy in the Triassic system of the Western Southern Alps. In: De Graciansky, P-C., Hardenbol, J., Jacquin, T., Vail, P. (Eds). Mesozoic and Cenozoic Sequence Stratigraphy of European Basins. *Soc. Sedim. Geolo. Spec. Public*., 60, 702-717.

García del Cura, M. A., Sanz-Moreno, M. E., De-los-Rios, M. A., Ascaso, C. 2013. Microbial dolomite in fresh water carbonate deposits. *Sedimentology* (accepted).

Garrett, P., 1970. Phanerozoic stromatolites: noncompetitive ecologic restriction by grazing and burrowing animals. *Science*, 169, 171-173.

Gerdes, G., Krumbein, W.E., Reineck, H. E. 1985. The depositional record of sandy, versicolored tidal flats (Mellum Island, southern North Sea). *J. Sediment. Petrol*., 55, 265–278.

Gianolla, P., Jacquin, T. 1998. Triassic sequence stratigraphic framework of western European basins. In: De Graciansky, P-C., Hardenbol, J., Jacquin, T., Vail, P. (Eds). Mesozoic and Cenozoic sequence stratigraphy of European Basins. *Soc. Sedim. Geolo. Spec. Public*., 60, 643-650.

Gianolla, P., Caggiati, M., Furin, S. 2011. Response of carbonate systems to sea-level drop: a case study from Middle Triassic of the Dolomites (Italy). *Abst., 28th IAS Meeting of Sediment*., Zaragoza, Spain.

Gianolla, P., Jacquin, T. 1998. Triassic sequence stratigraphic framework of western European basins. In: Graciansky, P. C., Hardenbol, J., Jacquin, T., Vail, P. (Eds). Mesozoic and Cenozoic sequence stratigraphy of European Basins. *Soc. Sedim. Geol., Spec. Publ*., 60, 643-650.

Goggin, V., Jacquin, T. 1998. A sequence stratigraphic framework of the marine and continental Triassic series in the Paris Basin, France. In: De Graciansky, P-C., Hardenbol, J., Jacquin, T., Vail, P. (Eds). Mesozoic and Cenozoic sequence stratigraphy of European Basins. *Soc. Sedim. Geolo. Spec. Public*., 60, 667-690.

Golubic, S., Browne, K. M., 1996. Schizothrix gebeleinii sp.nov. builds subtidal stromatolites, Lee Stocking Island, Bahamas. *Algol Stud*., 83, 273-290.

Gómez-Pérez, I., 2003. An Early Jurassic deep-water stromatolitic bioherm related to possible methane seepage (Los Molles Formation, Neuquén, Argentina). *Palaeogeo., Palaeoclim., Palaeoeco*., 201, 21-49.

Gradstein, F. M., Agterberg, F. P. Ogg, J. G., Hardenbol, J. Van Veen, P., Thierry, J., Huang, Z. 1994. A Mesozoic time scale. *Journ. Geoph. Res*., 99, 24051-24074.

Gradstein, F. M., Ogg, J. G. & Hilgen, F. J. 2012. On the geological time scale. *Newsletter Stratigraphy*, 45/2, 171-188

Haq, B. U., Hardenbol, J., Vail, P. R.1987. Chronology of fluctuating sea levels since the Triassic. *Science*, 235, 1156-1167.

Harris, M. T, Ellis, J & Purkis, S. J. 2013. Assessing the extent of carbonate deposition in early rift settings. *AAPG Bulletin*, 97, 27-60

Harris, M. T., 1994. The foreslope and toe-of-slope facies of the Middle Triassic Latemar buildup (Dolomites, Northen Italy). *J. Sed. Research*, 64, 132-145.

Harris, M. T.1993. Reef fabrics, biotic crusts and syndepositional cements of the Latemar reef margin (Middle Triassic), northern Italy. *Sedimentology*, 40, 383-401.

Harwood, C. L., Sumner, D.Y., 2011. Microbialites of the Neoproterozoic Beck Spring Dolomite, Southern California. *Sedimentology*, 58, 1648-1673.

Jahnert, R., Collins, L. B., 2011. Significance of subtidal microbial deposits in Shark Bay, Australia. *Mar. Geol*., 286, 106-111.

Jahnert, R., Collins, L. B., 2012. Characteristics, distribution and morphogenesis of subtidal microbial systems in Shark Bay, Australia. *Mar. Geol*., 303, 115-136.

Jahnert, R., Collins, L. B., 2013. Controls on microbial activity and tidal flat evolution in Shark Bay, Western Australia. *Sedimentology*, 60, 1071-1099.

Johnson, J. G. & Murphy, M. A.1984. Time-rock model for Siluro-Devonian continental shelf, western United States. *Geological Society America Bulletin*, 96, 567-587.

Kah, L. C., Grotzinger, J. P., 1992. Early Proterozoic (1.9 Ga) thrombolites of the Rocknest Formation, Nortwest Territories, Canada. *Palaios*, 7, 305-315.

Kahle, C. F., 2001. Biosedimentology of a Silurian thrombolite reef with meter-scale growth framework cavities. *Journal of Sed. Res*., 71 (3), 410-422.

Keim, L., Schlager, W., 2001. Quantitative compositional analysis of a Triassic carbonate platform (Southern Alps, Italy). *Sed. Geol.* 139, 261-283.

Kennard, J. M., 1994. Thrombolites and stromatolites within shale-carbonate cycles, Middle-Late Cambrian Shannon Formation, Amadeus Basin, Central Australia. In: Sarfati, J. B-S., Monty, C. L. V., (Eds.) *Phanerozoic stromatolites* II. Kluver.

Kennard, J. M., James, N. P., 1986. Thrombolites and stromatolites: two distinct types of microbial structures. *Palaios*, 1, 492-503.

Knorre, H.v. y Krumbein, W. E. 2000. Bacterial calcification. In: Riding, R., Awramik, S. M. (Eds.). *Microbial sediments*. Springer-Verlag, Heilderberg.

Lees, A., y Miller, J. 1985. Facies variation in Waulsortian buildups. Part 2: Mid-Dinantian buildups from Europe and North America. *Geol. J*., 20, 159-180.

Lehrmann, D. J., 1999. Early Triassic calcimicrobial mounds and biostromes of the Nanpanjiang basin, south China. *Geology*, 27, 359-362.

Logan, B. W., Cebulski, D. E., 1970. Sedimentary environments of Shark Bay, Western Australia. In: Logan, B. W., Davies, G. R., Read J. F., Cebulski, D. E., (Eds.). Carbonate sedimentation and environments, Shark Bay, Western Australia. *AAPG Memoir*, 13, 1-37.

Logan, B. W., Hoffman, P., Gebelein, C. D., 1974. Algal mats, cryptalgal fabrics, and structures, Hamelin Pool, Western Australia. In: Logan, B. W., Read, J. F., Hagan, G. M., Hoffman, P., Brown, R. G., Woods P. J., Gebelein, C. (Eds.) Evolution and diagenesis of Quaternary carbonate sequences, Shark Bay, Western Australia. *AAPG Memoir*, 22, 140-194.

Luis Dias, J. 2005. Tectônica, estratigrafia e sedimentaçâo no Andar Aptiano da margem leste brasileira. Boletim Geociências da Petrobras, Rio de Janeiro, 13, 1, 7-25.

Macintyre, I. G., Prufert-Bebout, L., Reid., R. P., 2000. The role of endolithic cyanobacteria in the formation of lithified laminae in Bahama stromatolites. *Sedimentology*, 47, 915-921.

Macintyre, I. G., Reid, R. P., Steneck, R. S., 1996. Growth history of stromatolites in a Holocene fringing reef, Stocking Island, Bahamas. *J. Sed. Research*, 66, 231-242.

Mancini, E. A., Llinás, C. L., Parcell, W. C., Aurell, M., Bádenas, B., Leinfelder, R. R., Benson, D. J. 2004. Upper Jurassic thrombolite reservoir play, northeastern Gulf of Mexico. *AAPG Bulletin*, 88, 11, 1573-1602.

Marangon, A., Gattolin, G., Della Porta, G. & Preto, N. 2011. The Latemar: A flat-topped, steep fronted platform dominated by microbialites and synsedimentary cements. *Sed. Geol*., 240, 97-114.

March, M. 1986. Conodontos del Triásico medio de los sectores meridionales de la Cordillera Ibérica y de los Catalánides. PhD Thesis, Valencia. 136p.

Marquez, A. 1983. Bivalvos del Triásico medio del sector meridional de la Cordillera Ibérica y de los Catalánides. PhD Thesis, Valencia. 429p.

Marzo, M. 1980. El Buntsandstein de los Catalánides: Estratigrafía y procesos de sedimentación. PhD Thesis, Univ. Barcel., 317 pp.

Mckenzie, D. P. 1978. Some remarks on the development of sedimentary basins. *Ear. Planet. Scien. Lett*., 40, 25-32.

Mercedes-Martín R., Salas R., Arenas C., 2013a. Facies heterogeneity and depositional models of a Ladinian (Middle Triassic) microbial-dominated carbonate ramp system (Catalan Coastal Ranges, NE Spain). *Journal of Marine and Petroleum Geology*, 46, 107-128.

Mercedes-Martín R., Salas R., Arenas C., 2013b. Microbial-dominated carbonate platforms during the Ladinian rifting: sequence stratigraphy and evolution of accommodation in a fault-controlled setting (Catalan Coastal Ranges, NE Spain). *Basin Research*, 25, 1-28.

Mercedes-Martín, R, Arenas C., Salas. R. 2013c. Controls on microbialite diversity and occurrence in the Ladinian (Middle Triassic) of the Catalan Basin (NE Spain). *Palaeogeo., Palaeoclim., Palaeoeco* (under review).

Merz-Preiß, M., Riding, R., 1999. Cyanobacterial tufa calcification in two freshwater streams: ambient environment, chemical thresholds and biological processes. *Sediment. Geol*. 126, 103– 124.

Monty C. L. V., 1967. Distribution and structure of Recent stromatolitic algal mats, eastern Andros Island, Bahamas. *Ann. Soc. Géol. Belg*., 90, 55-100.

Monty, C. L. V. 1995. The rise and nature of carbonate mud-mounds: an introductory actualistic approach. In: Monty, C.L.V, Bosence, D. W. J., Bridges, P. H., Pratt, B. R. (Eds).Carbonate mud-mounds: their origin and evolution. *Intern. Assoc. Sediment., Spec. Publ*., 23, 11-48.

Neumann, A. C., Macintyre, I. G. 1985. Reef response to sea level rise: keep-up, catch-up or give-up. Proceed. *Fifth Intern. Coral Reef Cong*., Tahiti, 3, 105-110.

Parcell, W. C. 2002. Sequence stratigraphic controls on the development of microbial fabrics and growth forms: implications for reservoir quality distribution in the Upper Jurassic (Oxfordian) Smackover Formation, Eastern Gulf Coast, USA. *Carbonates and Evaporites*, 17, 2, 166-181.

Peckman, J., Thiel, V., Michaels, W., Clari, P., Gaillard, C., Martire, L., Reitner, J. 1999. Cold seep deposits of Beauvoisin (Oxfordian; southeastern France) and Marmorito (Miocene; northern Italy): microbially induced authigenic carbonates. *Int. Journal. Eart. Sciences*, 88, 60-75.

Peckmann, J., Reimer, A., Luth, U., Luth, C., Hansen, B. T., Heinicke, C., Hoefs, J., Reitner, J. 2001. Methane-derived carbonates and authigenic pyrite from the northwestern Black Sea. *Marine Geology*, 177, 129–150.

Pentecost, A. 1985. Investigation of variation in heterocyst numbers, sheath development and false-branching in natural popuilations of Scytonemaceae (Cyanobacteria). *Arcean Hydrobiology*, 102, 343-353

Pentecost, A., 1991. Calcification processes in algae and cyanobacteria. In: Riding, R. (Ed.). *Calcareous algae and stromatolites*, Springer-Verlag, Berlin.

Permanyer, A. y Salas, R. 2005. Integrated thermal model, diagenetic history and oil correlation in Western Mediterranean, Spain. *IV ALAGO Workshop on Basin Modelling*, October 2005, Buenos Aires.

Playford, P. E., Cockbain, A. E., 1976. Modern algal stromatolites at Hamelin Pool, a hypersaline barred basin in Shark Bay, Western Australia. In: Walter M. R. (Ed.). Stromatolites. *Developments in Sedimentology*, 20, 193-249. Elsevier, Amsterdam.

Pratt, B. R. 1982. Stromatolitic framework of carbonate mud-mounds. *Jour. Sedimen. Res*., 52, 1203-1227.

Pratt, B. R., Haidl, F. M., 2008. Microbial pach reefs in Upper Ordovician Red River strata, Williston Basin, Saskatchewan: signal of heating in a deteriorating epeiric sea. In: Pratt, B. R., Holmden, C. (Eds.). Dynamics of epeiric seas. *Spec. Pap. Geol. Assoc. Can*. 48, 303-340.

Preto, N., Franceschi, M., Gattolin, G., Massironi, M., Riva, A., Gramigna, P., Bertoldi, L., Nardon, S., 2011. The Latemar: a Middle Triassic polygonal fault-block platform controlled by synsedimentary tectonics. *Sed. Geol*., 234, 1-18.

Pruss, S. B., Bottjer. 2005. The reorganization of reef communities following the end-Permian mass extinction. *Comp. Rend. Palev*., 4, 553-568.

Purdy, E. G., 1963. Recent calcium carbonate facies on the Great Bahama Bank. 1. Petrography and reaction groups. *J. Geol*., 71, 334-355.

Ramos A., Sopeña A., Sánchez-Moya A., Muñoz, A. 1996. Subsidence analysis, maturity modelling and hydrocarbon generation of the Alpine sedimentary sequence in the NW of the Iberian Ranges (Central Spain). *Cuadernos de Geología Ibérica*, 21, 23-53.

Reid, R. P., Macintyre, I. G., Steneck, R. S. A., Browne, K. M., Miller, T. E., 1995. Stromatolites in the Exuma Cays, Bahamas: uncommonly common. *Facies*, 33, 1-18.

Reid, R.P., Visscher, P. T., Decho, A.W., Stolz, J. F., Bebout, B. M., Dupraz, C., Macintyre, I. G., Paerl, H. W., Pinckney, J. L., Prufert-Bebout, L., Steppe, T. F., D. J. Desmarals. 2000. The role of microbes in accretion, lamination and early lithification of modern marine stromatolites. *Nature*, 406, 989-992.

Renaut, R. W., Jones, B., 2000. Microbial precipitates around continental hot Springs and geysers. In: Riding, R., Awramik, S. M. (Eds.). *Microbial sediments*. Springer-Verlag, Heilderberg.

Reolid, M y Nieto, L. M, 2010 Jurassic Fe–Mn macro-oncoids from pelagic swells of the External Subbetic (Spain): evidences of microbial origin. *Geologica Acta*, 8, 1–18

Rezende, M. F, Tonietto, S. N., Pope, M. C. 2012. Three-dimensional pore connectivity evaluation in a Holocene microbialite head. AAPG Search and Discovery Article. *AAPG Hedberg Conference, Microbial Carbonate Reservoir Charaterization,* Houston, Texas.

Riding R., Liang, L., 2005. Geobiology of microbial carbonates: metazoan and seawater saturation state influences on secular trends during the Phanerozoic. *Palaeogeography, Palaeoclimatology, Palaeoecology*, 219, 101-115.

Riding, R. 1991. Classification of microbial carbonates. In: Riding, R. (Ed.). *Calcareous algae and stromatolites*. Springer-Verlag, Berlin.

Riding, R. E, Awramik, S. M., 2000. *Microbial sediments*. Springer-Verlag Berlin Heildelberg.

Riding, R. Tomás, S., 2006. *Stromatolite reef crusts, Early Cretaceous, Spain: bacterial origin of in situ-precipitated peloid microspar? Sedimentology*, 53, 23-34.

Riding, R., 2000. Microbial carbonates: the geological record of calcified bacterial-algal mats and biofilms. *Sedimentology*, 47 (Suppl.), 179-214.

Riding, R., 2002. Biofilm architecture of Phanerozoic cryptic carbonate marine veneers. *Geology*, 30, 21-34.

Riding, R., 2011. Microbialites, stromatolites and thrombolites. In: Reitner., J. and V. Thiel (Eds), *Encyclopedia of Geobiology, Encyclopedia of Earth Science Series*, Springer, Heidelberg, pp. 635-654.

Rodríguez-Martínez, M., Reitner, J., Mas, R., 2011. Micro-framework reconstruction from peloidal-dominated mud mounds (Viséan, SW Spain). *Facies*, 56, 139-156.

Rosenberg, E., 1989. Biofilms on water-soluble substrates. In: Characklis, W.G., Wilderer, P.A. (Eds.), *Structure and Function of Biofilms*. Wiley, Chichester, U.K., pp. 59-72.

Rossi, C., Lozano, R. P., Isanta, N., Hellstrom, J., 2010 Manganese stromatolites in caves: El Soplao (Cantabria, Spain). *Geology*, 38, 1119-1122.

Russo, F., Mastandrea, A., Neri, C. 1998. Evoluzione degli organismi costruttori nelle piataforme Triassiche delle Dolomiti (Italia). *Soc. Geol. Ital. Memor.,* 53, 479-488.

Salas R., Guimera J., Mas R., Martin-Closas C., Melendez A., Alonso A., 2001. Evolution of the Mesozoic Central Iberian Rift System and its Cainozoic inversion (Iberian chain). In: Ziegler, P.A., Cavazza, W., Robertson, A.H.F., Crasquin-Soleau, S. (Eds.). Peri-Tethys memoir 6: Peri-Tethyan Rift/Wrechn Basins and Passive Margins. *Mém. Mus. Hist. Nat*. 186, 145–185.

Salas, R. Y Permanyer, A. 2003. Evidencias de generación de hidrocarburos en la formación de margas del Mas d'Ascla (Jurásico superior, Cadena Ibérica oriental) y su relación con el campo de Amposta de la Cuenca de Tarragona. *Boletín Geológico y Minero*, 114 (1): 75-86

Salas, R., Casas. A. 1993. Mesozoic extensional tectonics, stratigraphy and cristal evolution Turing the Alpine cycle of the eastern Iberian basin. *Tectonophysics*, 228, 33-55.

Sanz-Montero, M.E., Rodríguez Aranda, J.P. and García-del-Cura, M.A. (2008) Dolomite-silica stromatolites in Miocene lacustrine deposits from the Duero Basin Spain. The role of organotemplates in the precipitation of dolomite. *Sedimentology*, 55, 729–750.

Savard, M. M., Beauchamp, B., Veizer, J., 1996. Significance of aragonite cements around Cretaceous marine methane seeps. *J. Sed. Research*, 66, 430-438.

Schlager W. 2000. Sedimentation rates and growth potential of tropical, cool water and mud mound carbonate factories. In E. Insalaco, P.W. Skelton, T.J. Palmer, Carbonate Platform Systems: Components and Interactions. *Geological Society of London, Special Publications*, 178, 217–227.

Schmoker, J. W., Halley, R. B. 1982. Carbonate porosity versus depth: a predictable relation for south Florida. *Am. Assoc. Petrol. Geol.*, 66, 2561-2570.

Sclater, J. G., Christie, P. A. F. 1980. Continental stretching: an explanation of the post-mid Cretaceous subsidence of the Central North Sea Basin. *Journ. Geoph. Resear.*, 85, 3711-3739.

Seeling, M., Emmerich, A., Bechtädt, T., Zühlke, R., 2005. Accomodation/ sedimentantion development and massive early marine cementation: Latemar vs. Concarena (Middle/ Upper Triassic, Southen Alps). *Sed. Geol.*, 175, 439-457.

Senowbari-Daryan, B., 2013. Tubiphytes Maslov, 1956 and description of similar organisms from Triassic reefs of the Tethys. *Facies*, 59, 75-112.

Shapiro, R. S., 2000. A comment on the systematic confusion of thrombolites. *Palaios*, 15, 166-169.

Sharp, I., Verwer, K., Ferreira, H., Lapponi, F., Snidero, M., Machado, V., Holtar, E., Swart, R., Marsh, J., Gindre, L., Puigdefagregas, C, Fejerkov, M., 2013. Pre- and Post-Salt Non-Marine Carbonates of the Namibe Basin, Angola. Microbial carbonates in Space and Time: implications for global exploration and production. *The Geological Society*, London.

Sole de Porta N., Calvet F. & Torrento L. 1987. Análisis palinológico del Triásico de los Catalánides (NE España). *Cuadernos de Geología Ibérica*, 11, 237-254.

Spadafora, A., Perri, E, McKenzie, J. A., Vasconcelos, C. 2010. Microbial biomineralization processes forming modern Ca:Mg carbonate stromatolites. *Sedimentology*, 57, 27-40.

Spence G. H., Tucker M. E. 2007. A proposed integrated multi-signature model for peritidal cycles in carbonates. *Journal of Sedimentary Research*, 77, 797-808.

Steckler, M. S., Watts, A. B. 1978. Subsidence of the Atlantic-type continental margin off New York. *Eart. Plan. Scien. Lett*., 41, 1-13.

Steneck, R. S., Miller, T. E., Reid, R. P., Macintyre, I. G., 1993. Ecological factors controlling the distribution and abundance of intertidal stromatolites, Stocking Island, Bahamas. *Geol. Soc. America*, Abstract 25/6.

Sumner, D. Y., 2000. Microbial versus environmental influences on the morphology of late Archean fenestrated microbialites. In: Riding, R., Awramik, S. M. (Eds.). *Microbial sediments*. Springer-Verlag, Heilderberg.

Terra, G.J.S, Rodrigues, E. B., Freire, E. B., Lykawka, R., Raja Gabaglia, G. P., Hernández, R. M., Hernández, J. I. 2012. Salta Basin, Argentina: a good analog for Phanerozoic lacustrine microbialite-bearing reservoirs. *AAPG Search and Discovery Article. AAPG Hedberg Conference, Microbial Carbonate Reservoir Charaterization,* Houston, Texas.

Tonietto, S. N., Shane, E. K., Ahr, W. M., Pope, M. C. 2012. Pore type characterization and petrophysical properties on microbial carbonate reservoirs. *AAPG Search and Discovery Article. AAPG Hedberg Conference, Microbial Carbonate Reservoir Charaterization*, Houston, Texas.

Tucker M. E., Marshall J. 2004. Diagenesis and geochemistry of Upper Muschelkalk (Triassic) buildups and associated facies in Catalonia (NE Spain): a paper dedicated to Francesc Calvet. *Geologica Acta*, 4, 257-269.

Van der Kooij, B., Immenhauser, A., Steuber, T., Bahamonde Rionda, J. R., Meríno Tomé, O. 2010. Controlling factors of volumetrically important marine carbonate cementation in deep slope settings. *Sedimentology*, 57, 1491-1525.

Vargas H., Gaspar-Escribano J.M., López-Gómez J., Van Wees J-D., Cloetingh S., De La Horra R., Arche, A., 2009. A comparison of the Iberian and Ebro Basins during the Permian and Triassic, Eastern Spain: A quantitative subsidence modelling approach. *Tectonophysics*, 474, 160-183.

Vargas, H. 2002. Análisis y comparación de la subsidencia entre las cuencas Ibérica y Ebro Central durante el Pérmico y Triásico y su relación con el relleno sedimentario. PhD. Thesis, Madrid.

Via, L. Villalta, J. F., Esteban, M. 1977. Paleontología y paleoecología de los yacimientos fosilíferos del Muschelkalk superior entre Alcover y Montral (Montañas de Prades, Província de Tarragona). *Cuad. Geol. Iber.*, 4, 247-256.

Vilas, L., Martín-Chivelet, J., Arias, C. 2003. Integration of subsidente and sequence stratigraphic análisis in the Cretaceous carbonate platforms of the Prebetic (Jumilla-Yecla Region), Spain. *Palaeogeo., Palaeoclimat., Palaeoecol*., 200, 107-129.

Virgili, C. 1958. El Triásico de los Catalánides. *Bol. Inst. Geol., Min., Esp*., 69, 1-856.

Virgili, C., Sopeña, A., Ramon, A., Arche, A. Hernando, A. 1983. El relleno posthercínico y el cominenzo de la sedimentación Mesozoica. *Libr. Jub. Jos. María Rios*, Mad., 2, 25-36.

Visscher, P. T., Reid, R. P., Bebout, B, M. 2000. Microscale observations of sulfate reduction: Correlation of microbial activity with lithified micritic laminae in modern marine stromatolites . *Geology*, 28, 919-922

Watts, A. B. 1981. The U.S. Atlantic continental margin: subsidence history, crustal structure and thermal evolution: Geology of passive continental margins. In: Geology of passive continental margins: history, structure and sedimentology record (with special emphasis on the Atlantic margin). Bally, A. W., Watts, A. B., Grow, J. A. Manspeizer, W., Bernoulli, D., Schreiber, C., Hunt, J. M. (Eds.). *AAPG. Educat. Cours. Not. Ser*. 19, 1-24.

Webb, G. E., 1987. Late Mississippian thrombolite bioherms from the Pitkin Formation of northern Arkansas. *Geol. Soc. America Bull*., 99, 686-698.

Weber L. J., Francis, B. P., Harris, P. M.and Clark, M. 2003. Stratigraphy, lithofacies, and reservoir distribution, Tengiz field, Kazakhstan. In Ahr, W. M., Harris, P. M., Morgan, W. A., Somerville, I. D. (Eds.). Permo-Carboniferous carbonate platforms and reefs. SEPM Special Publication 78 and *AAPG Memoir* 83, 351-394.

Whittle, G. L., Kendall, C.G. St. C, Dill, R. F. Rouch, L., 1993. Carbonate cement fabrics displayed: a traverse across the margin of the Bahamas Platform near Lee Stocking Island in Exuma Cays. *Mar. Geology*, 110, 213-243.

Winlaw, H. D., Matthews, R. K., 1974. Origin and significance of grapestone, Bahamas Islands. *J. Sediment. Petrol*., 44, 921-927.

Ziegler, P. A. 1988. Evolution of Arctic-North Atlantic and the Western Tethys. *AAPG. Mem*. 43, 198pp.

Ziegler, P. A., 1982. Triassic rifts and facies patterns in Western and Central Europe. *Geolog. Runds*. 71, 747-772.

Anejo

Artículo 1:

Mercedes-Martín R., Salas R., Arenas C. 2013a. Microbial-dominated carbonate platforms during the Ladinian rifting: sequence stratigraphy and evolution of accommodation in a fault-controlled setting (Catalan Coastal Ranges, NE Spain). *Basin Research*, 25, 1-28.

Basin Research

IAS EAGE

Basin Research (2013) **25**, 1–28, doi: 10.1111/bre.12026

Microbial-dominated carbonate platforms during the Ladinian rifting: sequence stratigraphy and evolution of accommodation in a fault-controlled setting (Catalan Coastal Ranges, NE Spain)

R. Mercedes-Martín,* R. Salas* and C. Arenas†

**Departament de Geoquímica, Petrologia i Prospecció Geològica, Facultat de Geologia, Universitat de Barcelona, C/Martí i Franquès s/n, Barcelona, 08028, Spain*

†*Departamento de Ciencias de la Tierra, Área de Estratigrafía, Universidad de Zaragoza, C/Pedro Cerbuna, 12, Zaragoza, 50009, Spain*

ABSTRACT

The Upper Muschelkalk sedimentary record constitutes a major transgressive pulse of north-eastern Iberia during the Ladinian. This record is arranged in two transgressive–regressive (T–R) sequences formed by two stepped microbial-dominated carbonate ramp systems where accommodation was mainly controlled by extensional faults. This study seeks to gain new insights into how the evolution of syn-rift subsidence controls the creation of accommodation space, the depositional styles and, especially, the palaeogeographical domains where specific microbialites developed (thrombolites and stromatolites). Thrombolite bodies (at least 40 m thick) display two types of architecture, biostromal and mud-mounded and stromatolite bodies (at least 7 m thick) consist of tabular and domed, head-shaped morphologies. Domed and mounded forms are usually developed during stages of increasing accommodation rates, low-to flat-nelief forms tend to grow in association with periods of low accommodation rates. A sea-level fall of at least 50 m occurred at the end of the Early Ladinian leaving the platform subaerially exposed. As a result, a prominent karst with significant erosional incisions and profuse collapse breccia fillings was formed in the inner and middle ramp settings. The resultant subaerial unconformity bounds T–R sequences 1 and 2. Subsidence curves display two stages of rapid/decelerated total subsidence, constituting two discrete rift/post-rift pulses in the large Triassic rifting period: (i) Buntsandstein – Middle Muschelkalk, and (ii) Late Muschelkalk – Imon Formation (Rhaetian). The second pulse is characterized by a rapid syn-rift subsidence during the Late Muschelkalk, and a decelerated post-rift subsidence throughout the deposition of Keuper facies and Imon Formation. The Late Muschelkalk rapid syn-rift pulse of total subsidence produces gains in accommodation, which controls the development of the stromatolites and thrombolites (biostromes and mud-mounds).

INTRODUCTION

During the Triassic, western and central Europe underwent crustal extension owing to the break-up of Pangaea and the westward expansion of the Neotethyan Ocean. The Triassic Iberian and Catalan basins developed in the Late Permian–Triassic rifting stage (Salas & Casas, 1993) and two marine transgressive–regressive carbonate successions were deposited along the eastern margins of the Iberian plate (Iberia) during the Ladinian (237–228.7 Ma, according to Ogg *et al.*, 2008).

Correspondence: R. Mercedes-Martín, Departament de Geoquímica, Petrologia i Prospecció Geològica, Facultat de Geologia, Universitat de Barcelona, C/ Martí i Franquès s/n, Barcelona 08028, Spain. E-mail: rmercedes@ub.edu.

In many other mid-Triassic epicontinental settings of the Tethys margins, such as France (Goggin & Jacquin, 1998), Germany (Aigner, 1985; Hagdorn, 1991; Feist-Burkhardt *et al.*, 2008; Palermo *et al.*, 2010), Poland (Szulc, 1993, 2000), the western Carpathians (Jaglarz & Szulc, 2003) and Hungary (Török, 1998; Piros, 2002), considerable thicknesses of marine carbonates were deposited, giving rise to extensive carbonate successions characterized by the preferential development of ramp-like carbonate platforms (Bleahu *et al.*, 1996; Haas & Budai, 1995, Rüffer & Zühlke, 1995).

After the demise of metazoan reefs in the end-Permian extinction (Erwin, 1994; Flügel & Senowbari-Daryan, 2001), microbial biostromes and microbial reefs proliferated during the Early Triassic (Lehrmann, 1999; Flügel & Senowbari-Daryan, 2001; Pruss & Bottjer, 2005) and

became a notable carbonate factory. During the Middle Triassic, the Southern Calcareous Alps (Dolomites region) developed isolated carbonate platforms dominated by microbial components (automicrite fabrics *sensu* Neuweiler *et al.*, 1999) and syndepositional cements (Blendinger, 1994, 1996; Keim & Schlager, 2001). Ladinian platform margins with greater taxonomic diversity than Anisian (Russo *et al.*, 1998) were colonized by binding organisms (cyanobacteria, encrusting Porifera and *Tubiphytes*), with organomicrites and abundant cements prevailing over skeletal components. The Middle Triassic Latemar platform of Dolomites is a flat-topped, steep-fronted microbial platform where carbonate production along the margin and slope occurs in mud-mound type (*sensu* Schlager, 2000). The main components are microbialite (clotted peloidal micrite crusts, stromatolites or *Tubiphytes*) and cements (Harris, 1993; Emmerich *et al.*, 2005; Marangon *et al.*, 2011). Thus, most carbonate platforms and reefs of the Dolomites are now regarded as mud-mound platforms dominated by microbialites (Brandner *et al.*, 1991; Harris, 1993; Blendinger, 1994, 1996; Flügel & Senowbari-Daryan, 2001; Marangon *et al.*, 2011).

Microbes formed mound-shaped and biostromal carbonate buildups during the early Triassic reef gap. In the absence of metazoans, microbial reefs developed during this survival phase, acting as framework builders, bafflers and binders (Pruss & Bottjer, 2005). Moreover, microbial communities played a key role in the enhancement of the rigidity and stability of reef structures during their predominance throughout the Triassic. Some Middle Triassic reefs were formed exclusively by abundant and morphologically diverse microbial crust types.

Schlager (2000) highlighted the role of cool-water and especially mud-mound carbonate factories as an alternative to the tropical shoal-water factories in the Phanerozoic. Schlager (2003) considered the rates of growth potential of the mud-mound factory (renamed benthic automicrite factory by Pomar & Hallock, 2008) to be about the same (80–90%) as the tropical standard, taking into account the aggradation capability of the system as a substitute for sediment production by volume or mass. Some authors have stressed the significance of biotically induced carbonate precipitates in the formation of mounds and other microbial reef carbonates through time (Chafetz & Buczynski, 1992; Blendinger, 1994, 1996; Monty, 1995; Pratt, 1995; Reitner & Neuweiler, 1995; Webb, 1996; Riding, 2000; Riding & Awramik, 2000; Keim & Schlager, 2001; among others). These micrites were precipitated by a complex interplay of inorganic and organic chemical reactions, with microbial activity and decaying organic matter playing a central role (Monty, 1995; Schlager, 2000).

For this reason, estimating the growth potential, ecological importance and role of microbial factories in rapid syn-rift subsidence may help to elucidate some key issues of microbial carbonate formation. The Middle Triassic of the Tethys constitutes one of the most interesting periods to better understand the impact of microbialites in sedimentary systems.

This study provides fresh insights into the evolution and sedimentary architecture of a 150-km-long Middle Triassic (Ladinian) microbial-dominated carbonate platform system during a period of syn-rift rapid subsidence. Furthermore, our study estimates the evolution of accommodation space along the basin and through each identified Trangressive–Regressive sequence, and sheds light on how fault-induced subsidence controls the depositional styles and palaeogeographical domains where specific microbialites developed (both thrombolites and stromatolites).

GEOLOGICAL SETTING AND STRATIGRAPHY

The study area is located in the Catalan Coastal Ranges (Fig. 1). The Catalan Coastal Ranges developed by inversion of the Mesozoic rifts during the Palaeogene (Salas *et al.*, 2001). The outcrops of the present day Triassic Catalan Basin are about 300 km long and 200 km wide with a NE–SW trend. The basin opened towards the SE into the Neotethys sea, whereas the fully marine facies graded into more clastic-dominated facies towards the western and northern parts of the basin adjacent to the Spanish Meseta (Calvet *et al.*, 1990).

The Permian to Middle Triassic graben systems of Iberia, as in other areas of central and southern Europe, were closely related to the rapid southward propagation of the northern Europe–Greenland sea rift and the westward propagation of the Neotethys sea. This resulted in the formation of a complex system of grabens and horsts, many of which are superimposed on Permo–Carboniferous fracture systems (Ziegler, 1982, 1988). During the opening of the western Neotethys (the North Atlantic and the Bay of Biscay), Iberia was repeatedly affected by extensional tectonics giving rise to several large intraplate Mesozoic rift systems (Salas *et al.*, 2001).

The Late Permian and Mesozoic evolution of Iberia can be divided into three major rift cycles and post-rift stages (Salas & Casas, 1993; Ramos *et al.*, 1996; Salas *et al.*, 2001). One of them is the Late Permian–Triassic rift cycle, which broadly affected the eastern part of the Iberian plate.

Using more accurate analytical techniques, the Salas & Casas (1993) Late Permian–Triassic rift cycle could be divided into several syn-rift and post-rift phases (Vargas *et al.*, 2009). These authors differentiated up to four syn-rift phases and one general post-rift extensional phase in the Iberian Chain, and up to three syn-rift and two post-rift phases in the Triassic basement of the Tertiary Ebro Basin. In the Iberian Chain, the first syn-rift rapid subsidence phase took place in the Autunian (Early Permian). Later, during the Thüringian (Late Permian), a second syn-rift phase occurred in this area. The third rifting phase took place between the Scythian and the Ladinian.

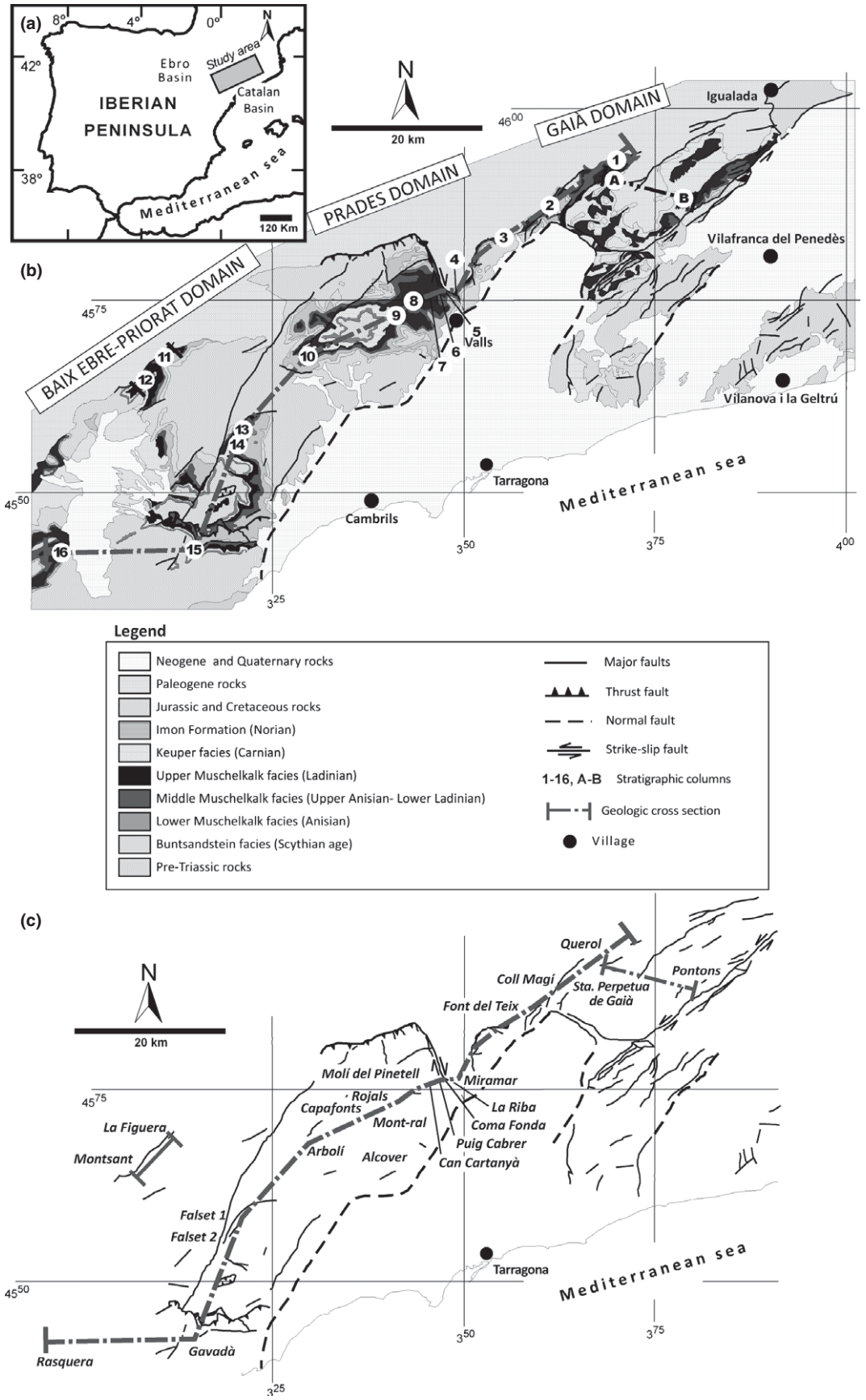

Fig. 1. (a) Location of the study area and nearby basins. (b) Geological map of the Catalan Basin showing the main rock types and Alpine structure (modified after Institut Cartogràfic de Catalunya). (c) Main localities used in the text. See legend for further details.

The Carnian and Norian stages corresponding to the Keuper facies underwent a general post-rift phase of thermal subsidence. The last rapid tectonic subsidence phase appeared during the Rhaetian (Late Triassic) and lasted until the Early Jurassic.

Moreover, the Triassic basement of the Tertiary Ebro Basin underwent a different subsidence pattern during the Triassic. This area displayed an initial and rapid subsidence phase during the Early–Middle Triassic (Scythian to Ladinian). In some areas later, short post-rift stage took place at the start of the Carnian. A second syn-rift phase occurred in the Middle Carnian and thereafter a second post-rift period between the uppermost Carnian and the Norian. The third rapid tectonic subsidence phase started in the earliest Rhaetian and lasted until the Early Jurassic (Vargas *et al.*, 2009).

Subsidence evolution during the Triassic strongly suggests that the Ladinian stage was a period of ubiquitous rapid syn-rift subsidence in the eastern part of the Iberian plate, where extensive carbonate deposits developed.

Broadly speaking, these Triassic fault-controlled basins were filled with sediments attributed to Germanic facies during the Late Permian and Triassic. These facies are characterized by a tripartite stratigraphical subdivision, with the lower part comprising continental Buntsandstein clastics and red beds, the middle part being composed of marine Muschelkalk carbonates, evaporites and red beds, and the upper part consisting of tidal and sabkha deposits of the Keuper facies (Virgili *et al.*, 1983).

The Muschelkalk facies (Anisian to Ladinian, Middle Triassic) consist of two marine carbonate units separated by a siliciclastic–evaporite unit. The first carbonate unit is Anisian in age and corresponds to the so-called Lower Muschelkalk facies, which has been widely recorded in the Triassic Catalan Basin (Marzo, 1980; Calvet & Ramon, 1987; and Calvet *et al.*, 1990). The second carbonate unit, which is the most important, is well represented in the Triassic Catalan Basin. This unit is divided into two depositional sequences of Ladinian age according to Calvet & Tucker (1995) (Fig. 2).

The thickness of the Upper Muschelkalk varies from around 100 m in the northern part of the study area to over 140 m in the south. The Upper Muschelkalk record of the Triassic Catalan Basin was subdivided by Calvet *et al.* (1987) into three palaeogeographical domains, from north-east to south-west: the Gaià domain, the Prades domain and the Baix Ebre-Priorat domain (Fig. 1).

The Upper Muschelkalk facies is constituted by various lithostratigraphic units (Fig. 2) in these domains (Calvet *et al.*, 1987). These authors recognized four units in the Gaià domain, which, from base to top, are as follows: (i) Rojals oolitic limestones-dolomites; (ii) Benifallet bioturbated limestones-dolomites; (iii) Querol stromatolites; and (iv) Capafonts dolomites, marls, shales, stromatolites and supratidal breccias. In the Prades domain, the Upper Muschelkalk has been divided into five units, from base to top: (i) the Rojals unit; (ii) the Benifallet unit; (iii) la Riba mud-mounds; (iv) Alcover laminated dolomites; and (v) the Capafonts unit. In the Baix Ebre-Priorat domain, the Upper Muschelkalk consists of five units, which, from base to top, are as follows: (i) the Rojals unit; (ii) the Benifallet unit; (iii) Rasquera limestones-dolomites and shales with *Daonella* (Calvet & Tucker, 1988); (iv) Tivissa limestones-dolomites and shales; and (v) the Capafonts unit. The lowermost stratigraphic units (Rojals and Benifallet) and the uppermost ones (Capafonts) are present in all domains (Fig. 2).

The sequence stratigraphic analysis of Calvet & Tucker (1995) interpreted the Middle Muschelkalk evaporites and marls and the Rojals unit (high-energy tidal oolitic limestone-dolomite deposits) as the lowstand systems tract of the first sequence (LST1). The transgressive systems tract(TSTI) is constituted by the Benifallet unit (lagoonal to shoal bioturbated limestones-dolomites). Furthermore, the highstand systems tract of this sequence in the Prades domain is composed of the la Riba mud-mound unit (Fig. 2), where the Alcover unit onlaps the la Riba unit, indicating the presence of a sequence boundary at this point in the succession (Fig. 2).

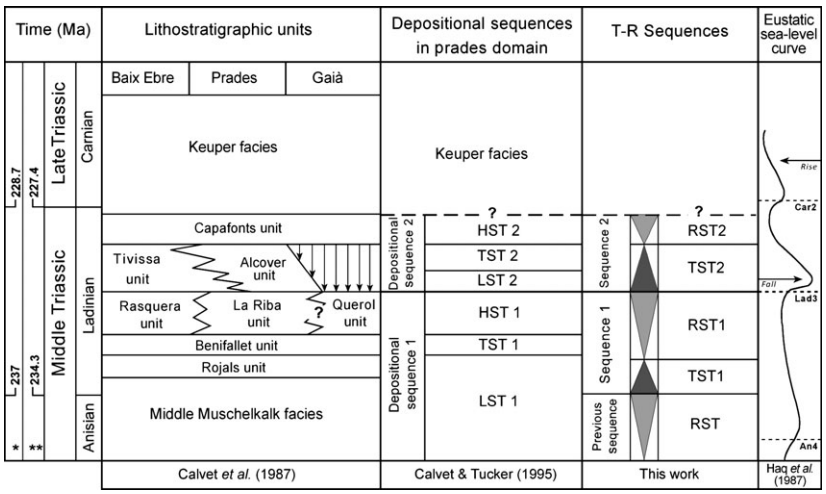

Fig. 2. (a) Lithostratigraphic framework of the Catalan Basin during part of the Middle Triassic, modified after Calvet *et al.* (1987). Palaeogeographical domains are also indicated. Absolute ages from Ogg *et al.* (2008)* and Gradstein *et al.* (1994)**. Depositional sequences defined in the Prades domain by Calvet & Tucker (1995). Ladinian Transgressive–Regressive sequences (T–R sequences) proposed in this study. Short-term eustatic curve of Haq *et al.* (1987).

In the Prades domain, the lowstand systems tract of the second sequence (Calvet & Tucker, 1995) comprises the lower part of the Alcover unit, although these authors do mention that this facies could also represent the early-transgressive systems tract. The Capafonts unit has a regressive character and constitutes the highstand systems tract (Fig. 2).

Calvet *et al.* (1990) suggested that the Rojals and the Benifallet units are Lower Ladinian. According to Goy (1995), the Rasquera unit is thought to be Lower Ladinian (Fassanian) in age, and the Tivissa and Alcover units are Upper Ladinian (Longobardian). Using palynomorphs, Solé *et al.* (1987) gave an Upper Ladinian age to the Capafonts unit.

Most of the Triassic Upper Muschelkalk carbonates of the study area are partly to totally dolomitized, although relict primary fabrics can be recognized. Tucker & Marshall (2004) concluded that the dolomitization of the la Riba unit took place through circulating seawater, probably induced by sea-level changes during the deposition of the Alcover unit or shortly after.

METHODS

Fieldwork was undertaken on 18 well-exposed stratigraphic sections from localities between Pontons and Rasquera, which were measured across a NE–SW 150-km-long exposure of the Catalan Coastal Ranges. Six of the sections were measured in the proximal domain, six were logged in the central domain and the remaining seven sections in the distal domain. The base of Keuper facies (Carnian in age) was plotted as a datum of the stratigraphic sections in the correlation panels. In addition, the stratigraphic data from the la Figuera-Montsant and Santa Perpetua de Gaià-Pontons sections were projected over the main cross-section transect. The sequence stratigraphic terminology used in the correlation panel follows the concepts of Catuneanu *et al.* (2009, 2011).

A detailed stratigraphic and sedimentological analysis was carried out for each section adopting the ideas proposed by Spence & Tucker (2007) when identifying the bounding surfaces between each parasequence and parasequence set in the field. Furthermore, microfacies analyses were performed on more than 200 thin sections and on 150 polished slabs of samples collected during the fieldwork campaign.

As for the sequence stratigraphic methodology, the transgressive–regressive (T–R) sequence stratigraphic model (Johnson & Murphy, 1984; Embry & Johannessen, 1992) was used to recognize the stratigraphic surfaces (summarized in Catuneanu *et al.* 2009). These surfaces are subaerial unconformities (SU), transgressive surfaces (TS), maximum regressive surfaces or zones (MRS/MRZ) (Catuneanu *et al.* 2009, 2011) and maximum flooding zones (MFZ, *sensu* Strasser *et al.*, 1999).

Line drawings of outcrop photomosaics were made to identify the architecture of the sedimentary bodies, the stratal terminations and their overall sequence stratigraphic relationships in the study area.

To explain the accommodation changes, quantitative subsidence analyses were carried out on three selected stratigraphic sections belonging to the different domains, using standard back-stripping methods (Steckler & Watts, 1978; Sclater & Christie, 1980; Watts, 1981; Bond & Kominz, 1984). The variables used in these techniques involved lithology, absolute age and palaeobathymetry values that were estimated from fossil assemblages, sedimentary facies and depositional environments. To compare the subsidence curves in this study with those of the previous one (Vargas *et al.*, 2009), the absolute ages of Gradstein *et al.* (1994) were used. Equivalences with absolute ages from Ogg *et al.* (2008) are provided in Fig. 2.

Total subsidence (decompacted) was calculated from the stratigraphic record for each sedimentary section selected. Corrections for compaction were made using standard porosity–depth relationships for each lithology following Sclater & Christie (1980) and Schmoker & Halley (1982). No eustatic corrections were performed. A regional quantitative estimation of accommodation was obtained from the total subsidence corrected with estimated palaeobathymetries following the procedure in Vilas *et al.* (2003).

A graphic model displaying the variations in accommodation space in the basin for each T–R sequence was also performed to this end, the maximum flooding zone of each T–R sequence was used as a datum. This method enabled the variations in accommodation in each systems tract along the T–R sequences to be assessed.

FACIES ASSOCIATIONS AND ARCHITECTURE

Seventeen facies assemblages ranging from inner to outer platform environments were described using lithology, depositional texture, skeletal and nonskeletal components, sedimentary features and stratigraphic context. Each facies association represents a specific sedimentary environment depending on the inferred hydraulic conditions, the type of sediment produced and the palaeogeographical background. The recognition of large-scale architectures with a specific distribution in time and space of sedimentary facies and heterogeneities enabled each facies group to be included in a specific depositional setting across the carbonate platform succession: basin, external shoal, sheltered lagoon, internal shoal, beach-barrier and tidal-flat deposits showing more open-marine conditions towards the SW (Mercedes *et al.*, 2011). The facies assemblages studied are described and classified in Tables 1 and 2 and illustrated in Figs 3–5, and the facies architectures are shown in Figs S1–S3, 6. A chart displaying the correlation between the different sedimentary sections and the lateral distribution of facies assemblages is presented in Fig. S4.

Table 1. Facies classification and interpretation of sedimentary environments in the study area

Type of facies	Facies assemblage	Description	Main constituents	Secondary constituents	Sedimentary features	Depositional environments
Coarse-grained grainstone facies associations	F1	Oolitic grainstone	Ooids	Bivalves; peloids (locally)	Low-angle cross-bedding, plane-parallel and herringbone stratification; hummocky cross-stratification (locally); herringbone and wavy lamination; climbing ripples (locally); massive bedding (locally); tidal bundles, tidal channels; basal lag deposits (locally); erosive bases	Marine shallowsubtidal shoals, moderate to high energy conditions. Above fair-weather wave base. Inner-middle ramp
	F2	Cross-bedded skeletal grainstone	Ooids, unidentified bioclasts	Ostracods, gastropods, foraminifera, peloids, intraclasts, litoclasts; cortoids (locally)	Undulous and low-angle cross-bedding, plane-parallel and herringbone stratification; herringbone, ripple, plane-parallel and wavy lamination; climbing ripples (locally); massive bedding (locally); tidal bundles, tidal bars, tidal channels; basal lag deposits (locally); microbial laminations (rare); erosive bases	Marine shallow subtidal beach-barrier island; high energy conditions. Above fair-weather wave base. Internal shoals. Inner ramp
	F3	Peloidal and skeletal wackestone to packstone	Peloids, fragments of bivalves and echinoids	Microoncoids, fragments of gastropods, crinoids; intraclasts	Massive or nodular bedding; herringbone, plane-parallel, ripple and wavy lamination; hummocky cross-stratification (locally); unidentified burrows, hardgrounds and borings (locally); erosive bases	Marine shallow-water, moderate to high energy conditions. Intertidal to subtidal. Above fair-weather wave base. Beach-barrier island? to shoreface carbonate sands
	F4	Oncolitic-oolitic-peloidal floatstone and grainstone	Oncoids, ooids, peloids,intraclasts, fragments of bivalves and echinoids	Fragments of ostreids, echinoids, gastropods, dasyclad algae; cortoids and aggregates (locally)	Massive or nodular bedding; Plane-parallel to low-angle cross-bedding stratification; Erosive bases; Unidentified burrows and root plants; plane-parallel, herringbone, wavy and ripple lamination; tidal bundles and tidal channels; basal lag deposits (locally); hardgrounds and Fe/Mn encrustations	Marine shallow-water, moderate to high energy conditions. Subtidal. Above fair-weather wave base. Sheltered lagoon.
	F5	Bioturbated wackestone and packstone with grainstone	Oncoids, ooids, fragments and whole skeletons of bivalves and echinoids	Black pebble intraclasts; planctonic foraminifera; conodonts	Massive, nodular and undulous bedding. Plane-parallel lamination (rare). Unidentified burrows and ichnofauna	Below fair-weather wave base, moderate energy conditions. Subtidal. Middle ramp
	F6	Wackestone to floatstone of molluscs interbedded with packstone of echinoderms	Oncoids and microoncoids, fragments of crinoids, bivalves and echinoids	Fragments of gastropods; peloids; Microproblematica; foraminifera	Low-angle cross-bedding, ripple, plane-parallel and wavy lamination; massive bedding (locally); tidal bundles; basal lag deposits (locally); unidentified escaping burrows; erosive bases	Marine shallow-water, moderate to high energy conditions. Above fair-weather wave base. Subtidal. Middle ramp

(Continued)

Table 1 (Continued)

Type of facies	Facies assemblage	Description	Main constituents	Secondary constituents	Sedimentary features	Depositional environments
Muddy facies associations	F7	Strongly burrowed skeletal mudstone to wackestone	Fragments of bivalves and echinoids, quartz grains	Fragments of gastropods, peloids, carbonatic intraclasts	Massive or nodular bedding, *Planolites* ichnofauna; *Thalassinoides* ichnofauna (locally); plane-parallel, ripple and wavy lamination (locally); tidal channels and tidal bars; tidal bundles (locally), hummocky cross-stratification (rare); conglomerate lag deposits (locally); slump-scars and carbonate breccias (rarely)	Marine shallow-water, moderate to high energy conditions. Above fair-weather wave base. Hypersaline intertidal to subtidal sheltered lagoons and tidal flats
	F8	Burrowed skeletal mudstone to packstone interbedded with marls	Peloids, fragments of bivalves and echinoids	Fragments of gastropods, intraclasts, *Tubiphytes,* foraminifera; cephalopods, crinoids, brachiopods, ostreids, bryozoans and ostracods (rare); oncoids, aggregates (rare); quartz grains (locally)	Massive or nodular bedding; plane-parallel, wavy and ripple lamination (occassionally); unidentified burrows; *Planolites* ichnofauna; *Thalassinoides* ichnofauna (locally); erosive bases; channelized deposits (calciturbidites?) and slumps (locally); hardgrounds and Fe/Mn mineralizations	Below storm wave base, moderate to low energy conditions. Deep subtidal. Outer ramp.
	F9	Thin-bedded laminated dolomicrite-dolomudstone	Fragments and whole skeletons of molluscs and macroinvertebrates	Small fragments of bivalves and other unidentified skeletal components	Event-bedding stratification; plane-parallel and ripple lamination (locally); Deep-water ichnofauna; unidentified burrows and borings; gas-bubble casts; evaporite moulds; hardgrounds and Fe/Mn encustrations (locally)	Below fair-weather wave base, low-energy restricted conditions. Subtidal. Middle-outer ramp
Microbialites and related facies associations	F10	Planar and domal stromatolites	Microbial laminations (domal and planar in shape)	Flat-pebble intraclasts (locally)	Microbial laminations (plane-parallel and domal), birdeyes and fenestral fabrics, teppe structures, karst related structures, hardgrounds, pseudomorphs after evaporite minerals	Marine shallow-water, moderate energy conditions. Hypersaline intertidal to supratidal flats. Inner ramp
	F11	Ooidal-peloidal stromatolites	Microbial laminations (domal and planar in shape), ooids, peloids	Aggregates, flat-pebble intraclasts; Bahamite peloids (locally); Quarz grains	Microbial laminations (planar paralel and domal), birdeyes and fenestral fabrics; tepee structures; plane-parallel, herringbone, wavy and ripple lamination (locally); microhardgrounds, borings; tidal channels (rare)	Marine shallow-water, moderate to high energy conditions. Intertidal to subtidal. Above fair-weather wave base. Internal fore-shoals. Inner ramp

(Continued)

Table 1 (Continued)

Type of facies	Facies assemblage	Description	Main constituents	Secondary constituents	Sedimentary features	Depositional environments
	F12	Microbial-peloidal thrombolites	Peloids, micropeloids, Microproblematica (*Garwoodia, Tubiphytes, Cayeuxia*)	Intraclasts, bivalves, oncoids, quarz grains, foraminifera	Massive or nodular bedding; erosive bases (locally); microbial laminations	Below fair-weather wave base, low to moderate energy conditions. Subtidal. Outer ramp.
	F13	Calcimicrobial boundstone with bioclasts	Calcimicrobes, fragments of bivalves, gastropods	Fe/Mn encrustrations and hardgrounds (locally)	Massive bedding; plane-parallel and ripple lamination (locally); Microbial laminations (domal and planar in shape); Birdeyes and fenestral fabrics	Marine shallow-water, moderate to high energy conditions. Above fair-weather wave base. Intertidal. Middle ramp
	F14	Coral-microbial boundstone to rudstone	Scleractinian corals, worm tubes, sponges?, peloids, organomicrites	Intraclasts, fragments of bivalves; foraminifera, serpulids, Microproblematica *(Garwoodia, Girvanella*?, *Tubiphytes*),	Massive bedding, hardgrounds, unidentified burrows (locally)	Marine shallow-water, moderate to high energy conditions. Above fair-weather wave base. Subtidal. Middle ramp
	F15	Laminated packstone of oncoids and peloids	Oncoids, peloids, intraclasts, fragments of bivalves and echinoids	Peloidal micrite and filamentous microbial remains	Massive bedding; microbial laminations (planar paralel and domal), birdeyes and fenestral fabrics; ripple and plane-parallel lamination (locally); Calcite pseudomorphs after evaporite minerals	Marine shallow-water, moderate energy conditions. Intertidal to supratidal flats. Inner-middle ramp
	F16	Packstone to rudstone of dasyclads, bioclasts and peloids	Intraclasts, peloids, fragments of Dasyclad algae, *Tubiphytes*	Fragments of bivalves, gastropods, echinoids; foraminifera, Microproblematica; Microbial boundstones and skeletal stromatolites (locally)	Massive bedding to low-angle cross-bedding, plane-paralel and ripple lamination. Hardgrounds and Fe/Mn encrustrations (locally); Erosive bases	Marine shallow-water, moderate to high energy conditions. Above fair-weather wave base. Subtidal. Middle ramp
	F17	Foreslope dolomitic breccias	Carbonate clasts	Microproblematica encrusters	Massive to coarsely bedding. Poor to moderate sorting; polymictic composition; heterometric; clast-supported and mud-supported (locally); subangular to subrounded clasts.	Below fair-weather wave base to hemipelagic, low-energy conditions. Subtidal. Outer ramp

Table 2. Features of microbial-related structures of facies F10, F11 and F12.

Type of facies	Facies assemblage	Description	Features of microbial-related structures	
Microbialitic facies associations	F10	Planar and domal stromatolites	Type 1 *Geometry*: stratiform, tabular, rarely dome-shaped *Thickness*: 5 m *Width*: - *Lateral extension*: at least 30 Km *Internal structure*: vertically stacked, flat-laminated to undulatory laminae *Microstructure*: alternation of dark and light dolomite layers Light: ochre dolospar/microdolospar laminae (up to 7 mm thick) Dark: grey, wavy micrite laminae (up to 3 mm thick) Continuity: consistent to irregularly variable. *Other remarks*: small dome-shaped bodies (up to 15 cm high and 20 cm wide) and low synoptic relief bodies with a conical profile (up to 2 cm high and 5 cm wide)	Type 2 *Geometry*: large, head-shaped, domed buildups commonly linked laterally *Thickness*: 2 m *Width*: 6 m *Lateral extension*: at least 20 km *Internal structure:* planar, smooth laminae. Wavy to slightly wrinkled (lower part). Flat-laminated to undulatory (upper part) *Microstructure*: alternation of dark and light dolomite layers Light: ochre/brown dolospar/microdolospar laminae (up to 1 mm thick) Dark: grey, dolomitic laminae (up to 2 mm thick) Continuity: highly consistent *Other remarks*: some small, isolated spaced intermingled domes (up to 10 cm high and 15 cm wide)
	F11	Ooidal-peloidal stromatolites	*Geometry*: Stratiform stromatolites and low-relief hemielliptical microbial buildups *Thickness*: 3 m *Width*: 2 m *Lateral extension*: at least 40 Km *Internal structure*: vertically stacked, flat laminated laminae *Microstructure*: alternation of oolitic grainstone layers and tabular intervals Oolitic grainstone layers: smooth, planar to slightly wavy (sub-millimetre to a few decimetres thick) Tabular intervals: light grey to dark, wavy, massive to clotted dolomicrite and microdolospar laminae (a few millimetres to centimetres thick) Continuity: regularly variable	
	F12	Microbial-peloidal thrombolites	*Geometry*: extensive flat-relief biostromes *Thickness*: 14–40 m *Width*: – *Lateral extension*: at least 45 km *Internal structure*: clotted and peloidal fabric. Rounded to elongated mesoclots surrounded by interframework cavities *Microstructure*: Mesoclots: massive, dense, dark-coloured microcrystalline masses, rounded, amoeboid and arborescent in shape Interframework cavities: with infilling of mudstone to wackestone composed of clotted micrite textures, peloids and micropeloids of irregular shapes and sizes *Other remarks*: microbial remains (e.g. bacteria) and encrusting calcified microfossils (*Garwoodia*, *Tubiphytes*, *Cayeuxia*?, *Microcodium*?). Micropeloidal to peloidal cloudy micrite textures. Microproblematica organisms and various skeletal components	*Geometry*: high-relief bioherms *Thickness*: 14–40 m *Width*: 50–100 m *Lateral extension*: at least 45 km

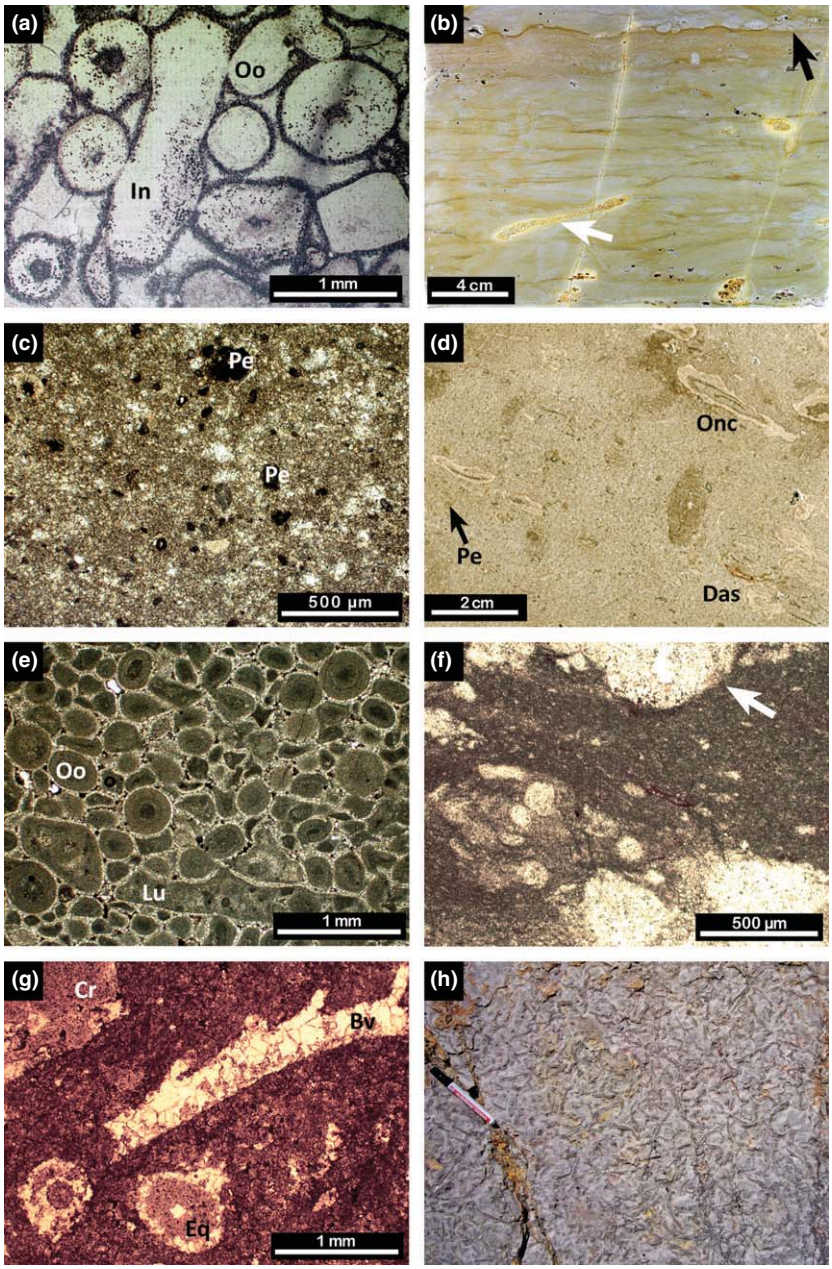

Fig. 3. Photomicrographs and outcrop photographs of representative microfacies assemblages. (a) Oolitic grainstone with ooids (Oo), intraclasts (In) (Facies Assemblage F1; Table 1). (b) Cross-bedded skeletal grainstone shown in polished slab. Undulous and low-angle cross-bedding with ripple lamination and bioturbation traces (white arrow) are observed. Small hardground surfaces are also present (black arrow) (Facies Assemblage F2; Table 1). (c) Peloidal and skeletal wackestone to packstone showing a dolomitized matrix with small peloids (Pe) (Facies Assemblage F3; Table 1). (d) Oncolitic-oolitic-peloidal floatstone and grainstone showing abundant oncoids (Onc) coating elongated dasyclad skeletons (Das) and peloids (Pe) (Facies Assemblage F4; Table 1). (e) Polished slab of the same facies as (d), with well-sorted oolitic grainstone (Oo), some coated-grains (lumps: Lu) (Facies Assemblage F4; Table 1). (f) Bioturbated wackestone and packstone interbedded with grainstone. It shows a wackestone matrix with small peloids and bivalves and unidentified ichnofauna (white arrow). (Facies Assemblage F5; Table 1). (g) Wackestone to floatstone of molluscs interbedded with packstone of echinoderms. A wackestone matrix with large bivalve skeletons (Bv), fragments of crinoids (Cr) and echinoid spines (Eq). (Facies Assemblage F6; Table 1). (h) Outcrop photograph of strongly burrowed skeletal mudstone and wackestone facies showing the bioturbated fabric produced by *Planolites* sp. and other worm-shaped trace fossils. Pencil is 15 cm long (Facies Assemblage F7; Table 1).

For the sake of simplicity, the facies assemblages were grouped into three large facies associations based on sediment composition: (i) coarse-grained grainstone facies associations; (ii) muddy facies associations; and (iii) microbialites and related facies associations.

Coarse-grained grainstone facies associations

Six types of coarse-grained carbonate facies were identified in the Ladinian strata of the study area: oolitic

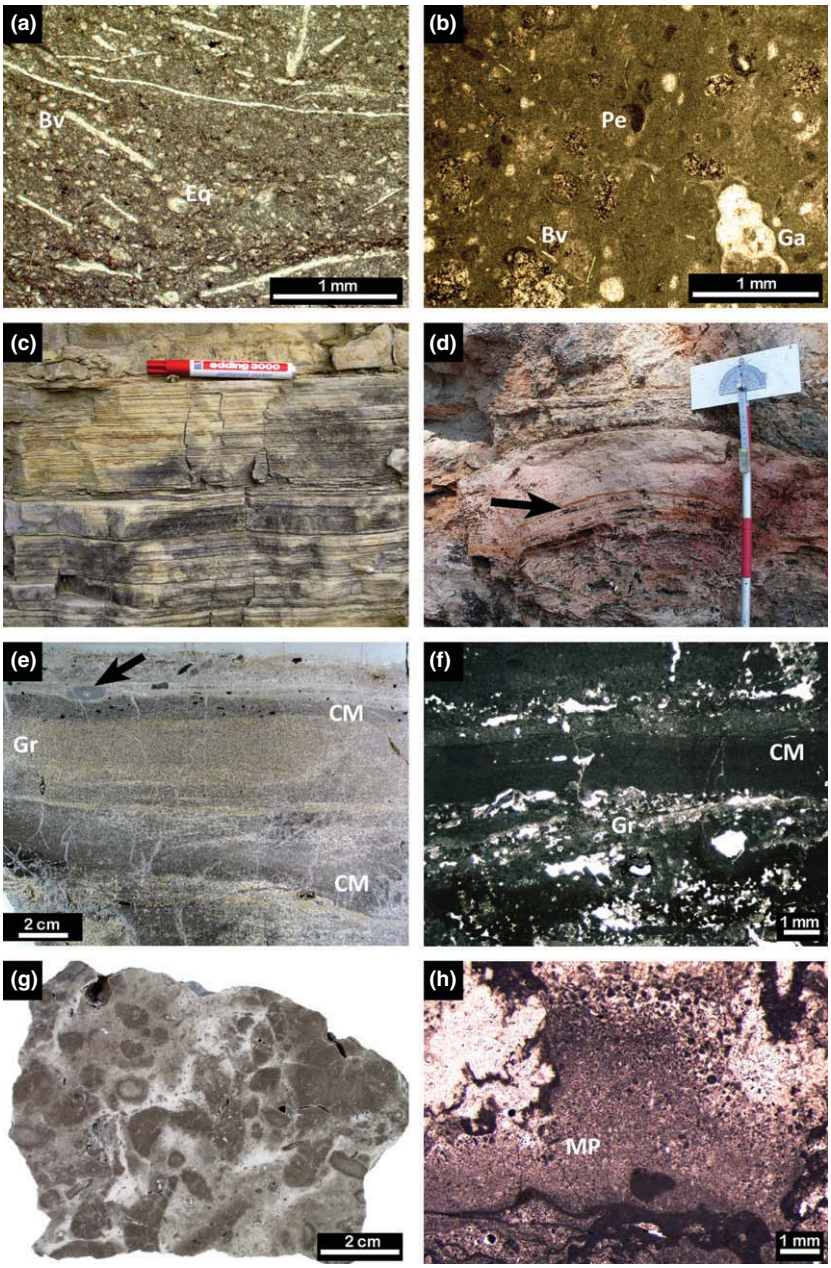

Fig. 4. Photomicrographs and outcrop photographs of representative microfacies assemblages (a) Strongly burrowed skeletal mudstone to wackestone facies with fragments of flattened bivalves (Bv) and echinoid spines (Eq) (Facies Assemblage F7; Table 1). (b) Burrowed skeletal mudstone to packstone interbedded with marls. Peloids (Pe), fragments of bivalves (Bv), echinoids and gastropods (Ga) are present in a muddy matrix (Facies Assemblage F8; Table 1). (c) Outcrop photograph of the thin-bedded laminated dolomicrite-dolomudstone showing the crudely plane-parallel laminated facies. Ripple lamination is usually observed (upper left). The marker is 15 cm long (Facies Assemblage F9; Table 1). (d) Planar and domal stromatolites shown in an outcrop picture of 80-cm-thick stromatolitic dome. Note the fenestral fabric across the macroscopic laminae (black arrow) (Facies Assemblage F10; Table 1 and 2). (e) Polished slab photograph of ooidal-peloidal stromatolites showing the macroscopic alternation of layers. Grainstone layers (Gr) show an extensive moldic and keystone porosity. Some intraclastic layers (black arrow) cap the clotted micrite layers (CM) (Facies Assemblage F11; Table 1 and 2). (f) The same facies as (e) displaying an alternation of massive to clotted micrite layers (CM) with smooth, planar to slightly wavy oolitic-peloidal grainstone intervals (Gr) (Facies Assemblage F11; Table 1 and 2). (g) Polished slab of microbial-peloidal thrombolites showing the macroscopic rounded to elongated dark grey coloured mesoclots surrounded by interframework cavities filled with dense to clotted micrite (Facies Assemblage F12; Table 1 and 2). (h) Same facies as (g) displaying cavities containing a filling of mudstone to wackestone composed of clotted micrite textures, peloids and micropeloids (MP) (Facies Assemblage F12; Tables 1 and 2).

grainstone and cross-bedded skeletal grainstone (F1 and F2); peloidal and skeletal wackestone to packstone (F3); oncolitic-oolitic-peloidal floatstone to grainstone (F4); bioturbated wackestone and packstone interbedded with grainstone (F5); and wackestone-floatstone of molluscs interbedded with packstone of echinoderms (F6).

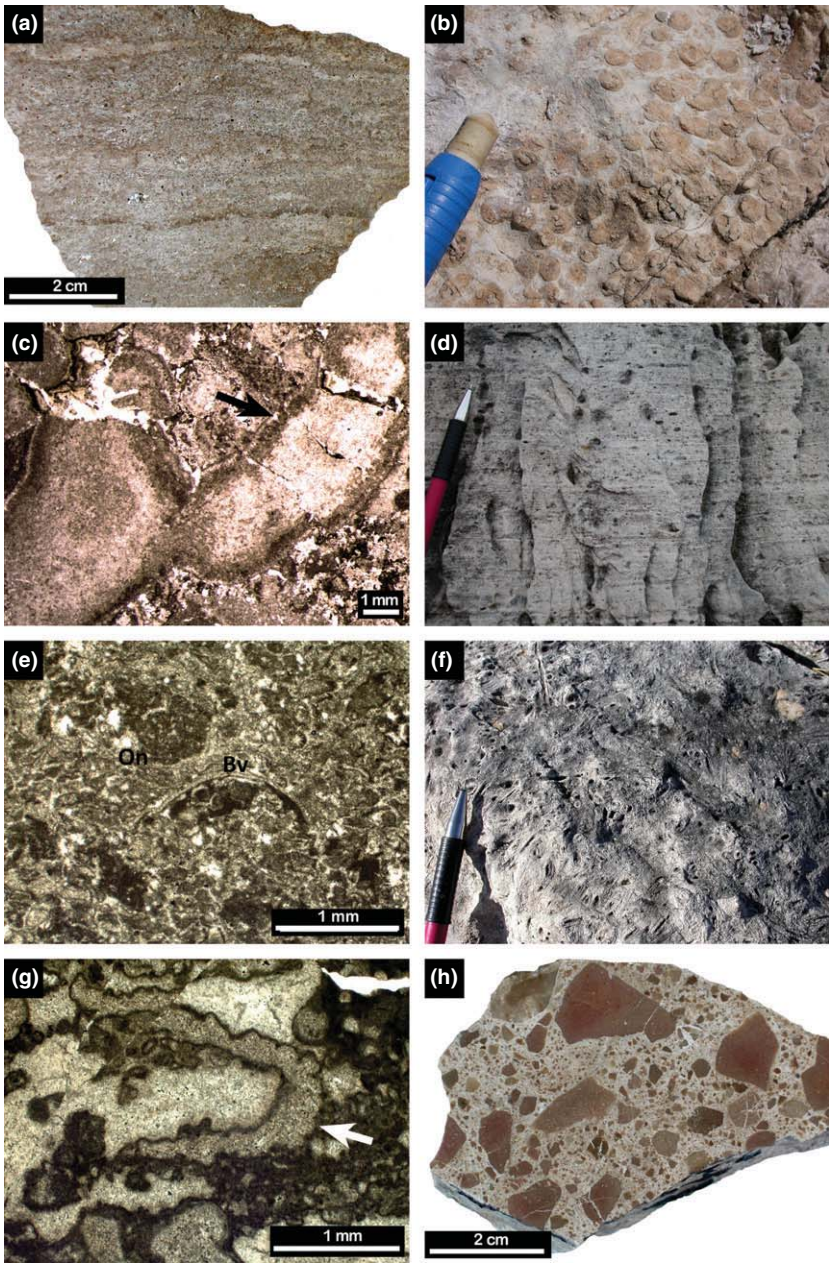

Fig. 5. Photomicrographs and outcrop photographs of representative microfacies assemblages. (a) Polished slab of calcimicrobial boundstone with bioclasts, a flat-laminated microbial bindstone, locally with Fe/Mn incrustations and hardgrounds (darker laminae). Birdeyes and fenestral fabrics are common along the macroscopic laminae (Facies Assemblage F13; Table 1). (b) Outcrop photograph of coral-microbial boundstone to rudstone, showing a small coral reef colony with rounded corallites in a muddy matrix (fragment scale is 3 cm long) (Facies Assemblage F14; Table 1). (c) The same facies as (b) in thin section showing dolomitized wackestone to packstone with branching scleractinian corals (black arrow). (Facies Assemblage F14; Table 1). (d) Outcrop photograph of laminated packstone of oncoids and peloids with plane-parallel laminated fabrics and abundant vuggy porosity (Facies Assemblage F15; Table 1). (e) The same facies as (d) showing a packstone with bivalves (Bv) and oncoids (On) surrounded by organomicrites with clotted and peloidal fabrics (Facies Assemblage F15; Table 1). (f) Outcrop photograph of packstone to rudstone of dasyclads, bioclasts and peloids showing the accumulation of elongated dasyclads talli (scale is 7 cm long) (Facies Assemblage F16; Table 1). (g) The same facies as (f) showing longitudinal sections of dasyclad algae (white arrow) incrusted by *Tubiphytes* sp. (Facies Assemblage F16; Table 1). (h) Polished slab photograph foreslope dolomitic breccias of poorly to moderately sorted, polymict, matrix supported breccias derived from the mud-mound flanks (Facies Assemblage F17; Table 1).

This facies association consists of decimetre to metre-thick (up to 8 m in some cases), light grey to brown limestones composed of dolomitized wackestone to grainstone and locally floatstone texture. They commonly exhibit low-angle cross-bedding with plane-parallel, herringbone, ripple and wavy lamination, but massive to nodular bedding is also present. Tidal bundles, tidal channels and basal lag deposits with beds

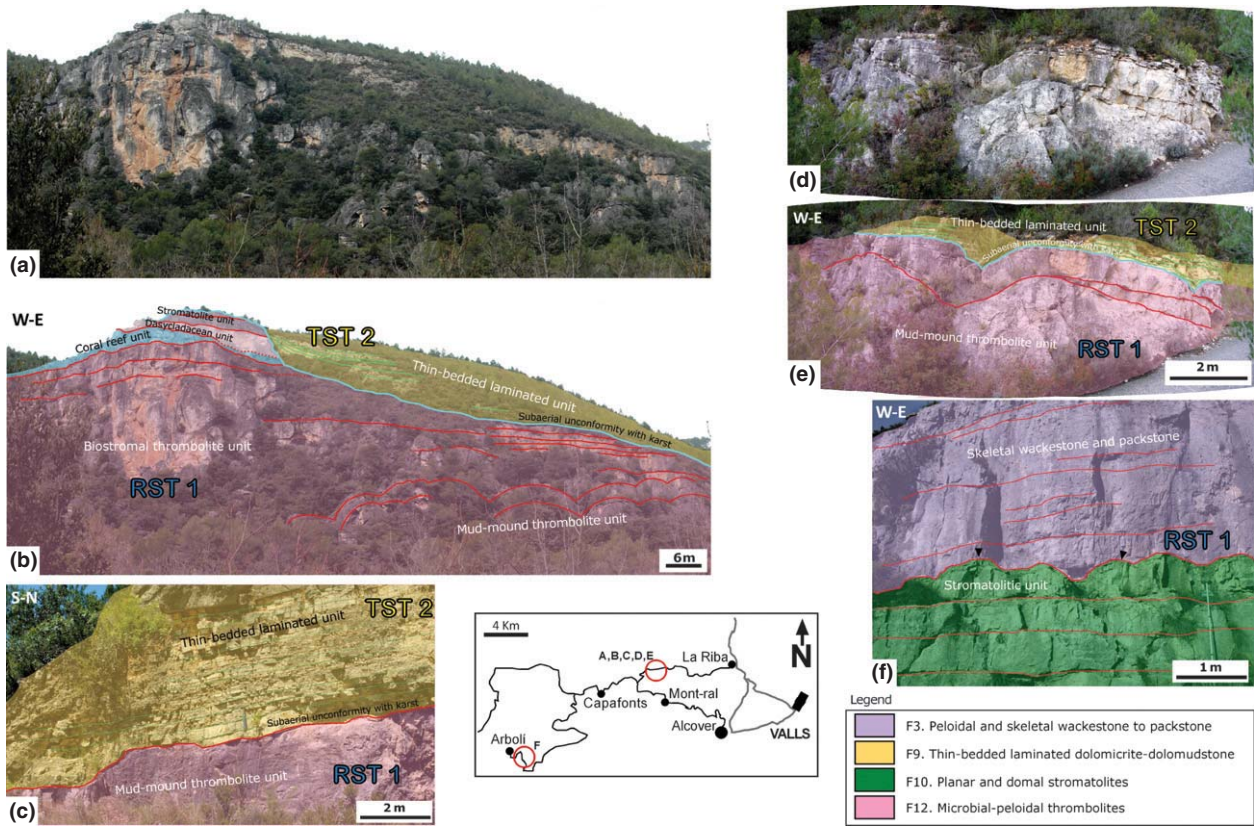

Fig. 6. Several microbial outcrops in the Prades domain and their geometries, facies relationships and sequence stratigraphic interpretation (see map for location). (a) Outcrop photomosaic of the boundary between T–R sequences 1 and 2, near Molí del Pinetell section (la Riba). See legend for more details. (b) Line-drawing interpretation showing the boundary (turquoise blue line) between T–R sequences 1 and 2 and their facies associations. Note that the biostromal thrombolite unit shows a tabular geometry along the flanks. A metre-thick mud-mound thrombolitic unit is recorded at the base of some biostromes. (c) Line-drawing and sequence stratigraphic interpretation showing the boundary between T–R sequences 1 and 2, located near the Molí del Pinetell section. This boundary is characterized by a paleokarstic surface. The mud-mound thrombolitic unit represents the base of the biostromal thrombolitic unit of (b). (d) A metre-thick mud-mound thrombolitic unit present at the base of the biostromal thrombolitic unit shown in (b). (e) Line-drawing and sequence stratigraphic interpretation of the previous photograph showing the facies associations and the boundary between T–R sequences 1 and 2. (f) Line-drawing and sequence stratigraphic interpretation of the western and shallowest microbial deposits in the Arbolí section. Dome-shaped stromatolitic bodies cropping out in this area (black arrows).

displaying erosive and irregular bases are also a common feature. The major components of this lithofacies association are rounded to sub-rounded, well-sorted ooids (diameter up to 2 mm). Peloids, sub-spherical to ellipsoidal type-C oncoids and microoncoids (diameter up to 7 mm), intraclasts, cortoids, fragments and complete specimens of bivalves and gastropods, echinoid spines and plates, crinoid stems and benthic foraminifera are the most common components. Among the secondary components are black pebbles, fragments of ostreids, conodonts and lumps, planktonic foraminifera, microproblematica and dasyclad thalli (Fig. 3a–g).

This facies association, which characterizes the inner and middle ramp depositional environments, developed in shallow subtidal marine settings, under moderate to high energy conditions, mainly above the fair-weather wave base zone. Typical subenviroments are marginal beach-barrier island areas, shoreface carbonate sands, internal or external shoals (*sensu* Colombié & Strasser, 2005) and sheltered lagoons.

Muddy facies associations

Three common types of muddy carbonate facies were documented in the Ladinian strata of the study area: strongly burrowed mudstone to wackestone (F7); burrowed skeletal mudstone to packstone interbedded with marls (F8), and thin-bedded laminated dolomicrite-dolomudstone (F9).

This facies association is usually formed by the alternation of centimetre to decimetre-thick packages of massive to nodular-bedded bioturbated dolomudstone to dolowackestone with light to dark grey, argillaceous burrowed marls or locally mud-supported thin-bedded dolomites (up to 6 m thick). In some areas, this facies association is composed mainly of brown to light grey, centimetre to decimetre-thick packages of finely laminated dolomites (Figs 3h and 4a–c). According to the degree of biogenic modification in the substrate, the presence of laminated intervals is conspicuous in outcrop. The most characteristic components are fragments or whole skeletons of bivalves (diameter up to 3 mm, *Daonella* and *Posidonia* shells

are frequent), small echinoid spines (around 10 μm), subrounded and high sphericity quartz grains (around 6 μm) and peloids (diameter up to 0.8 mm). The secondary components of this lithofacies association are fragments of gastropods, cephalopods, brachiopods, ostreids, crinoids, ostracods, bryozoan, benthic foraminifera (nodosarian) and microproblematica (*Tubiphytes*). The nonskeletal common elements are oncoids, lumps and carbonatic intraclasts. The beds display irregular and locally erosive bases and massive to nodular bedding. Plane-parallel and wavy to ripple laminations are also common in the sandy intervals. Tidal bars and channelized deposits are also present and are formed by a lateral accretion of finely laminated muddy deposits (rarely tidal bundles). The limestone beds show evidence of bioturbation giving rise to irregular and diffuse bases and decimetre-thin and rhythmically bedded stratification. *Planolites* and small-sized *Thalassinoides* ichnoassemblages were commonly recognized. In some settings, there is an abundant biota of soft-bodied marine macroinvertebrates and vertebrates. Exquisitely preserved whole specimens of a wide range of nektonic and planktonic taxa, especially osteichthyan fish, sauropterygian reptiles, arthropods, echinoderms, decapods, mollusca, brachiopods, insects and terrestrial plant remains can be found in certain levels (Via *et al.*, 1977; Cartaña, 1994; Fregenal-Martínez *et al.*, 1995).

This type of facies association is interpreted to have formed in different sedimentary settings, from inner to outer ramp environments. Shallow marine water, from moderate to high energy conditions to deep-water, low-energy conditions, were recorded. Subenvironments include hypersaline intertidal to subtidal sheltered lagoons and bioturbated tidal flats (above fair-weather wave base) to restricted marine basins (below fair-weather wave base).

A number of authors have reported the bioturbated facies in other Middle Triassic settings of the Tethys: in the Hungarian Carpathians (Török, 1998), the Northern Calcareous Alps (Rüffer & Bechstädt, 1998), the Southern Alps (Maurer & Schlager, 2003) and Southern Poland (Jaglarz & Uchman, 2010). The restricted muddy deposits resemble some of those reported in other areas along the margin of the Tethys during the Late Jurassic with laminated limestones and exceptional marine fossil preservation, such as the famous Solnhofen, Eichstätt and Nusplingen localities (Keupp, 1977; Barthel *et al.*, 1990; Fürsich *et al.*, 2007).

Microbialites and related facies associations

Eight types of boundstone and carbonate-related facies were recognized in the Ladinian strata of the study area: planar and domal stromatolites (F10); ooidal-peloidal stromatolites (F11); microbial-peloidal thrombolites (F12); calcimicrobial boundstone with bioclasts (F13); coral-microbial boundstone to rudstone (F14); laminated packstone of oncoids and peloids (F15); packstone to rudstone of dasyclads, bioclasts and peloids (F16); and foreslope dolomitic breccias (F17).

Organic boundstones

In the study area, organic boundstones (F10–F15) occur in the form of microbialites (stromatolites and thrombolites of Kennard & James, 1986; Figs 4d–h and 5a, d, e) and coral boundstone (Fig. 5b, c). Stromatolites usually develop two types of geometries: stratiform and tabular forms (Type 1 biostromes), and domed, head-shaped forms (Type 2 biostromes). Locally, Type 2 biostromes are developed above Type 1 biostromes. The two types form deposits at least 20 km wide, attaining thicknesses of several metres (up to 5 m) (Fig. S1).

The two types of thrombolites occur as extensive flat-relief biostromes (Type 1, biostromal thrombolite unit) and high-relief adjacent bioherms (Type 2, mud-mound thrombolite unit) (Figs S2, S3, 6).

The planar and domal stromatolites (F10) are interpreted as having formed in shallow marine environments in the inner–middle ramp, in hypersaline intertidal to supratidal flats subenvironments with moderate energy conditions. The scarcity and low diversity of subtidal-associated macrofauna and the presence of laminoid-fenestral fabrics after evaporite minerals probably indicate arid conditions with significant departures from normal marine salinities (Fig. 4d). These hypersaline conditions could have inhibited predation and competition of marine invertebrates and favoured the development of such microbialites in the inner ramp settings. The occurrence of microkarst horizons inside the microbialitic bodies is evidence of relatively short periods of subaerial exposure, indicating an intertidal rather than subtidal origin of the stromatolites. The well-defined manifestation of pseudomorph of evaporite minerals and the preferential accumulation of intraclasts (flat-pebble reworked clasts) also suggest intermittent intertidal to supratidal-sabkha subenvironments in arid to semi-arid coastal plains.

The depositional environments would be similar to those in Hamelin Pool, Shark Bay, Western Australia (Logan *et al.*, 1974; Awramik & Riding, 1988; Browne *et al.*, 2000): an enclosed marine basin with a semi-arid climate.

The ooidal-peloidal stromatolites (F11) consist of dolomitized oolitic-peloidal grainstone alternating with millimetre-thick micritic laminae (Fig. 4e). Stratiform and low-relief hemi-elliptical buildups are the most common geometries of these microbial deposits. Large biostromes are produced by the alternation of stacked flat-laminated intervals. These biostromes reach a thickness of up to 3 m in outcrop, correlating with a width of at least 40 km, and are arranged in deepening-upward cycles. The internal structure consists of smooth, planar to slightly wavy oolitic grainstone layers from sub-millimetre to a few decimetres in thickness. The grainstone layers alternate between light and dark grey, wavy, massive and clotted dolomicrite and microdolospar laminae (few millimetres to centimetres in thickness, Fig. 4f).

This lithofacies is interpreted to have been deposited in a shallow-water marine environment (intertidal to subtid-

al), with moderate to high energy hydraulic conditions, above the fair-weather wave base on the basis of the depositional texture and components. The depositional environment suggested for this lithofacies would correspond to an internal fore-shoal in the inner ramp (Colombié & Strasser, 2005).

The microbial-peloidal thrombolites (F12) consist of extensive, decimetre to metre-thick, massive to nodular-bedded, mainly nonlaminated (thrombolitic) microbialites that may include minor stromatolite intervals. The predominant texture of this lithofacies association is a massive peloidal mudstone-wackestone, although packstone and grainstone are present locally. The seismic-scale thrombolitic successions constitute up to 14-m-thick continuous packages of texturally uniform sedimentary bodies (attaining an overall thickness of 40 m) with a lateral extension of at least 45 km. All these successions are characterized by an internal macroscopic clotted and massive peloidal fabric (Aitken, 1967; Burne & Moore, 1987) despite the presence of packstone and grainstone (Fig. 4g, h). These deposits are composed mainly of peloids and micropeloids, which accounts for over 30–40% of the volume of the thin sections studied. Intraclasts, rock fragments, oncoids and detrital quartz grains are also common nonskeletal constituents. Benthic foraminifera, microproblematica (*Garwoodia*, *Tubiphytes*, *Cayeuxia*? and other cryptic forms), gastropods, microbial crusts (porostromate calcified microbes) and fragments of bivalves were identified among the skeletal components. The thrombolitic deposits are interpreted to have been deposited below the fair-weather wave base region in subtidal open-marine environments with low to moderate energy conditions on the basis of the depositional texture, components and faunal predominance.

The coral-microbial boundstone to rudstone (F14) consists of metre-thick, light grey, massive to nodular-bedded, dolomitized beds of wackestone to packstone of bioclasts containing layers of boundstone of patch-coral reefs, stromatolites and sponges (Figs 5b, c). The upper part of this lithofacies contains more stromatolites and sponges. Small-sized stromatolites (up to 15 cm wide) coexist with patch-reefs. The depositional environment suggested for this lithofacies association would correspond to a shallow subtidal, open-marine setting under moderate to high energy conditions.

Related facies

A number of carbonate-related facies (F16 and F17) are closely associated with the aforementioned microbialite facies. The related facies commonly overlie the microbial-peloidal thrombolites (Type 1 and Type 2, thrombolite units) (Figs 5f–h, S2 and S3)

This facies association is composed of light grey to yellowish, decimetre to metre-thick, massive to nodular-bedded wackestone to packstone or rudstone deposits. Low-angle cross-bedding and ripple and plane-parallel lamination may be present. Evidence of hardground and Fe–Mn-rich encrustations and bioturbation is present locally. The main components are fragments of bivalves, gastropods, benthic foraminifera, serpulids, disarticulated fragments of *Diplopora*-like dasyclad green algae, echinoid spines and plates, worm tubes, microproblematica (*Garwoodia, Girvanella*? and *Tubiphytes*), micropeloidal micrite, peloids, quartz grains and intraclasts. Warm water conditions and water depth in the range of a few metres are inferred from the abundance of dasyclad skeletal components. This depositional environment would constitute a back-reef area with a restricted platform carbonate deposition.

Similarly, carbonate breccia deposits are frequently associated with the tops of the thrombolitic units. The lithological composition of the clasts is commonly polymictic and is variable in shape (ranging from millimetres to decametres). They are generally subangular and poorly to moderately sorted and have a low sphericity. The groundmass is formed by a dolomitized fine-grained and also coarse-grained sedimentary matrix depending on the setting of the accumulation. The clasts are commonly encrusted and bored by microproblematica. This lithofacies is interpreted as having been deposited on the seaward flanks of the microbial-peloidal boundstone of the middle and outer ramps. The eroded reef material and organisms forming the more open-marine microbial buildups were resedimented downslope, below the fair-weather wave base. Low-energy and subtidal conditions are attributed to these breccia deposits.

SEQUENCE STRATIGRAPHIC INTERPRETATION

Two major transgressive–regressive (T–R) sequences were identified because of the vertical distribution of facies and the recognition of different stratigraphic surfaces with a sequence stratigraphic significance. These sequences span almost the entire duration of the Ladinian, i.e. about 9 Ma (according to Ogg *et al.*, 2008). The studied succession was subdivided according to Embry & Johannessen's (1992) T–R sequence model. This model highlights the importance of SU and facilitates the recognition of MRS. This sequence stratigraphic approach was adopted because an extensive subaerial unconformity with karst was recorded along the basin. Moreover, evidence of transgressions and regressions was documented.

A chart displaying the correlation between the different sedimentary sections and their sequence stratigraphic interpretation is shown in Fig. S5.

Transgressive–regressive sequence 1

A re-establishment of marine carbonate sedimentation followed a period of siliciclastic and evaporite deposition that characterized the continental Middle Muschelkalk facies (Anisian-Lowermost Lower Ladinian age). The basal boundary of T–R sequence 1 is thus represented by

a transgressive surface that separates the regressive deposits of the Middle Muschelkalk (below) from the Upper Muschelkalk marine sediments (above).

An early-transgressive phase of the first transgressive systems tract was responsible for the deposition of a widely distributed peritidal carbonate facies (up to 10 m thick). These deposits are formed by extensive (*ca.* 100 km across) shoals (facies F1) interbedded with tidal flats containing facies F10 that crop out from Rasquera to Miramar (Figs S4 and S5). These high to moderate energy deposits thicken basinwards and show slightly retrogradational to aggradational stacking patterns, belonging to the inner ramp depositional settings. The initial transgressive pulse was not recorded in the sections of the Gaià domain. The scarcity or absence of skeletal components in the oolitic shoal subenvironments and the preservation of the stromatolitic intervals strongly suggest environmental stress, i.e. hypersaline marine conditions. As a result, the depositional model for the first transgressive wedge of T–R sequence 1 corresponds to a stepped carbonate ramp owing to the large lateral continuity of tabular strata and to the low-gradient depositional profile.

A second early-transgressive wedge (up to 12 m thick) recorded in T–R sequence 1 is made up of extensive lagoonal bioturbated muddy deposits. It corresponds to the second transgressive pulse characterized by aggradational stacking patterns and low to moderate energy subtidal deposits that thicken slightly basinwards (Figs S4 and S5). These low diversity, homogeneous deposits, completely burrowed by *Planolites* and other ichnofauna, suggest the existence of environmental stress conditions (hypersalinity) over the ramp. Similar facies have been described for the Middle Triassic of the Hungarian Carpathians (Török, 1998), the Southern Alps (Maurer & Schlager, 2003) and the Tatra Mountains in Poland (Jaglarz & Uchman, 2010). The uniformity of the thicknesses and the lateral continuity of the facies suggest that the depositional profile of this wedge developed under quiescent tectonic conditions. The Gaià domain records this second transgressive pulse near Miramar and Font del Teix as a result of progressive backstepping and the creation of accommodation space in a landward direction.

The late-transgressive phase includes the most widespread sedimentary event recorded during the TST1 with the development of diverse sedimentary environments and facies from the inner to middle-outer ramps (Fig. S4). During this stage, carbonate bank sedimentation took place near Puigcabrer in a mainly shallow subtidal shoreface with moderate energy conditions. Moreover, an extensive tidal-flat environment with an intertidal to shallow subtidal sheltered lagoon developed in the back-shoal area of the ramp (Gaià domain). These deposits show aggrading to slightly retrograding stratal patterns and are observed in a NE-trending outcrop running from Miramar to Pontons. The strong bioturbation and low diversity and small size of the metazoans characterizing the facies F7 point to severe environmental conditions inherited from the previous stage, which inhibited the growth of invertebrate communities.

Furthermore, on the seaward margin of the ramp, more open-marine basinal deposits are characterized by facies F8. The deepest area extended over tens of metres from Molí del Pinetell to Gavadà, with considerable thickness, suggesting a relatively low-gradient depositional profile from the ramp margin to the basin. Deepening and fining-upward cycles with a progressive increase in marl content towards the top and retrogradational stacking patterns are recorded in these basinal deposits. Minor storm-derived channelized deposits are locally interbedded.

The latest transgressive pulse associated with the TST1 of the first sequence is marked by the local acceleration of fault-induced subsidence, which differentiated the inner ramp setting from the surrounding ramp. In the Gaià domain, the generation of accommodation space by means of minor NE-dipping faults near Font del Teix contributed to the deposition of facies F1 (up to 32 m thick and 45 km wide). This high-energy tidal-influenced carbonate deposit thickens to the NE and SE, showing tidal bundles accreting as bars and low-angle planar cross-bedding migrating towards the SW. Its internal architecture reveals the backstepping of interbedded tidal flats composed of high continuity stromatolitic intervals cropping out mainly between Coll Magí and Pontons. Retrogradational stacking patterns (reflooding and deepening phases *sensu* Spence & Tucker, 2007) and thickening and thinning-upward cycles are recorded at the scale of parasequence (Figs S4 and S5).

The top of the TST1 is traced by the maximum flooding zone (MFZ) of T–R sequence 1. The criteria for identifying the MFZ vary according to the setting of the basin. In the inner ramp (Gaià domain), the MFZ was placed on top of the widespread last marl unit that overlies facies F1. In the middle ramp settings (Prades domain), the MFZ could be interpreted to represent a phase of nondeposition with sediment starvation, local hardgrounds, borings and encrusting organisms. The MFZ was placed at the top of fining-upward deposits in sharp contact with the overlying microbial deposits (facies F12), which exhibit prograding and shallowing-upward stacking patterns. However, in deeper water settings (ramp slope and outer ramp), the MFZ is identified at the bottom of coarse-grained calciturbidites and slumped-slide deposits (facies F8). The MFZ marks an abrupt sedimentary shift in facies and an increase in water depth. The change from retrogradational stacking patterns below the surface to progradational stacking patterns above the surface suggests that the sedimentation rate started to outpace the rate of base-level rise, favouring the shedding of resedimented carbonates downslope.

Above the MFZ, the regressive systems tract developed during the late stage of base-level rise, generating a normal regressive succession whose deposits are dominated by aggradational and progradational stratal patterns. During the RST1, a rapid subsidence associated with the generation of SW-dipping fault half-grabens considerably altered

the basin architecture, i.e. the compartmentalization of the basin into different sub-basins. The master fault, which controlled the creation of accommodation space, was located between Miramar and Coma Fonda (la Riba fault, Prades domain), although its conjugate equivalent (the Ulldemolins-Gandesa fault, the Prades domain) also created blocks tilted to the NE near Arbolí (Fig. 7). This caused the differential accumulation of more than 80 m of sediments in the northern areas and less than 20 m in the southern ones (a dissimilar thickness also noted by Gómez & Guimerà, 1999). Deposition during this stage was characterized by spectacular, widely distributed microbial deposits from facies F10 in the inner ramp (Fig. S1) to facies F12 in the middle-outer ramp (Figs S2, S3 and 6). The ubiquity of microbial deposits along the sedimentary environments of the basin during this stage suggests a major environmental control (hypersaline, anoxia) that favoured the conditions for their formation.

In the Gaià domain, hypersaline intertidal and supratidal flats developed in a protected embayment where peritidal prograding carbonates were deposited in shallowing-upward cycles. Microbial carbonates are significant here because of their high accumulation rate. This domain is characterized by an extensional tectonic quiescence due to the slower rate of accommodation space. However, the Prades domain recorded a rapid fault-induced subsidence giving rise to the largest space available for sedimentation, mainly in the northern part of the half-graben. A catch-up phase took place with an extensive development of mainly aggrading to slowly prograding microbial biostromes and mud-mounds (facies F12), reaching up to 50 m in thickness. In this domain, the late RST1 is characterized by the sedimentation of facies F15 that grew above the microbial deposits. Facies F15 frequently embedded in a framework of peloidal micrite developed patch-reefs. In addition, facies F16 also occupied wide areas capping the previous facies F15. The two facies F15 and F16 gave rise to marked prograding geometries as a result of the decrease in the available space. Grainstone and rudstone spread out from the platform tops when the rate of sediment production started to exceed the rates of relative sea-level rise and subsidence. These materials prograded leeward, resulting in large clinoforms, which downlapped the MFZ. Panoramic examples of east-dipping prograding clinoforms (Fig. S3) can be identified in the Prades domain between the Can Cartanyà and Coma Fonda localities.

The transition from the middle to outer ramps occurs in the Baix Ebre-Priorat domain between la Figuera and Rasquera (Figs S4 and S5). During the RST1, this

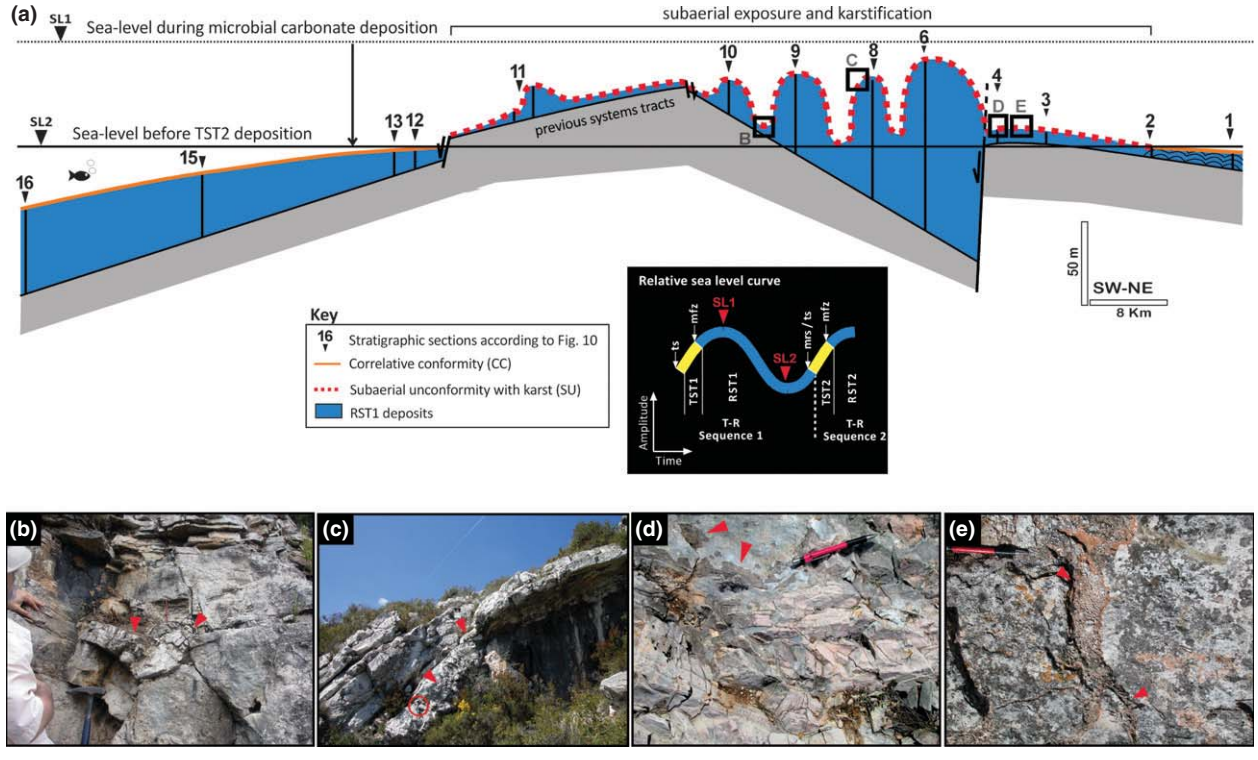

Fig. 7. The stepped carbonate ramp profile of T–R sequence 1, between Pontons and Rasquera. (a) Evolution of the sea level between the onset of sea-level fall (SL1) and the end of regression (SL2). Note that the significant sea-level fall produced an extensive subaerial exposure area affecting the inner to outer ramp domains. (b, c, d and e). Karst examples associated with the subaerial exposure in the boundary between T–R sequence 1 and 2. (b) V-structures on top of the mud-mound thrombolitic unit (red arrows). (c) Cemented mosaic packbreccias (red arrows) over the flanks of the mud-mound thrombolitic unit. Hammer is 32 cm long. (d) Cemented rubble floatbreccia (red arrows) filling the karstified stromatolitic host rock near the Miramar section. Pencil is 15 cm long. (e) Particulate rubble packbreccia fillings (red arrows) affecting the western part of the Gaià domain (Miramar section).

domain developed a SW-dipping fault, generating a small step around the Montsant section coeval with the deposition of facies F8 that extends basinwards. Some microbial mud-mounds (up to 20 m thick) developed in the proximal part of this domain (near la Figuera) (Figs S4 and 7). Facies F17 derived from the mud-mounds were deposited on the foreslope margins of these buildups and on the toe-of-slope (located in Montsant and Falset) during the late RST1. The cycles observed in the RST1 deposits in this area exhibit a shallowing and coarsening-upward trend and display few storm events and gravity-flow deposits. This suggests that the synchronous microbial buildups that developed on the platform margin could have prevented granular sediments from being shed downslope. The restricted slump-slide deposits and carbonate turbidites are only present in the vicinity of the slope and are much less common in the distal parts of the basin (Fig. S4). In the Rasquera section, the RST1 is composed of several shallowing and coarsening-upward parasequences first described by Calvet & Tucker (1988). Most of these cycles consist of 7 m-thick marlstone-shale facies. Towards the south, there is an increase in thickness of the marlstone units (interpreted as basinal facies) and marlstone-interbedded limestone units (interpreted as deep-distal ramp facies).

Sea level started to fall after the sedimentation of the late-stage RST1 deposits. As a result, the previous microbial-dominated highstand platform was subaerially exposed and widely karstified (at least 50 m of sea-level fall), shutting down the carbonate factories (Fig. 7). The extensive subaerial unconformity between Coll Magí and la Figuera is used in this study as a sequence boundary (SB), limiting T–R sequences 1 and 2 (Calvet & Tucker, 1995) (Fig. S5). Distinct karstic dissolution cavities, collapse breccias and v-structures (Figs 7b–e) are recognized coevally along the basin. Both the microbial buildups and their reefal caps in the Prades domain were subaerially exposed. No evidence of subarerial exposure with karst was observed in the stromatolitic buildups at Querol and Pontons (Gaià domain). This is probably due to the differential subsidence and subsequent NE tilting mainly in this area below the sea level. However, the western part of the Gaià domain (near the Miramar section) remained partially uplifted and subaerially karstified (Figs 7b–e).

Trangressive–regressive sequence 2

Above the RST1, the TS exhibits a sparsely developed hardground with ferruginous crusts, Fe-rich nodules, encrusting organisms, borings and abundant macrofauna, and is superimposed on the SB landwards (e.g. to the east of la Figuera 1 section, Fig. S5). Thus, the subaerial unconformity that separates T–R sequences 1 and 2 becomes a composite sequence boundary because the transgressive surface meets the sequence boundary.

There is little evidence of hardground and colonization by opportunistic communities in the middle and inner ramp settings probably because of the ravinement scouring effect of waves and tides during transgression. However, in offshore environments (Falset), the transgressive surface has a high preservation potential because it is overlain by fine-grained mudstone and wackestone deposited below the storm wave base (SWB).

During the early TST2, the highstand subaerially exposed ramp was progressively flooded. A complex system of shoals, sheltered lagoons and internal fore-shoals developed progressively inshore during the TST2 (Fig. S4). Rapidly induced subsidence by the two conjugate major faults (la Riba and Ulldemolins-Gandesa faults) continued during the TST2, with the middle ramp setting being the most subsided area.

The incipient transgressive phase can be recorded in the middle ramp at Mont-ral and Arbolí (Fig. S4), starting with the deposition of facies F9. These low-energy, restricted marine and deep subtidal deposits are prominent in the inter-reef microbial depressions where restricted areas remained isolated and filled during the early-transgressive stage (considered as a possible lowstand deposits by Calvet & Tucker (1995). At the same time, offshore environments were characterized by the deposition of open-marine facies (facies F5) that onlapped the correlative conformity and the TS. These deposits locally contain high-energy storm-induced beds whose sediments were derived from more proximal settings. The source of these sediments was an active area of oolitic shoal formation (near Falset and la Figuera) whose deposits underwent backstepping. These oolitic shoals acted as a barrier. These deposits favoured the formation of *ca.* 30-km-wide sheltered lagoons composed of retrogradational stacking patterns and characterized by thickening-upward cycles (reflooding phase *sensu* Spence & Tucker, 2007) in facies F4. This facies is interpreted to belong to the middle ramp, attaining a thickness of between 15 and 60 m. In some protected areas inside the lagoon and detached from landward margins, facies F14 formed coevally with facies F4.

In the Gaià domain (Fig. S4), a new extensional pulse activity during the late stage of the TST2 accelerated the rapid subsidence through a SW-dipping master fault located between Querol and Santa Perpetua de Gaià (Fig. S4). This fault led to the creation of available space for an internal shoal and beach-barrier deposition and its internal fore-shoal. These sedimentary complexes are characterized by backstepping architecture, retrogradational stacking patterns and progressively thinning-upward cycles (deepening phase *sensu* Spence & Tucker, 2007; predominance of facies F11). In this area, internal shoals and beach-barrier island deposits composed of facies F1 and F2 were established between Coll Magí and Pontons. Moreover, the associated transitional fore-shoals composed of facies F11 are widely distributed in this domain, recording marked shifts in thicknesses across the inner ramp.

During the RST2, fault-induced subsidence continued in the Prades domain disminishing in the Gaià and Priorat-Baix Ebre domains. The RST2 displays a thickness of

over 50 m, aggrading to slightly prograding stacking patterns and shallowing-upward cycles composed of facies F14. This is the characteristic of intermittent intertidal to supratidal-sabkha coastal plain subenvironments. Arid to semi-arid conditions are indicated by abundant pseudomorphs of evaporite minerals.

Above this succession, the maximum regressive zone marks the transition to the widely distributed Keuper facies (Carnian in age) composed of evaporitic mud-flat deposits (Fig. S4). This surface, which is characterized by a facies shift from peritidal carbonates to evaporites, marls and sporadic red beds, was used as a datum for all the stratigraphic sections because of its extensive lateral continuity.

ARCHITECTURE OF THE MICROBIAL-DOMINATED T–R SEQUENCE 1

The architectural stratal patterns of the facies associations under study enabled us to ascribe the T–R sequence 1 to the carbonate ramp model of Ahr (1973) and Read (1982, 1985) and Burchette & Wright (1992). The T–R sequence 1 was examined in detail because it contains the thickest and the most widespread microbial facies in this area (Fig. S6).

According to Tucker *et al.* (1993), T–R sequence 1 (Fig. S6) would correspond to a carbonate ramp model. The TST1 and the RST1 show some of the diagnostic criteria attributable to this kind of carbonate platform. The depositional profile of T–R sequence 1 displays the following facies zonation: (i) an inner ramp characterized by (a) cyclic lagoonal muddy bioturbated carbonates with restricted biota, (b) agitated oolitic shoal, back-barrier sediments, commonly sheet-like grainstone units and (c) tidal-flat environments with peritidal sediments and microbially laminated carbonates; (ii) a middle ramp exhibiting (a) deeper ramp argillaceous lime mudstone-wackestone, nodular bedding, bioturbation and commonly open-marine faunas, (b) discrete thin storm-generated, fining-upward sequences and (c) microbial mud-mounds and biostromes; and (iii) an outer ramp displaying: (a) an abundance of slumped-slide slope carbonate deposits and channelized thin coarse-grained calciturbidite successions, (b) local carbonate foreslope breccias and (c) heavily cemented microbial mud-mounds.

The restored depositional profile of T–R sequence 1 (Fig. S6) accounts for a low-angle gradient platform defined by a significant NE-dipping step induced by the la Riba fault in the Prades domain. This fracture was active during the whole deposition of T–R sequence 1 and gave rise to the stepped ramp profile of the depositional model. A minor SW-dipping step is located near the Montsant section in the Baix Ebre-Priorat domain (Fig. S6) and controls the basin morphology of the outer ramp environment, resulting in instability, slumping and resedimentation of some carbonate deposits.

EVOLUTION OF ACCOMMODATION SPACE

A model showing an estimation of the evolution of accommodation space along the basin for each T–R sequence was constructed (Fig. 8). To this end, the thicknesses of the sedimentary sections were plotted using the maximum flooding zone as a datum. This method is useful because it is independent of the carbonate factory and the sedimentation rate. The results show a graphic representation of the net space available for deposition.

The sedimentary record of the TST1 of T–R sequence 1 (Fig. 8a) shows no significant changes in accommodation along the basin. The smaller accommodations are recorded near the Puigcabrer and Molí del Pinetell sections (Prades domain), and also in the Rasquera section (Baix Ebre-Priorat domain), suggesting that the depocentres are in the Prades and Gaià domains. A generalized stage of uniform development of accommodation took place during the TST1. During the RST1 of T–R sequence 1, the basin configuration changed notably (Fig. 8a). A marked depocentre developed in the Prades domain between the Coma Fonda and Arbolí sections (Fig. 8a). However, the Gaià and Baix Ebre-Priorat domains (Fig. 8a) became areas with decreasing available space for sedimentation with respect to the previous systems tract. Because of the heterogeneous accommodations in the Prades domain, a fault-controlled half-graben was responsible for the huge increase in accommodation in this area. The la Riba fault between the Miramar and Coma Fonda sections gave rise to a marked heterogeneity in the available space for deposition between the Prades and Gaià domains. At the same time, the Baix Ebre-Priorat domain records smaller variations in accommodation (Fig. 8a). A small change in accommodation is observed in the sketch near the la Figuera and Montsant sections, providing evidence for the presence of a step in this area (Figs 7 and 8a).

During the TST2 of T–R sequence 2 (Fig. 8b), a marked compartmentalization of the basin occurred, giving rise to three major sedimentary domains, coinciding with the Gaià, Prades and Baix Ebre-Priorat domains. These areas were delimited from each other by two main fault systems: the la Riba fault and the Montsant step. An overall increase in accommodation values triggered by a fault-controlled subsidence is observed in these areas during the TST2.

The sedimentation of the RST2 of T–R sequence 2 (Fig. 8b) is marked by the large reduction in accommodation in the Baix Ebre-Priorat domain. The accommodation rate in the Gaià domain is reduced with respect to the TST2.

Accommodation changes and subsidence

Three stratigraphic sections (Pontons, Puigcabrer and Rasquera, Fig. 9a) were analysed in the three different domains of the Triassic Catalan Basin to calculate the

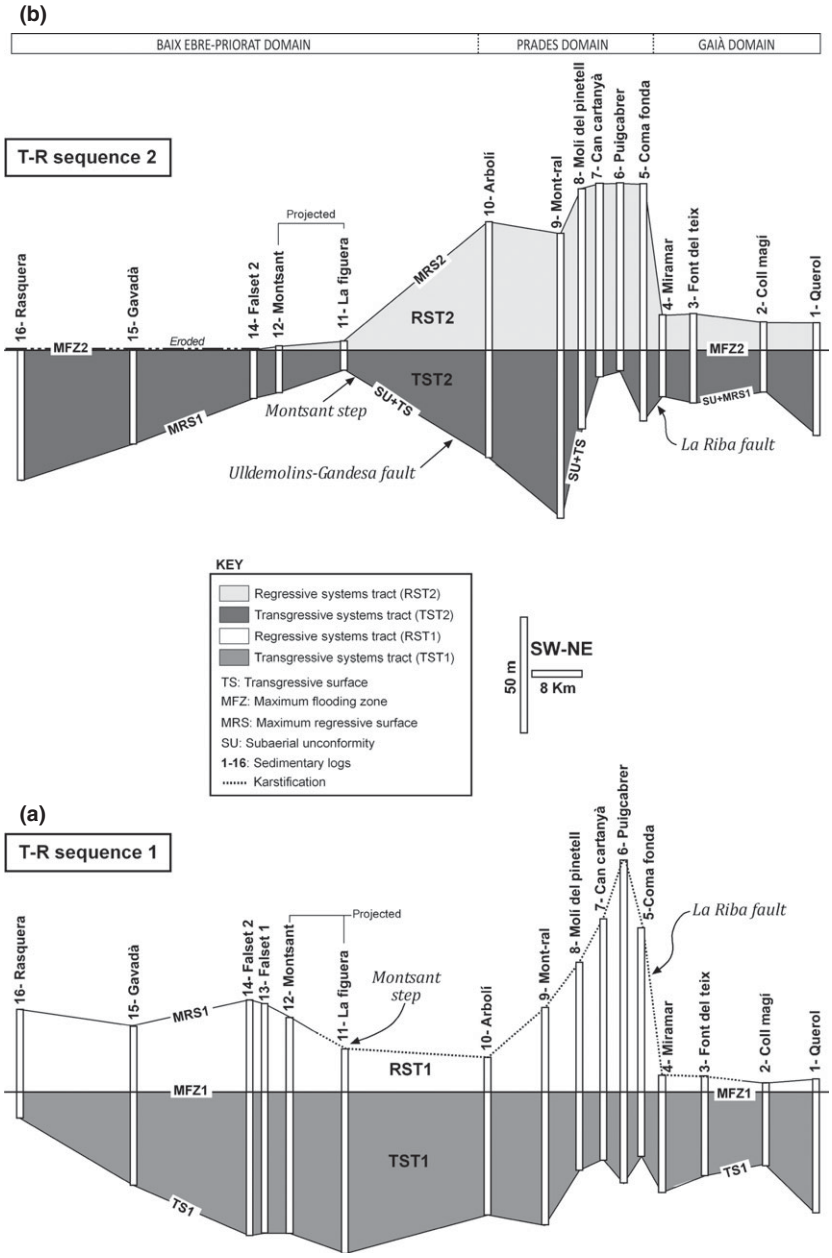

Fig. 8. Querol-Rasquera correlation of the stratigraphic thicknesses taking the maximum flooding zone (MFZ) of each T–R sequence as a datum. The variations in accommodation along the basin are shown graphically. See the legend for further details. (a) Variation in accommodation in T–R sequence 1 along the basin. The main features are the homogeneity in the sedimentary record during the TST1 and the increase in sedimentary thicknesses around the Prades domain during the RST1 stage. (b) Variation in accommodation in T–R sequence 2 along the basin. In this case, the heterogeneity distribution of the sedimentary record during the TST2 reveals an increase in accommodation in the Prades and the Baix Ebre domains. During RST2, the Prades domain acted as an important depocentre according to the stratigraphic thicknesses recorded in this area.

total subsidence curves with palaeobathymetry corrections (Fig. 9b). These curves represent a fairly accurate evolution of accommodation during the Triassic in the study area.

Specific measurements of the Triassic strata belonging to Buntsandstein, Muschelkalk and Keuper facies were also carried out at selected sites to calculate the Triassic total subsidence curves. Despite small differences in magnitude, the three curves of total subsidence display the same general pattern (Fig. 9b). In all sections, the curves show an initial episode of decelerated subsidence represented by the sediments of the Buntsandstein facies (Scythian, 244.8–240.2 Ma). A later phase, which is characterized by an episode of rapid subsidence comprising the Lower Muschelkalk carbonate facies (Late Anisian, 240.2–237.1 Ma), was observed in all the stratigraphic sections. The Middle Muschelkalk facies is represented by a decelerating subsidence stage (237.1–233 Ma). Rapid subsidence resumes during the sedimentation of the Upper Muschelkalk facies (Ladinian, 233–227.4 Ma), attaining 470 m of total subsidence. This period is marked by a resumption of a rapid subsidence in all the stratigraphic sections, which was particularly fast in the Prades domain. In this domain, the development of a fault-controlled half-graben is linked to this rapid subsidence stage controlling the deposition of Upper Muschelkalk facies. However, during the Carnian and Norian stages (233–209.6 Ma) of Keuper facies sedimentation, a significant decelerating trend in subsidence is recorded in all the sections and domains analysed. Finally, during the Rhaetian (209.6–205.7 Ma), the highest decelerating subsidence occurred in the Catalan basin, giving rise to the deposition of shallow marine limestones and dolomites of the Imon Formation (Arnal *et al.*, 2002).

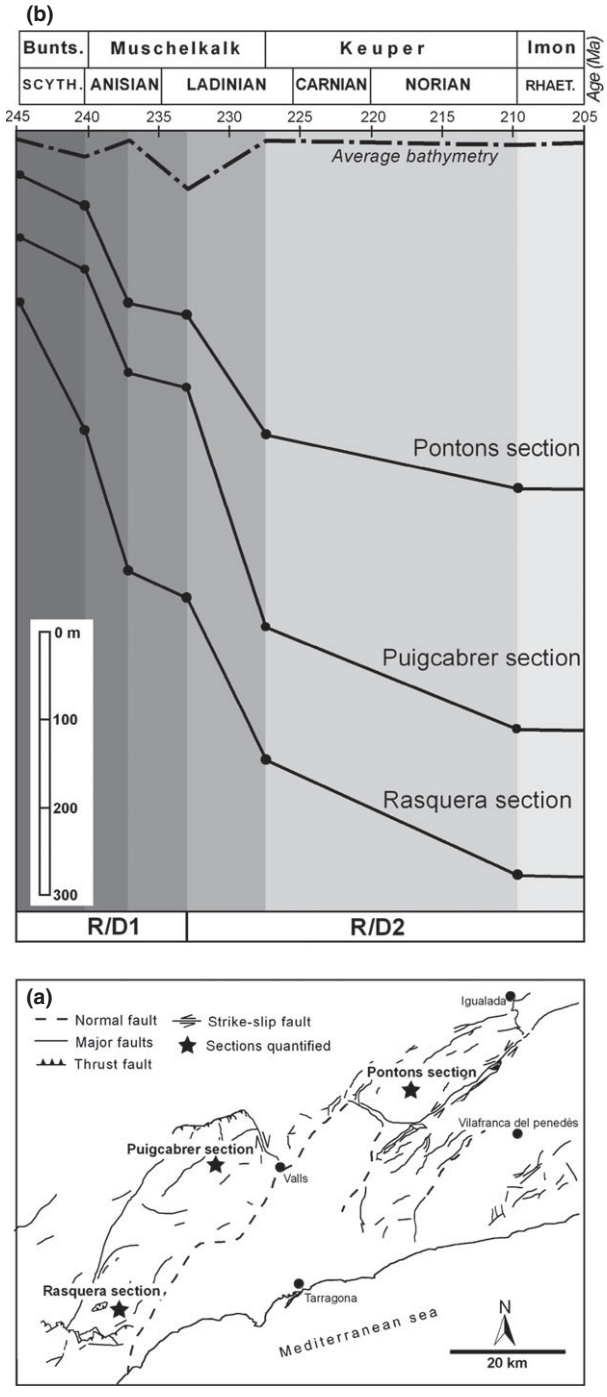

Fig. 9. (a) Schematic tectonic map of the Catalan Basin showing the location of the different sections used in the quantitative subsidence analysis. (b) Decompacted total subsidence curves corrected for paleobathymetries representing total accommodation. The average bathymetry curve is also indicated. Absolute ages are from Gradstein *et al.* (1994). R/D1 and R/D2: Stages of rapid/decelerated total subsidence.

All three curves display a similar shape with two major differentiated parts of rapid/decelerated (R/D) total subsidence, representing two discrete rift/post-rift pulses in the largest Triassic rifting stage. The first pulse (R/D1 in Fig. 9b) is defined by a rapid syn-rift subsidence from 244.8 to 237.1 Ma including the Buntsandstein and Lower Muschelkalk facies, and a decelerated post-rift subsidence including the Middle Muschelkalk facies (237.1–233 Ma). The second pulse (R/D2 in Fig. 9b) is also characterized by a rapid syn-rift subsidence from 233 to 227.4 Ma corresponding to the Upper Muschelkalk facies, and a decelerated post-rift subsidence from 233 to 205.7 Ma, matching the Keuper facies and the Imon Formation.

The rapid syn-rift pulses of total subsidence correspond to the main extensional periods of fault activity and a reactivation of tilting blocks producing gains in accommodation. The slower post-rift pulses of total subsidence indicate local periods of thermal re-equilibration of the crust heated during previous fracture phases (McKenzie, 1978; Salas *et al.*, 2001), thereby giving rise to accommodation losses.

The results obtained in this study are in agreement with the modern quantitative subsidence analysis carried out by Vargas (2002) and Vargas *et al.* (2009) for the Triassic deposits of the areas of the Iberian Chain and the Ebro Basin. Three syn-rift phases and two post-rift stages have been identified in the Ebro Basin. In the eastern part of the Ebro Basin, the Triassic basement subsidence at the Monzón-1 and Lérida-1 wells (Vargas *et al.*, 2009) bears a close resemblance to that in the Catalan Coastal Ranges. In these wells, up to two periods of rapid subsidence (Scythian to Middle Anisian and Upper Anisian to Lower Carnian) have been reported and two stages of decelerated subsidence (Middle Anisian to Upper Anisian and Middle Carnian to Upper Norian) have been described (Vargas *et al.*, 2009). Calvet *et al.* (1990) also calculated the sedimentation rates, using a decompacted subsidence curve (total subsidence) for the Triassic period. According to these authors, two phases of extension took place, each followed by a regional subsidence stage. The first phase enabled the deposition of the syn-rift Buntsandstein and post-rift Lower Muschelkalk facies. Subsequently, the second phase permitted the syn-rift Middle Muschelkalk sedimentation followed by the post-rift Upper Muschelkalk facies. This interpretation regards the clastic facies as syn-rift, and the carbonate facies as post-rift (regional subsidence) deposits. Nevertheless, the subsidence curve of Calvet *et al.* (1990) also displays a rapid subsidence segment in the start of the carbonate deposition during the Lower and Upper Muschelkalk.

DISCUSSION

Controls on microbialite growth and morphology

Microbialites are the result of a complex interaction among biological, ecological and physical factors that play a key role in their formation, shape and internal architecture (Logan *et al.*, 1974; Pratt, 1982, 1995; Burne & Moore, 1987; Andres & Reid, 2006; Pratt & Haidl, 2008). Five main types of microbialitic facies were described in

the study area, corresponding to five types of facies assemblages (F10, F11, F12, F13 and F14) from laminated stromatolites to microbial thrombolites. Each microbialitic facies developed under different environmental conditions (e.g. water energy, salinity, depth, nutrients, oxygen) and palaeogeographical context, giving rise to distinct deposits characterized by a specific macroscopic shape and internal features. The discussion will only focus on microbial facies F10 and F12 because of their growth potential and palaeogeographical and stratigraphical significance along the basin.

The water column (bathymetry), i.e. the available space for sedimentation, plays an important part in the morphology, dimensions and vertical stacking trends of the Triassic stromatolites under study. The two major microbial facies recognized in the study area enabled us to reconstruct the environmental factors involved in the internal anatomy and external architecture of the microbialites: i) Planar and domal stromatolites (F10); and ii) Microbial-peloidal thrombolites (F12).

The planar and domal stromatolites (F10)

During the RST of the first sequence, progradational stacking patterns were recorded in the inner ramp settings with peritidal shallowing-upward cycles. The intertidal and supratidal parts of these cycles are well developed between Coll Magí and Pontons despite the presence of some shallow subtidal intervals (with few bivalve shells and tiny oolites). In this region, two types of microbialite developed in a back-shoal setting: a first stage of planar stromatolites (Type 1 biostromes) and a second overlying stage of domal stromatolites (Type 2 biostromes).

The vertical transition between Type 1 and Type 2 biostromes is explained in terms of increasing accommodation rather than a change in the type of microbial community. The physical expression, the nature and arrangement of the alternating dark and light-coloured laminae are similar in the two types. However, Type 2 biostromes show less spacing, undulatory to wrinkled, slightly domed laminae. In this case, the increase in available space enabled the microbial mats to build small domes that progressively became enveloped by the subsequent microbial stages, giving rise to large domal stromatolites of metric to decametric height.

During this systems tract, high-energy oolitic subtidal grainstones were located around Font del Teix and may have acted as a palaeogeographical barrier, reducing the physical stress and erosion effect of waves and currents. These deposits favoured the restricted conditions (hypersalinity) in the back-shoal environment colonized by Type 1 and Type 2 biostromes.

The evidence suggesting a stressed environment associated with hypersalinity are (i) the occurrence of intervals characterized by abundant lenticular pores and birdseye structures filled with calcite pseudomorphs of evaporite minerals, (ii) an increasing proportion of chert nodules resembling primary anhydrite nodules, (iii) the presence of locally well-preserved small intraclastic breccia layers and (iv) the scarcity and low diversity of marine invertebrates (bivalves or gastropods) or their traces. This suggests an arid/semi-arid environment subjected to moderately restricted marine conditions with high salinities and evaporation rates.

Furthermore, some domal stromatolites display centimetre-sized microkarst evidence showing profuse dissolution of the microbial laminae during periods of subaerial exposure, suggesting deposition under lower upper intertidal conditions.

The palaeogeographical context of Type 1 and Type 2 biostromes resembles the well-known example of Shark Bay, Hamelin Pool in Western Australia. The hypersaline embayment of Shark Bay (Logan & Cebulski, 1970; Logan *et al.*, 1974) exhibits stromatolitic units developed in elevated salinities. These conditions would restrict the growth of microbial grazers and other competitors (Garrett, 1970; Logan *et al.*, 1974), even favouring the persistence of coccoid cyanobacteria (Seong-Joo *et al.*, 2000).

Microbial-peloidal thrombolites (F12)

The two types of thrombolitic geometries (Type 1 and Type 2) accumulated during the RST1, which was a period of increasing accommodation in the Prades and the Baix Ebre-Priorat domains, dominated by aggradational and progradational stacking patterns and mainly fine-grained pelagic–hemipelagic sedimentation. The first stage of microbial accretion occurred during the early phase of the RST1, when the Prades and the Baix Ebre-Priorat domains started to undergo a generalized fault-controlled long-term subsidence. As a result, flooded areas became important settings for accommodation and subsequent widespread thrombolite development. These microbial deposits nucleated commonly on a substrate of skeletal and peloidal packstone and grainstone (facies F3) disseminated over the middle and outer ramps in the form of lenses and sand bodies of a few metres thick. The compartmentalization of the Prades and Baix Ebre-Priorat domains enhanced the diversification of the ecological biotopes. Type 1 biostromal thrombolites constituted the first microbial subtidal colonizers and occupied a large extension of the subsiding middle and outer ramps (from Coma Fonda to E Arbolí, and W Arbolí and la Figuera). They attained a thickness of up to 14 m in the areas where the growth potential matched the rate of sea-level rise (keep-up). Similarly, Arbolí was a preferential site for dome-shaped intertidal stromatolitic deposition (facies F10, Fig. 6f) as this location remained slightly uplifted owing to differential subsidence.

During the late phase of the RST1, which is traditionally defined by much lower rates of sea-level rise and stronger progradational stacking patterns (Catuneanu, 2006), the eastern part of the Prades domain underwent accelerated fault-controlled subsidence, which created greater accommodation near the la Riba extensional fault. These conditions were suitable for thrombolite building to

sea level (catch-up growth of Kendall & Schlager, 1981; Neumann & Macintyre, 1985 and James & Bourque, 1992), resulting in the extensive development of high-relief Type 2 microbial mounds in the area. Moreover, near la Figuera (Baix Ebre-Priorat domain), a similar process took place, favouring the formation of several Type 2 microbial mounds. Type 1 biostromal thrombolites developed in the areas where accommodation was less significant (between Arbolí and Mont-ral) and where the microbial growth potential closely matched the rate of sea-level rise. Once thrombolitic mounds reached sea level, open-marine biota colonized the tops of the mounds developing reefal facies (*sensu* Calvet & Tucker, 1995). According to these authors, the reefal facies (facies F14) was formed by scleractinian corals, sponges, calcareous algae and molluscs and is interpreted to have been deposited under normal marine conditions (water depths of 5–20 m). A progressive shallowing-upward trend was recorded above the reefal facies with a vertical succession of packstone to rudstone of dasyclads (F16) and peritidal deposits of calcimicrobial boundstone (F13). Facies F13, F15 and F16 exhibit extensive NE-prograding geometries over the thrombolitic mounds near Cartanyà and Puigcabrer. These geometries correspond to the outbuilding phase during which excess sediment was deposited on the flanks.

Eustatic sea-level changes during the Ladinian

The marked sea-level fall recorded at the top of the RST1 platform of T–R sequence 1 is well documented in other Triassic basins of the Tethys such as the Southern Calcareous Alps, the Paris Basin, the North Sea, the Barents Sea and the German Basin (Gianolla & Jacquin, 1998). According to these authors, the new calibration of sequence stratigraphic interpretations in Tethyan and Boreal Triassic deposits gave rise to four second-order T–R cycles throughout the Western Europe. The top of the second T–R cycle (R2 in Gianolla & Jacquin, 1998) corresponds to the maximum regression recording a great regional unconformity (Biddle, 1984; Brandner, 1984; Haq *et al.*, 1987). These unconformities are commonly associated with visible karst surfaces, large carbonate megabreccia deposits and the erosional truncation of the slope front and margins, and erosional incisions.

In the south-western Barents Sea, Skjold *et al.* (1998) tentatively identified the uppermost sequence of the Ladinian strata using seismic profiles. A sand-rich interval probably represents the lowstand systems tract, which shows a partially eroded contact below the base of the Carnian materials.

Goggin & Jacquin (1998) distinguished the uppermost Ladinian–lower Carnian sequence K1 in the intracratonic Paris Basin. The K1 sequence boundary has been identified as an erosional unconformity illustrating erosional truncation of the previous sand-rich deposits. Regional tilting occurred in the westward portion of the basin along sequence boundary K1.

In the Southern Alps, Gaetani *et al.* (1998) also recognized the uppermost Ladinian sequence in the Esino carbonate platform, whose basal sequence boundary is locally defined by a deep karstification event (maximum 80 m; Jadoul & Frisia, 1988; Feist-Burkhardt *et al.*, 2008) in the inner platform. A megabreccia body is present in more basinal positions.

In the Southern Alps (Northern Italy), Gianolla *et al.* (1998, 2011) highlighted the uppermost Ladinian major unconformity that corresponds to a strong karst surface on top of the Sciliar Dolomite 3, Esino Limestones 3 and San Salvatore Dolomite 3. In the basins of the western Dolomites, the sequence boundary coincides with a large submarine erosional surface at the base of the Marmolada Conglomerate.

The significant subaerial unconformity capping the top of the Ladinian T–R cycle is also identified in other regions worldwide, such as the Sverdrup Basin in the Canadian Arctic Archipelago (Embry, 1988).

CONCLUSIONS

The Ladinian stratigraphic record of the Catalan Basin displays a large diversity of carbonate facies assemblages whose distribution is mainly controlled by syn-rift subsidence, which also affected the Middle Triassic strata of the Iberian and Ebro Basins. A refined sedimentological and facies analyses provided the framework for subdividing the sedimentary record into two T–R sequences. These sequences reflect an internal third-order sea-level-influenced cyclicity characterized by specific stacking patterns. The two T–R sequences can be regarded as examples of carbonate ramps with low-gradient depositional angles and lateral relationships of facies belts. In particular, the depositional model of the microbial-dominated T–R sequence 1 consists of a stepped ramp. T–R sequence 1 (Lower Ladinian) contains the most developed microbial deposits, such as stromatolites in the inner ramp (at least 7 m thick) and thrombolites in the middle ramp (at least 40 m thick). T–R sequence 2 (Upper Ladinian) is mainly characterized by the occurrence of oolitic stromatolites in the inner ramp and internal shoals and sheltered lagoons in the middle-outer ramp.

A sea-level drop of at least 50 m occurred in the Uppermost Lower Ladinian leaving the platform subaerially exposed. As a result, a prominent karst with significant erosional incisions and profuse collapse breccia fillings was formed in the inner and middle ramp settings. The resultant subaerial unconformity bounds the two T–R sequences. This unconformity is in line with the widespread sea-level fall described in several other coeval basins of the western Tethys and in the Canadian Arctic Archipelago.

Differential rapid syn-rift subsidence is the main controlling factor in accommodation and also in the depositional styles in the T–R sequences. Accommodation plays a key role in controlling the meso and macroscale

morphologies of the microbialites. Domed and mounded forms developed during the stages of increasing accommodation rates, whereas stratiform and biostromal morphologies grew in association with periods of low accommodation rates.

The extensional tectonic regime played a major part in several palaeogeographical domains and in their associated palaeoecological niches where specific microbialites developed. Stromatolites developed in a hypersaline-protected embayment in the inner ramp of T–R sequence 1, whereas large thrombolite mounds managed to grow in open-marine conditions with evaporite precipitation in the middle ramp. These departures from normal salinities and environmental stress were most probably triggered by local palaeogeographical barriers and intensified by the arid to semi-arid climate.

ACKNOWLEDGEMENTS

This study is dedicated to the memory of Professor Francesc Calvet, who made a significant contribution to the study of the Triassic in the Catalan Coastal Ranges. We are indebted to Mateu Esteban (External Consultant, Repsol-Ypf) for his valuable comments on the manuscript and for fruitful discussions in the field, and to Joan Guimerà for his helpful criticism of an earlier version of the manuscript. We gratefully acknowledge the comments and suggestions of Maurice E. Tucker, who, together with Francesc Calvet, set up the modern stratigraphic framework of the area. Thanks are due to Marc Aurell for his constructive advice. Grateful thanks are also extended to two anonymous reviewers whose detailed comments and suggestions considerably improved the manuscript. Isabel Montanez is warmly thanked for the editorial advice and G. von Knorring for English revision. Funding was supplied by Repsol Exploración, S.A, through the E&P director Carlos Macellari, and the Spanish government's I+D+i research project CGL2008-04916, the Consolider-Ingenio 2010 programme under CSD 2006-0004 'Topo-Iberia' and the Grup Consolidat de Recerca 'Geologia Sedimentària' (2009SGR-1451).

The Paratge Natural d'Interès Nacional de Poblet provided facilities and assistance in gaining access to the Protected Natural Area of Serra de l'Ermita, where some fieldwork was carried out.

SUPPORTING INFORMATION

Additional Supporting Information may be found in the online version of this article:

Figure S1. (a) Planar and domal stromatolites (F10) overlain by oolitic grainstone (F1) in the Gaia domain in the Querol section. (b) Line-drawing interpretation showing the boundary (black line) between T–R sequence 1 and 2. (c) Sequence stratigraphic interpretation exhibiting the key stratigraphic surfaces, facies associations and a synthetic stratigraphic section (right part). See legend for further details. Note the onlap stratal terminations of facies association F1 over the domed geometries characterizing the upper parts of the facies association F10. (d) Outcrop photograph showing flat laminated and tabular examples occurring at the base of the facies asso-ciation F10. The hammer is 32 cm long. (e) Polished slab of the basal parts of facies association F10. (f) Oolitic grainstone (facies association F1) displaying silicified ooids.

Figure S2. (a) The mounded geometry of the facies association F12 and the NE large leeward prograding geometries (facies association F15 and F16) downlapping the top of the mud-mound thrombolitic unit (F12, right part) in the Prades domain along the Brugent river, near the village of la Riba. (b) Line-drawing interpretation of the previous photomosaic showing the boundary (turquoise blue line) between T–R sequencess 1 and 2. (c) Sequence stratigraphic interpretation of the previous photomosaic showing the key stratigraphic surfaces, facies associations and geometries of sedimentary bodies. See legend for further details. Note the onlap stratal terminations of the facies association F4 above the subaerial unconformity with karst (black line).

Figure S3. The 150-Km-long platform to basin correlation along the Middle Triassic Catalan Basin, between Pontons and Rasquera, displaying the main facies assemblages. The data derived from the stratigraphic sections between la Figuera-Montsant and Santa Perpetua de Gaia-Pontons are projected on to the main cross-section. Note that the vertical scale has been exaggerated to show the depositional geometries and facies associations. The Prades domain is controlled by two major synsedimentary faults: the la Riba fault to the tyeast and the Ulldemolins-Gandesa fault to the west. The Gaia domain includes sections A, B and 1 to 4, the Prades domain sections 5–10, and the Baix Ebre-Priorat domain sections 11–16.

Figure S4. The 150-Km-long platform to basin correlation along the Middle Triassic Catalan Basin, between Pontons and Rasquera, displaying the main facies assemblages. The data derived from the stratigraphic sections between la Figuera-Montsant and Santa Perpetua de Gaia-Pontons are projected on to the main cross-section. Note that the vertical scale has been exaggerated to show the depositional geometries and facies associations. The Prades domain is controlled by two major synsedimentary faults: the la Riba fault to the east and the Ulldemolins-Gandesa fault to the west. The Gaia domain includes sections A, B and 1 to 4, the Prades domain section 5–10, and the Baix Ebre-Priorat domain sections 11–16.

Figure S5. Sequence stratigraphic interpretation along the 150-Km-long platform to the basin transect of Fig. S4. See legend for more details. The T–R sequence interpretation is based on Embry & Johannessen (1992).

Figure S6. Restored depositional profile of the microbial-dominated T–R sequence 1 (sea level during the microbial carbonate deposition). The unconformity (MRS + TS) is used as a datum for the correlation.

Accommodation of the microbial deposits in the Prades domain is controlled by a major half-graben. (a) Depositional profile shows a vertical exaggeration 9200. (b) Depositional profile shows only a vertical exaggeration 920 without stratigraphic sections. The architecture and continuity of facies distribution suggest a depositional model like a stepped carbonate ramp.

REFERENCES

Ahr, W. M. (1973) The carbonate ramp – an alternative to the shelf model. *Trans. Gulf Coast Assoc. Geol. Soc.*, **23**, 221–225.

Aigner, T. (1985) Storm depositional systems, dynamic stratigraphy in modern and ancient shallow marine sequences. In: *Lecture Notes in Earth Sciences 3* (Ed. by G.M. Friedman, H.J. Neugebauer & A. Seilacher), pp. 1–171. Springer, Berlin.

Aitken, J.D. (1967) Classification and environmental significance of crytalgal limestones and dolomites, with illustrations from the Cambrian and Ordovician of south western Alberta. *J. Sed. Petrol.*, **37**, 1163–1178.

Andres, M.S. & Reid, R.P. (2006) Growth morphologies of modern marine stromatolites: a case study from Highborne Cay, Bahamas. *Sed. Geol.*, **185**, 319–328.

Arnal, I., Calvet, F., Márquez, L., Márquez-Aliaga, A. & Solé De Porta, N. (2002) The epeiric carbonate platform (Imón and Isábena Formations) of the Upper Triassic from the Northeastern Iberian Peninsula. *Acta Geol. Hisp.*, **37**, 299–328.

Awramik, S.M. & Riding, R. (1988) Role of algal eukaryotes in subtidal columnar stromatolite formation. *Proc. Natl Acad. Sci. USA*, **85**, 1327–1329.

Barthel, K.W., Swinburne, N.H.M & Conway Morris, S. (1990) *Solnhofen: A Study in Mesozoic Palaeontology*. Cambridge University Press, Cambridge. 236 pp.

Biddle, K.T. (1984) Triassic sea level changes and the Ladinian-Carnian stage boundary. *Nature*, **308**, 631–633.

Bleahu, M., Mantea, G, Bordea, S., Panin, S., Stefănescu, M., Sikić, K., Haas, J., Kovacs, S., Pero, C. S., Berczi-Makk, A., Konrad, G. Y., Nagy, E., Ralisch-Felgenhauer, E. & Torok, A. (1996) Triassic facies types, evolution and paleogeographic relations of the Tisza Megaunit. *Acta Geol. Hung.*, **37**, 187–234.

Blendinger, W. (1994) The carbonate factory of Middle Triassic buildups in the Dolomites, Italy: a quantitative analysis. *Sedimentology*, **41**, 1147–1159.

Blendinger, W. (1996) The carbonate factory of Middle Triassic buildups in the Dolomites, Italy: a quantitative analysis [Reply]. *Sedimentology*, **43**, 402–404.

Bond, G.C. & Kominz, M.A. (1984) Construction of tectonic subsidence curves for the early Paleozoic miogeocline, southern Canadian Rocky Mountains: implications for subsidence machanisms, age of break-up, and crustal thinning. *Geol. Soc. Am. Bull.*, **95**, 155–173.

Brandner, R. (1984) Meeresspiegelschwankungen und tektonik in der Trias der NW-Tethys. *Jarb. Geol. Bunder.*, **126**, 435–475.

Brandner, R., Flügel, E. & Senowbari-Daryan, B. (1991) Microfacies of carbonate slope boulders: indicator of the source area (Middle Triassic: Mahlknecht Cliff, Western Dolomites). *Facies*, **25**, 279–296.

Browne, K.M., Golubic, S. & Seong-Joo, L. (2000) Shallow marine microbial carbonate deposits. In: *Microbial Sediments* (Ed. by R.E. Riding & M. Awramik), pp. 233–249. Springer-Verlag, Heilderberg.

Burchette, T.P. & Wright, V.P. (1992) Carbonate ramp depositional systems. *Sed. Geol.*, **79**, 3–57.

Burne, R.V. & Moore, L.S. (1987) Microbialites; organosedimentary deposits of benthic microbial communities. *Palaios*, **2**, 241–254.

Calvet, F. & Ramon, X. (1987) Estratigrafía, sedimentología y diagenesis del Muschelkalk inferior de los Catalánides. *Cuad. Geol. Ibérica*, **11**, 141–169.

Calvet, F. & Tucker, M.E. (1988) Outer ramp cycles in the Upper Muschelkalk of the Catalan Basin, northeast Spain. *Sed. Geol.*, **57**, 185–198.

Calvet, F. & Tucker, M.E. (1995) Mud-mound with reefal caps in the upper Muschelkalk (Triassic), eastern Spain. *Spec. Publ. Int. Assoc. Sed.*, **23**, 311–333.

Calvet, F., March, M. & Pedrosa, A. (1987) Estratigrafía, sedimentología y diagenesis del Muschelkalk superior de los Catalánides. *Cuad. Geol. Ibérica*, **11**, 171–197.

Calvet, F., Tucker, M.E. & Henton, J.M. (1990) Middle Triassic carbonate ramp systems in the Catalan Basin, northeast Spain: facies, systems tracts, sequences and controls. *Spec. Publ. Int. Assoc. Sed.*, **9**, 79–108.

Cartaña, J. (1994) Noves aportacions paleontològiques al Muschelkalk superior de les Muntanyes de Prades: el cas del Pinetell. *Quaderns de Vilaniu*, **25**, 67–93.

Catuneanu, O. (2006). *Principles of Sequence Stratigraphy*. Elsevier, Amsterdam, 375 pp.

Catuneanu, O., Abreu, V., Bhattacharya, J.P., Blum, M.D., Dalrymple, R.W., Eriksson, P.G., Fielding, C.R., Fisher, W.L., Galloway, W.E., Gibling, M.R., Giles, K.A., Holbrook, J.M., Jordan, R., Kendall, C.G.ST.C., Macurda, B., Martinsen, O.J., Miall, A.D., Neal, J.E., Nummedal, D., Pomar, L., Posamentier, H.W., Pratt, B.R., Sarg, J.F., Shanley, K.W., Steel, R.J., Strasser, A., Tucker, M.E. & Winker, C. (2009) Towards the standardization of sequence stratigraphy. *Earth-Sci. Rev.*, **92**, 1–33.

Catuneanu, O., Galloway, E., Kendall, G.St.C., Miall, A.D., Posamentier, H.W., Strasser, A. & Tucker, M. E. (2011) Sequence stratigraphy: methodology and nomenclature. *Newsl. Stratigr.*, **44**, 173–275.

Chafetz, H.S. & Buczynski, C. (1992) Bacterially induced lithification of microbial mats. *Palaios*, **7**, 277–293.

Colombié, C. & Strasser, A. (2005) Facies, cycles, and controls on the evolution of a keep-up carbonate platform (Kimmeridgian, Swiss Jura). *Sedimentology*, **52**, 1207–1227.

Embry, A.F. (1988) Triassic sea-level changes: evidence from the Canadian Arctic Archipelago. In: *Sea-Level Changes – An Integrated Approach* (Ed by C.K. Wilgus, B.S. Hastings, C.G.St.C. Kendall, H.W. Posamentier, C.A. Ross & J.C. Van Wagoner) *Soc. Sed. Geol. Spec. Publ.*, **42**, 2.

Embry, A.F. & Johannessen, E.P. (1992) T-R sequence stratigraphy, facies analysis and reservoir distribution in the uppermost Triassic-Lower Jurassic succession, Western Sverdrup Basin, Arctic Canada. In: *Arctic Geology and Petroleum Potential. Special Publication, 2* (Ed. by T.O. Vorren, E. Bergsager, O.A. Dahl-Stamnes, E. Holter, B. Johansen, E. Lie & T.B. Lund) *Norw. Petrol. Soc. Spec. Publ.*, **2**, 121–146.

Emmerich, A., Zamparelli, V., Bechstädt, T. & ZÜhlke, R. (2005) The reefal margin and slope of a Middle Triassic carbonate platform: the Latemar (Dolomites, Italy). *Facies*, **50**, 573–614.

Erwin, D.H. (1994) The Permo-Triassic extinction. *Nature*, **367**, 231–236.

Feist-Burkhardt, S., Götz, A.E., Szulc, J., Borkhataria, R., Geluk, M., Haas, J., Hornung, J., Jordan, P., Kempf, O., Michalik, J., Nawrocki, J., Reinhardt, L., Ricken, W., Röhling, H.G., Rüffer, T., Török, A. & Zühlke, R. (2008) Triassic. In: *The Geology of Central Europe. Volume 2: Mesozoic and Cenozoic* (Ed. by. T. McCann), pp. 749–821. The Geological Society, London.

Flügel, E & Senowbari-Daryan, B. (2001) Triassic reefs of the Tethys. In: *The History and Sedimentology of Ancient Reef Systems*(Ed. by. G. Stanley) *Top. Geobiol.*, **17**, 217–249.

Fregenal-Martínez, M, Meléndez, N. & Martínez-Delcòs, X. (1995) Montsec and Montral- Alcover, Two Konservat-Lagerstätten, Catalonia, Spain. Field trip guide book-II. International Symposium on Lithographic Limestones Institut d'Estudis Ilerdencs. Lleida, 12–29.

Fürsich, F.T., Werner, W., Schneider, S. & Mäuser, M. (2007) Sedimentology, taphonomy, and palaeoecology of a laminated plattenkalk from the Kimmeridgian of the northern Franconian Alb (southern Germany). *Palaeogeogr. Palaeoclimatol. Palaeoecol.*, **243**, 92–117.

Gaetani, M., Gnaccolini, M., Jadoul, F. & Garzanti, E. (1998) Multiorder sequence stratigraphy in the Triassic system of the Western Southern Alps. In: *Mesozoic and Cenozoic Sequence Stratigraphy of European Basins* (Ed. by P-C. De Graciansky, J. Hardenbol, T. Jacquin & P. Vail) *Soc. Sed. Geol. Spec. Publ.*, **60**, 702–717.

Garrett, P. (1970) Phanerozoic stromatolites: noncompetitive ecologic restriction by grazing and burrowing animals. *Science*, **169**, 171–173.

Gianolla, P. & Jacquin, T. (1998) Triassic sequence stratigraphic framework of western European basins. In: *Mesozoic and Cenozoic Sequence Stratigraphy of European Basins* (Ed. by P.C. Graciansky, J. Hardenbol, T. Jacquin & P. Vail) *Soc. Sed. Geol. Spec. Publ.*, **60**, 643–650.

Gianolla, P., De Zanche, V. & Mietto, P. (1998) Triassic sequence stratigraphy in the Southern Alps (Northern Italy): definition of sequences and basin evolution. In: *Mesozoic and Cenozoic Sequence Stratigraphy of European Basins* (Ed. by P-C. De Graciansky, J. Hardenbol, T. Jacquin & P. Vail) *Soc. Sed. Geol. Spec. Publ.*, **60**, 719–747.

Gianolla, P., Caggiati, M. & Furin, S. Response of carbonate systems to sea-level drop: a case study from Middle Triassic of the Dolomites (Italy). Abst., 28th IAS Meeting of Sediment., Zaragoza, Spain, 2011.

Goggin, V. & Jacquin, T. (1998) A sequence stratigraphic framework of the marine and continental Triassic series in the Paris Basin, France. In: *Mesozoic and Cenozoic Sequence Stratigraphy of European Basins* (Ed. by P-C. De Graciansky, J. Hardenbol, T. Jacquin & P. Vail) *Soc. Sed. Geol. Spec. Publ.*, **60**, 667–690.

Gómez, M. & Guimerà, J. (1999) Estructura alpina de la Serra de Miramar y del NE de las Muntanyes de Prades (Cadena Costero Catalana). *Rev. Soc. Geol. Esp.*, **12**, 405–418.

Goy, A. (1995) Ammonoideos del Triásico Medio de España: Bioestratigrafía y Correlaciones. *Cuad. Geolog. Iber.*, **19**, 21–60.

Gradstein, F.M., Agterberg, F.P., Ogg, J.G., Hardenbol, J., Van Veen, P., Thierry, J & Huang, Z. (1994) A Mesozoic time scale. *J. Geo. Res.*, **99**, 24051–24074.

Haas, J & Budai, T. (1995) Upper Permian-Triassic facies zones in the Transdanubian Range. *Rivis. Italian. Paleont. Stratig.*, **101**, 249–266.

Hagdorn, H. (1991) The Muschelkalk in Germany – an introduction. In: *Muschelkalk – A field Guide* (Ed. by H. Hagdorn, T. Simon & J. Szulc), pp. 7–21. Goldsechneck-Verlag, Werner, Korb.

Haq, B.U., Hardenbol, J. & Vail, P.R. (1987) Chronology of fluctuating sea levels since the Triassic. *Science*, **235**, 1156–1167.

Harris, M.T. (1993) Reef fabrics, biotic crusts and syndepositional cements of the Latemar reef margin (Middle Triassic), northern Italy. *Sedimentology*, **40**, 383–401. 867.

Jadoul, F. & Frisia, S. (1988) Le Evinosponge: ipotesi genetiche di cementi calcitici nella piattaforma ladinica delle Prealpi lombarde (Alpi Meridionali). *Riv. Ital. Paleontol. Stratigr.*, **94**, 81–104.

Jaglarz, P. & Szulc, J. (2003) Middle Triassic evolution of the Tatricum sedimentary basin: an attempt of sequence stratigraphy to the Wierchowa Unit in the Polish Tatra Mountains. *Ann. Soc. Geol. Pol.*, **73**, 169–182.

Jaglarz, P. & Uchman, A. (2010) A hypersaline ichnoassemblage from the Middle Triassic carbonate ramp of the Tatricum domain in the Tatra Mountains, Southern Poland. *Palaeogeogr. Palaeoclimatol. Palaeoecol.*, **292**, 71–81.

James, N.P. & Bourque, P-A. (1992) Reefs and mounds. In: *Facies Models. Response to Sea Level Change* (Ed by R.G. Walker & N.P. James), pp. 323–349. Geological Association of Canada, Ontario, Canada.

Johnson, J.G. & Murphy, M.A. (1984) Time-rock model for Siluro-Devonian continental shelf, western United States. *Geol. Soc. Am. Bull.*, **96**, 567–587.

Keim, L. & Schlager, W. (2001) Quantitative compositional analysis of a Triassic carbonate platform (Southern Alps, Italy). *Sed. Geol.*, **139**, 261–283.

Kendall, C.G.St. C. & Schlager, W. (1981) Carbonates and relative changes in sea level. *Mar. Geol.*, **44**, 181–212.

Kennard, J.M. & James, N.P. (1986) Thrombolites and stromatolites: two distinct types of microbial structures. *Palaios*, **1**, 492–503.

Keupp, H. (1977) Ultrafazies und Genese der Solnhofener Plattenkalke (Oberer Malm, Südliche Frankenalb). *Abdh. Naturhist. Gesell. Nürn.*, **37**, 1–128.

Lehrmann, D.J. (1999) Early Triassic calcimicrobial mounds and biostromes of the Nanpanjiang basin, south China. *Geology*, **27**, 359–362.

Logan, B.W. & Cebulski, D.E. (1970) Sedimentary environments of Shark Bay, Western Australia. In: *Carbonate Sedimentation and Environments, Shark Bay, Western Australia* (Ed by B.W. Logan, G.R. Davies, J.F. Read & D. E Cebulski) *Am. Assoc. Petrol. Geol. Mem.*, **13**, 1–37.

Logan, B.W., Hoffman, P. & Gebelein, C.D. (1974) Algal mats, cryptalgal fabrics, and structures, Hamelin Pool, Western Australia. In: *Evolution and Diagenesis of Quaternary Carbonate Sequences, Shark Bay, Western Australia*. (Ed. by B.W. Logan, J.F. Read, G.M. Hagan, P. Hoffman, R.G. Brown, P.J. Woods & C. Gebelein) *Am. Assoc. Petrol. Geol.*, **22**, 140–194.

Marangon, A., Gattolin, G., Della Porta, G. & Preto, N. (2011) The Latemar: a flat-topped, steep fronted platform dominated by microbialites and synsedimentary cements. *Sed. Geol.*, **240**, 97–114.

Marzo, M. (1980) El Buntsandstein de los Catalánides: Estratigrafía y procesos de sedimentación. PhD Thesis, University of Barcelona, Barcelona.

Maurer, F. & Schlager, W. (2003) Lateral variation in sediment composition and bedding in Middle Triassic interplatform basins (Buchenstein Formation, southern Alps, Italy). *Sedimentology*, **50**, 1–22.

McKenzie, D.P. (1978) Some remarks on the development of sedimentary basins. *Earth Planet. Sci. Lett.*, **40**, 25–32.

Mercedes, R., Arenas, C. & Esteban, M. (2011) Ladinian carbonate sedimentation during Triassic rifting: sequence stratigraphy and evolution of accommodation in a fault-controlled setting (Catalan Coastal Ranges, Spain). In: *Abstracts, 28th IAS Meeting of Sedimentology, Zaragoza, Spain* (Eds. B. Bádenas, M. Aurell & A.M. Alonso-Zarza), p. 496. University of Zaragoza, Zaragoza.

Monty, C.L.V. (1995) The rise and nature of carbonate mudmounds: an introductory actualistic approach. In: *Carbonate Mud-Mounds: Their Origin and Evolution* (Ed by C.L.V. Monty, D.W.J. Bosence, P.H. Bridges & B.R. Pratt) *Inter. Assoc. Sed. Spec. Publ.*, **23**, 11–48.

Neumann, A.C. & Macintyre, I.G. (1985) Reef response to sea level rise: keep-up, catch-up or give-up. *Proc. Fifth Int. Coral Reef Cong. Tahiti*, **3**, 105–110.

Neuweiler, F., Gautret, P., Volker, T., Lange, R., Michaelis, W. & Reitner, J. (1999) Petrology of Lower Cretaceous carbonate mud mounds (Albian, N. Spain): insights into organomineralic deposits of the geological record. *Sedimentology*, **46**, 837–859.

Ogg, J.G., Ogg, G. & Gradstein, F.M. (2008) *The Concise Geological Time Scale*. Cambridge University Press, Cambridge, 177 pp.

Palermo, D., Aigner, T., Nardon, S. & Blendinger, W. (2010) Three-dimensional facies modelling of carbonate sand bodies: Outcrop analog study in an epicontinental basin (Triassic, southwest Germany). *Am. Assoc. Petrol. Geol.*, **94**, 475–512.

Piros, O. (2002) Anisian to Carnian carbonate platform facies and dasycladacean biostratigraphy of the Aggtelek Mountains, Northeastern Hungary. *Acta. Geol. Hung.*, **45**, 119–151.

Pomar, L. & Hallock, P. (2008) Carbonate factories: a conundrum in sedimentary geology. *Earth-Sci. Rev.*, **87**, 134–169.

Pratt, B.R. (1982) Stromatolitic framework of carbonate mudmounds. *J. Sed. Res.*, **52**, 1203–1227.

Pratt, B.R. (1995). The origin, biota and evolution of deep-water mud-mounds. In: *Carbonate Mud-Mounds: Their Origin and Evolution*. (Ed by C.L.V. Monty, D.W.J. Bosence, P.H. Bridges & B.R. Pratt) *Int. Assoc. Sed. Spec. Publ.*, **23**, 49–123.

Pratt, B.R. & Haidl, F.M. (2008) Microbial pach reefs in Upper Ordovician Red River strata, Williston Basin, Saskatchewan: signal of heating in a deteriorating epeiric sea. In: *Dynamics of Epeiric Seas* (Ed by B.R Pratt & C. Holmden) *Geol. Assoc. Can. Spec. Pap.*, **48**, 303–340.

Pruss, S.B. & Bottjer, D.J. (2005) The reorganization of reef communities following the end-Permian mass extinction. *Comp. Rend. Palev.*, **4**, 553–568.

Ramos, A., Sopeña, A., Sánchez-Moya, A. & Muñoz, A. (1996) : Subsidence analysis, maturity modelling and hydrocarbon generation of the Alpine sedimentary sequence in the NW of the Iberian Ranges (Central Spain). *Cuad. Geol. Ibérica*, **21**, 23–53.

Read, J.F. (1982) Carbonate platforms of passive (extensional) continental margins: types, characteristics and evolution. *Tectonophysics*, **81**, 195–212.

Read, J.F. (1985) Carbonate platform facies models. *Am. Assoc. Petrol. Geol.*, **69**, 1–21.

Reitner, J. & Neuweiler, F. (1995) Mud mounds: recognizing a polygenetic spectrum of fine –grained carbonate buildups. In: *Mud Mounds: A Polygenetic Spectrum of Fine-Grained Carbonate Buildups* (Ed. by J. Reitner, F. Neuweiler, P. Dingle, G. Flajs, Ch. Hensen, H. Hüssner, R. Leinfelder, B. Kaufmann, H. Keupp, D. Meischner, J. Paul, P Schäfer, P. Vigener, K. Warnke & H. Weller) *Facies*, **32**, 2–4.

Riding, R.E. (2000) Microbial carbonates: the geological record of calcified bacterial-algal mats and biofilms. *Sedimentology*, **47** (suppl 1), 179–214.

Riding, R.E. & Awramik, M. (2000) *Microbial Sediments*. Springer-Verlag, Heilderberg.

Rüffer, T. & Bechstädt, T. (1998) Triassic sequence stratigraphy in the western part of the Northern Calcareous Alps (Austria). In: *Mesozoic and Cenozoic Sequence Stratigraphy of European Basins* (Ed. by P.C. Graciansky, J. Hardenbol, T. Jacquin & P. Vail) *Soc. Sed. Geol. Spec. Publ.*, **60**, 751–761.

Rüffer, T. & ZÜhlke, R. (1995) Sequence stratigraphy and sea-level changes in the Early to Middle Triassic of the Alps: a global comparison. In: *Sequence Stratigraphy and Depositional Response to Eustatic, Tectonic and Climatic Forcing* (Ed. by B. Haq), pp. 161–207. Kluwer, Dordrecht.

Russo, F., Mastandrea, A. & Neri, C. (1998) Evoluzione degli organismi costruttori nelle piataforme Triassiche delle Dolomiti (Italia). *Soc. Geol. Ital. Mem.*, **53**, 479–488.

Salas, R. & Casas, A. (1993) Mesozoic extensional tectonics, stratigraphy and cristal evolution turing the Alpine cycle of the eastern Iberian basin. *Tectonophysics*, **228**, 33–55.

Salas, R., Guimera, J., Mas, R., Martin-Closas, C., Melendez, A. & Alonso, A. (2001) Evolution of the mesozoic central iberian Rift System and its Cainozoic inversion (Iberian chain). In: *Peri-Tethys Memoir 6: Peri-Tethyan Rift/Wrechn Basins and Passive Margins* (Ed. by P.A. Ziegler, W. Cavazza, A.H.F. Robertson & S. Crasquin-Soleau) *Mém. Mus. Hist. Natl.*, **186**, 145–185.

Schlager, W. (2000) Sedimentation rates and growth potential of tropical, cool water and mud mound carbonate factories. In: *Carbonate Platform Systems: Components and Interactions* (Ed. by E. Insalaco, P.W. Skelton & T.J. Palmer) *Geol. Soc. London Spec. Publ.*, **178**, 217–227.

Schlager, W. (2003) Benthic carbonate factories of the Phanerozoic. *Int. J. Earth Sci. (Geol Rundsch)*, **92**, 445–464.

Schmoker, J.W. & Halley, R.B. (1982) Carbonate porosity versus depth: a predictable relation for south Florida. *Am. Assoc. Petrol. Geol.*, **66**, 2561–2570.

Sclater, J.G. & Christie, P.A.F. (1980) Continental stretching: an explanation of the post-mid Cretaceous subsidence of the Central North Sea Basin. *J. Geophys. Res.*, **85**, 3711–3739.

Seong-Joo, L., Browne, K.M. & Golubic, S. (2000) On stromatolite lamination. In: *Microbial Sediments* (Ed by R.E. Riding & M. Awramik), pp. 16–25. Springer-Verlag, Heilderberg.

Skjold, L.J., Van Veen, P.M., Kristensen, S-E. & Rasmussen, A.R. (1998) Triassic sequence stratigraphy of the southwestern Barents Sea. In: *Mesozoic and Cenozoic Sequence Stratigraphy of European Basins* (Ed. by P-C. De Graciansky, J. Hardenbol, T. Jacquin & P. Vail) *Soc. Sed. Geol. Spec. Publ.*, **60**, 651–666.

Sole, N, Calvet, F. & Torrento, L. (1987) Analisis palinologico del Triasico de los Catalanides (NE Espana). *Cuad. Geol. Iber.*, **11**, 237–254.

Spence, G.H. & Tucker, M.E. (2007) A proposed integrated multi-signature model for peritidal cycles in carbonates. *J. Sed. Res.*, **77**, 797–808.

Steckler, M.S. & Watts, A.B. (1978) Subsidence of the Atlantic-type continental margin off New York. *Earth Planet. Sci. Lett.*, **41**, 1–13.

Strasser, A., Pittet, B., Hillgärtner, H. & Pasquier, J-B. (1999) Depositional sequences in shallow carbonate-dominated sedimentary systems: concepts for a high-resolution analysis. *Sed. Geol.*, **128**, 201–221.

Szulc, J. (1993) Early Alpine tectonics and lithofacies sucession in the Silesian part of the Muschelkalk Basin. In: *Muschelkalk, Schöntaler Symposium 1991* (Ed. by H. Hagdorn & A. Seilacher) *Sonderbände der Gesellschaft für Naturkunde in Württemberg*, **2**, 19–28. Goldschnek, Sttutgart, Korb.

Szulc, J. (2000) Middle Triassic evolution of the Northern Peri-Tethys area influenced by early opening of the Tethys Ocean. *Ann. Soc. Geol. Pol.*, **70**, 1–48.

Török, Á. (1998). Controls on development of Mid-Triassic ramps: examples from southern Hungary. In: *Carbonate Ramps*. (Ed. by V.P. Wright & T.P. Burchette) *Geol. Soc. London Spec. Publ.*, **149**, 339–367.

Tucker, M.E. & Marshall, J. (2004) Diagenesis and geochemistry of Upper Muschelkalk (Triassic) buildups and associated facies in Catalonia (NE Spain): a paper dedicated to Francesc Calvet. *Geol. Act.*, **4**, 257–269.

Tucker, M.E., Calvet, F. & Hunt, D. (1993) Sequence stratigraphy of carbonate ramps: systems tracts, models and application to the Muschelkalk carbonate platforms of eastern Spain. *Spec. Publ. Int. Assoc. Sed.*, **18**, 397–415.

Vargas, H. (2002) Análisis y comparación de la subsidencia entre las cuencas Ibérica y Ebro Central durante el Pérmico y Triásico y su relación con el relleno sedimentario. PhD Thesis, Universidad Complutense de Madrid, Madrid.

Vargas, H., Gaspar-Escribano, J.M., López-Gómez, J., Van Wees, J-D., Cloetingh, S., De La Horra, R. & Arche, A. (2009) A comparison of the Iberian and Ebro Basins during the Permian and Triassic, Eastern Spain: a quantitative subsidence modelling approach. *Tectonophysics*, **474**, 160–183.

Via, L., Villalta, J.F. & Esteban, M. (1977) Paleontología y paleoecología de los yacimientos fosilíferos del Muschelkalk superior entre Alcover y Montral (Montañas de Prades, Província de Tarragona). *Cuad. Geol. Ibérica*, **4**, 247–256.

Vilas, L., Martín-Chivelet, J. & Arias, C. (2003) Integration of subsidente and sequence stratigraphic análisis in the Cretaceous carbonate platforms of the Prebetic (Jumilla-Yecla Region), Spain. *Palaeogeogr. Palaeoclimatol. Palaeoecol.*, **200**, 107–129.

Virgili, C., Sopeña, A., Ramon, A., Arche, A. & Hernando, A. (1983) El relleno posthercínico y el cominenzo de la sedimentación Mesozoica. *Libr. Jub. Jos. María Rios, Mad.*, **2**, 25–36.

Watts, A.B. (1981) The U.S. Atlantic continental margin: subsidence history, crustal structure and thermal evolution: Geology of passive continental margins. In: *Geology of Passive Continental Margins: History, Structure and Sedimentology Record (With Special Emphasis on the Atlantic Margin)*. (Ed. by A.W. Bally, A.B. Watts, J.A. Grow, W. Manspeizer, D. Bernoulli, Schreiber C.& J.M. Hunt) *Am. Assoc. Petrol. Geol. Educ. Cours. Not. Ser.*, **19**, 1–24.

Webb, G.E. (1996) Was Phanerozoic reef history controlled by the distribution of non-enzymatically secreted reef carbonates (microbial carbonate and biologically induced cement)? *Sedimentology*, **43**, 947–971.

Ziegler, P.A. (1982) Triassic rifts and facies patterns in Western and Central Europe. *Geol. Runds.*, **71**, 747–772.

Ziegler, P.A. (1988) Evolution of Arctic-North Atlantic and the Western Tethys. *Am. Assoc. Petrol. Geol. Mem.*, **43**, 198.

Manuscript received 16 April 2012; In revised form 31 January 2013; Manuscript accepted 16 March 2013.

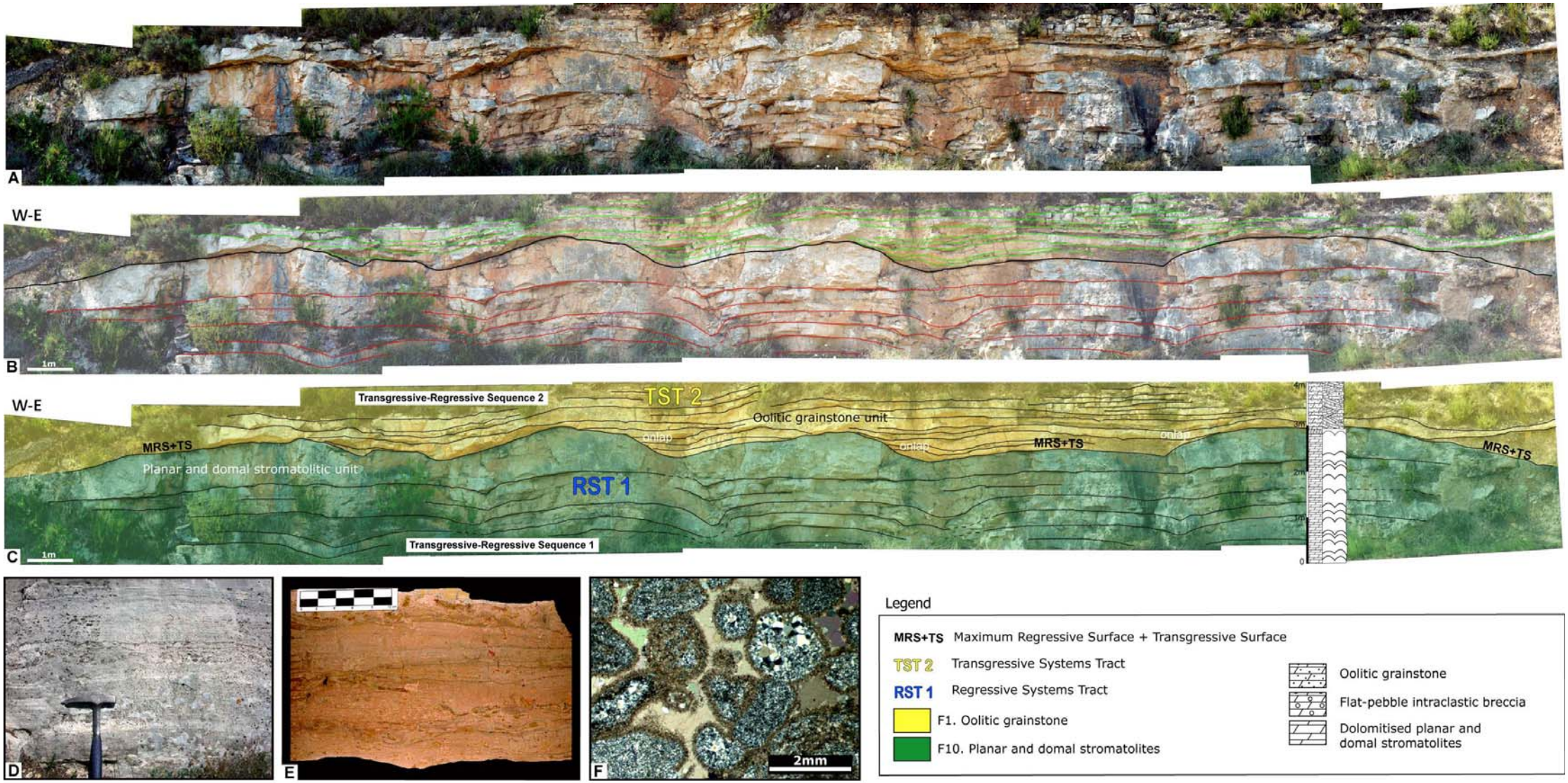
A
W-E
B
1m
W-E
Transgressive-Regressive Sequence 2
TST 2
Oolitic grainstone unit
onlap
onlap
onlap
MRS+TS
MRS+TS
MRS+TS
Planar and domal stromatolitic unit
RST 1
Transgressive-Regressive Sequence 1
C
1m
4m
3m
2m
1m
0
D
E
F
2mm
Legend
MRS+TS Maximum Regressive Surface + Transgressive Surface
TST 2 Transgressive Systems Tract
RST 1 Regressive Systems Tract
F1. Oolitic grainstone
F10. Planar and domal stromatolites
Oolitic grainstone
Flat-pebble intraclastic breccia
Dolomitised planar and domal stromatolites

Figure. S1

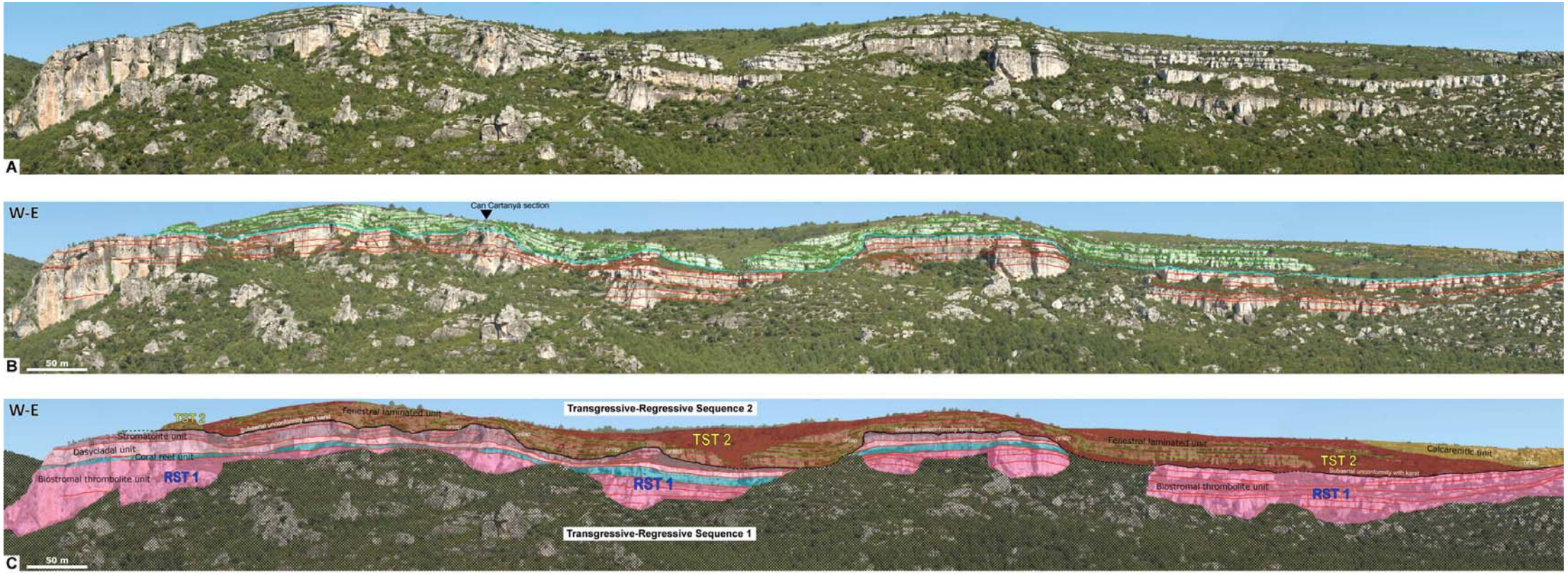
A
W-E
Can Cartanyà section
B
50 m
W-E
TST 2
Fenestral laminated unit
Transgressive-Regressive Sequence 2
Stromatolite unit
Dasycladal unit
Coral reef unit
Bioestromal thrombolite unit
RST 1
TST 2
RST 1
Fenestral laminated unit
Calcarenitic unit
TST 2
Bioestromal thrombolite unit
RST 1
Transgressive-Regressive Sequence 1
C
50 m
Legend
F4. Oncolitic-oolitic-peloidal floatstone and grainstone
F12. Microbial-peloidal thrombolites
F13. Calmicrobial boundstone with bioclasts
F14. Coral-microbial boundstone to rudstone
F15. Laminated packstone of oncoids and peloids
F16. Packstone to rudstone of dasyclads, bioclasts and peloids
TST 2 Transgressive Systems Tract
RST 1 Regressive Systems Tract
Covered

Figure. S2

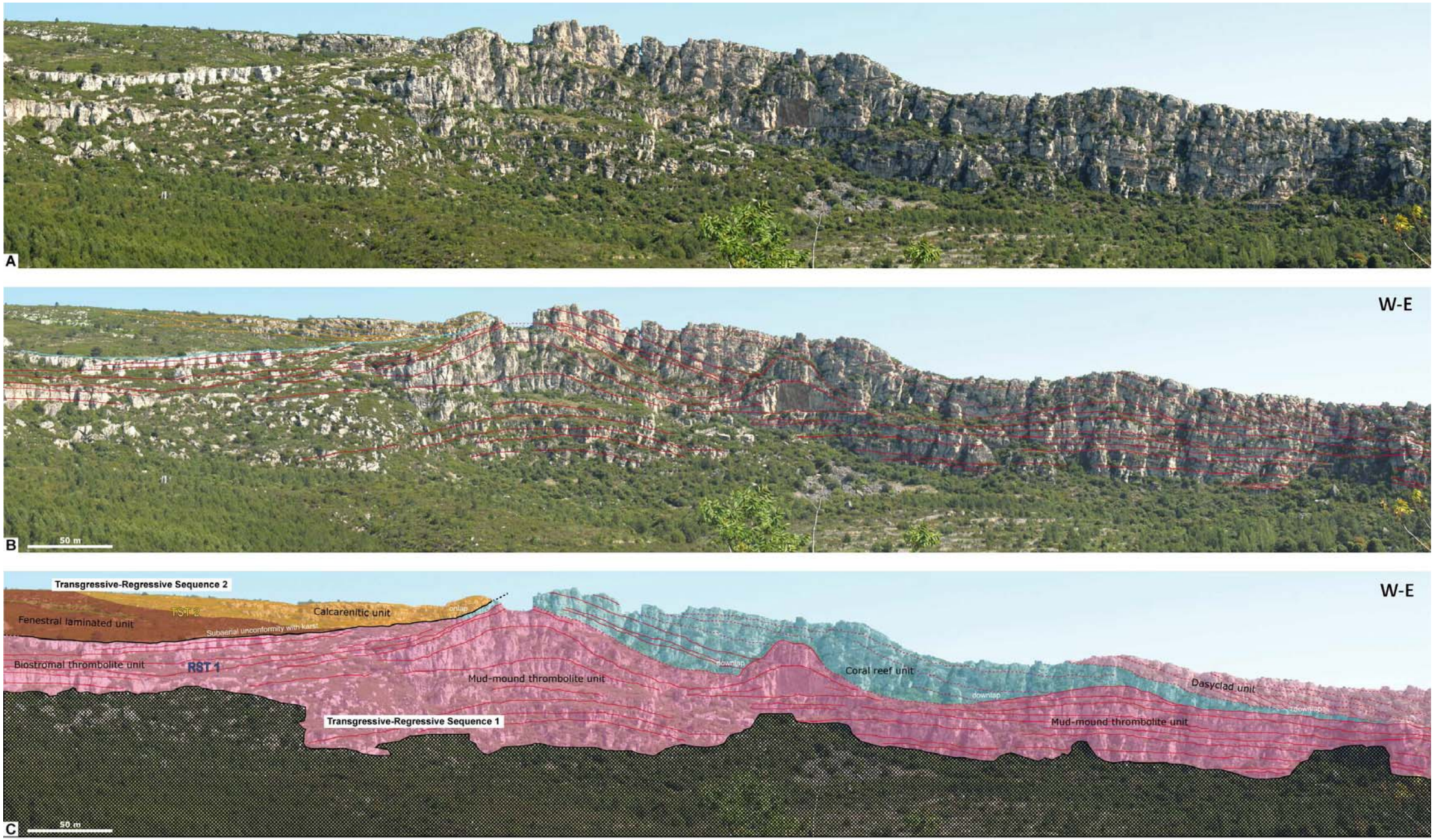
A
B
W-E
50 m
C
W-E
Transgressive-Regressive Sequence 2
TST 2
Fenestral laminated unit
Calcarenitic unit
onlap
Subaerial unconformity with karst
Biostromal thrombolite unit
RST 1
Mud-mound thrombolite unit
downlap
Coral reef unit
Dasyclad unit
Transgressive-Regressive Sequence 1
Mud-mound thrombolite unit
50 m
Legend
F4. Oncolitic-oolitic-peloidal floatstone and grainstone
F12. Microbial-peloidal thrombolites
F14. Coral-microbial boundstone to rudstone
F15. Laminated packstone of oncoids and peloids
F16. Packstone to rudstone of dasyclads, bioclasts and peloids
TST 2 Transgressive Systems Tract
RST 1 Regressive Systems Tract
Covered

Figure. S3

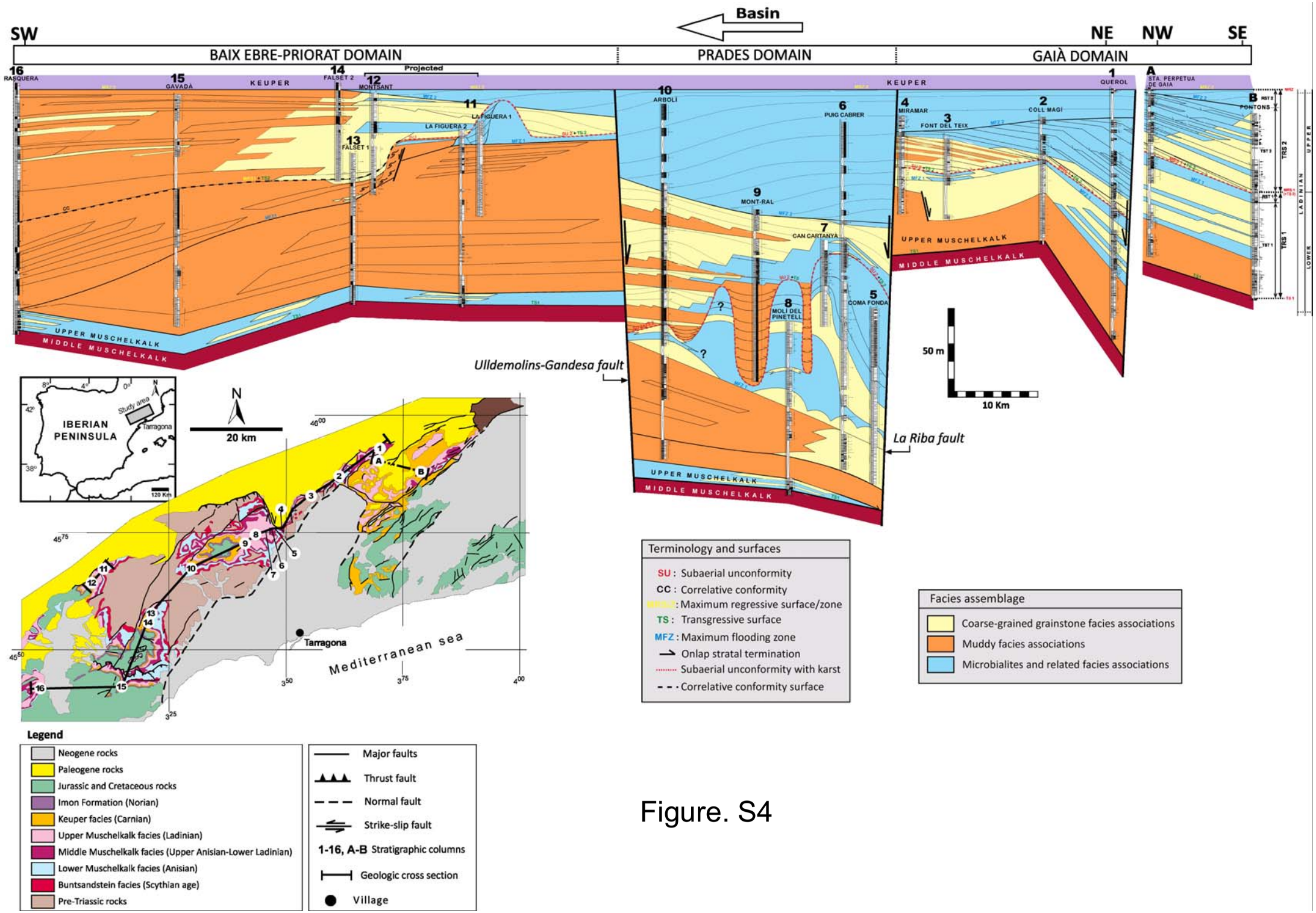
SW
Basin
NE
NW
SE
BAIX EBRE-PRIORAT DOMAIN
PRADES DOMAIN
GAIÀ DOMAIN
Projected
KEUPER
UPPER MUSCHELKALK
MIDDLE MUSCHELKALK
16 RASQUERA
15 GAVASA
14 FALSET 2
13 FALSET 1
12 MONTSANT
11 LA FIGUERA 1
LA FIGUERA 2
10 ARBOLI
9 MONT-RAL
8 MOLI DEL PINETELL
7 CAN CARTANYA
6 PUIG CABRER
5 COMA FONDA
4 MIRAMAR
3 FONT DEL TEIX
2 COLL MAGI
1 QUEROL
A STA. PERPETUA DE GAIA
B PONTONS
Ulldemolins-Gandesa fault
La Riba fault
50 m
10 Km
TRS 2
TRS 1
LADINIAN
UPPER
LOWER
IBERIAN PENINSULA
Study area
Tarragona
120 Km
N
20 km
Mediterranean sea
Terminology and surfaces
SU : Subaerial unconformity
CC : Correlative conformity
MRSZ : Maximum regressive surface/zone
TS : Transgressive surface
MFZ : Maximum flooding zone
Onlap stratal termination
Subaerial unconformity with karst
Correlative conformity surface
Facies assemblage
Coarse-grained grainstone facies associations
Muddy facies associations
Microbialites and related facies associations
Legend
Neogene rocks
Paleogene rocks
Jurassic and Cretaceous rocks
Imon Formation (Norian)
Keuper facies (Carnian)
Upper Muschelkalk facies (Ladinian)
Middle Muschelkalk facies (Upper Anisian-Lower Ladinian)
Lower Muschelkalk facies (Anisian)
Buntsandstein facies (Scythian age)
Pre-Triassic rocks
Major faults
Thrust fault
Normal fault
Strike-slip fault
1-16, A-B Stratigraphic columns
Geologic cross section
Village

Figure. S4

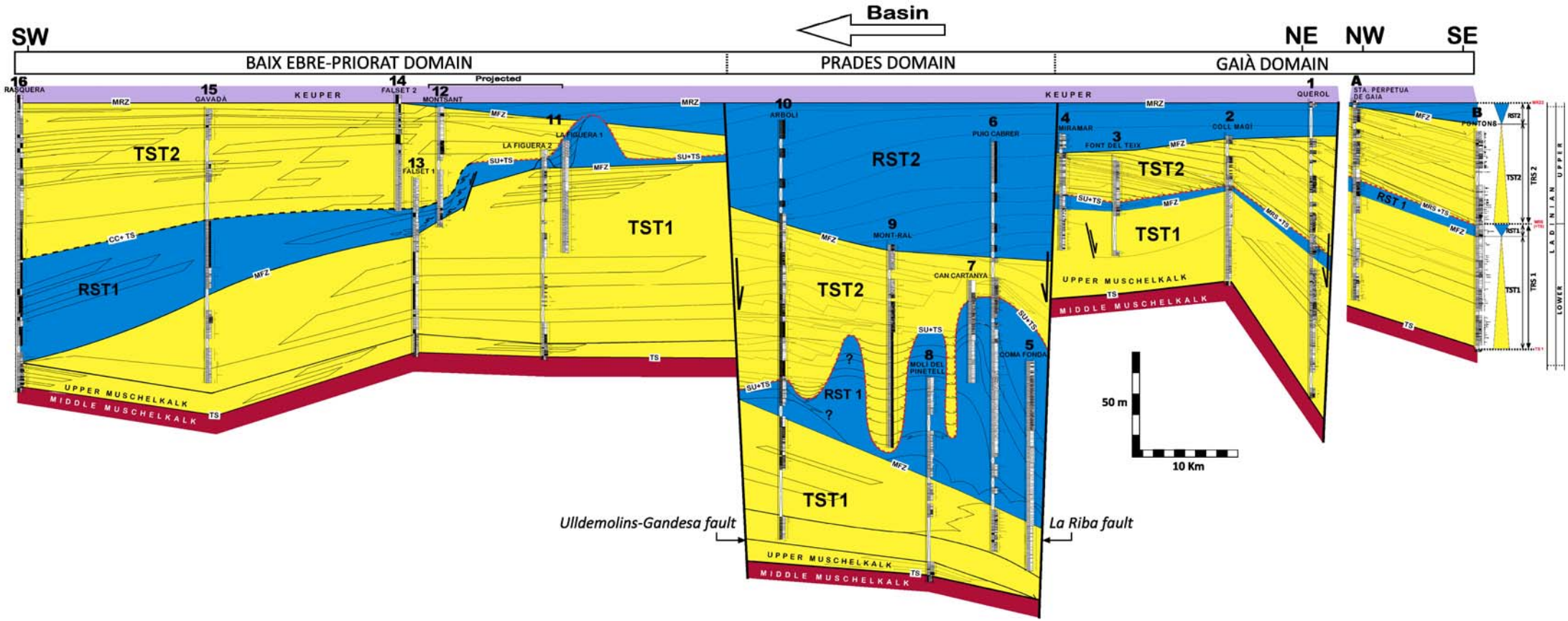

Colour squeme	T-R Sequences	Systems Tracts and Surfaces	Tipology of Surfaces
	Keuper facies	TST: Transgressive Systems Tract	CC/SU
	RST2	RST: Regressive Systems Tract	MRZ
	TST2	CC: Correlative conformity	MRS/TS
	RST1	SU: Subaerial unconformity	MFZ
	TST1	MRS/Z: Maximum Regressive Surface/ Zone	TS
	Middle Muschelkalk facies	TS: Transgressive Surface	
		MFZ: Maximum Flooding Zone	

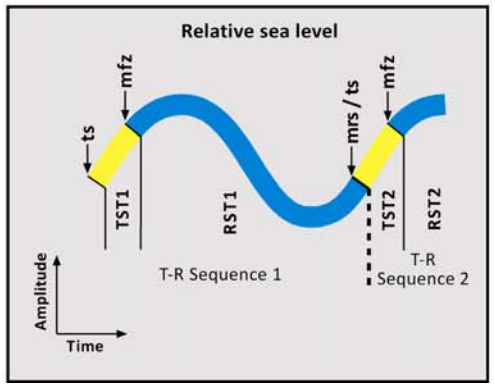

Figure. S5

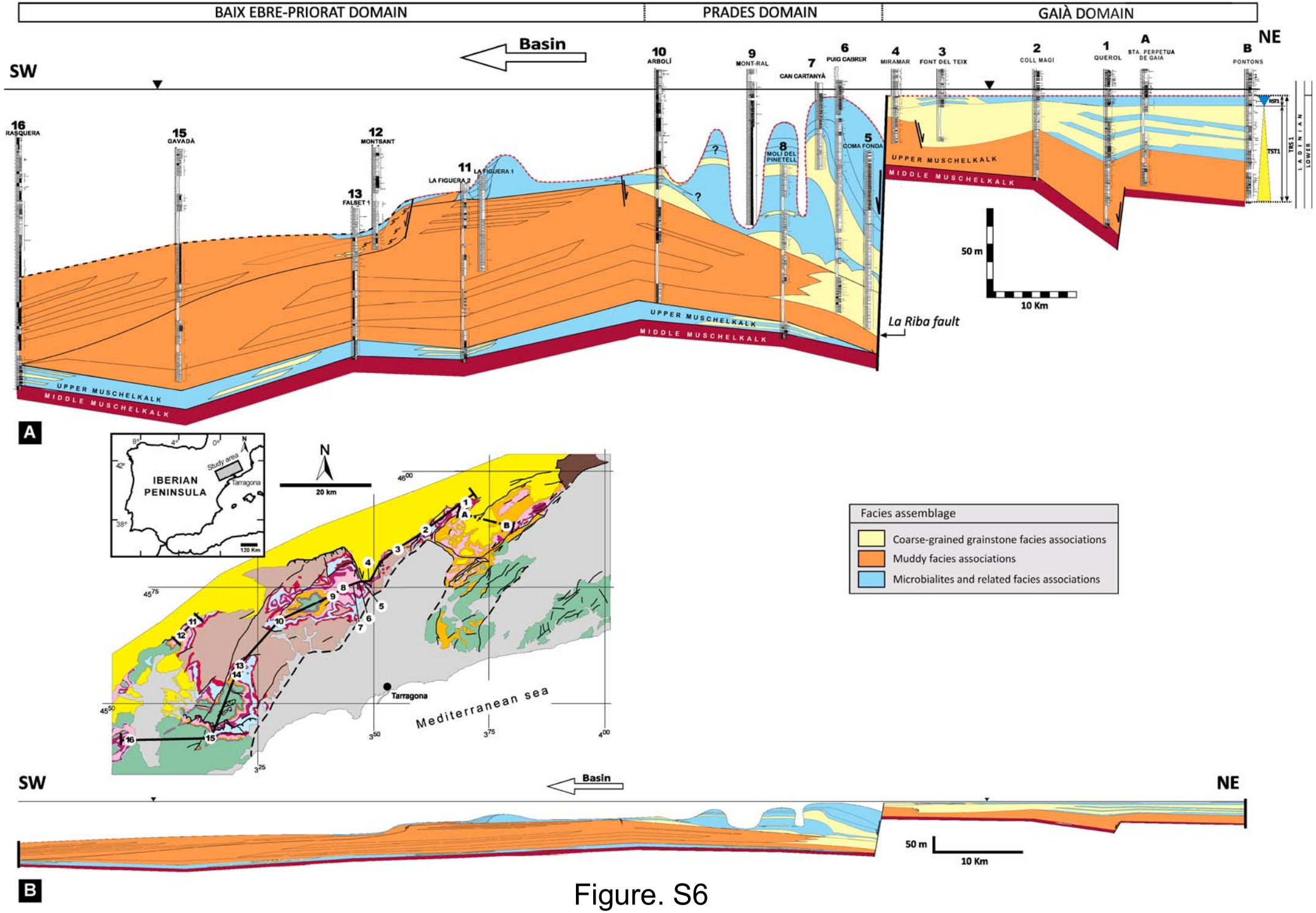
BAIX EBRE-PRIORAT DOMAIN
PRADES DOMAIN
GAIÀ DOMAIN
SW
NE
Basin
16 RASQUERA
15 GAVADÀ
12 MONTSANT
13 FALSET 1
11 LA FIGUERA 1
LA FIGUERA 2
10 ARBOLÍ
9 MONT-RAL
8 MOLÍ DEL PINETELL
7 CAN CARTANYÀ
6 PUIG CABRER
5 COMA FONDA
4 MIRAMAR
3 FONT DEL TEIX
2 COLL MAGI
1 QUEROL
A STA. PERPETUA DE GAIA
B PONTONS
UPPER MUSCHELKALK
MIDDLE MUSCHELKALK
La Riba fault
50 m
10 Km
RST1
TST1
TRS 1
LADINIAN
LOWER
A
IBERIAN PENINSULA
Study area
Tarragona
120 Km
N
20 km
Facies assemblage
Coarse-grained grainstone facies associations
Muddy facies associations
Microbialites and related facies associations
Mediterranean sea
Tarragona
B

Figure. S6

Artículo 2:

Mercedes-Martín R., Salas R., Arenas C. 2013b. Facies heterogeneity and depositional models of a Ladinian (Middle Triassic) microbial-dominated carbonate ramp system (Catalan Coastal Ranges, NE Spain). *Journal of Marine and Petroleum Geology*, 46, 107-128.

Marine and Petroleum Geology 46 (2013) 107–128

Contents lists available at SciVerse ScienceDirect

Marine and Petroleum Geology

journal homepage: www.elsevier.com/locate/marpetgeo

Facies heterogeneity and depositional models of a Ladinian (Middle Triassic) microbial-dominated carbonate ramp system (Catalan Coastal Ranges, NE Spain)

R. Mercedes-Martín [a,*], R. Salas [a], C. Arenas [b]

[a] Departament de Geoquímica, Petrologia i Prospecció Geològica, Facultat de Geologia, Universitat de Barcelona, C/Martí i Franquès s/n, 08028 Barcelona, Spain
[b] Departamento de Ciencias de la Tierra, Área de Estratigrafía, Universidad de Zaragoza, C/Pedro Cerbuna, 12, 50009 Zaragoza, Spain

ARTICLE INFO

Article history:
Received 6 March 2013
Received in revised form
27 May 2013
Accepted 6 June 2013
Available online 19 June 2013

Keywords:
Ramp architecture
Heterogeneity
Microbialite
Porosity
Sequence stratigraphy
Ladinian
Depositional models
Catalan Coastal Ranges

ABSTRACT

The Ladinian sedimentary successions record a major transgressive pulse of northeastern Iberia during the Middle Triassic. This record is arranged in two transgressive–regressive (T–R) sequences formed by two fault-block microbial and shoal-dominated carbonate ramps. The main factor controlling the creation of accommodation space is the differential rapid syn-rift subsidence, which induces the generation of palaeogeographical barriers that played a key role in the sedimentary architecture and microbial development.

The facies architecture of these ramps was reconstructed by means of facies analysis and sequence stratigraphy. T–R sequence 1 corresponds to a fault-block carbonate ramp system dominated by microbialites and oolitic shoals. T–R sequence 2 represents a fault-block carbonate ramp system mainly characterised by lagoons and shoals.

The diverse types of microbialites (stromatolites and thrombolites) are widely represented in the inner and middle ramp settings, reaching a width of 45 km and an average thickness of 40 m. T–R sequence 1 contains the most noticeable microbial deposits, stromatolites in the inner ramp (up to 7 m thick) and thrombolites in the middle ramp (up to 40 m thick). T–R sequence 2 is mainly characterised by the occurrence of oolitic stromatolites in the inner ramp and internal shoals and sheltered lagoons in the middle ramp. Microbialites exhibit a fabric-selective ancient porosity which is currently occluded by coarse calcite and quartz cements. The most common types of ancient porosity are interlaminar, vuggy and mouldic (grain dissolution and evaporite replacement).

The studied carbonate ramps can be used as an analogue for ancient microbialite reservoirs in rapidly subsiding depositional areas, with a high diversity of microbial deposits formed in restricted to open marine conditions, with a wide array of ancient porosity and a well-known sequence stratigraphic context.

1. Introduction

The architecture and evolution of carbonate platforms are commonly interpreted on the basis of their response to fluctuations in relative sea-level, changes in accommodation space and productivity because of the development of sequence stratigraphy and its application to carbonate depositional systems (Hardie and Shinn, 1986; Sarg, 1988; Crevello et al., 1989; Goldhammer et al., 1990; Handford and Loucks, 1993; Hunt and Tucker, 1992, 1993; Catuneanu et al., 2011). In extensional basins, differential subsidence plays a major role in the configuration of carbonate platform types, in the evolution of accommodation space (Bosence, 2005), and in the facies architecture (distribution in time and space of sedimentary facies).

The Ladinian succession of the Catalan Coastal Ranges provides an excellent opportunity to study the facies heterogeneities (facies architecture and porosity distribution) and the sedimentary evolution of the Middle Triassic in the western margin of the Tethys. The Ladinian microbial-dominated carbonate system developed across more than 150-km-long transect during a period of rapid syn-rift subsidence (Mercedes-Martín et al., 2013) where fault-induced subsidence created accommodation space. The modern sequence stratigraphic survey was first carried out by Calvet et al. (1990) and

* Corresponding author. Tel.: +34 93 4031165.
E-mail address: rmercedes@ub.edu (R. Mercedes-Martín).

0264-8172/$ – see front matter © 2013 Elsevier Ltd. All rights reserved.
http://dx.doi.org/10.1016/j.marpetgeo.2013.06.004

Calvet and Tucker (1995). Recently, Mercedes-Martín et al. (2013) have provided a more refined stratigraphic framework for subdividing the Ladinian sedimentary record into two transgressive–regressive (T–R) sequences where distinct microbialites developed (thrombolites and stromatolites). These sequences constitute examples of carbonate ramp-like records, with low-gradient depositional angles and large continuity of facies.

During the Middle Triassic, other basins of the Tethys developed carbonate platforms dominated by microbial carbonates (automicrite fabrics *sensu* Neuweiler et al., 1999) and syndepositional cements (Blendinger, 1994; Keim and Schlager, 2001), as in the Southern Calcareous Alps (Dolomites region). In this area, most of the Anisian buildups were dominated by binding microbialites lacking primary frameworks (Russo et al., 1998). Ladinian platform margins were dominated by binding organisms (cyanobacteria, encrusting Porifera and *Tubiphytes*), with organomicrites and abundant cements dominating skeletal components. More than 50% of the slope components of the Middle Triassic Marmolada platform are composed of boundstone, microbial crusts, early cements and *Tubiphytes* (Blendinger, 1994). Similarly, margin and slope carbonate production of the Middle Triassic Latemar platform (Dolomites) and Sella massif (Southern Alps, Northern Italy) occur in mud mound-type (sensu Schlager, 2000), i.e. microbialite and cements (Harris, 1993; Keim and Schlager, 2001; Emmerich et al., 2005; Marangon et al., 2011).

Moreover, the discovery of hydrocarbon reservoirs associated with microbial carbonates such as in the Upper Jurassic of Gulf of Mexico (Mancini et al., 2004), the Carboniferous of Kazakhstan (Collins et al., 2006) or the Lower Cretaceous of Campos Basin, Brazil (Luis Dias, 2005) has prompted new research into the formation of microbially influenced carbonates, the nature of their morphology and how they developed into significant reservoir-scale structures (Awramik and Buchheim, 2012). This knowledge has proved useful in predicting the occurrence of well-developed microbialite bodies within well-constrained depositional models.

Lately, Harris et al. (2013) assessed the styles of carbonate deposition in some early rift settings where microbial processes and their products (microbialites and tufa) were predominant. The Triassic Catalan Basin could be regarded as an ancient analogue that combines the restricted marine carbonate deposition in an extensional tectonic setting (as in the Red Sea) with the microbialite diversity that developed in response to environmental changes (Shark Bay).

In this paper, we focus on the facies analysis of the Ladinian microbial dominated carbonate ramps exposed in outcrops between Pontons and Rasquera (Catalan Coastal Ranges, NE Spain). The primary objectives of this study are: a) to characterise the facies associations according to their depositional environments (inner, middle and outer ramp) within the ramp, b) to give an architectural pattern of distribution in time and space of sedimentary facies, and c) to generate a two-dimensional heterogeneity model encompassing architecture and trends of porosity in microbial facies.

These results improve the understanding of the sedimentary facies belts of microbial-dominated carbonate ramps during the Middle Triassic, which is a period of abundant development of microbial carbonates worldwide. In addition, this work sheds new light on the heterogeneous distribution and coexistence of the facies (grainy, muddy and microbial facies assemblages), and quantifies and characterises the ancient porosity of microbialite facies for reservoir characterisation purposes.

2. Geological setting and stratigraphy

The study area is located in the Catalan Coastal Ranges (Fig. 1), which developed through inversion of the Mesozoic rifts during the Paleogene (Salas et al., 2001). The outcrops of the Triassic Catalan Basin are about 300 km long and 200 km wide, trending NE–SW. The basin opened towards the SE into the Neotethys sea with the result that the fully marine facies graded into more clastic-dominated facies towards the western and northern parts of the basin close to the Spanish Meseta (Calvet et al., 1990).

During the opening of the western Neotethys, Iberia underwent extensional tectonic regime, and several large intraplate Mesozoic rift systems developed (Salas et al., 2001; García-Senz and Salas, 2011).

The Late Permian – Mesozoic evolution of Iberia can be divided into three major rift cycles and post-rift stages (Salas and Casas, 1993; Ramos et al., 1996; Salas et al., 2001). One of them is the Late Permian–Triassic rift cycle, which affected the eastern part of the Iberian plate. Vargas et al. (2009) subdivided the Late Permian–Triassic rift cycle of Salas and Casas (1993) into several syn-rift and post-rift phases.

In addition, Vargas et al. (2009) affirmed that a generalized phase of rapid subsidence during the Early-Middle Triassic (Olenekian to Ladinian) occurred in the Ebro Basin and Iberian Chain (Spain). The subsidence evolution during the Triassic strongly suggests that the Ladinian stage was a period of ubiquitous rapid syn-rift subsidence in the eastern part of the Iberian plate, where large carbonate deposits developed at this time (Mercedes-Martín et al., 2013).

In general, these Triassic fault-controlled basins were filled with sediments attributed to Germanic facies during Late Permian and Triassic times. These facies are characterised by a tripartite stratigraphical subdivision, with the lower part comprising continental Buntsandstein clastics and red beds, the middle part formed by marine Muschelkalk carbonates, evaporites and red beds, and the upper part consisting of tidal and sabhka deposits of the Keuper facies (Virgili et al., 1983).

In the Catalan Coastal Ranges, the Muschelkalk facies (Anisian to Ladinian) is made up of two marine carbonate units separated by a siliciclastic-evaporite unit. The second carbonate unit is extremely well represented in the Triassic Catalan Basin and has been interpreted as a depositional sequence spanning the Middle and Upper Muschelkalk (Calvet et al., 1990). Later, Calvet and Tucker (1995) proposed the division of the Ladinian into two depositional sequences corresponding to two major Upper Muschelkalk marine pulses (Fig. 2).

The thickness of the Upper Muschelkalk varies from around 100 m in the northern part of the study area to over 140 m in the south. The Upper Muschelkalk record of the Triassic Catalan Basin was subdivided into three palaeogeographical domains, from north-east to south-west: the Gaià domain, the Prades domain and the Baix Ebre–Priorat domain (Calvet and Ramon, 1987) (Fig. 1).

Mercedes-Martín et al. (2013) subdivided the Ladinian sedimentary record into two T–R sequences corresponding to two low-angle, microbial-dominated carbonate ramps, where thrombolites and stromatolites developed from inner to outer ramp settings. An extensive subaerial unconformity with a prominent karst, significant incision (up to 60 m) and abundant collapse breccia fillings bounds the two T–R sequences. T–R sequence 1 (lower ramp) contains the most prominent microbial deposits, i.e. stromatolites in the inner ramp (at least 7 m thick) and thrombolites in the middle ramp (ca. 40 m thick). T–R sequence 2 (upper ramp) is mainly characterised by the occurrence of oolitic stromatolites in the inner ramp and internal shoals and sheltered lagoons in the middle ramp.

Following the biostratigraphic framework of Sole de Porta et al. (1987) and Goy (1995), the T–R sequence 1 is Lower Ladinian (Fassanian) in age, and the T–R sequence 2 belongs to the Upper Ladinian (Longobardian).

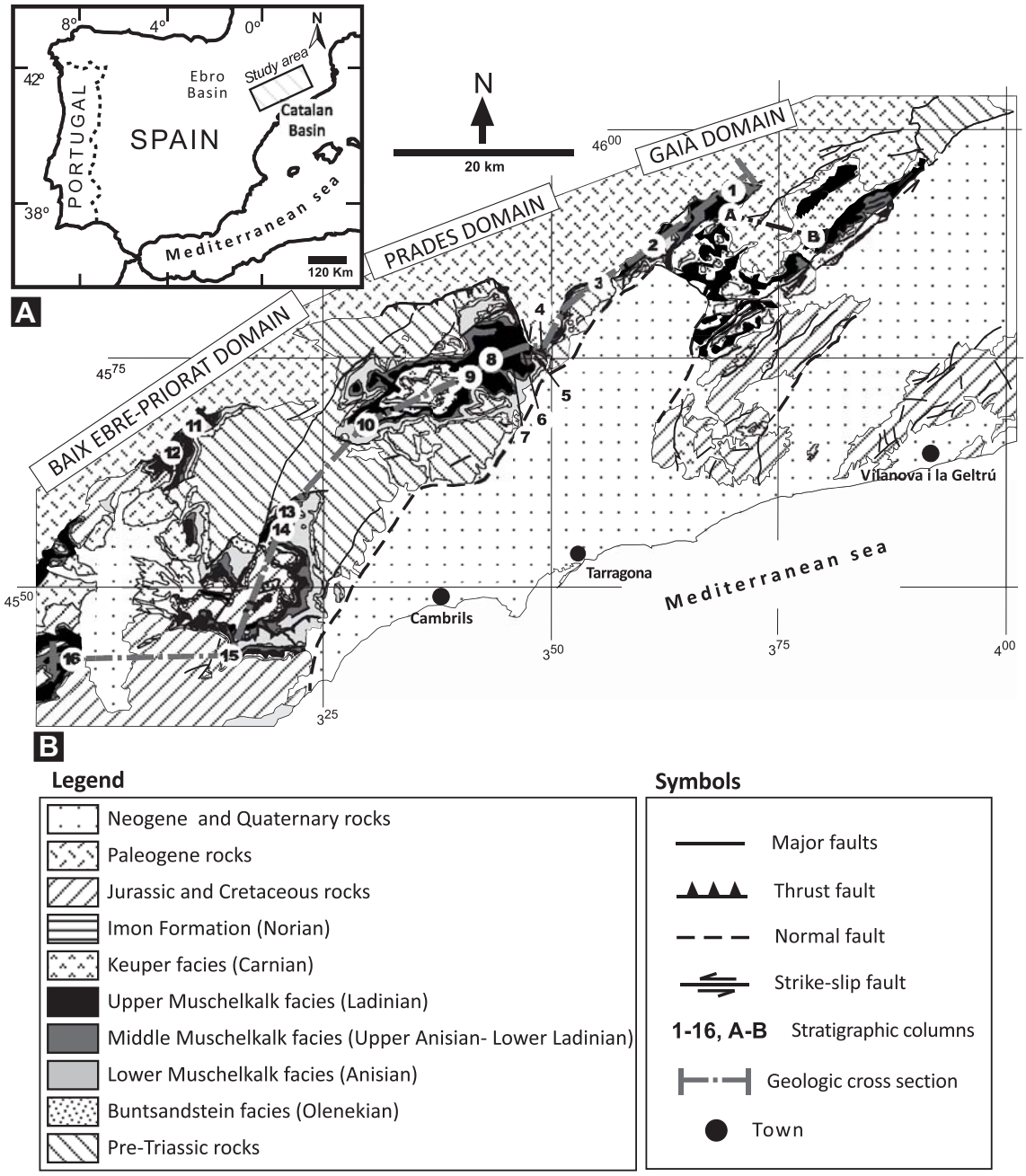

Figure 1. (A) Location of the study area and nearby basins. (B) Geological map of the Catalan Basin showing the main rock types and the geological transect studied (modified from Mercedes-Martín et al., 2013). Numbers refer to stratigraphic sections in Figures 3, 10 and 11.

3. Methods

The study is based on 18 outcrop sections described from localities between Pontons and Rasquera and measured across a NE to SW 150 km-long exposure of the Catalan Coastal Ranges (Fig. 1). The sections were chosen for their stratigraphic completeness and their low tectonic overprint. In the correlation panels, the base of the Keuper facies (Carnian in age) was considered as a datum of the stratigraphic sections. In addition, the stratigraphic data from the La Figuera and Montsant sections and Santa Perpetua de Gaià-Pontons were projected over the main cross-section transect. The sequence stratigraphic terminology used in the correlation panel follows the concepts of Catuneanu et al. (2009, 2011).

Sedimentological interpretations are based on facies and microfacies analyses using standard techniques. More than 300 samples were prepared as thin sections for microfacies examination. Furthermore, 150 polished slabs were also used for textural and compositional analyses.

The transgressive–regressive (T–R) sequence stratigraphic model (Johnson and Murphy, 1984; Embry and Johannessen, 1992) was used to identify stratigraphic surfaces (summarized in Catuneanu, 2006). The proposal advanced by Spence and Tucker (2007) was adopted to identify the bounding surfaces between each parasequence and parasequence set in the field and the carbonate peritidal cycle model. The concepts of Burchette and Wright (1992) were used for subdividing the carbonate ramp environments and the classification of Bosence (2005) for carbonate

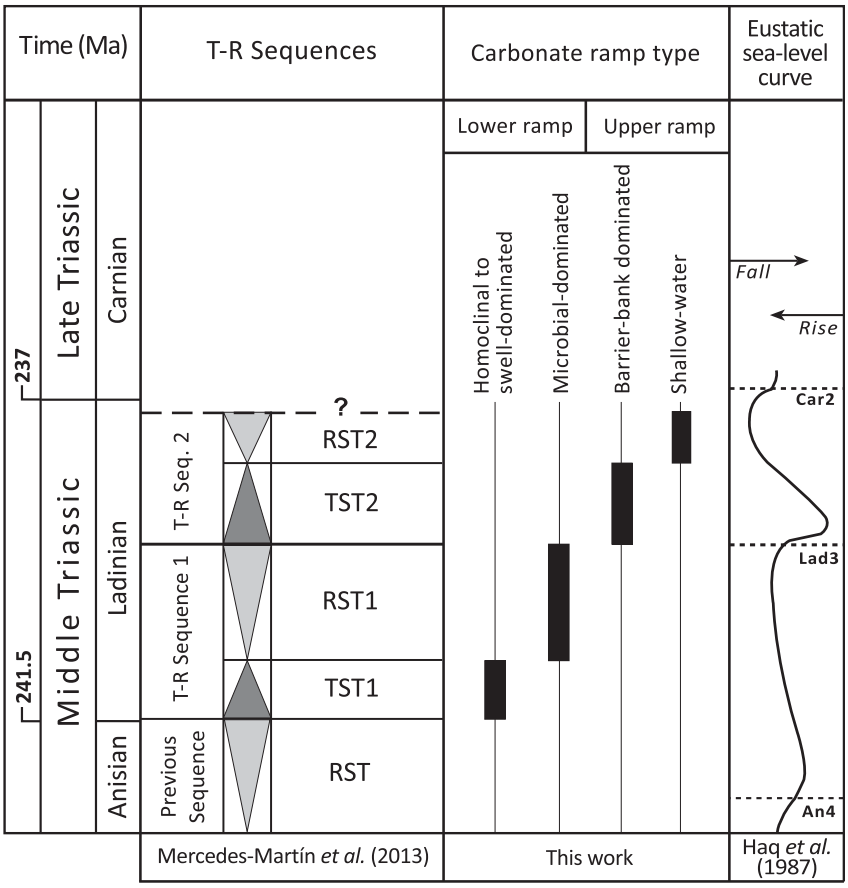

Figure 2. Carbonate ramp types developed during the Middle Triassic Catalan Basin and their sequence stratigraphic framework. Absolute ages from Gradstein et al. (2012) and short-term eustatic curve from Haq et al. (1987).

platform types according to their tectonic setting. The terms 'internal' and 'external shoals' separated by a 'sheltered lagoon' come from Colombié and Strasser (2005). The term 'microbialite' is used *sensu* Burne and Moore (1987).

Photograph-based outcrop panels and line drawings were used for correlation and evaluation of large-scale depositional geometries and the architecture of the sedimentary bodies across the study area.

Modal 2D ancient cemented porosity determinations were obtained from thin sections by point counting and visual estimation. Choquette and Pray's (1980) pore space scheme was used for porosity classification and terminology.

4. Facies heterogeneities

Seventeen facies ranging from inner ramp to outer ramp environments have been described on the basis of lithology, depositional texture, skeletal and non-skeletal components and sedimentary structures and summarized in Mercedes-Martín et al. (2013). The facies are described and arranged in three large groups on the basis of texture (Fig. 3): coarse-grained facies group (Table 1); muddy facies group (Table 2), and microbialites and related facies group (Table 3). They are illustrated in Figures 4, 5 and 6.

A chart displaying the correlation among the different sedimentary sections and the lateral distribution of facies is presented in Figure 3. Each facies represents a specific sedimentary environment characterised by specific hydraulic conditions, carbonate factory and inherited palaeotopography. The recognition of large-scale architectures with a particular distribution of sedimentary facies and heterogeneities through time and space enables us to assign each facies to a specific depositional environment within the inner, middle and outer ramp settings: basin, external shoal, sheltered lagoon, internal shoal, beach-barrier and tidal flat, showing more open marine conditions towards the SW (Mercedes-Martín et al., 2013).

4.1. Coarse-grained facies group

Six main types of coarse-grained carbonate facies were identified in the Ladinian strata of the study area (Mercedes-Martín et al., 2013) and displayed in Figure 3 and Table 1: oolitic grainstone (F1, Fig. 4A–C); cross-bedded grainstone (F2, Fig. 4D and E); peloidal and skeletal wackestone to packstone (F3; Fig. 4F and G); oncolitic–oolitic–peloidal floatstone to grainstone (F4, Fig. 4H and I); bioturbated wackestone and packstone interbedded with grainstone (F5, Fig. 4J and K), and wackestone to floatstone of mollusks interbedded with packstone of echinoderms (F6, Fig. 5A and B).

4.2. Muddy facies group

Three common types of muddy carbonate facies have been recognized (Mercedes-Martín et al., 2013) and arranged in Figure 3 and Table 2: strongly burrowed bioclastic mudstone and wackestone alternating with argillaceous dolomitic layers (F7, Fig. 5C and D); burrowed skeletal mudstone to packstone interbedded with marls (F8, Fig. 5E and F), and thin-bedded laminated dolomudstone (F9, Fig. 5G and H).

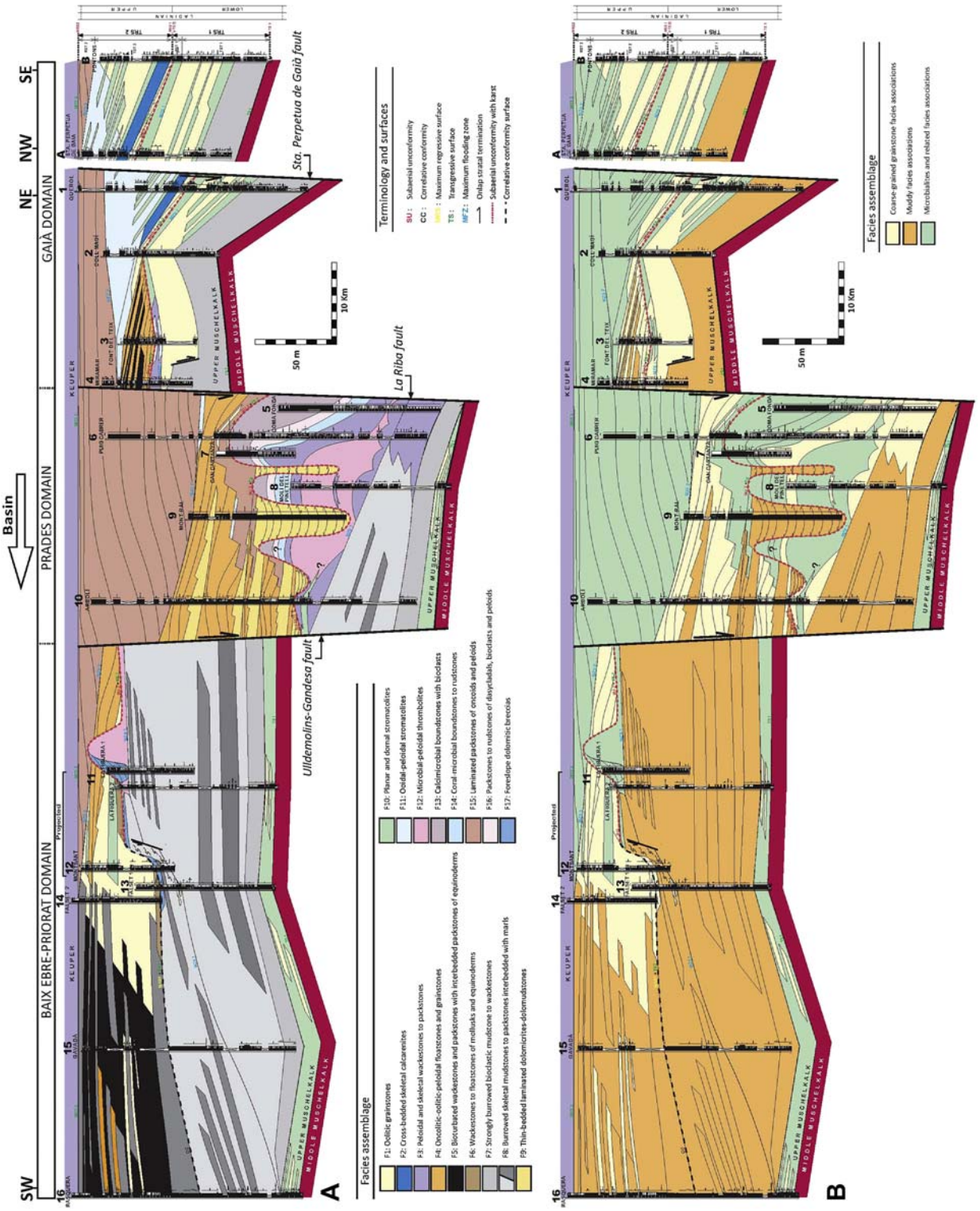

Figure 3. (A) The platform-to-basin facies correlation across the Middle Triassic Catalan Basin. The data derived from the stratigraphic sections between La Figuera-Montsant and Santa Perpetua de Gaià-Pontons are projected to the main cross section. See Figure 1A for location of the sections. Note that the vertical scale has been exaggerated. (B) The same geological profile displaying the three main groups of facies assemblages (modified from Mercedes-Martín et al., 2013).

Table 1
Coarse-grained grainstone facies group and interpretation of sedimentary environments and their occurrence in the lower and upper ramp. (*) Facies developed within an intraplatform trough located in the middle ramp.

Facies	Components	Sedimentary structures	Depositional environments	Ramp setting					
				Lower ramp			Upper ramp		
				Inner	Middle	Outer	Inner	Middle	Outer
F1 Oolitic grainstone Figure 4A–C	Ooids, peloids (locally); bivalves	Low-angle cross bedding, plane parallel and herringbone stratification; hummocky cross stratification (locally); herringbone and wavy lamination; climbing ripples (locally); massive bedding (locally); tidal bundles, tidal channels; basal lag deposits (locally); erosive bases	Marine shallow subtidal shoals, moderate to high energy conditions. Above fair-weather wave base. Some resedimented sheets below fair-weather wave base.	X	–	–	X	X	–
F2 Cross-bedded skeletal grainstone Figure 4D, E	Ooids, peloids, intraclasts, cortoids (locally); gastropods, foraminifera	Undulous and low-angle cross bedding, plane parallel and herringbone stratification; herringbone, ripple, plane parallel and wavy lamination; climbing ripples (locally); massive bedding (locally); tidal bundles, tidal bars, tidal channels; basal lag deposits (locally); microbial lamination (rare); erosive bases	Marine shallow subtidal beach-barrier island; high energy conditions. Above fair-weather wave base. Internal shoals.	X	–	–	–	–	–
F3 Peloidal and skeletal wackestone to packstone Figure 4F and G	Peloids, intraclasts, microoncoids, bivalves, gastropods, crinoids and echinoids	Massive or nodular bedding; herringbone, plane parallel, ripple and wavy lamination; hummocky cross stratification (locally); unidentified burrows, hardgrounds and borings (locally); erosive bases	Marine shallow-water, moderate to high energy conditions. Intertidal to subtidal. Above fair-weather wave base. Beach-barrier island? To shoreface carbonate sands (*)	X	X	–	–	–	–
F4 Oncolitic–oolitic–peloidal floatstone and grainstone Figure 4H and I	Oncoids, ooids, peloids, intraclasts, cortoids and aggregates (locally); bivalves, ostreids, dasyclad algae, gastropods and echinoids	Massive or nodular bedding; plane parallel to low-angle cross-bedding stratification; erosive bases; unidentified burrows and root plants; plane parallel, herringbone, wavy and ripple lamination; tidal bundles and tidal channels; basal lag deposits (locally); hardgrounds and Fe/Mn encrustations	Marine shallow-water, moderate to high energy conditions. Subtidal. Above fair-weather wave base. Sheltered lagoon.	–	–	–	X	X	–
F5 Bioturbated wackestone and packstone with grainstone Figure 4J and K	Oncoids, black pebble intraclasts; ooids, bivalves, echinoids, foraminifera, conodonts	Massive, nodular and undulous bedding. Plane parallel lamination (rare); unidentified burrows and ichnofauna	Below fair-weather wave base, moderate energy conditions. Subtidal.	–	–	–	–	X	–
F6 Wackestone to floatstone of mollusks interbedded with packstone of echinoderms Figure 5A and B	Oncoids, peloids, microoncoids; crinoids, gastropods, bivalves, echinoids, foraminifera, microproblematica	Low-angle cross bedding, ripple, plane-parallel and wavy lamination; massive bedding (locally); tidal bundles; basal lag deposits (locally); unidentified escaping burrows; erosive bases	Marine shallow-water, moderate to high energy conditions. Above fair-weather wave base.	–	–	–	X	–	–

4.3. Microbialites and related facies group

The following boundstone-type textures and carbonate-related facies have been recognized in the study area (Mercedes-Martín et al., 2013) and are shown in Figure 3 and summarized Table 3: planar and domal stromatolites (F10, Fig. 5I–L); ooidal–peloidal stromatolites (F11, Fig. 6A–D); microbial-peloidal thrombolites (F12, Fig. 6E–I); calcimicrobial boundstone with bioclasts (F13, Fig. 6J); coral-microbial boundstone to rudstone (F14, Fig. 6I–L); laminated packstone of oncoids and peloids (F15, Fig. 6I, M and N); packstone to rudstone of dasyclads, bioclasts and peloids (F16, Fig. 6I, O, P and Q) and foreslope dolomitic breccias (F17, Fig. 6R).

5. Porosity distribution in microbialites

Microbialite samples belonging to facies F10, F11, F12 and F15 were analysed for porosity purposes. In thin sections (Figs. 7, 8 and 9), ancient porosity appears to be occluded by spar calcite cements and less commonly by quartz cements. Most of the open porosity present in thin sections (up to 20%) has a weathering origin. This porosity was not used for quantification purposes because it is not noteworthy for reservoir studies. Cemented porosity values were estimated by counting the occluded pore spaces. Nevertheless, the analysis of some partially cemented cavities provided insights into microbialite porosity types.

5.1. Porosity distribution in microbialites

Although microbialitic facies (stromatolites and thrombolites) are well represented in the Gaià and Prades domains of the Ladinian platform (Fig. 3B), microbialite occurrence are more restricted in the Baix Ebre–Priorat domain.

The TST1 (Transgressive Systems Tract 1) records abundant stromatolites (facies F10) along the entire platform. This systems

Table 2
Muddy facies group and interpretation of sedimentary environments and their occurrence in the lower and upper ramp. (*) Facies developed within an intraplatform trough located in the middle ramp.

Facies	Components	Sedimentary structures	Depositional environments	Ramp setting					
				Lower ramp			Upper ramp		
				Inner	Middle	Outer	Inner	Middle	Outer
F7 Strongly burrowed skeletal mudstone to wackestone Figure 5C and D	Bivalves, echinoids, gastropods; peloids, intraclasts, quartz grains	Massive or nodular bedding, *Planolites* ichnofauna; *Thalassinoides* ichnofauna (locally); plane parallel, ripple and wavy lamination (locally); tidal channels and tidal bars; tidal bundles (locally), hummocky cross stratification (rare); conglomerate lag deposits (locally); slump-scars and carbonate breccias (rarely)	Marine shallow-water, moderate to high energy conditions. Above fair-weather wave base. Hypersaline intertidal to subtidal sheltered lagoons and tidal flats	X	X	–	–	–	–
F8 Burrowed skeletal mudstone to packstone interbedded with marls Figure 5E and F	Peloids, bivalves, echinoids, gastropods, cephalopods, crinoids, brachiopods, ostreids, bryozoans, foraminifera, *Tubiphytes*; intraclasts, oncoids, aggregates, quartz grains (locally)	Massive or nodular bedding; plane parallel, wavy and ripple lamination (occassionally); unidentified burrows; *Planolites* ichnofauna; *Thalassinoides* ichnofauna (locally); erosive bases; channelized deposits (calciturbidites?) and slumps (locally); hardgrounds and Fe/Mn mineralizations	Below storm wave base, moderate to low energy conditions. Deep subtidal.	–	X	X	–	–	–
F9 Thin-bedded laminated dolomudstone Figure 5G and H	Fragments and whole skeletons of mollusks and macroinvertebrates	Event-bedding stratification; plane parallel and ripple lamination (locally); deep water ichnofauna; unidentified burrows and borings; gas-bubble casts; evaporite moulds; hardgrounds and Fe/Mn encustrations (locally)	Below fair-weather wave base, low energy restricted conditions. Periodically hypersaline and anoxic. Subtidal. (*)	–	X	–	–	–	–

tract represents the most widespread and most homogeneous microbial event, giving rise to tabular and stratiform bodies which contain modal porosities up to 10% (Table 4). The RST1 (Regressive Systems Tract 1) constitutes thicker successions of microbialites and a wider spectrum of forms: stromatolites (facies F10) in the Gaià domain and thrombolites (facies F12) in the Prades domain. The overall modal porosities range between 5 and 20%. During the TST2 (Transgressive Systems Tract 2), ooidal–peloidal stromatolites are recorded in the Gaià domain (facies F11) and microbial-related deposits in the Prades domain (facies F15). The porosity varies between 10 and 15% (Table 4). The RST2 (Regressive Systems Tract 2) contains the thickest microbial-related deposits (facies F15) and are distributed along all the domains. Modal porosity may attain up to 15% (Table 4).

5.2. Types of porosity in the planar and domal stromatolites (facies F10)

Stromatolites usually contain two types of geometries: stratiform and tabular forms (Type 1 biostromes), and domed, head-shaped forms (Type 2 biostromes). Locally, Type 2 biostromes are developed above Type 1 biostromes, giving rise to extensive sedimentary bodies. Stromatolites develop interlaminar voids and vuggy porosity (Table 4). The former porosity may be enlarged by early to late dissolution processes to become a vuggy porosity. Modal porosity values are up to 10%. These voids (Fig. 7A, B and E–I) consist of millimetre sized (commonly between 1 and 3 mm) elongated to patch cavities parallel to stromatolitic laminae. Horizons of abundant porosity may be surrounded by layers of dense carbonate material that lacks visible macroporosity. In some cases, evidence of unconnected cavities is available. They are thought to constitute former sites of bacterial body accretion, microbial mats and calcimicrobes (as mm-sized *Cayeuxia*) which subsequently degraded and were filled with micrite to microspar calcite cements. Vuggy porosity (Fig. 7A and C) consists of millimetre sized (between 5 and 10 mm), irregularly elongated and subspherical cavities mainly developed subparallel to microbial laminations and occasionally cutting across them. Dissolution may start from fenestral pores and interlaminar voids and are later occluded by blocky calcite cements.

5.3. Types of porosity in the ooidal–peloidal stromatolites (facies F11)

The ooidal–peloidal stromatolites consist of dolomitised oolitic–peloidal grainstone alternating with millimetre thick micritic laminae (Fig. 8). Stratiform geometries and low-relief hemi-elliptical microbial buildups are the most common architectures of these microbial deposits.

Porosity in ooidal–peloidal stromatolites includes vuggy and mouldic types. The two types consist of millimetre to sub-millimetre size pores and cavities. Vuggy porosity may attain up to 15% of modal values whereas mouldic porosity may attain up to 20%.

Vuggy porosity (Fig. 8A–E) consists of millimetre sized (up to 5 mm width) irregular, dendritic to subangular patch cavities developed in the grainstone layers. They are widely distributed across the grainy intervals suggesting that a dissolution process took place prior to cementation.

Mouldic porosity is widely distributed in the grainstone horizons of the oolitic–peloidal stromatolites. This fabric-selective porosity affects ooids, oncoids, peloids and other lithoclasts generating a low to moderate inter-pore connectivity. Pores are less than 1 mm in width (Fig. 8E and F, Table 4). Mouldic pores are not currently occluded by coarse sparry calcite cements and often present relict calcitic rims, suggesting subsequent leaching processes.

5.4. Types of porosity in the microbial-peloidal thrombolites (facies F12)

The microbial-peloidal thrombolites consist of extensive, decimetre to metre-thick, massive to nodular bedded, mainly non-

Table 3
Microbialites and related facies group and interpretation of sedimentary environments and their occurrence in the lower and upper ramp. (*) Facies developed within an intraplatform trough located in the middle ramp.

Facies	Components	Sedimentary structures	Depositional environments	Ramp setting					
				Lower ramp			Upper ramp		
				Inner	Middle	Outer	Inner	Middle	Outer
F10 Planar and domal stromatolites Figure 5I–L	Microbial remains (filaments and coccoids, and calcimicrobes); flat-pebble intraclasts (locally)	Microbial, flat to undulate lamination, alternating dark and light dolomite intervals, submillimetre to mm thick; birdeyes and fenestral fabrics; teppe structures; karst related structures; hardgrounds; pseudomorphs of evaporite minerals	Marine shallow-water, moderate energy conditions. Hypersaline intertidal to supratidal flats.	X	–	–	X	–	–
F11 Ooidal–peloidal stromatolites Figure 6A–D	Microbial laminations (domal and planar in shape), ooids, peloids, aggregates, flat-pebble intraclasts, bahamite peloids (locally); quartz grains	Alternating ooidal–peloidal (grainstone) and micritic intervals (flat to undulate lamination), mm to cm thick; fenestral and keystone fabrics; tepee structures; plane parallel, herringbone, wavy and ripple lamination (locally); microhardgrounds, borings; tidal channels (rare)	Marine shallow-water, moderate to high energy conditions. Intertidal to subtidal. Above fair-weather wave base. Internal fore-shoals.	X	–	–	X	–	–
F12 Microbial-peloidal thrombolites Figure 6E–I	Peloids, micropeloids, intraclasts, oncoids, quartz grains; Microproblematica (*Garwoodia, Tubiphytes, Cayeuxia*), bivalves, foraminifera	Massive or nodular bedding; erosive bases (locally); microbial lamination (cm thick intervals of facies F10)	Below fair-weather wave base to below storm wave base, low to moderate energy conditions.	–	X	X	–	–	–
F13 Calcimicrobial boundstone with bioclasts Figure 6J	Calcimicrobes, bivalves, gastropods; Fe/Mn encrustrations and hardgrounds (locally)	Microbial laminated biostromes; plane parallel and ripple lamination (locally); microbial flat and domal lamination; birdeyes and fenestral fabrics	Marine shallow-water, moderate to high energy conditions. Above fair-weather wave base (*)	–	X	–	–	–	–
F14 Coral-microbial boundstone to rudstone Figure 6I, K and L	Scleractinian corals, bivalves, foraminifera, serpulids, worm tubes, sponges?, Microproblematica (*Garwoodia, Girvanella?, Tubiphytes*), micropeloidal micrite; intraclasts, peloids	Massive bedding, hardgrounds, unidentified burrows (locally)	Marine shallow-water, moderate to high energy conditions. Above fair-weather wave base (*)	–	X	–	–	–	–
F15 Laminated packstone of oncoids and peloids Figure 6I, M and N	Oncoids, peloids, intraclasts; bivalves and echinoids, filamentous microbial remains	Massive bedding; microbial flat and domal lamination; birdeyes and fenestral fabrics; ripple and plane parallel lamination (locally); calcite pseudomorphs of evaporite minerals	Marine shallow-water, low energy conditions. Intertidal to supratidal flats.	X	–	–	X	–	–
F16 Packstone to rudstone of dasyclads, bioclasts and peloids Figure 6I, O, P and Q	Intraclasts, peloids, Dasyclad algae, bivalves, gastropods, echinoids; foraminifera, microproblematica (*Tubiphytes*), microbial boundstones and skeletal stromatolites (locally)	Massive bedding to low angle cross-bedding, plane-parallel and ripple lamination; hardgrounds and Fe/Mn encrustrations (locally); erosive bases	Marine shallow-water, moderate to high energy conditions. Above fair-weather wave base (*)	–	X	–	–	–	–
F17 Foreslope dolomitic breccias Figure 6R	Carbonate clasts; microproblematica encrusters	Massive to coarsely bedding; clast-supported and mud-supported fabrics (locally), polymictic composition, poor to moderate sorting, heterometric and subangular to subrounded clasts	Below fair-weather wave base, low energy conditions. Subtidal.	–	–	X	–	–	–

laminated (thrombolitic) microbialites. Microbial-peloidal thrombolites usually contain vugs that are often occluded by sparry calcite cements or euhedral crystals of quartz. This mouldic porosity is secondary in origin since it is produced during the replacement of dolomite by evaporite minerals (anhydrite or gypsum) (Tucker and Marshall, 2004). Depending on the effectiveness of this replacement, some vugs are partially open and could become sites for porosity development. Modal porosity values attain a maximum of 10% (Fig. 8G and H, Table 4). In addition, there are some vugs that also developed within cements in this microbial facies after early dolomitisation processes linked to circulation of seawater (Tucker and Marshall, 2004) (Fig. 8I). Although facies F12 could develop some kind of mouldic porosity, this facies is commonly a non-porous facies. The reason for this is that their components (in-situ generated micropeloidal to peloidal cloudy micrite masses) are usually surrounded by early marine fibrous and coalescent mamelons with compound fans of botryoidal cavity-filling cements which grew coevally with microbial fabrics.

5.5. Types of porosity in the laminated packstone of oncoids and peloids (facies F15)

These microbial deposits develop a flat-laminated to domal internal organization, and constitute tabular and stratiform bodies of a consistent lateral continuity and vertically stacked laminae. Porosity in facies F15 attain a homogeneous distribution of millimetre size elongated pores sometimes displaying a cauliflower-like external morphology. Modal porosity values are up to 15% (Fig. 9,

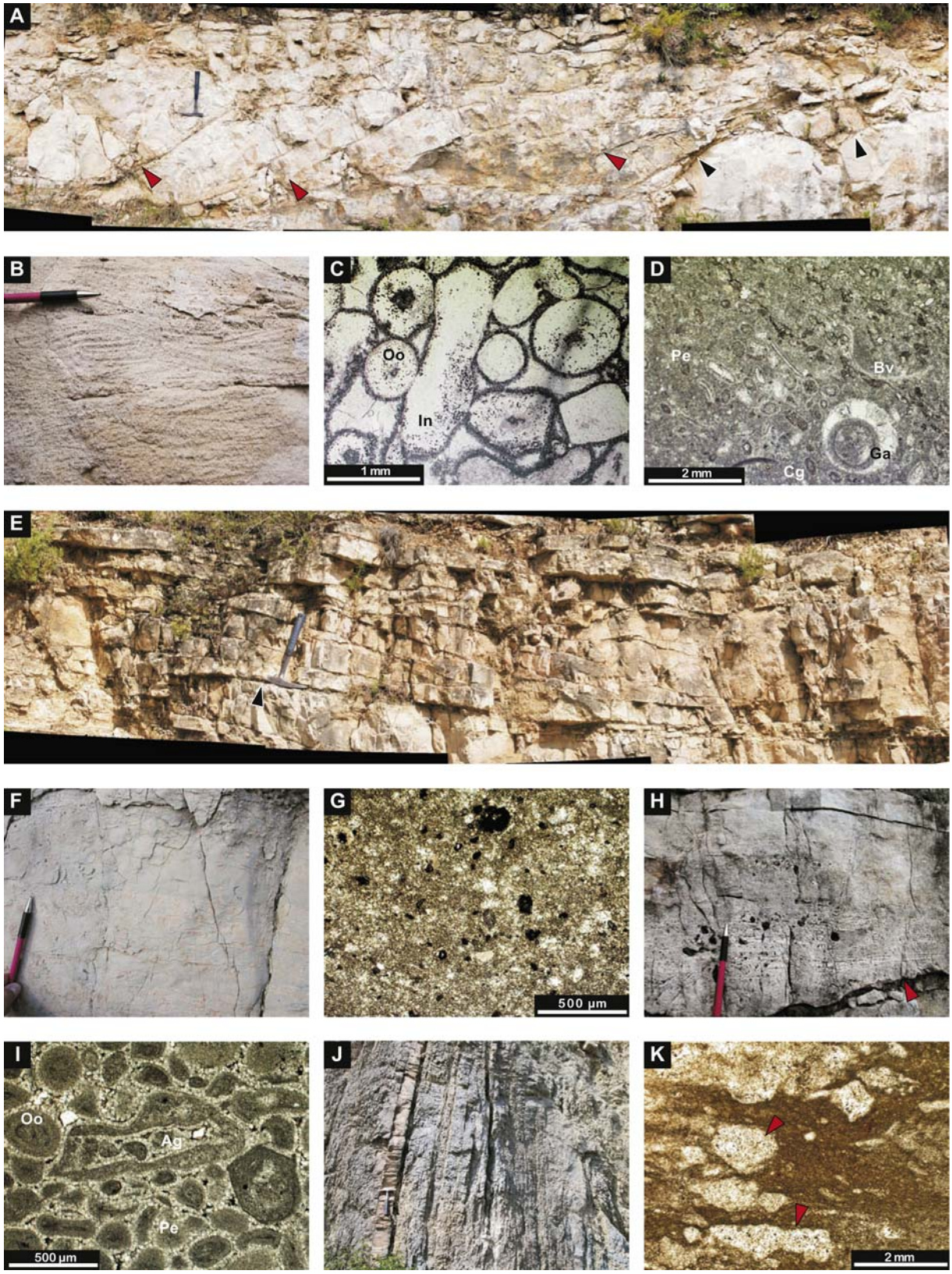

Figure 4. Photomicrographs and outcrop photographs of representative microfacies. (A) Outcrop photomosaic of the oolitic grainstone (facies F1) showing cross-bedded tidal bundles (red arrows) above a preexisting tidal channel (black arrows). (B) Detail of herringbone and ripple laminations on facies F1. (C) Photomicrograph of the oolitic grainstone facies showing intraclasts (In) and ooids (Oo). (D) Photomicrograph of cross-bedded skeletal grainstone (facies F2) with gastropod shells (Ga), bivalves (Bv), coated grains (Cg) and peloids (Pe). (E) Outcrop photomosaic of facies F2 displaying prograding tidal bundles with low-angle cross bedding above an erosive base (black arrow). (F) Peloidal and skeletal wackestone to packstone (facies F3) showing nodular bedding and bioturbation. (G) Photomicrograph of facies F3 with small peloids and intraclasts. (H) Outcrop detail of oncolitic-oolitic peloidal floatstone and grainstone (facies F4) with oncoids and flat-pebble intraclasts. The red arrow indicates an erosive base. (I) Photomicrograph of facies F4 displaying aggregates (Ag), ooids (Oo) and peloids (Pe). (J) Outcrop photograph of bioturbated wackestone and packstone with grainstone (facies F5). Note the nodular and undulous bedding. (K) Detail of facies F5 displaying a muddy matrix with evidence of bioturbation (red arrows). (For scale: pencil 15 cm long; hammer 32 cm long). (For interpretation of the references to colour in this figure legend, the reader is referred to the web version of this article.)

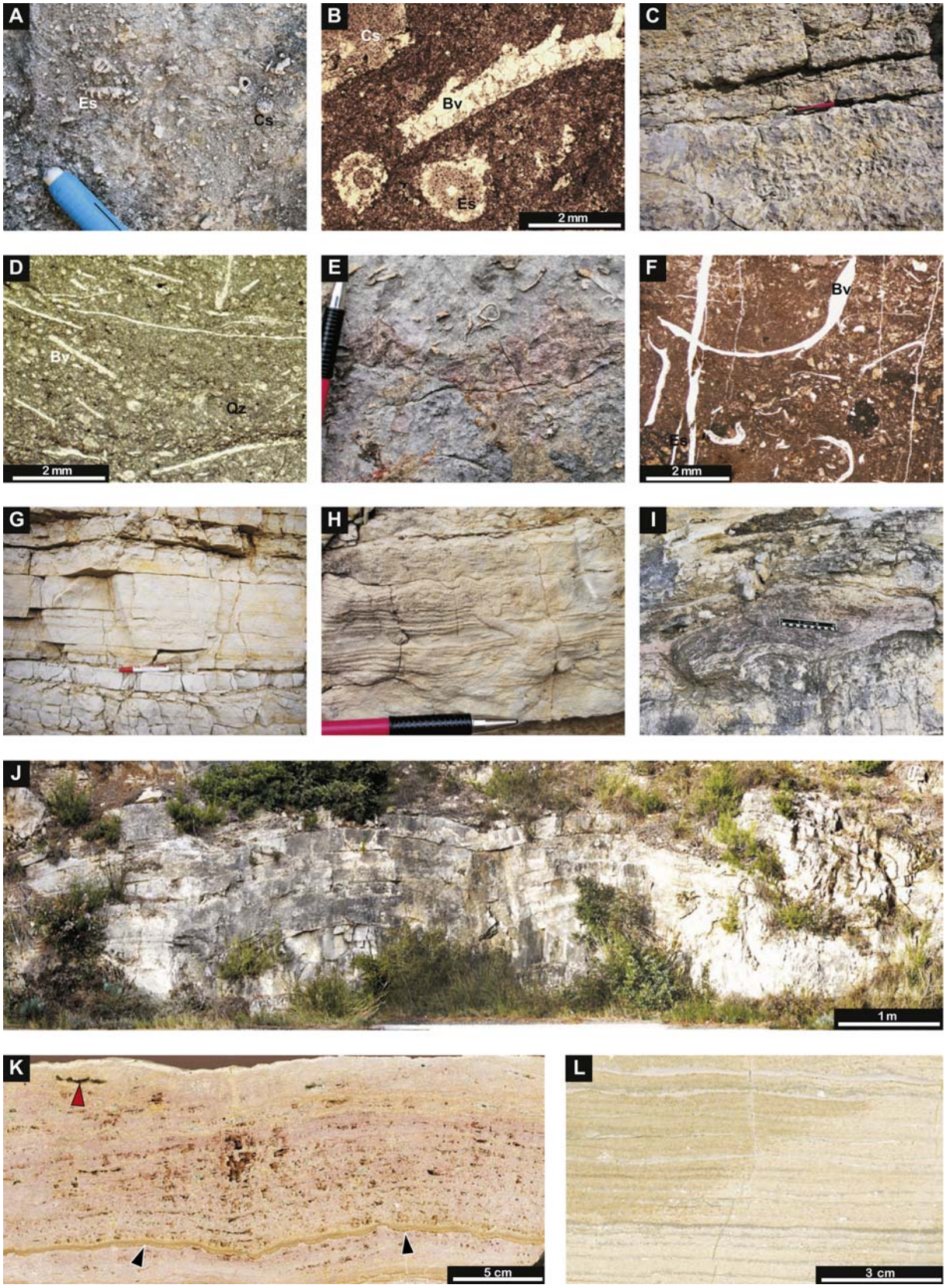

Figure 5. Photomicrographs and outcrop photographs of representative microfacies. (A) Outcrop detail of wackestone to floatstone of mollusks with packstone of echinoderms (facies F6). This facies shows a wackestone matrix with fragments of crinoid ossicles (Cs) and echinoid spines (Es). (B) Photomicrograph of facies F6 showing bivalve fragments (Bv), echinoid spine sections (Es) and crinoid ossicles (Cs). (C) Outcrop photograph of the strongly burrowed skeletal mudstone to wackestone (facies F7), showing nodular bedding and abundant *Planolites* ichnofauna. (D) Photomicrograph of facies F7 with frequent bivalve skeletons (Bv), peloids and some quartz grains (Qz). (E) Outcrop detail showing the burrowed skeletal mudstone to packstone interbedded with marls (facies F8). Whole specimens of bivalves and gastropods are observed. (F) Photomicrograph of facies F8 with

Table 4). Mouldic porosity consists of small sized (up to 3 mm width), elongated to subelliptical cavities representing pseudomorphs after evaporite minerals and anhydrite rosettes. These pores are occluded by blocky to granular calcite cements which are widely distributed in specific intervals of this facies.

6. Stratigraphic architecture and depositional models of the Ladinian ramps

The correlation between the 18 stratigraphic sections measured in the study area (Fig. 3) is based on the continuity of strata and characteristics of distinct stratigraphic surfaces (Mercedes-Martín et al., 2013). Stratigraphic surfaces were identified on the basis of the nature of the facies in contact across the surface, and the geometry of stratal terminations associated with each particular surface (Catuneanu, 2006). In the study area, four main types of sequence stratigraphic surfaces can be correlated across the platform to basin transect: the TS (transgressive surface), the MFZ (maximum flooding zone), the MRZ (the maximum regressive zone) and the SU (subaerial unconformity). These surfaces and the stacking patterns enabled us to identify two T–R Sequences in the Ladinian (Mercedes-Martín et al., 2013).

A major TS is identified above the continental sediments belonging to the Middle Muschelkalk facies. This surface can be correlated between Rasquera and Pontons and is characterised by a sharp lithological contrast which separates the continental red beds and clastics of the Middle Muschelkalk below from the fully marine carbonate sediments of the Upper Muschelkalk above (Fig. 3). This surface is overlain by 1) planar and domal stromatolites, 2) oolitic grainstone, or 3) finely laminated to massive dolomudstone, representing lateral facies changes related to distinct depositional conditions. This TS represents the bottom of the T–R Sequence 1 and can be clearly identified in the Prades and Baix Ebre–Priorat domains.

The MFZ marks the end of the shoreline transgression from a reflooding phase below (thickening-upwards parasequences) to a shallowing phase above (single shallowing-upwards parasequences) in the T–R Sequence 1 or a deepening phase below to a static shallow-water phase above in the T–R Sequence 2 (*sensu* Spence and Tucker, 2007). In the T–R Sequence 1, this change in stacking patterns can be easily recognized in the inner ramp portion of the platform by a conspicuous facies shift from oolitic shoals below (subtidal deposits) to planar and domal stromatolites above (intertidal deposits). A marked condensed surface with a hardground and evidence of starvation is recorded above the oolitic shoals in the more open marine parts of the inner ramp (around Miramar section, Fig. 3).

The MRZ of the T–R Sequence 1 is traceable in the inner ramp portion of the Gaià domain between the Coll Magí and Santa Perpetua de Gaià sections (Fig. 3). This surface marks the change from shoreline regression to subsequent transgression based on a change in stacking patterns from a shallowing phase below (single shallowing-upwards parasequences) to a deepening phase above (thinning-upwards parasequences *sensu* Spence and Tucker, 2007). Some transgressive deposits (Santa Perpetua de Gaià section) onlap the MRZ, providing evidence of backstepping beach deposits (cross-bedded oolitic grainstone) above the previous regressive materials (planar and domal stromatolites). The MRZ corresponding to the T–R Sequence 2 is located at the base of the regressive materials corresponding to the Keuper facies (evaporitic mud-flats and sabkhas).

The SU is an extensive surface that can be correlated at regional scale along the Gaià and the Prades domains. It is associated with a significant sea-level fall giving rise to subaerial processes and erosional incision (Figs. 3 and 10C). This surface, which is considered as an unconformity bounding the T–R Sequences 1 and 2, is accompanied by dissolution and karstification of the inner ramp stromatolitic deposits and middle ramp microbial biostromes and mud-mounds of T–R Sequence 1. In the Arbolí section, the SU is replaced by a younger TS at the contact between RST1 and TST2, generating a composite surface formed by ferruginous-rich deposits and hardgrounds. The epikarstic cavities and the associated packbreccia and floatbreccia fillings (*sensu* Morrow, 1982) are generally observed between the Miramar and La Figuera sections (Mercedes-Martín et al., 2013).

The distribution of sedimentary facies in time and space (stratigraphic architecture, Fig. 10) is controlled by the geotectonic evolution of the sedimentary basin, the type and rate of carbonate production, and the preferential location of deposition. The evolution of the stratigraphic architecture is divided in four stages. Each stage is characterised by the occurrence of specific facies in each depositional environment (inner, middle and outer ramp) within the ramp (Fig. 3A; Tables 1–3).

6.1. The first transgressive stage

The first transgressive stage corresponds to the first Ladinian transgression over the Middle Muschelkalk continental red beds, the TST1 of Figure 10A.

During the first pulse of this stage, extensive deposits accumulated in an inner ramp environment which was located between Miramar and Rasquera. These deposits are composed of carbonate tidal flats composed of wide-ranging planar stromatolites (facies F10) which are interbedded within small-scale oolitic shoals (facies F1). At this time, no middle or outer ramps environments were recorded in the study area.

The second pulse of this stage is characterised by the development of extensive muddy subtidal flat subenvironments between Miramar and Rasquera (middle-outer ramps environments), and intertidal to shallow-subtidal sheltered lagoons between Miramar and Pontons (inner ramp environment). In fact, these environments consist of strongly burrowed skeletal mudstone to wackestone (facies F7), but they are separated by a small bank formed by peloidal and skeletal wackestone to packstone (facies F3).

The last pulse of the first transgressive stage is dominated by the sedimentation of extensive subtidal oolitic shoals (facies F1) in the inner ramp environment (Miramar to Pontons) and by deep subtidal burrowed mudstone to packstone interbedded with marls (facies F8) in the outer ramp environment (Miramar to Rasquera). The coeval development of the la Riba fault played a key role in the facies arrangement, thicknesses of sedimentary bodies and the distribution of sedimentary subenvironments during the transgressive stage.

6.2. Widespread microbial settlement

The parasequences of the RST1 show a shallowing-upwards trend and mainly aggrading and prograding stacking patterns.

fragments of bivalves (Bv), echinoid spines (Es) and peloids. (G) Outcrop photograph of thin-bedded laminated dolomudstone showing plane parallel lamination (facies F9). (H) Detail of facies F9 displaying unidentified escaping burrows. (I) Outcrop detail of planar and domal stromatolite (facies F10) showing domal geometries. (J) Panoramic photomosaic of the facies F10 displaying metric domal buildups in outcrop (Type 2 biostromes, head-shaped). (K) Polished slab of a stromatolite dome (facies F10) showing its internal laminae and interlaminar voids (red arrow). Some microkarstic horizons are also visible (black arrows). (L) Polished slab showing the lamination of a planar stromatolite (facies F10) consisting of an alternation of dark and light dolomite layers (Type 1 biostromes, stratiform). For scale: pencil, rubber and marker are 15 cm long. (For interpretation of the references to colour in this figure legend, the reader is referred to the web version of this article.)

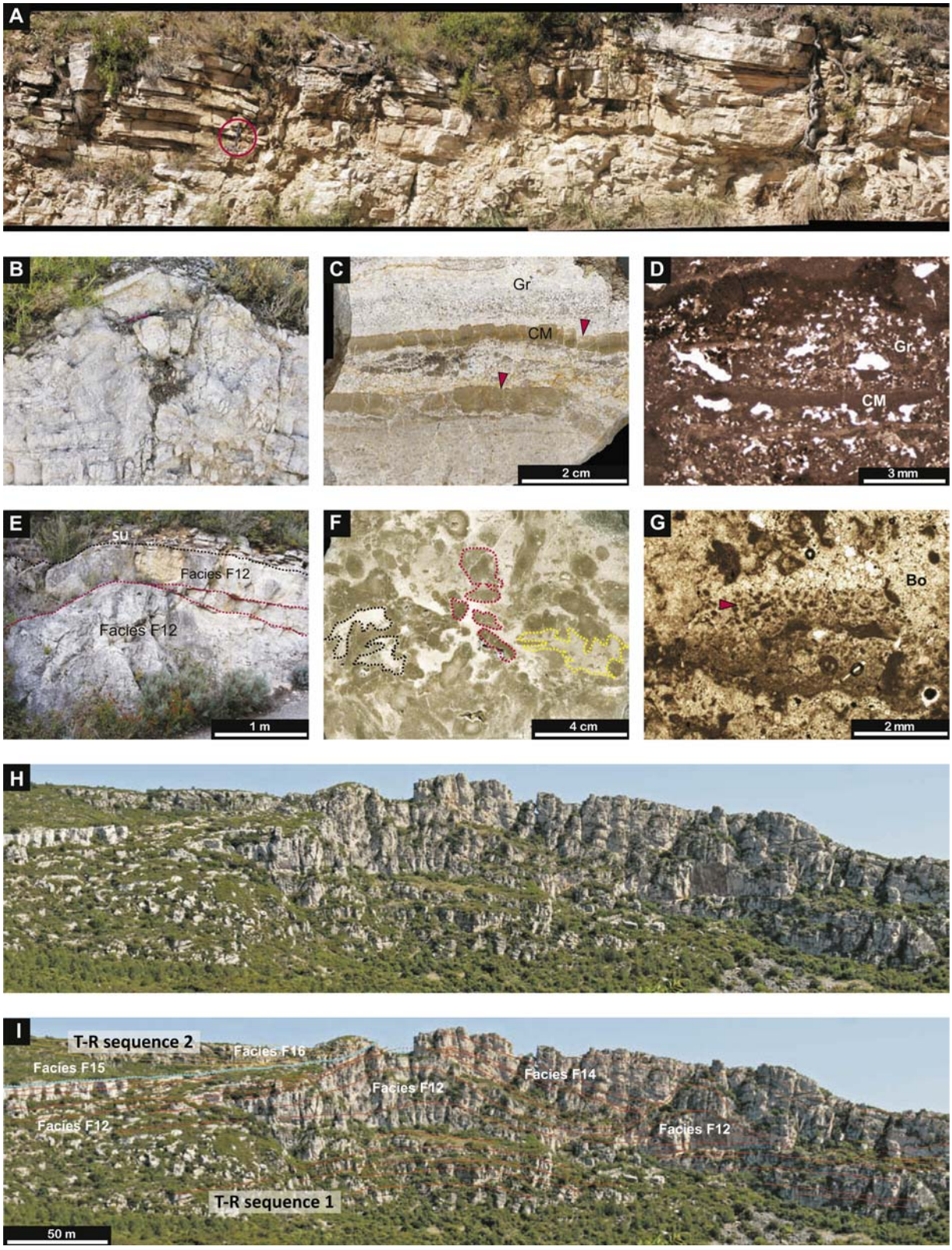

Figure 6. A–B. Photomicrographs and outcrop photographs of representative microfacies. (A) Outcrop photomosaic showing the ooidal–peloidal stromatolite (facies F11) displaying metric domal geometries. (B) Outcrop detail of facies F11 displaying a small stromatolitic dome. Note the heterogeneous centimetric layers exhibiting some convolute structures. (C) Polished slab of facies F11 with an alternation of oolitic grainstone layers (Gr) and clotted micrite layers (CM). Note the microkarstic dissolution surfaces on top of the muddy intervals (red arrows). (D) Photomicrograph of facies F11 displaying an alternation of thick oolitic layers (Gr) with thin clotted micrite layers (CM). (E) Photograph of the microbial-peloidal thrombolites (facies F12) in outcrop. The red dotted lines represent stratigraphic surfaces within the thrombolite mounds. The black dotted line is a karstic surface and the subaerial unconformity (SU) bounding T–R sequences 1 and 2. (F) A polished slab of the microbial-peloidal thrombolite. Yellow dotted lines represent interframework cavities composed of light clotted micrite textures whereas red dotted lines enclose the mesoclots constituted by darker micropeloidal to peloidal cloudy micrite. Dark dotted lines enclose pale white botryoidal and fibrous marine cements (G) Photomicrograph of facies F12 displaying cavities containing a filling of mudstone to wackestone

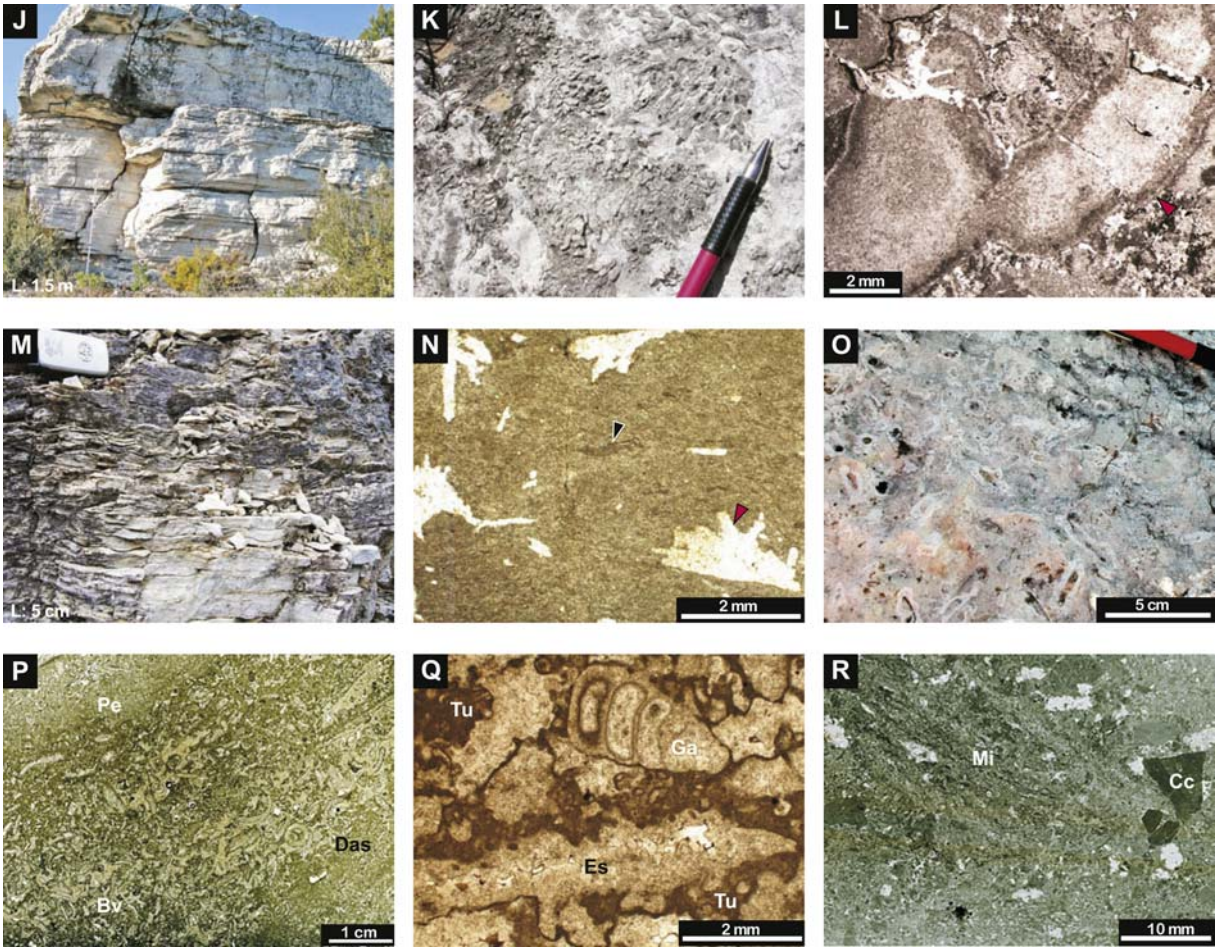

Figure 6. (*continued*).

During the RST1, microbial carbonates were the most important carbonate factories along inner and outer-middle ramp environments. In the inner ramp, planar and domal stromatolites (facies F10) developed under hypersaline conditions, whereas in the middle and outer-middle ramp environments considerable microbial biostromes and mud-mounds (facies F12) accumulated under restricted to open-marine conditions. Fault-induced syn-rift subsidence led to a severe compartmentalization of the Prades domain, generating a large depocentre in this area. As a result, a wide variation in thickness is recorded in this domain (Fig. 10B). A large diversity of facies mainly calcimicrobial boundstone (facies F13), coral-microbial boundstone (facies F14) and packstone to rudstone of dasyclads (facies F16) locally cap the microbial biostromes and mud mounds. Steep prograding flanks are observed in the eastern part of the Prades domain indicating the presence of a considerable depocentre in this area as a result of the la Riba fault. By contrast, aggradational geometries are more locally recorded in the western part of the Prades domain forming extensive tabular facies belts. During this stage, the outer ramp environment was located in the Baix Ebre–Priorat domain. Around the Montsant section a SW-dipping escarpment developed coeval with the deposition of burrowed mudstone to packstone (facies F6) that extends basinwards.

6.3. Widespread development of sheltered lagoons and shoals

Prior to this stage, a sea level drop of at least 50 m (Fig. 10C) kept the Gaià and Prades domains subaerially exposed and karstified. The resultant incised surface is a subaerial unconformity. At that time, several areas in Gaià, Prades and Baix Ebre–Priorat domains became important depocentres for carbonate deposition. There is no evidence of subaerial karstification in the northern part of the Gaià domain, suggesting that the blocks tilted towards the NE

composed of clotted micrite textures, peloids and micropeloid layers (red arrow) and botryoidal cements (Bo). (H–I) Panoramic photomosaic of Type 2 mud-mound thrombolitic unit and associated facies near the Molí del Pinetell section (village of la Riba). Line-drawing interpretation showing the geometries, facies relationships and boundary between T–R sequence 1 and 2 (turquoise blue line). (J) Outcrop expression of the calcimicrobial boundstone with bioclasts (facies F13). (K) Outcrop photograph of coral-microbial boundstone to rudstone (facies F14), consisting of a small coral reef colony with several rounded corallites in a muddy matrix. (L) Photomicrograph of facies F14 with dolomitised wackestone to packstone with branching scleractinian corals (red arrow). (M) Outcrop photograph of laminated packstone of oncoids and peloids (facies F15) displaying wavy microbial lamination. (N) Thin-section photograph of facies F15 composed of peloidal matrix with oncoids (black arrow) and calcite pseudomorphs of evaporite minerals (red arrow). (O) Outcrop photograph of packstone to rudstone of dasyclads, bioclasts and peloids (facies F16) showing abundant coated elongated dasyclad talli. (P). Polished slab of facies F16 displaying a rudstone texture composed of dasyclad sections (Das), bivalve fragments (Bv) and peloids (Pe). (Q) Photomicrograph of facies F16 with gastropod shells (Ga), elongated echinoid spines (Es) encrusted with *Tubiphytes* sp. (Tu). (R) Polished slab of foreslope dolomitic breccia (facies F17) with microproblematica crusts (Mi) and carbonate clats (Cc). For scale: hammer 32 cm long; pencil 15 cm long and car key 6 cm long. (For interpretation of the references to colour in this figure legend, the reader is referred to the web version of this article.)

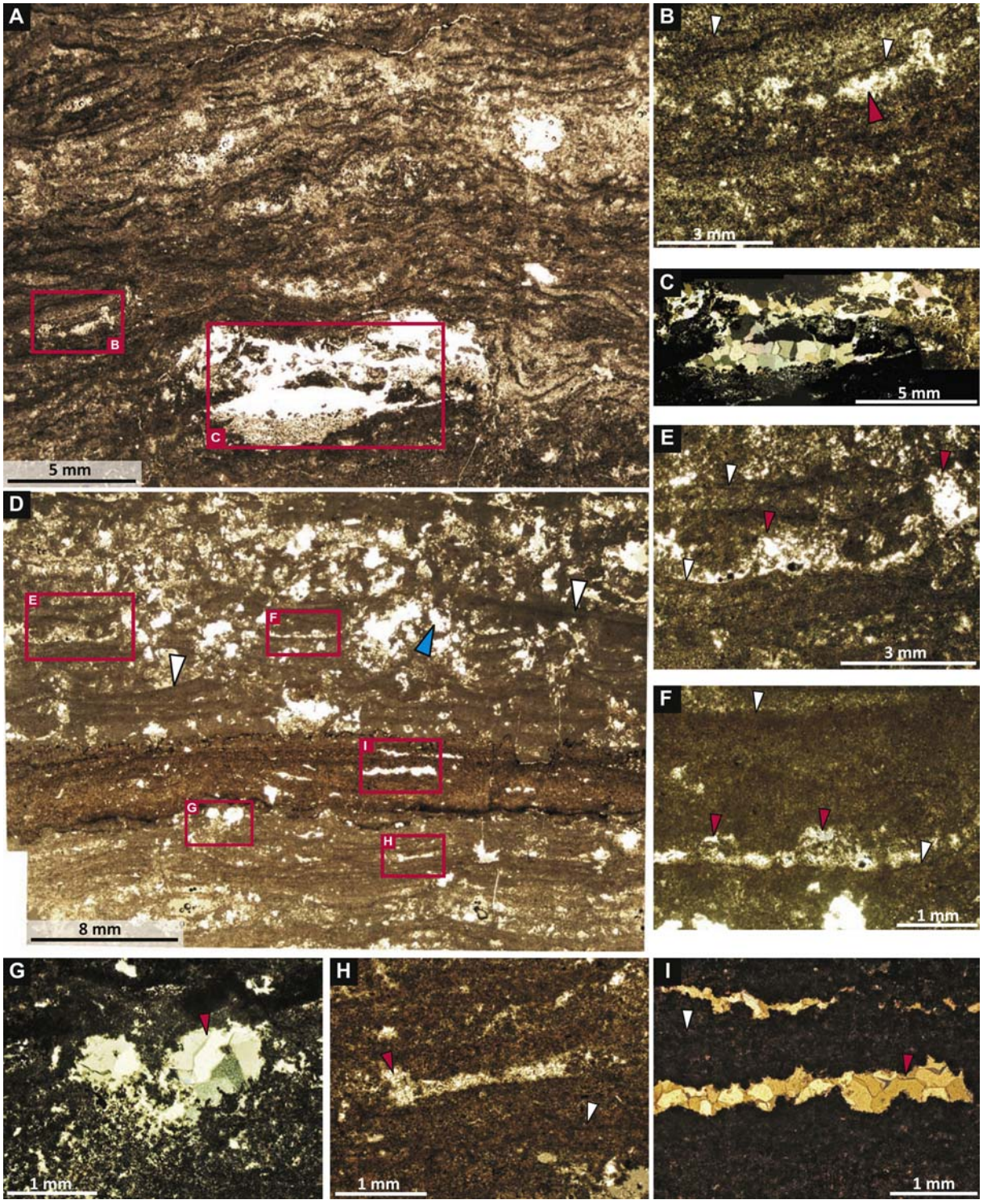

Figure 7. Photomicrographs displaying examples of the ancient porosity in the planar and domal stromatolites (facies F10)occluded by calcite cements. (A) Laminated fabric displaying different types of pores and cavities. Note the continuous, undulate and wavy microbial laminae. (B) Cemented interlaminar voids (red arrow) following the microbial lamination (white arrow). Cross-polarised light. (C) Vuggy porosity filled with blocky and granular calcite cements. Cross-polarised light. (D) Microbial laminations exhibiting some examples of porosity types. Note the subparallel laminae (white arrows). (E) Interlaminar voids within a laminated fabric (white arrows) displaying a convex morphology associated with former sites of microbial vertical accretion (red arrows). Cross-polarised light. (F) Some interlaminar voids filled with sparite (red arrows) were apparently occupied by calcimicrobes and microbial mats which define the laminated fabric (white arrows). Cross-polarised light. (G) Cemented interlaminar voids (red arrow) developed below wavy laminae. Cross-polarised light. (H, I) Elongated interlaminar voids (red arrow) are developed parallel to laminae (white arrow) and are subsequently filled with blocky calcite cement. Cross-polarised light. (For interpretation of the references to colour in this figure legend, the reader is referred to the web version of this article.)

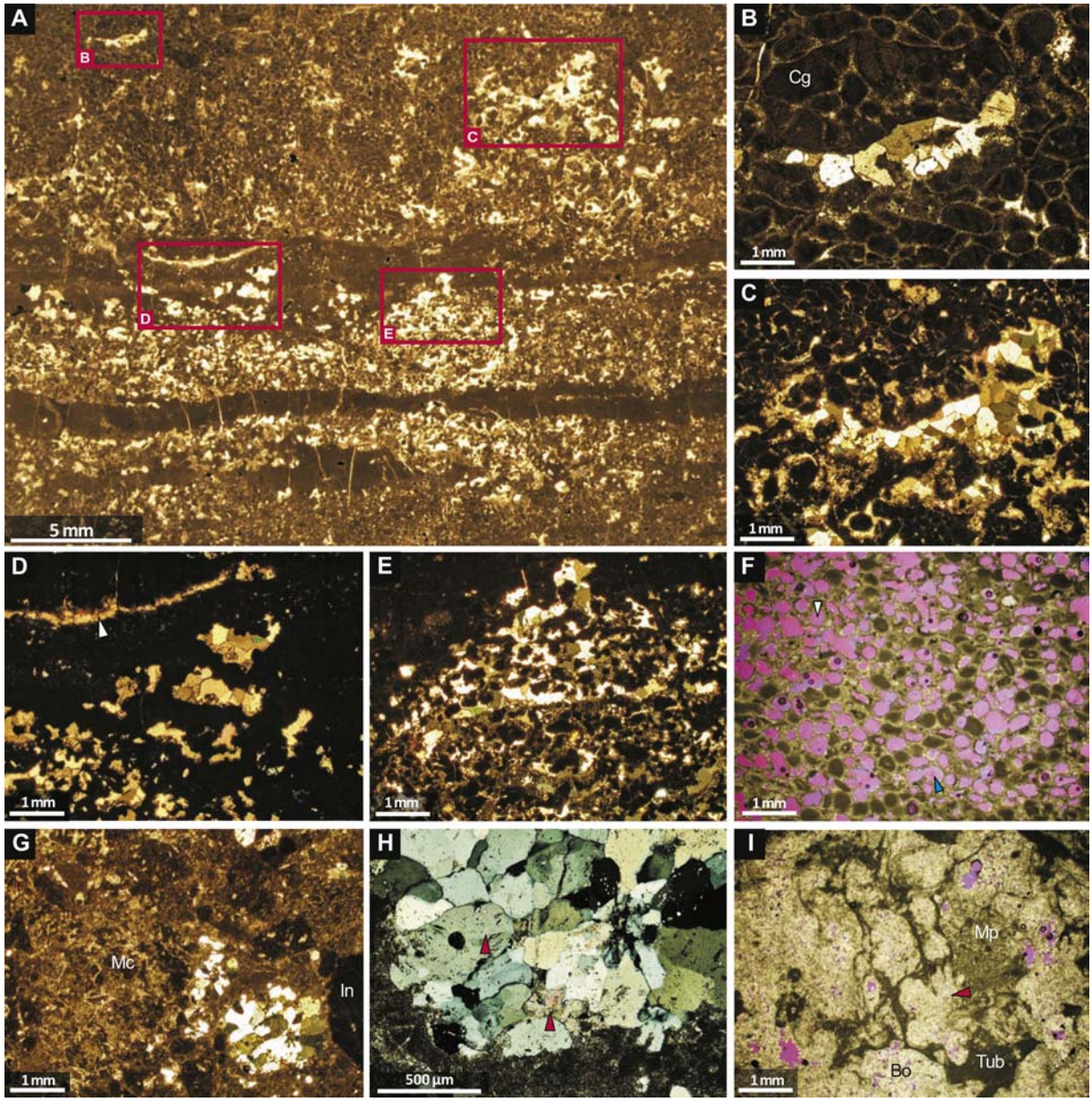

Figure 8. Photomicrographs displaying examples of the ancient porosity in the ooidal–peloidal stromatolites (facies F11, A to F) and microbial-peloidal thrombolites (facies F12, G to I), cemented by blocky calcite cements. (A) Thin section displaying the internal fabric of facies F11 with an alternation of grainy with muddy layers. Cross-polarised light. (B) Vuggy porosity occluded by a sparry calcite cement. Note the irregular cutting across the coated grains (Cg). Cross-polarised light. (C) Vuggy porosity in grainy intervals. (D) Selective vuggy porosity developed within a muddy interval and filled with sparry calcite cements. Note the elongated and subparallel fenestral cavity (white arrow). Cross-polarised light. (E) Vuggy porosity in grainy intervals. An initial intergranular porosity enhanced by selective leaching may have originated the vuggy porosity which is now occluded by sparry calcite cements. Cross-polarised light. (F) Abundant mouldic porosity (white arrows) affecting ooids and peloids. Note an interconnected vuggy porosity which evolves from a previous mouldic porosity. Pink colour indicates open pore spaces. (G) Microbial-peloidal thrombolite formed by Microproblematica crusts (Mc) and carbonate intraclasts (In) displaying occluded porosity (white masses). (H) Detail of a quartz cemented cavity with tiny anhydrite inclusions (red arrows). (I) Microbial-peloidal thrombolite showing abundant botryoidal cements (Bo) surrounded by *Tubiphytes* crusts (Tub) and micropeloidal masses (Mp). Pink colour indicates open pore spaces. (For interpretation of the references to colour in this figure legend, the reader is referred to the web version of this article.)

(Fig. 10C). During this stage, corresponding to the TST2 (Fig. 10D), bioturbated wackestone and packstone (facies F5) accumulated as open marine facies, in a proximal outer ramp environment (Falset to Rasquera). Besides, the middle ramp environment was constituted by external shoals (Falset to Montsant) formed by thick coarse-grained grainstone deposits (facies F1) and a very extensive sheltered lagoon (Montsant to Coll Magí) formed by oncolitic–oolitic–peloidal floatstones and grainstones (facies F4). Thinning and fining-upwards parasequences are recorded. In addition, the inner-middle ramps environments (Gaià domain, from Coll Magí to Pontons) were formed by internal shoals at this time dominated by cross-bedded calcarenites and oolitic grainstone (facies F1 and F2) and also internal fore-shoals characterised by broad belts of ooidal–peloidal stromatolites (facies F11).

6.4. The last marine shallowing stage

The deposits of this period (RST2, Fig. 10E) are widely represented in Prades and Gaià domains; important heterogeneous thicknesses of laminated packstone of oncoids (facies F15) filled the

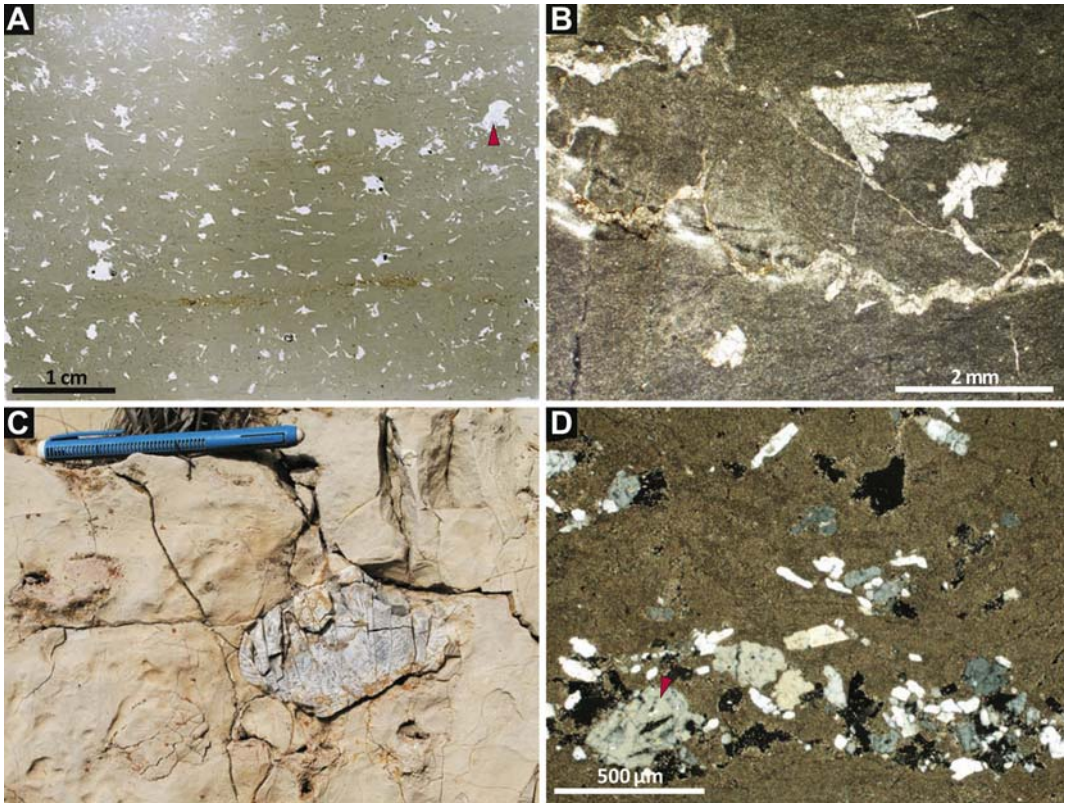

Figure 9. Photomicrographs displaying examples of the ancient porosity in the laminated packstone of oncoids and peloids (facies F15). (A) Thin section displaying the internal fabric of facies F15. (B) Mouldic porosity with pseudomorph crystals after evaporite minerals filled with blocky calcite cements. (C) Subespherical silicified masses in outcrop interpreted as a late replacement of evaporite nodules. (D) Mouldic porosity filled with granular quartz cements containing small inclusions of anhydrite (red arrow). Cross-polarised light. For scale: pencil 15 cm long. (For interpretation of the references to colour in this figure legend, the reader is referred to the web version of this article.)

basin between Pontons and Montsant. These materials deposited in an inner ramp environment as intertidal and supratidal flats, giving rise to aggradational to progradational stacking patterns recorded at the scale of parasequence. Both the Ulldemolins-Gandesa and la Riba faults played a leading role in the configuration of this remarkable depocentre of shallow marine deposits.

6.5. Depositional models of the Ladinian carbonate platform

A spatial and temporal distribution of sedimentary facies has been conducted for a carbonate ramp system in the Ladinian of the Catalan Basin. Detailed field work allowed us to build a precise sequence stratigraphic framework based on the identification of stratigraphic surfaces and outcrop and seismic scale depositional geometries. An accurate recognition of fractures and regional faults is essential for restoring the original depositional profile, and constraining the subsidence values/accommodation space of each domain in order to construct reliable depositional models.

The Ladinian fault-controlled syn-rift carbonate system developed in the Triassic Catalan Basin was constituted by two types of carbonate ramps (lower and upper) corresponding to T–R sequence 1 and 2 respectively (see Mercedes-Martín et al., 2013).

The T–R sequence 1 (Lower Ladinian) is interpreted as a fault-block ramp, with a TST1 defined by two sedimentary pulses and a

Table 4
Depositional and reservoir attributes of microbialite facies. Porosity values are referred to ancient porosity occluded by calcite cements.

Facies	Dimensions	Structure	Morphotypes	Depositional environment and constraints	Systems tracts	Porosity types/values
F10 Planar and domal stromatolites Figure 7	At least 20 km wide At least 7 m thick	Laminated	Type 1 Biostromes (stratiform) Type 2 Biostromes (head-shaped)	Restricted to hypersaline Attached to coarse-grained substrates Associated to marine flooding surfaces Moderate energy conditions	TST1 RST1 TST2	Interlaminar voids Ancient vuggy up to 10%
F11 Ooidal–peloidal stromatolites Figure 8A–F	At least 40 km wide At least 3 m thick	Laminated	Stratiform geometries Low-relief hemi-elliptical	Semi-restricted to open-marine Attached to coarse-grained substrates Associated to transgressive surfaces Moderate to high energy conditions	TST2	Ancient vuggy up to 15% Mouldic (grain dissolution) up to 20%
F12 Microbial-peloidal thrombolites Figure 8G–I	At least 45 km wide At least 40 m thick	Thrombolitic	Type 1 Biostromal thrombolites Type 2 Mud-mound thrombolites	Semi-restricted to open-marine Attached to coarse-grained substrates Associated to marine flooding surfaces Low to moderate energy conditions	RST1	Mouldic (evaporite replacement) up to 10%
F15 Laminated packstone of oncoids and peloids Figure 9	At least 100 km wide At least 70 m thick	Laminated	Flat laminated and locally domal	Open marine Attached to coarse-grained substrates Associated to maximum flooding surfaces Low energy conditions	RST2	Mouldic (evaporite replacement) up to 15%

RST1 formed by one sedimentary pulse (Fig. 10). The first stage of the TST1 is mainly characterised by a widespread microbial carbonate colonization event over the previous Middle Muschelkalk continental sequence, giving rise to a homoclinal ramp depositional profile. The second stage of the TST1 is made up of a muddy facies throughout the ramp, especially in the middle-outer ramp, and extensive coarse-grained grainstone blanket deposits in the inner ramp. A swell-dominated fault-block ramp model is inferred for the second stage of the TST1. Synsedimentary faulting activity in the Gaià domain caused by la Riba fault modified the basin physiography by creating subsiding areas that developed specific depositional environments during the TST1.

The RST1 contains the most prominent microbial deposits, such as stromatolites in the inner ramp (up to 10 m thick) and thrombolites in the middle ramp (up to 40 m thick). During this stage, the Prades domain became an important subsiding area where large thicknesses of biostromal and mud-mound thrombolitic units proliferated owing to the increasing accommodation space triggered by the la Riba fault. In addition, the Gaià domain experienced less pronounced gains in accommodation space which permitted the inner ramp to develop coeval conspicuous planar and domal stromatolites. The depositional model for this stage would correspond to a microbial-dominated fault-block ramp.

The T–R sequence 2 (Upper Ladinian) is also defined as a fault-block ramp mainly controlled by the Ulldemolins-Gandesa and la Riba faults (Fig. 10). The TST2 is characterised by a wide settlement of well-developed sheltered lagoons and external-internal shoals showing a great lateral continuity of facies (more than 140 km across the basin), from inner to middle-outer ramp subenvironments. The prolonged active role of the Ulldemolins-Gandesa and the la Riba faults allowed the Prades domain to maintain its subsiding character and accommodate tens of metres of carbonate deposits. Oncolitic-oolitic floatstone and grainstone formed in sheltered lagoons in this location. In addition, huge oolitic stromatolites were mainly deposited in the inner ramp settings as internal fore-shoals. Variable thicknesses are recorded in the Gaià domain because of the Sta. Perpetua de Gaià fault. The depositional model corresponds to a barrier-bank dominated fault-block ramp.

The RST2 is exclusively formed by laminated packstone of oncoids and peloids that were deposited in extensive peritidal flats occupying more than 100 km of the inner and middle ramp. During this stage, the Ulldemolins-Gandesa and la Riba faults were active, generating a considerable amount of accommodation space that was filled with shallowing-upwards deposits. A shallow-water fault-block ramp is assumed for the RST2.

7. Discussion

The study on facies architecture allowed us to better understand some key points of the constructional dynamics of the Ladinian carbonate ramp system in the Catalan Basin. The basinal and tectonic settings of carbonate platforms control their occurrence, the overall 2-D platform morphology, and the large-scale stratigraphic features and depositional sequences (Bosence, 2005). In spite of the syn-rift compartmentalisation of the Catalan Basin during the Ladinian (Mercedes-Martín et al., 2013), the irregularities of the antecedent topography were compensated by significant rates of carbonate production. As a result, the geometry of sedimentary bodies and the continuity of facies belts indicate a ramp-like depositional setting. A good example of this trend is observed during the RST1 in the Prades domain, where a marked difference in sedimentary thickness is recorded between the footwall block (Miramar) and the hangingwall block (Coma Fonda) through La Riba fault. This suggests that the rate of subsidence, increasing the accommodation space, was offset by the rate of microbial carbonate growth (facies F12 to F16). In other words, the space available for deposition was promptly filled with facies F12 to F16 predominantly characterised by microbial components, giving rise to a fault-block carbonate ramp depositional profile. The evidence for this depositional model is the lack of platform margins associated to fault scarps and the absence of well-defined talus slope facies associated with those active faults. Although, in other cases, as in the proximity of Montsant, the tilting of blocks associated with synsedimentary faults gave rise to narrow mud-rich debris flows and slumped deposits indicating small scarps. In the intrashelf trough of the Prades domain, the infill of sediments consists of middle-ramp facies and there is not any evidence of basinal marly facies. Thus, this trough can not be considered as an intrashelf basin.

In contrast, the ratio between the creation of accommodation space and the production of carbonates was notably different in other Middle Triassic regions of the Tethys. The late Anisian Latemar carbonate platform (western Dolomites) is an example of a polygonal fault-block isolated carbonate buildup that grew during an episode of extremely high subsidence (Preto et al., 2011). The platform interior displays well layered peritidal shallowing-upwards cycles with aggradational geometries. The slope is dominated by gravitational processes, and composed of megabreccia facies and coarse turbidites and slumps with progradational geometries (Marangon et al., 2011). The Ladinian Marmolada platform, which is an isolated carbonate platform limited by synsedimentary faults, was forced to aggrade, resulting in a sharp facies contrast between bedded platform deposits and the foreslope talus deposits. This talus is constituted by clinoforms of limestone megabreccias interfingered with pelagic basinal sediments (Blendinger, 1986). In these Italian examples, the rate of fault displacement exceeded that of carbonate deposition generating a tectonic asymmetry which resulted in a distinctive facies differentiation. This rate triggered the development of small-scale isolated carbonate platforms on structural highs and organic-rich intrashelf basins in grabens. There is no sedimentary evidence supporting this pattern in the Ladinian carbonate platforms of the Catalan Basin.

In addition, the Latemar platform (Harris, 1993; Marangon et al., 2011) contains abundant microbial and early-cement dominated boundstones preferentially located on the platform margin and slope (2D areal estimate: 750 m width and 875 m thick). Similarly, the Lower Carboniferous Tengiz, which is an isolated carbonate platform (Weber et al., 2003; Collins et al., 2006), displays an abundant in-situ microbial boundstone and cement-rich facies mainly located at the transition between outer-platform and upper-slope and also on the upper and middle slope facies (2D areal estimate: 416 m width and 250 m thick). These examples show that 2D areal distribution of microbialite facies in synsedimentary isolated carbonate platforms is generally limited to the platform margin and slope displaying narrow wedges of progradational clinoforms. By contrast, the synsedimentary fault-block ramps of the Ladinian Catalan Basin are characterised by mainly stratiform, sheet-like continuous microbial facies belts of considerable lateral extension with 2D areal estimate up to 45 km width and 40 m thick in thrombolites, and up to 30 Km width and 7 m thick in stromatolites (Fig. 11, Table 4).

Differential rapid syn-rift subsidence was the main factor controlling accommodation and also the depositional styles observed in the T–R sequences 1 and 2. Accommodation played a key role on the geometry of the microbialites (stromatolites and thrombolites) at the meso and macroscale. Domed and mounded bodies developed during the stages of increasing accommodation rates, whereas biostromal morphologies grew in association with periods of lower accommodation rates. In the case of stromatolites (facies F10), the vertical transition between Type 1 biostromes (stratiform)

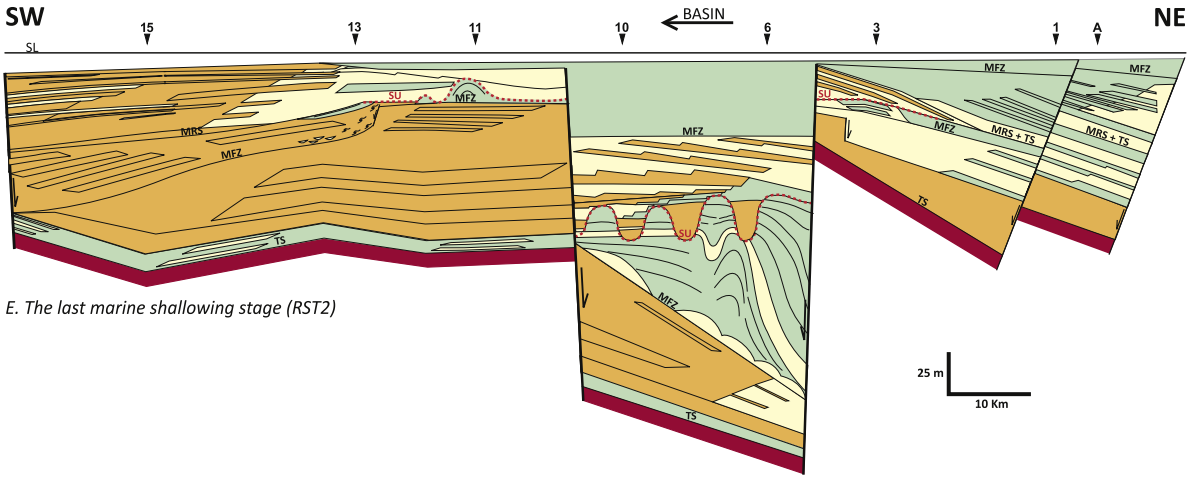

E. The last marine shallowing stage (RST2)

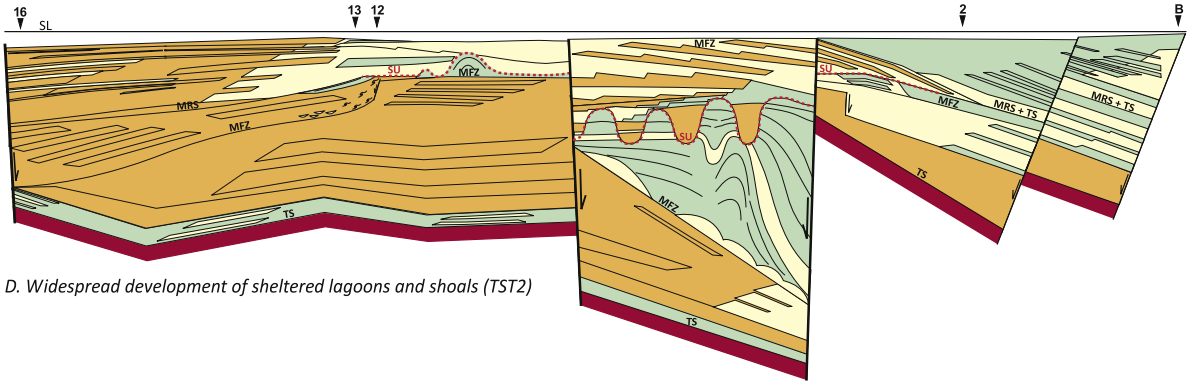

D. Widespread development of sheltered lagoons and shoals (TST2)

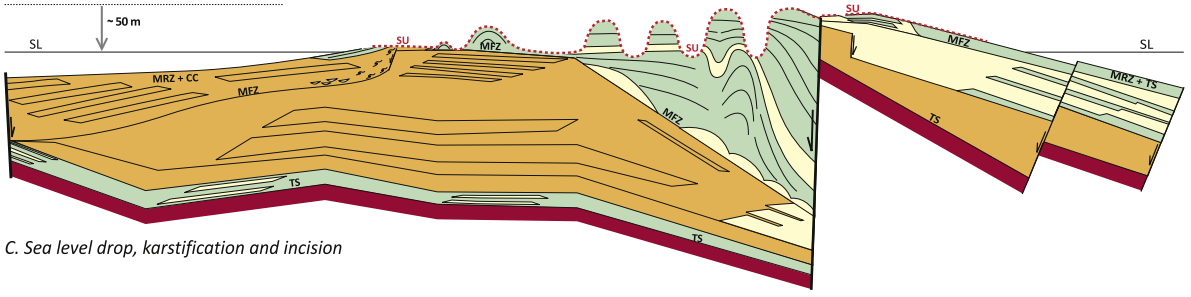

C. Sea level drop, karstification and incision

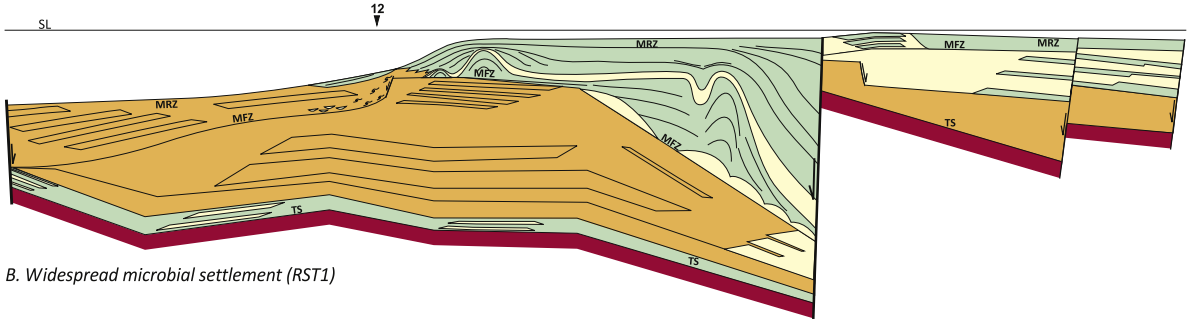

B. Widespread microbial settlement (RST1)

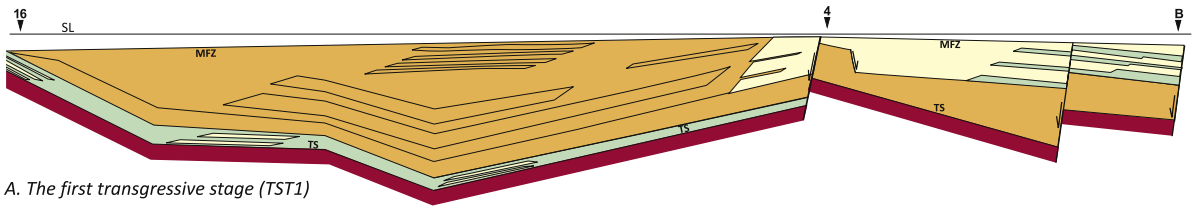

A. The first transgressive stage (TST1)

and Type 2 biostromes (head-shaped) is explained in terms of increasing accommodation rather than in relation to a change in the type of microbial community (Mercedes-Martín et al., 2013) (Table 4). In addition, the eastern part of the Prades domain underwent accelerated fault-controlled subsidence, which created greater accommodation near the la Riba fault. These conditions were not suitable for thrombolite growth, since they built to relative sea-level rise in order to adapt to the new suddenly water table conditions (oxygen, temperature, nutrients, water chemistry, input of detrital carbonate material, light?). This resulted in the extensive development of high-relief Type 2 thrombolite mounds of facies F12 (Table 4).

Moreover, the extensional tectonic regime, which compartmentalised the basin into the Gaià and Prades domains, created different palaeoecological niches where microbialites developed. In T–R sequence 1, stromatolites developed in a hypersaline protected embayment such as Shark Bay, Australia triggered by local palaeogeographical barriers in the inner ramp (Gaià domain), whereas large thrombolites could grow in open-marine conditions with limited input of siliciclastic sediment, in the middle ramp (Prades domain).

In recent years, microbialites have monopolized attention in both academia and the oil industry because of the increased interest in biomineralization processes and products (see revision in Dupraz et al., 2009) and in the last decade because of the possible accumulation of hydrocarbons in their successions (Parcell, 2002; Adams et al., 2005; Collins et al., 2006; Ahr, 2009; Awramik and Buchheim, 2012). Microbial carbonate pore type characterisation is crucial to an appropriate evaluation of their petrophysical properties and reservoir potential (Rezende et al., 2012; Tonietto et al., 2012). Microbial textures show a considerable heterogeneity and complexity reflecting the biological processes of microbialite formation (Ahr, 2008, 2009). Moreover, the distinction between depositional porosity and diagenetically altered porosity is noteworthy in carbonate reservoir characterisation.

In the case of the Upper Jurassic Smackover thrombolites (Mancini et al., 2004), the reservoir quality and distribution within the microbial mounds are largely controlled by the distribution of microbial fabrics and growth types (Parcell, 2002). Although depositional facies remained the primary control on reservoir quality, the diagenetic processes (early marine and burial diagenesis; Benson, 1985) exerted a significant influence on reservoir quality. Porosity in the Smackover thrombolite boundstones is a mixture of shelter and fenestral porosity overprinted by secondary dolomite intercrystalline and vuggy porosity (Mancini et al., 2004). In the case of the Catalan Basin, the Ladinian microbialites show a marked fabric-selective ancient porosity linked to the depositional environment. This porosity is affected by several diagenetic stages (marine diagenesis, exposure diagenesis, dolomitisation and late sulphate replacement; Tucker and Marshall, 2004).

Microbial facies F10 exhibits a fenestral porosity (interlaminar voids) apparently associated with the early diagenetic degradation of microbial mats and calcimicrobes, and facies F11 displays a well-sorted grain fabric with abundant mouldic porosity related to high-energy environments (Table 4). Furthermore, facies F12 develops a common secondary vuggy porosity which affects dolomite fabrics and also an evaporite mouldic porosity. Facies F15 develops a mouldic porosity produced during the replacement of dolomite by evaporite minerals (Table 4).

Moreover, as noted by Tucker and Marshall (2004), mouldic porosity characterised by pseudomorph crystals after evaporite minerals is common in facies F12 (Fig. 8G and H). These authors recorded many vugs in the thrombolite facies partly filled with coarse calcite crystals and also quartz cements and chert with small anhydrite-bearing inclusions. The origin of these vugs has been attributed to dissolution of local patches of gypsum/anhydrite which replaced the dolomite. The evidence of sulphate replacement is also recorded in facies F15 (Fig. 9, Table 4) and locally in facies F10. As pointed out by Tucker and Marshall (2004), this replacement could have been contemporaneous with deposition of facies F9 (thin bedded laminated dolomudstone, Fig. 3), when the basin was periodically subjected to hypersaline and anoxic conditions, or during a shallow burial shortly after the deposition of the evaporitic Keuper facies (Carnian). In fact, the presence of evaporite deposits above microbial facies could produce a degradation of the reservoir quality through evaporite precipitation and subsequent pore obliteration (Schröder et al., 2005).

Another similarity between the Ladinian microbialites in the Catalan Basin and the Oxfordian Smackover thrombolites is that they are both dolomitised. Extensive dolomitisation resulted in effective dolomite intercrystalline and vuggy porosities that acted to improve reservoir connectivity of all the Oxfordian thrombolite types (Mancini et al., 2004). Dolomitisation of the Smackover thrombolites has been interpreted as a relatively early diagenetic event because of the interplay of palaeotopography, fluctuations of the sea level, restrictive nature of ocean circulation due to barriers and an arid climate (Benson and Mancini, 1999). Similarly, Ladinian microbialites (facies F12) have been affected by an aragonite dissolution-dolomite cementation (Tucker and Marshall, 2004) which generated a fabric-retentive dolomitised fibrous or spar cements with a drusy fabric. According to Tucker and Marshall (2004), this suggests early dolomitisation, before the sediment stabilised to calcite. In addition, these authors suggested that the vugs generated within reefal facies (facies F14) after the dolomitisation of the marine botryoidal cements. In fact, thrombolite facies records post-dolomitisation early vugs and marine botryoidal cements embedded within clotted micrite matrix or coated by microbial *Tubiphytes* crusts (Fig. 8I). Thus, early dolomitisation could increase the original porosity of Ladinian thrombolites (facies F12), enhancing their pore connectivity and reservoir quality through vugs. Moreover, Ladinian microbialites may have undergone an increase in porosity during or after the late diagenetic replacement of the sulphates by quartz and coarse calcite cements. However, the impact of this diagenetic process on pore generation and occlusion of microbialitic facies remains to be studied more fully.

Understanding facies heterogeneities depends considerably on the specific sedimentary architecture which is linked to the basin evolution, sea level fluctuations and their palaeoenvironmental constraints, and also on porosity distribution, which is dependent on the nature of pore-filling fluids and the diagenetic evolution (Rezende et al., 2012; Terra et al., 2012; Tonietto et al., 2012). This knowledge has far-reaching implications for microbial reservoir characterisation. Accordingly, our work provides an integrated vision of microbial-dominated carbonate ramps in marine settings

Figure 10. Architectural evolution during the Ladinian of the Catalan Basin. (A) The first transgressive stage (TST1) gave rise to a homoclinal and later to swell-dominated carbonate ramp. (B) The RST1 corresponds to a widespread microbial settlement of stromatolites and thrombolites during a period of remarkable syn-rift subsidence. A microbial-dominated fault-block carbonate ramp was developed. (C) Extensive subaerial incision and karstification took place after a sea level drop of at least 50 m. (D) Widespread development of sheltered lagoons and shoals accumulated during the TST2 giving rise to a barrier-bank dominated ramp. (E) The last marine shallowing stage (RST2) corresponds to a period of extensive peritidal deposition and development of a shallow-water carbonate ramp. Numbers on top refer to stratigraphic sections in Figure 3.

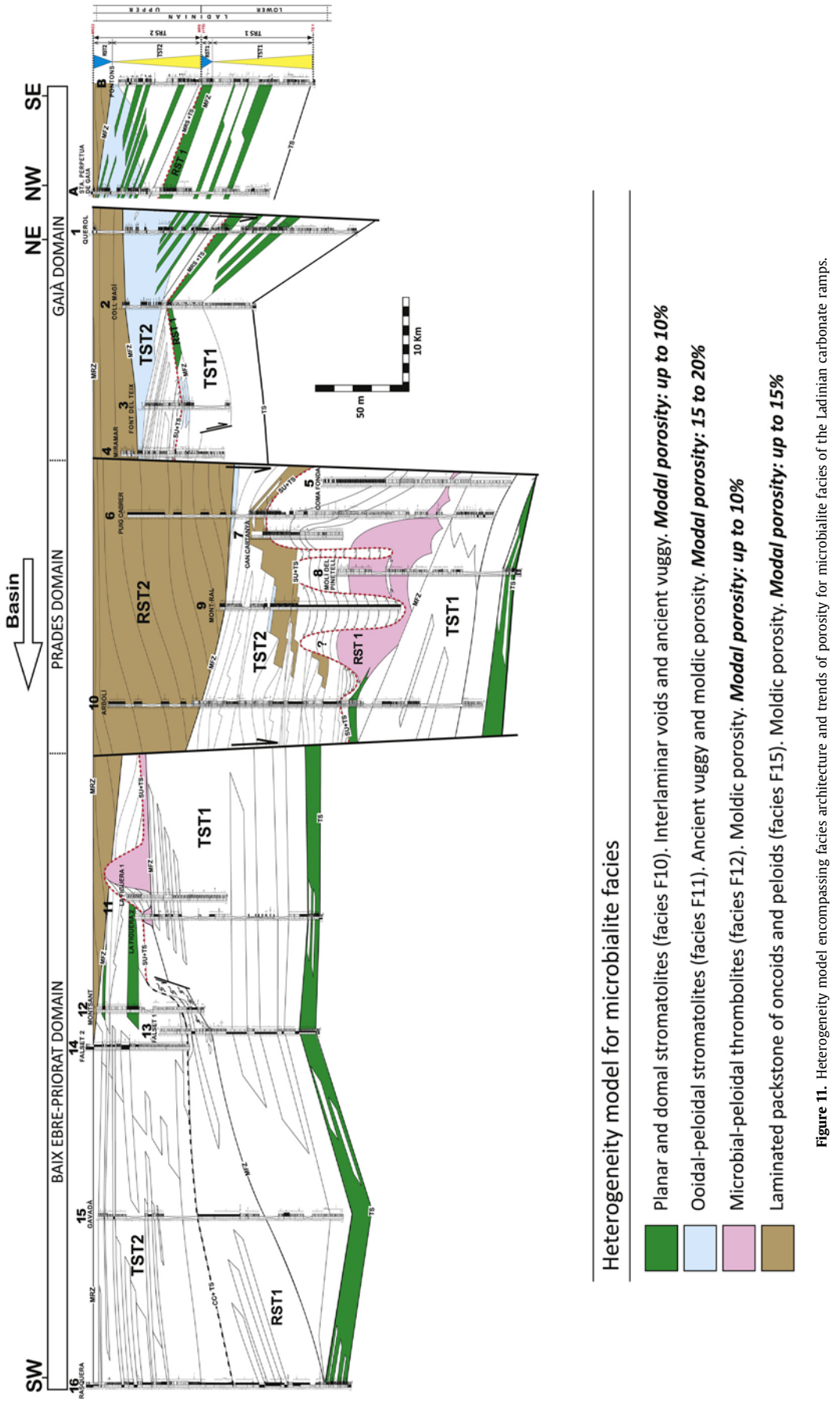

Figure 11. Heterogeneity model encompassing facies architecture and trends of porosity for microbialite facies of the Ladinian carbonate ramps.

because the Triassic Catalan Basin is a well-studied syn-rift basin, with a refined sedimentary framework (Mercedes-Martín et al., 2013). This allowed us to place the microbialites within a precise sequence stratigraphic context, and to characterise them as reservoir units using modal porosity values and sedimentary architectures (Fig. 11).

However, additional work is warranted to better understand the diagenetic processes affecting depositional and non-depositional porosity (cementation history, impact of dolomitisation, leaching processes) and their influence on pore geometry and connectivity. Further study on microbialite microstructure is required to characterise the microbial textures and fabrics of Triassic stromatolites and thrombolites to predict the mechanisms and preferential sites for early and late porosity generation.

8. Summary and conclusions

The record of Ladinian carbonate platforms of the Catalan Basin was studied in detail using a modern sequence stratigraphic approach. The distribution of carbonate facies and accommodation space is mainly controlled by fault-induced subsidence, which also caused basin compartmentalization. Detailed sequence stratigraphic and sedimentological analysis provided the framework for subdividing the Ladinian sedimentary record into two transgressive–regressive sequences showing internal third-order sea-level cyclicity. These two T–R sequences can be interpreted as having been deposited on a fault-block carbonate ramp model, with low-gradient depositional angles and wide lateral continuity of facies belts.

The T–R sequence 1 (Lower Ladinian) contains the most prominent microbial deposits, such as stromatolites in the inner ramp (up to 7 m thick) and thrombolites in the middle ramp (up to 40 m thick). The TST1 corresponds to a swell-dominated fault-block carbonate ramp model and the RST1 conforms to a microbial-dominated fault-block carbonate ramp.

The T–R sequence 2 (Upper Ladinian) is mainly constituted by marine oolitic stromatolites in the inner ramp and internal shoals and a sheltered lagoon in the middle-outer ramp. The TST2 corresponds to a barrier-bank dominated fault-block carbonate ramp model and the RST2 is inferred to be a shallow-water fault-block carbonate ramp.

Different palaeogeographical barriers developed coevally with regional syn-sedimentary fractures, giving rise to a specific lateral and vertical facies shifts (architecture). Some of these physical barriers coincided with 1) the abrupt lateral facies change from muddy facies group to coarse-grained facies group (e.g. the transition from the Prades domain to the Gaià domain in the TST1); 2) the abundance of microbial-peloidal thrombolites (e.g. biostromal and mud-mound thrombolite bodies of RST1 prospered in the Prades domain, a marked area of subsidence); 3) the stromatolite proliferation (e.g. the planar and domal stromatolite unit of RST1 grew in a restricted hypersaline embayment protected from the physical stress and erosion effect of waves and currents); and 4) the development of external shoals and sheltered lagoons in TST2. The previous stepped configuration of the RST1 provided the appropriate palaeogeographical framework for this specific arrangement of sedimentary environments.

Microbialites flourish during third-order regressive periods and are volumetrically the prime constituent in all sedimentary domains (RST1 and RST2). Their deposits display a marked lateral extension and mainly sheet-like, tabular bodies (up to 45 km width and 40 m thick in thrombolites and up to 30 km width and 7 m thick in stromatolites). Besides, microbial carbonates are proportionately more evident in the inner and middle portions of the ramp. On the other hand, coarse-grained and muddy facies are more conspicuous and more extensive during third-order transgressive periods (TST1 and TST2) and are volumetrically more prominent in the middle and outer portions of the ramp.

Modal porosity studies suggest that microbialites develop an original fabric selective porosity: interlaminar voids up to 10% (facies F10) and mouldic porosity by grain dissolution up to 20% (facies F11). A secondary ancient vuggy porosity filled with mosaic blocky calcite cements is also recorded attaining up to 15% (facies F10 and F11). A mouldic porosity due to evaporite replacement is observed in facies F12 and F15 with modal values of up to 15%. In addition, the microbialite bodies of the Ladinian Catalan Basin are characterised by mainly stratiform, sheet-like continuous microbial facies belts of considerable lateral extension. These attributes (porosity and architecture) make microbialite facies appropriate candidates for reservoir modelization.

The Ladinian microbial-dominated carbonate ramps represent an invaluable analogue that may be applied to fault-block microbial-dominated carbonate ramps rich in stromatolites and thrombolites and to basins that developed during a syn-rift regime of rapid subsidence.

Acknowledgements

We would like to dedicate this paper to the memory of Jordi Maria de Gibert, who died while he was engaged in a work on Triassic ichnofaunas. We are indebted to Ioan Bucur and Bruno Granier for micropalaeontological determinations and to G. v. K. for revising the English of the manuscript. We are grateful to Marc Aurell and an anonymous reviewer for their useful comments and criticism on the manuscript.

We gratefully acknowledge Repsol Exploración, S.A, and the Spanish government's I + D + i research project CGL2008-04916, the Consolider-Ingenio 2010 programme under CSD 2006–0004 "Topo-Iberia" and the Grup Consolidat de Recerca "Geologia Sedimentària" (2009SGR-1451), for funding.

References

Adams, E.W., Grotzinger, J.P., Watters, W.A., Schröder, S., McCormick, D.S., Al-Siyabi, A., 2005. Digital characterization of thrombolite-stromatolite reef distribution in a carbonate ramp system (terminal Proterozoic, Nama Group, Namibia). AAPG Bulletin 89, 1293–1318.

Ahr, W.M., 2008. Geology of Carbonate Reservoirs: The Identification, Description, and Characterization of Hydrocarbon Reservoirs in Carbonate Rocks. John Wiley & Sons, p. 277.

Ahr, W.M., 2009. Microbial Carbonates as Hydrocarbon Reservoirs. AAPG Search and Discovery Article. AAPG Annual Convention and Exhibition, Denver, Colorado.

Awramik, S.M., Buchheim, H.P., 2012. The Quest for Microbialite Analogs to the South Atlantic Pre-salt Carbonate Hydrocarbon Reservoirs of Africa and South America. HGS International Dinner Meeting talk. URL: http://www.hgs.org/node/4875.

Benson, D.J., 1985. Diagenetic controls on reservoir development and quality, Smackover Formation of southwest Alabama. Gulf Coast Association of Geological Societies Transactions 35, 317–326.

Benson, D.J., Mancini, E.A., 1999. Diagenetic influence on reservoir development and quality in the Smackover updip basement ridge play, southwest Alabama. Gulf Coast Association of Geological Societies Transactions 49, 96–101.

Blendinger, W., 1986. Isolated stationary carbonate platforms: the Middle Triassic (Ladinian) of the Marmolada area, Dolomites, Italy. Sedimentology 33, 159–183.

Blendinger, W., 1994. The carbonate factory of Middle Triassic buildups in the Dolomites, Italy: a quantitative analysis. Sedimentology 41, 1147–1159.

Bosence, D., 2005. A genetic classification of carbonate platforms based on their basinal and tectonic settings in the Cenozoic. Sedimentary Geology 175, 46–72.

Burchette, T.P., Wright, V.P., 1992. Carbonate ramp depositional systems. Sedimentary Geology 79, 3–57.

Burne, R.V., Moore, L.S., 1987. Microbialites; organosedimentary deposits of benthic microbial communities. Palaios 2, 241–254.

Calvet, F., Ramon, X., 1987. Estratigrafía, sedimentología y diagenesis del Muschelkalk inferior de los Catalánides. Cuadernos de Geología Ibérica 11, 141–169.

Calvet, F., Tucker, M.E., 1995. Mud-mound with reefal caps in the upper Muschelkalk (Triassic), eastern Spain. Special Publications of the International Association of Sedimentologists 23, 311–333.

Calvet, F., Tucker, M.E., Henton, J.M., 1990. Middle Triassic carbonate ramp systems in the Catalan Basin, northeast Spain: facies, systems tracts, sequences and controls. Special Publications of the International Association of Sedimentologists 9, 79–108.

Catuneanu, O., 2006. Principles of Sequence Stratigraphy. Elsevier, Amsterdam, p. 375.

Catuneanu, O., Abreu, V., Bhattacharya, J.P., Blum, M.D., Dalrymple, R.W., Eriksson, P.G., Fielding, C.R., Fisher, W.L., Galloway, W.E., Gibling, M.R., Giles, K.A., Holbrook, J.M., Jordan, R., Kendall, C.G.St.C., Macurda, B., Martinsen, O.J., Miall, A.D., Neal, J.E., Nummedal, D., Pomar, L., Posamentier, H.W., Pratt, B.R., Sarg, J.F., Shanley, K.W., Steel, R.J., Strasser, A., Tucker, M.E., Winker, C., 2009. Towards the standardization of sequence stratigraphy. Earth-Science Reviews 92, 1–33.

Catuneanu, O., Galloway, E., Kendall, C.G.St.C., Miall, A.D., Posamentier, H.W., Strasser, A., Tucker, M.E., 2011. Sequence stratigraphy: methodology and nomenclature. Newsletter Stratigraphy 44, 173–275.

Choquette, P.W., Pray, L., 1980. Geological nomenclature and classification of porosity in sedimentary carbonates. AAPG Bulletin 54, 207–250.

Colombié, C., Strasser, A., 2005. Facies, cycles, and controls on the evolution of a keep-up carbonate platform (Kimmeridgian, Swiss Jura). Sedimentology 52, 1207–1227.

Collins, J.F., Kenter, J.A.M., Harris, P.M., Kuanysheva, G., Fischer, D.J., Steffen, K.L., 2006. Facies and reservoir-quality variations in the Late Visean to Bashkirian outer platform, rim, and flank of the Tengiz buildup, Precaspian Basin, Kazakhstan. In: Harris, P.M., Weber, L.J. (Eds.), Giant Hydrocarbon Reservoirs of the World: From Rocks to Reservoir Characterization and Modelling, AAPG Memoir, 88/SEPM Special Publication, pp. 55–95.

Crevello, P.D., Wilson, J.L., Sarg, J.F., Read, J.F., 1989. Controls on carbonate platform development. Society of Economic Paleontologists and Mineralogists, Special Publication 44, 405.

Dupraz, C., Reid, P.R., Braissant, O., Decho, A.W., Norman, R.S., Visscher, P.T., 2009. Processes of carbonate precipitation in modern microbial mats. Earth-Science Reviews 96, 141–162.

Embry, A.F., Johannessen, E.P., 1992. T–R sequence stratigraphy, facies analysis and reservoir distribution in the uppermost Triassic-Lower Jurassic succession, Western Sverdrup Basin, Arctic Canada. In: Vorren, T.O., Bergsager, E., Dahl-Stamnes, O.A., Holter, E., Johansen, B., Lie, E., Lund, T.B. (Eds.), Arctic Geology and Petroleum Potential, Special Publication, *2*. Norwegian Petroleum Society, pp. 121–146.

Emmerich, A., Zamparelli, V., Bechstädt, T., Zühlke, R., 2005. The reefal margin and slope of a Middle Triassic carbonate platform: the Latemar (Dolomites, Italy). Facies 50, 573–614.

García-Senz, J., Salas, R., 2011. Sedimentary response to continental rifting in Iberia. In: Bádenas, B., Aurell, M., Alonso-Zarza, A.M. (Eds.), Abstracts, 28th IAS Meeting of Sedimentology, Zaragoza, Spain, p. 37.

Goldhammer, R.K., Dunn, P.A., Hardie, L.A., 1990. Depositional cycles, composite sea-level changes, cycles stacking patterns, and hierarchy of stratigraphic forcing – examples from platform carbonates of the Alpine Triassic. Geological Society of America Bulletin 102, 535–562.

Goy, A., 1995. Ammonoideos del Triásico Medio de España: Bioestratigrafía y Correlaciones. Cuadernos de Geología Ibéricia 19, 21–60.

Gradstein, F.M., Ogg, J.G., Hilgen, F.J., 2012. On the geological time scale. Newsletter Stratigraphy 45/2, 171–188.

Handford, C.R., Loucks, R.G., 1993. Carbonate depositional sequences and systems tract – responses of carbonate platforms to relative sea-level changes. In: Loucks, B., Sarg, R.J. (Eds.), Carbonate Sequence Stratigraphy: Recent Developments and Applications. AAPG Bulletin vol. 57, 3–41.

Haq, B.U., Hardenbol, J., Vail, P.R., 1987. Chronology of fluctuating sea levels since the Triassic. Science 235, 1156–1167.

Hardie, L.A., Shinn, E.A., 1986. Carbonate depositional environments, modern and ancient, part 3: tidal Flats. Colorado School of Mines Quarterly 81, 1–74.

Harris, M.T., 1993. Reef fabrics, biotic crusts and syndepositional cements of the Latemar reef margin (Middle Triassic), northern Italy. Sedimentology 40, 383–401.

Harris, M.T., Ellis, J., Purkis, S.J., 2013. Assessing the extent of carbonate deposition in early rift settings. AAPG Bulletin 97, 27–60.

Hunt, D., Tucker, M.E., 1992. Stranded parasequences and the forced regressive wedge systems tract: deposition during sea-level fall. Sedimentary Geology 81, 1–9.

Hunt, D., Tucker, M.E., 1993. Sequence stratigraphy of carbonate shelves with an example from the mid-Cretaceous (Urgonian) of southeast France. In: Posamentier, H.W., Summerhayes, C.P., Haq, B.U., Allen, G.P. (Eds.), Sequence Stratigraphy and Facies Associations, International Association Sedimentologists, Special Publication, 18, pp. 307–341.

Johnson, J.G., Murphy, M.A., 1984. Time-rock model for Siluro-Devonian continental shelf, western United States. Geological Society America Bulletin 96, 567–587.

Keim, L., Schlager, W., 2001. Quantitative compositional analysis of a Triassic carbonate platform (Southern Alps, Italy). Sedimentary Geology 139, 261–283.

Luis Dias, J., 2005. Tectônica, estratigrafia e sedimentação no Andar Aptiano da margem leste brasileira. Boletim Geociências da Petrobras, Rio de Janeiro 13 (1), 7–25.

Mancini, E.A., Llinás, C.L., Parcell, W.C., Aurell, M., Bádenas, B., Leinfelder, R.R., Benson, D.J., 2004. Upper Jurassic thrombolite reservoir play, northeastern Gulf of Mexico. AAPG Bulletin 88 (11), 1573–1602.

Marangon, A., Gattolin, G., Della Porta, G., Preto, N., 2011. The Latemar: a flat-topped, steep fronted platform dominated by microbialites and synsedimentary cements. Sedimentary Geology 240, 97–114.

Mercedes-Martín, R., Salas, R., Arenas, C., 2013. Microbial-dominated carbonate platforms during the Ladinian rifting: sequence stratigraphy and evolution of accommodation in a fault-controlled setting (Catalan Coastal Ranges, NE Spain). Basin Research (in press).

Morrow, D.W., 1982. Descriptive field classification of sedimentary and diagenetic breccia fabrics in carbonate rocks. Bulletin of Canadian Petroleum Geology 30, 227–229.

Neuweiler, F., Gautret, P., Volker, T., Lange, R., Michaelis, W., Reitner, J., 1999. Petrology of Lower Cretaceous carbonate mud mounds (Albian, N. Spain): insights into organomineralic deposits of the geological record. Sedimentology 46, 837–859.

Parcell, W.C., 2002. Sequence stratigraphic controls on the development of microbial fabrics and growth forms: implications for reservoir quality distribution in the Upper Jurassic (Oxfordian) Smackover Formation, Eastern Gulf Coast, USA. Carbonates and Evaporites 17 (2), 166–181.

Preto, N., Franceschi, M., Gattolin, G., Massironi, M., Riva, A., Gramigna, P., Bertoldi, L., Nardon, S., 2011. The Latemar: a Middle Triassic polygonal fault-block platform controlled by synsedimentary tectonics. Sedimentary Geology 234, 1–18.

Ramos, A., Sopeña, A., Sánchez-Moya, A., Muñoz, A., 1996. Subsidence analysis, maturity modelling and hydrocarbon generation of the Alpine sedimentary sequence in the NW of the Iberian Ranges (Central Spain). Cuadernos de Geología Ibérica 21, 23–53.

Rezende, M.F., Tonietto, S.N., Pope, M.C., 2012. Three-dimensional pore connectivity evaluation in a Holocene microbialite head. AAPG Search and Discovery Article. In: AAPG Hedberg Conference, Microbial Carbonate Reservoir Charaterization, Houston, Texas.

Russo, F., Mastandrea, A., Neri, C., 1998. Evoluzione degli organismi costruttori nelle piataforme Triassiche delle Dolomiti (Italia). Memorie della Società Geologica Italiana 53, 479–488.

Salas, R., Casas, A., 1993. Mesozoic extensional tectonics, stratigraphy and crystal evolution during the Alpine cycle of the eastern Iberian basin. Tectonophysics 228, 33–55.

Salas, R., Guimera, J., Mas, R., Martin-Closas, C., Melendez, A., Alonso, A., 2001. Evolution of the Mesozoic Central Iberian rift system and its Cainozoic inversion (Iberian chain). In: Ziegler, P.A., Cavazza, W., Robertson, A.H.F., Crasquin-Soleau, S. (Eds.), 2001. Peri-Tethys Memoir 6: Peri-Tethyan Rift/Wrechn Basins and Passive Margins, vol. 186. Mémoire Museum Historie Naturelle, pp. 145–185.

Sarg, J.F., 1988. Carbonate sequence stratigraphy. In: Wilgus, C.K., Hastings, B.S., Kendall, C.G.St.C., Posamentier, H.W., Ross, C.A., Van Wagoner, J.C. (Eds.), Sea-Level Changes – an Integrated Approach, Society of Sedimentary Geologists Special Publications, 42, pp. 155–182.

Schlager, W., 2000. Sedimentation rates and growth potential of tropical, cool water and mud mound carbonate factories. In: Insalaco, E., Skelton, P.W., Palmer, T.J. (Eds.), Carbonate Platform Systems: Components and Interactions, Geological Society of London, Special Publications, 178, pp. 217–227.

Schröder, S., Grotzinger, J.P., Amthor, J.E., Matter, A., 2005. Carbonate deposition and hydrocarbon reservoir development at the Precambrian-Cambrian boundary: the Ara Group in South Oman. Sedimentary Geology 180, 1–28.

Sole de Porta, N., Calvet, F., Torrento, L., 1987. Análisis palinológico del Triásico de los Catalánides (NE España). Cuadernos de Geología Ibérica 11, 237–254.

Spence, G.H., Tucker, M.E., 2007. A proposed integrated multi-signature model for peritidal cycles in carbonates. Journal of Sedimentary Research 77, 797–808.

Terra, G.J.S., Rodrigues, E.B., Freire, E.B., Lykawka, R., Raja Gabaglia, G.P., Hernández, R.M., Hernández, J.I., 2012. Salta Basin, Argentina: a Good Analog for Phanerozoic Lacustrine Microbialite-bearing Reservoirs. AAPG Search and Discovery Article. In: AAPG Hedberg Conference, Microbial Carbonate Reservoir Charaterization, Houston, Texas.

Tonietto, S.N., Shane, E.K., Ahr, W.M., Pope, M.C., 2012. Pore Type Characterization and Petrophysical Properties on Microbial Carbonate Reservoirs. AAPG Search and Discovery Article. In: AAPG Hedberg Conference, Microbial Carbonate Reservoir Charaterization, Houston, Texas.

Tucker, M.E., Marshall, J., 2004. Diagenesis and geochemistry of Upper Muschelkalk (Triassic) buildups and associated facies in Catalonia (NE Spain): a paper dedicated to Francesc Calvet. Geologica Acta 4, 257–269.

Vargas, H., Gaspar-Escribano, J.M., López-Gómez, J., Van Wees, J.-D., Cloetingh, S., De La Horra, R., Arche, A., 2009. A comparison of the Iberian and Ebro Basins during the Permian and Triassic, Eastern Spain: a quantitative subsidence modelling approach. Tectonophysics 474, 160–183.

Virgili, C., Sopeña, A., Ramon, A., Arche, A., Hernando, A., 1983. Libro Jubilar a Jose María Rios, Madrid. El relleno posthercínico y el comienzo de la sedimentación Mesozoica, vol. 2, pp. 25–36.

Weber, L.J., Francis, B.P., Harris, P.M., Clark, M., 2003. Stratigraphy, lithofacies, and reservoir distribution, Tengiz field, Kazakhstan. In: Ahr, W.M., Harris, P.M., Morgan, W.A., Somerville, I.D. (Eds.), Permo-carboniferous Carbonate Platforms and Reefs, SEPM Special Publication 78 and AAPG Memoir 83, pp. 351–394.

Artículo 3:

Mercedes-Martín R., Arenas C., Salas R. 2013c. Controls on microbialite diversity and occurrence in the Ladinian (Middle Triassic) of the Catalan Basin (NE Spain). *Palaeogeography, Palaeoclimatology, Palaeoecology*.

PALAEO 3

Palaeogeography, Palaeoclimatology, Palaeoecology

An International Journal for the Geo-Sciences

16/09/13

To whom it may concern,

I hereby certify that the paper by Ramon Mercedes-Martín et al. entitled "Controls on microbialite diversity and occurrence in the Ladinian (Middle Triassic) of the Catalan Basin (NE Spain)" is in review for the journal Palaeogeography, Palaeoclimatology, Palaeoecology.

Sincerely,

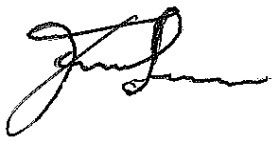

Finn Surlyk
Editor-in-Chief
Professor, University of Copenhagen

Controls on microbialite diversity and occurrence in the Ladinian (Middle Triassic) of the Catalan Basin (NE Spain)

R. Mercedes-Martín[1], C. Arenas[2] and R. Salas[1]

1: Departament de Geoquímica, Petrologia i Prospecció Geològica, Facultat de Geologia, Universitat de Barcelona, C/ Martí i Franquès s/n, 08028, Barcelona, Spain. rmercedes@ub.edu , +34 93 4031165

2: Departamento de Ciencias de la Tierra, Área de Estratigrafía, Universidad de Zaragoza, C/ Pedro Cerbuna, 12, 50009, Zaragoza, Spain.

Abstract

The microbial-dominated carbonate ramps of the Ladinian (Middle Triassic) Catalan Basin host a wide variety of microbialites which grew in association with a rapid fault-induced syn-rift period. Three types of microbialites were analysed for the first time on the basis of their external features, internal textures and microbial and non-microbial processes: stromatolites s.s., ooidal-peloidal stromatolites and thrombolites. These microbialites recorded a concomitant occurrence during the Fassanian regressive stage, and juxtaposition of microbial facies (stromatolites s.s. and ooidal-peloidal stromatolites) during the Longobardian transgressive stage. The simultaneous distribution of these microbialites provides insights into the growth mechanisms, diversity of microbial components, interplay of microbial and the non-microbial contribution and the paleoenvironmental constraints of their initiation and development. Despite the involvement of microbial processes in their accretion, a number of extrinsic factors such as salinity, water energy, sediment supply, type of substratum, and widespread and anomalous oceanographic conditions were instrumental in the growth of these microbialites. The coeval occurrence of these microbialites offers an excellent opportunity to compare their successions with the recent case studies in Shark Bay (Australia), the Exuma Cays (Bahamas), and the ancient Dolomites (Italy-Alps). In addition, we discuss the possible fault-controlled hydrothermal fluid circulation responsible for the corrosion and pervasive botryoidal and fibrous marine cementation, which is concomitant with microbial accretion in thrombolites

Keywords

Microbialite, Stromatolite, Thrombolite, Marine Cement, Ladinian, Catalan Basin

1. Introduction

The study of microbialite formation, their biotic and abiotic processes and the diversity of their products is a cutting-edge topic of research in sedimentary geology. Microbial mats are regarded as ecosystems with a large environmental tolerance living in almost all biotopes and extensively involved in the production, accumulation and diagenesis of sediment (Grotzinger and Knoll, 1999; Riding and Awramick, 2000; Dupraz et al., 2009; Riding, 2011).

A wide array of factors controls the diversity and typology of microbial deposits. These include the type of microbial community, hydrodynamic conditions, hydrochemistry, sedimentation patterns, type of substratum, and the overall ecological factors (salinity, temperature, nutrients and oxygenation), all of which play a prominent role in the development of microbial carbonates, their geometry and fabrics (Logan *et al.*, 1964; Hoffman, 1974; Monty, 1976; Kennard, 1994; Pratt, 1995; Mutti and Hallock, 2003; Riding and Liang, 2005; Andres and Reid, 2006).

Although stromatolites and thrombolites are well-known organosedimentary structures formed by the interplay of benthic microbial communities and their environment (Kennard and James, 1986; Burne and Moore, 1987; Kennard, 1994), the discrimination among such varied factors is not straightforward. Moreover, the fact that both types of microbialites may grow contemporaneously in the same broad environmental setting (Riding et al., 1991; Armella 1994; Kennard, 1994; Reid et al., 1995; Feldmann and McKenzie, 1998; Harwood and Sumner, 2011; Jahnert and Collins, 2012) prompts researchers to continue studying more cases to unravel the parameters responsible for their growth, morphology and mutual co-existence. Modern stromatolite and thrombolite associations of the Exuma Cays, Bahamas (Dravis, 1983; Dill et al., 1986; Reid et al., 1995; Feldmann and McKenzie, 1998; Planavsky and Ginsburg, 2009) and Shark Bay, Australia (Logan and Cebulski, 1970; Logan et al, 1974, Playford and Cockbain, 1976; Reid et al., 2003; Jahnert and Collins, 2013) have provided valuable data on microbialite textures, diversity of microbial processes and palaeoenvironmental constraints that represent interesting proxies for comparison with ancient microbialite systems.

The recent discovery of the hydrocarbon reservoirs in the Lower Cretaceous Pre-Salt of the Campos Basin (Dorobek et al., 2012) has led to further research on the various parameters involved in microbial-

related deposits (Awramik and Buchheim, 2012; Tonietto et al., 2012; Fagundes de Rezende and Pope, 2013), in particular those deposits formed in extensional settings (Harris et al., 2013; Sharp et al., 2013). The controversy about the contribution of biotic and abiotic processes to microbial-related deposits is still a matter of debate, both in marine and continental environments (Wright, 2013). In this context, the origin of massive marine botryoidal cements in microbialites needs further investigation.

The Middle Triassic (Ladinian) marine carbonate systems of the Catalan Basin constitute an interesting case study of syn-rift deposition that display the concomitant occurrence of stromatolites s.s., ooidal-peloidal stromatolites and thrombolites during a regressive stage, and also the juxtaposition of stromatolites s.s and ooidal-peloidal stromatolites in the same local environment during a transgressive stage. This coincidence offers the opportunity to decipher the palaeoenvironmental and palaeoecological conditions in order to provide insights into some key aspects of microbialite growth and co-existence. The refined sequence-stratigraphy framework (Mercedes-Martín et al., 2013a) and the facies architecture analysis (Mercedes-Martín et al., 2013b) carried out in the Ladinian Catalan Basin provide the basis to build two detailed microbialite depositional models which, in turn, can be compared and tested with recent (Bahamas and Shark Bay) and ancient (Dolomites) analogues.

The present paper seeks to 1) characterise the microbial carbonates of Ladinian age (stromatolites s.s., ooidal-peloidal stromatolites and thrombolites) focusing on their external and internal features, providing evidence of the processes and related textures, 2) shed light on the palaeoenvironmental constraints associated with their formation and synchronous occurrence, and 3) discuss the possible hydrothermal influence which may have favoured the development of thrombolites.

2. Geological setting

The study area is located in the Catalan Coastal Ranges (Fig. 1), which developed through inversion of the Mesozoic rifts during the Palaeogene (Salas *et al*. 2001). The microbialite deposits of the Ladinian Catalan Basin are superbly exposed in a NE-SW trending area 300 km in length and 200 km in width. The Triassic basin opened towards the SE into the Neotethys sea. The marine facies graded into more clastic-dominated facies towards the western and northern parts of the basin which were adjacent to the Spanish Meseta (Calvet *et al*. 1990).

Iberia was affected by extensional tectonics and several large intraplate Mesozoic rifts systems formed during the opening of the western Neotethys (Salas *et al*. 2001; García-Senz and Salas, 2011).

Extensive shallow carbonate platforms were established on the flanks of the Tethys Ocean during the Early and Middle Triassic, whereas deeper water carbonates and shales accumulated in the intervening troughs (Ziegler, 1982).

In addition, it is widely accepted that a generalized phase of rapid subsidence during the Early-Middle Triassic (Olenekian to Ladinian) took place in the Ebro Basin and Iberian Chain (Spain) (Vargas et al., 2009). The subsidence evolution during the Triassic indicates that the Ladinian stage was a period of widespread rapid syn-rift subsidence in the eastern part of the Iberian plate (Catalan Coastal Ranges), where extensive carbonate deposits formed at this time (Mercedes-Martín *et al.*, 2013a).

[Fig. 1. one and a half page width]

During Late Permian and Triassic times, these Triassic fault-controlled basins were filled with sediments attributed to Germanic facies. The threefold stratigraphical subdivision of these facies is constituted by a lower part comprising continental Buntsandstein clastics, a middle part formed by marine Muschelkalk carbonates, evaporites and red beds, and an upper part consisting of tidal and sabhka deposits of the Keuper facies (Virgili *et al.* 1983). In the Catalan Coastal Ranges, the carbonates belong to the Upper Muschelkalk facies (Ladinian in age) and are extremely well represented in outcrop. Calvet and Tucker (1995) proposed the division of the Ladinian into two depositional sequences corresponding to two major Upper Muschelkalk marine pulses (Fig. 2). The thickness of the Upper Muschelkalk varies from around 100 m in the northern part of the study area to over 140 m in the south. Their sedimentary record was subdivided into three palaeogeographical domains, from north-east to south-west: the Gaià domain, the Prades domain and the Baix Ebre-Priorat domain (Calvet & Ramon, 1987) (Fig. 1).

Stromatolites s.s. were first recorded in the Gaià domain by Calvet et al. (1990) and interpreted to be formed in tidal flat deposits. Moreover, the presence of 'mud-mounds' developing into reefal complexes in the Baix Ebre-Priorat domain was studied by Calvet and Tucker (1995) who proposed their deposition in a middle-ramp setting.

Mercedes-Martín et al. (2013a) subdivided the Ladinian sedimentary record into two T-R sequences corresponding to two low-angle, microbial-dominated fault-block carbonate ramps, where thrombolites and stromatolites developed from inner to outer ramp settings. T-R sequence 1 (Lower Ladinian, Fassanian) contains the most prominent microbial deposits, such as stromatolites s.s. in the inner ramp (at

least 7 m thick) and thrombolites in the middle ramp (ca. 40m thick). T-R sequence 2 (Upper Ladinian, Longobardian) is mainly characterised by the occurrence of ooidal-peloidal stromatolites and stromatolites s.s. in the inner ramp and internal shoals and sheltered lagoons in the middle-outer ramp (Fig. 2).

[Fig. 2. small column size]

3. Methods

The stratigraphic distribution and depositional environments of the microbialites were determined by measuring 18 complete detailed stratigraphic sections of the Ladinian record at three domains (Gaià, Prades and Baix Ebre-Priorat, Fig. 1). The present paper focuses on three selected sections, i.e. Querol, Font del Teix and Molí del Pinetell (Fig. 3 and 4). The superb lateral continuity of facies and the stratigraphic completeness along a NE to SW 150 km-long exposure allowed us to study the architecture of microbialite deposits at outcrop and seismic scales. Microbialites (*sensu* Burne and Moore, 1987) were studied from megastructural to microstructural scales (*sensu* Shapiro 2000). Photograph-based outcrop panels and line drawings were used for megastructural and macrostructural correlation of microbialitic bodies through the study area. Thrombolite microfacies were mapped and numbered over the thin-sections under the microscope in order to outline the distribution and relationships between their microtextures. The terms 'thrombolite' and 'mesoclot' follows the semantics of Shapiro (2000). Fifty-six samples were prepared as thin sections for the examination of microbial features (structures and textures) and 37 polished slabs were scanned at high resolution and used for mesostructural analysis of microbialites.

4. Microbialite sequence stratigraphy

A detailed facies analysis and sequence stratigraphy framework of the Ladinian Catalan Basin has been performed by Mercedes-Martín et al. (2013a, b). They recognised seventeen facies types from inner ramp to outer ramp depositional environments. Texturally, these facies have been arranged into three groups: muddy facies, coarse-grained facies, and microbialites and related facies. Three types of microbialite facies (see Table 1, 2 and 3) were analysed for the first time in the study area: stromatolites s.s, ooidal-peloidal stromatolites, and thrombolites (facies F10, F11 and F12 of Mercedes-Martín et al.,

2013a). Mercedes-Martín et al., (2013a, b) recognised two Transgressive-Regressive (T-R) sequences in the Ladinian that correspond to low-angle fault-block carbonate ramps. Stromatolites s.s. are well developed in T-R sequence 1 (Fassanian) and are poorly represented in T-R sequence 2 (Longobardian) (Fig. 2). They covered large areas throughout the Prades and Baix Ebre-Priorat domains during the Transgressive Systems Tract 1 (TST1) giving rise to sheet-like carbonate deposits (Fig. 3). During the Regressive Systems Tract 1 (RST1) stromatolites s.s. occurred in the Gaià domain forming extensive belts of planar and domal morphologies and formed under marine shallow-water conditions in hypersaline intertidal and supratidal flats (Mercedes-Martín et al., 2013a). Ooidal-peloidal stromatolites and stromatolites s.s are located mainly in the Gaià domain and developed during the TST2, and are adjoined to stromatolite s.s. deposits (Fig. 2, 3). These deposits show strong thickness heterogeneity owing to synsedimentary faulting. Ooidal-peloidal stromatolites formed under normal salinity, in marine shallow-water conditions, and intertidal/ subtidal environments, commonly internal fore-shoals (Mercedes-Martín et al., 2013a). Thrombolites developed during the RST1 giving rise to huge biostromal and mud-mound bodies in the Prades and Baix Ebre-Priorat domains (Fig. 2, 4). During the RST1, stromatolites s.s., ooidal-peloidal stromatolites and thrombolites concurred. Overall, thombolites formed in shallow subtidal open-marine environments, under low to moderate energy conditions and normal salinity (Mercedes-Martín et al., 2013a).

[Fig. 3. full page width]

[Fig. 4. full page width]

5. Microbialite types

The microbialite characteristics concerning the external morphology and texture are summarized in Tables 1, 2 and 3. Despite the pervasive and fabric-retentive dolomitisation undergone by the Ladinian carbonate rocks (Calvet et al., 1990; Tucker and Marshall, 2004), a large number of samples provided valuable information about the original textural attributes.

[Table 1. full page width]

[Table 2. full page width]

[Table 3. full page width]

180 5.1. Stromatolites s.s.

181 The most common buildups are tabular stromatolites (type 1, stratiform), whereas domed, head-
182 shaped forms (type 2, domal) are less abundant (Fig. 3, Fig. 5a-d, Fig. 6, Fig. 7 and Table 1).

183

184 5.1.1. Type 1: Stratiform stromatolites

185 These are composed of vertically stacked, flat- to undulatory-laminated intervals, a few millimeters
186 to 0.5 meters thick. In some cases the biostromes contain isolated, small dome-shaped bodies (up to 15
187 cm high and 20 cm wide) and occasionally low synoptic relief specimens with a conical profile (up to 2
188 cm high and 5 cm wide) (Fig. 5a to c). These biostromes are several meters thick (up to 5 m) and have a
189 lateral extension of at least 30 km. In some areas, they are overlain by larger domed stromatolite buildups
190 (Type 2) (Fig. 3 and 4). At mesoscopic scale, the laminae are continuous, smooth, planar, undulate and
191 occasionally wavy. Less commonly, convex, generally conical, laminae occur. Typically, the lamination
192 consists of an alternation of dark and light dolomicrite and dolosparite layers (Type A couplets, Fig. 6a,
193 b). The light ochre, dolosparite layers are commonly thicker than the darker, light grey, commonly wavy
194 dolomicrite layers. The two types of layers are commonly composed of several laminae. The mode of
195 accretion of the laminae gives way to a parallel stacking throughout the tabular bodies.

196

197 5.1.2. Type 2: Domal stromatolites

198 These stromatolites are characterised by large, head-shaped and domed buildups usually grouped
199 forming extensive deposits. These forms are developed over the Type 1 stromatolites. The domes have
200 close spacing and are commonly linked laterally (Fig. 5a, d). The buildups are up to 2 m high and 6 m
201 wide, becoming progressively larger towards the upper part of the stratigraphic section. Their lateral
202 extension is at least 20 km. Within a buildup, at mesoscopic scale, the laminae is commonly wavy to
203 slightly wrinkled in the lower stromatolitic part and flat to undulatory in the upper stromatolitic part (Fig.
204 6b). The lateral continuity of the laminae is highly consistent in the two parts. A number of small, isolated
205 domes (up to 10 cm high and 15 cm wide) are sporadically intermingled at centimeter scale. The texture
206 and pattern of the lamination is similar to that of Type 1 stromatolites, with an alternation of dark and
207 light dolomite layers (Type A couplets). The ochre/brown light-coloured, dolospar/microdolospar laminae
208 are normally thinner than the darker, light grey, dolomicrite laminae although sometimes dark and light
209 dolomicrite laminae are equal in thickness (Fig. 6). These stromatolitic buildups may include minor

centimetric layers of small flat-pebble intraclasts and decimeter-scale tepee structures (Fig. 3). Some evidence of microkarst and subsequent hardground was observed within the microbialitic bodies, as well as abundant fenestral fabrics and birdseye structures. Dolospar-filled pseudomorphs after evaporite minerals (with lenticular and rosette crystal shapes) are conspicuous in the fine-grained dolomitic intervals.

[Fig. 5. full page width]

5.1.3. Microscopic features

Both types of stromatolites display similar microstructure and texture. Light laminae consist of peloidal dolomicrite, microdolospar and dolospar. These laminae vary from 500 to 1500 μm in thickness, and have flat to gently ondulate profiles, generally with sharp bases and gradual upward passages to the dark laminae (Fig. 6). In some cases, the light laminae encompass domed structures (convex-upward bodies) that contain filamentous dolomicrite bodies subperpendicular to the domes (Fig. 6c); commonly, larger porosity is found at the base of the laminae and the domes, whereas denser and finer textures constitute the upper part. Isolated fan-like, filament-bearing dolomicrite bodies subperpendicular to the lamination may also be present in the light laminae. The dark laminae are made of dense dolomicrite, mostly peloidal, clotted and cloudy. Single laminae vary from 100 to 250 μm in thickness, and have undulate to gently domed profiles despite the existence of the laminae. Subperpendicular, isolated micrite filamentous bodies are found in the dark laminae and several of these filamentous remains and calcimicrobial bodies (*Cayeuxia*-like and other forms, Fig. 6d and e) are rooted in these laminae and protrude into the overlying light laminae (Fig. 6c and d). The filamentous remains evoke cyanobacterial bouquets (Fig. 7). Interlaminar voids (fenestral porosity) and ancient vuggy porosity filled with dolomite cements have also been recorded (Mercedes-Martín et al., 2013b). On the basis of shape, these fenestral pores are believed to correspond to ancient microbial mats which subsequently degraded and decayed (Fig. 6 d and e). Composite intervals consisting of several dark laminae are 2 to 4 mm thick. In some cases, these composite intervals contain micropeloidal to clotted dolomicrite masses cemented with dolosparite (Fig. 8a).

[Fig. 6. full page width]

5.1.4. Environmental interpretation

The stromatolites s.s. are interpreted as having formed in a shallow marine environment with moderate energy conditions (intertidal flats). The scarcity and low-diversity of macroinvertebrates and the presence of laminoid-fenestral fabrics after evaporite minerals indicate arid conditions with high evaporation and increased salinity. The absence of coarse sand-sized grains may indicate that this type of sediment was not available in these settings, or that the currents were too weak to transport the grain population. The occurrence of microkarst horizons accompanied by dissolution and subsequent accumulation of tiny ferruginous crusts in some domal heads provide evidence of relatively short periods of subaerial exposure. In addition, the occasional presence of well preserved, thin intraclastic breccia layers associated with the stromatolites supports deposition under shallow-marine conditions. Thus, an intertidal to shallow subtidal, rather than a subtidal environment for these stromatolites is consistent with the stratigraphic data, together suggesting an overall saline to hypersaline embayment associated with tidal flats.

[Fig. 7. small column size]

5.2. Ooidal-peloidal stromatolites

The ooidal-peloidal stromatolites consist of ooidal-peloidal grainstone layers alternating with dolomicritic intervals (Fig. 3 and 5e and f, Table 2). Stratiform and low-relief hemielliptical buildups are the most common geometries. Large biostromes are produced by the succession of flat laminated intervals. These biostromes can be up to 3 m thick and at least 40 km wide. The internal mesostructure consists of grainstone layers (smooth, planar to slightly wavy) that alternate with micritic layers (tabular to wavy). Ooidal grainstone layers are from sub-millimeter to 5 cm thick, and micritic intervals are a few µm to 2 cm thick. The thickness of the micritic layers was used to categorise two types of couplets: Type B and Type C. Type B couplets (Fig. 8b) attain several µm in thickness, whereas Type C couplets (Fig. 8c, d, e) are formed by micritic layers that exceed 100 µm in thickness. Type C couplets are more abundant than Type B (Table 2).

5.2.1. Grainstone intervals

The ooidal grainstone intervals (up to 5 cm-thick) are made of dark, subspherical, subrounded to rounded, moderately to well-sorted ooids (up to 0.3 mm in diameter), which are commonly micritized, featureless and show a microcrystalline texture (Fig. 8c and d). Peloids are the second most frequent

component in these intervals and often become the nuclei of some ooids. Peloids (up to 0.8 mm long) are rounded to subangular, fine-grained, elongated dark particles. Most peloids occur as micritized and recrystallized ooids (bahamite peloids), bioclasts and faecal pellets, giving rise to structureless microcrystalline brown grains. These peloids are subrounded and very well sorted (up to 0.5 mm in diameter). Ocassionally, ooids are fused at point contacts. Lumps (up to 5.6 mm in diameter) and less common grapestones (up to 7.2 mm long) are conspicuous components in the samples (Fig. 8f). These composite grains consist of well rounded, elliptical and spherical grains (often micritized ooids and peloids) with smooth and dense microcrystalline coatings, and dolosparitic cements between them. The coatings are composed of alternating thin, dark dolomicrospar laminae and light peloidal to micropeloidal cloudy dolomicrite laminae. Within the aggregate grains, the clotted and peloidal dolomicrite filling the interspaces between coated grains is occasionally replaced with neomorphic dolomicrosparite to equant dolosparite crystals (Fig. 8f). Oomouldic and ancient vuggy porosities have been observed in these intervals (Mercedes-Martín et al., 2013b) (Fig. 8h).

[Fig. 8a. full page width]

[Fig. 8b. full page width]

5.2.2. Dolomicritic intervals

The fine-grained, muddy intervals (from 10 μm to 2 cm thick) are composed of dark to light, massive to peloidal dolomicrite layers. These laminae are commonly parallel, flat and display a variable lateral continuity. The bases of the intervals overlie the ooidal layers generally through gradual transition. In some cases the tops of the dolomicritic laminae provide evidence of erosion with micro-scours filled with tiny ooids, giving rise to undulatory or wavy irregular profiles (Fig. 8d). Desiccation cracks are seldom present affecting these fine-grained intervals. Horizons of thin ferruginous crusts (< 20 μm-thick) are observed on top of the dolomicritic laminae. Furthermore, some of these horizons exhibit evidence of local remobilization suggesting metazoan disruption.

5.2.3. Microbial remains

These microbialites contain abundant microbial remains and provide evidence that microbial activity played an important role in their formation. Microbial filamentous remains are better recorded in the

dolomicritic intervals and they are commonly rooted in the dark, massive to peloidal dolomicrite laminae developing a complex network of chaotic and subperpendicular to subparallel microbial filaments (Fig. 8g and h). There are two types of filaments which vary in size. Small and spiraliform filaments are grouped forming bouquets, whereas thicker and rectilinear filaments are commonly isolated and disperse. Calcimicrobial bodies were not found in these intervals. Similarly, the grainy intervals are made of abundant aggregate grains (lumps and grapestones) whose laminated coatings are believed to be microbially mediated (e.g., accretion of thin, dark dolomicrospar laminae and light peloidal to micropeloidal cloudy dolomicrite envelops), despite the absence of specific microbial remains (Fig. 8f).

5.2.4. Environmental interpretation

According to the depositional texture and components, these stromatolites were deposited in a marine shallow-water subenvironment (mainly subtidal), above fair-weather wave base, under moderate to slightly high energy hydraulic conditions (Mercedes-Martín et al., 2013a). The presence of coated grains (ooids, peloids and aggregates) associated with this range of water energy suggests open marine conditions (Tucker and Wright, 1990; Flügel, 2004). The aggregate grains (lumps and grapestones) may indicate changing water energy conditions and low sedimentation rates as well as abundant marine cementation processes within intergranular voids (Winlaw and Matthews, 1974). In addition, the coated grains are moderately to well-sorted and are surrounded by small proportions of micritic matrix. The presence of micro-scours and borings in the micritic-microsparitic intervals filled with ooids strongly suggests that these muddy layers were early lithified prior to disruption processes. The alternation of grainy intervals and micritic intervals records successive periods of abundant coarse allochems and periods of mud accretion, suggesting a balance between allochem-bearing sediment accretion and subsequent lithification of the muddy intervals. These processes occurred in an internal fore-shoal subenvironment, as postulated by Mercedes-Martín et al. (2013b).

5.3. Thrombolites

Thrombolites consist of extensive, decimeter to meter-thick, massive to nodular bedded, mainly non-laminated dolomitic buildups that may include minor stromatolite intervals (centimeter-thick intervals of type 1 stromatolites). The thrombolitic successions are commonly decimeter thick and typically consist of continuous packages of texturally uniform sedimentary bodies, although an overall thickness of 40 m is

recorded in some sections. Thrombolites occur as extensive flat-relief biostromes (Type 1, stratiform thrombolites) and high-relief adjacent bioherms (Type 2, mud mound thrombolites) (Table 3). These two types crop out in the Prades and Baix-Ebre Priorat domains (Fig. 2) and attain a lateral extension of at least 45 km. Occasional high-relief, linked and isolated domal bodies (up to 4 m thick) are interlayered (Molí del Pinetell section, Fig. 4, Fig. 5g and h). This facies encompasses a secondary mouldic porosity related to the interstitial growth of evaporite minerals (anhydrite or gypsum; Tucker and Marshall, 2004).

5.3.1. Microscopic features

Thrombolites are composed of a mesoscopic clotted texture (Aitken, 1967; Burne & Moore, 1987), in which the different textural components are characterised as follows (Table 3).

Dense micritic mesoclots (Dmm). The mesoclots (*sensu* Kennard and James, 1986) represent the prime microbial constituents of the thrombolite framework. Mesoclots are constituted by dark-coloured, massive and dense microcrystalline masses, rounded, amoeboid and arborescent in shape and are up to 4 cm long. Microscopically, these masses are commonly constituted by different elements: 1) micropeloidal to peloidal cloudy dolomicritic veneers (calcified biofilms of Riding, 2002); 2) calcified microfossils (e.g. calcimicrobes: *Garwoodia* and *Cayeuxia*-like porostromate calcimicrobes, or Microproblematica: *Tubiphytes, Koivaella?, Isnella?* or *Tubiphytes*-like, *Archaeolithoporella*-like cryptic forms, Fig. 9, 10 and 11); 3) isolated and dispersed micropeloidal bodies of microbial origin (e.g. coccoid bacteria bushes and micropeloidal clusters, Fig. 11b and d), and 4) occasional isolated sponges (*Solenolmia manon manon*). Some Dmm display corrosion cavities subsequently filled by the micritic matrix and intraclastic-peloidal masses. These corrosion cavities are more abundant in the lower parts of the thrombolite bodies.

Micritic matrix (Mm). The micritic matrix between the mesoclots consists of homogeneous and structureless light mudstone and rarely wackestone of intraclasts. Some small quartz grains and peloids are occasionally embedded. In some areas, the dolomicrite is replaced with neomorphic microdolosparite patches. Overall, these micritic masses represent the original internal sediment devoid of disruption by bioturbation (Fig. 9c and d).

[Fig. 9. full page width]

Intraclastic-peloidal masses (Ipm). The interframework cavities are filled with intraclastic and peloidal wackestone. Peloids are rounded to subangular, and up to 0.4 mm long, and intraclasts are

subrounded to angular, with low sphericity and up to 1.5 mm long. Peloids and intraclasts grade from poorly to moderately sorted. Benthonic foraminifera, small gastropods, brachiopods, and fragments of pelecypods were recognized among the skeletal components. Occasionally, some intraclasts consist of reworked microbial components or crusts. There is evidence of neomorphic microsdoloparite to dolosparite replacing the dolomicritic matrix around intraclasts. The intraclastic-peloidal masses are present within the interspaces and cavities of the mesoclotted framework (Dmm), displaying an episodic filling with normal grading (Fig. 9 and 10).

[Fig. 10. full page width]

[Fig.11. full page width]

Botryoidal and fibrous cements (Bfc). Some samples contain abundant cavity-filling early marine cements (botryoidal and fibrous) that can constitute the 40 % of volume of the thin-sections. These cements are closely associated with the Dmm. In some cases microbial crusts/ biofilms encrust the outlines of the botryoidal and fibrous cements. In other cases, multiple generations of cement crusts occlude the pore spaces between the microbial components (porostromate calcimicrobes in Dmm) and the allochem-bearing components (Mm or Ipm) (Fig. 10d). Cements are volumetrically the most significant component in the upper parts of the thrombolite bodies. Some samples show remains of authigenic barite cements within dolomitic matrix.

5.3.2. Depositional environment

According to the macroscopic, mesoscopic and microscopic attributes (geometry and microbial origin of some components), the thrombolites are interpreted to be deposited below the fair-weather wave base region, in shallow subtidal open marine environments, under low to moderate energy conditions and within the photic zone. Thrombolites commonly nucleate over a coarse-grained substrate formed by peloidal and skeletal wackestone to packstone blankets in the middle ramp (Calvet and Tucker, 1995; Mercedes-Martín et al., 2013b) (Fig. 4). The presence of two types of cavity-filling sediments between the mesoclots (coarse-grained Ipm, and mud-sized Mm) suggests the fluctuation of water energy conditions. The accumulation of the Mm indicates periods of lower energy; in contrast, the Ipm is associated with periods of higher energy conditions while the microbial structure was growing. The

sorting of peloids and intraclasts and their low sphericity suggest an environment characterised by episodes of decreasing energy (intermittent rather than continuous source of hydraulic energy). The scarce occurrence of benthonic foraminifera, pelecypods and other skeletal organisms suggests rather open marine conditions. Accordingly, the presence of abundant botryoidal and fibrous cements indicates a syn-depositional lithification of the framework in an open marine environment. Authigenic barite cements may indicate hydrothermal activity associated to the formation of thrombolites.

6. Discussion

The three types of microbialite deposits discussed in this work reflect different environmental conditions for their formation through space and time. Hydrodynamics, salinity, water depth, type of substrate and sediment supply commonly control the growth morphology of microbialites in modern environments, giving rise to distinct microbial lithosomes structures, and textures (Reid et al., 1995; Feldmann and Mckenzie, 1997, 1998; Andrés et al., 2006; Jahnert and Collins, 2011). In addition, some biological factors (e.g., type of microbial communities and the diversity of associated microbial processes) may also account for the microstructural and textural features of microbialites (Riding and Awramik, 2000; Reid et al., 2000; Hillgärtner et al., 2001; Dupratz et al., 2009; Franks and Stolz, 2009; Allwood et al., 2007).

6.1. Environmental controls, growth history and microbial contribution

As suggested in other studies of microbial deposits (Andrés et al., 2006; Arenas and Pomar, 2010), Mercedes-Martín et al., (2013a) proposed that the water column (bathymetry) and therefore the available space for sedimentation (accommodation space) is a key factor that controls the external morphology and dimensions of the microbialites. The comprehensive study of the external architecture, internal structure and other sedimentological attributes, enable us to reconstruct the environmental factors that controlled the growth of the three types of microbialitic facies.

6.1.1. Stromatolites s.s.

These deposits chiefly formed during the RST-1 and TST-2 in the intertidal to shallow subtidal subenvironments of the inner ramp, where they attain the maximum thickness and size. These deposits commonly nucleated on a substrate of skeletal packstone, oolitic grainstone or intraclastic breccia,

lending support to the view that the type of substrate plays a major part in their initiation, as in the Bahamas (Reid et al, 1995), the Great Bank of Guizhou (Lehrmann, 1999) or in Shark Bay (Jahnert and Collins, 2012). The stratigraphic analysis reveals that thickest stromatolite deposits grew primarily in the intertidal zone of a back shoal environment, where the influence of waves and currents was limited and the coarse-sediment supply was apparently absent. Furthermore, the concomitant restricted conditions (high evaporation rates and hypersalinity) could have inhibited predation and competition of marine invertebrates accounting for its scarcity (Garrett, 1970; Browne et al., 2000) and contributing to the development of these microbialites in the inner ramp (Mercedes-Martín et al., 2013a). The transition from Type 1 (stratiform stromatolites) to Type 2 (domal stromatolites) through time is better explained by increasing accommodation space triggered by synrift faults (Mercedes-Martín et al., 2013a) than by a variation of microbial constructors (Sumner, 2000; Harwood and Sumner, 2011) or by a change from intertidal (shallowing) to subtidal (deepening) conditions (Arenas and Pomar, 2010). In Highborne Cay in the Bahamas, Andres and Reid (2006) and Eckman et al., (2008) suggest that the macro-scale growth morphologies of the stromatolites are primarily controlled by accommodation space, hydrodynamics and sedimentation patterns. There the sediment type and the mobility of grains control stromatolite height, distribution and morphology of stromatolites are controlled by the sediment type and the mobility of grains. Jahnert and Collins (2011, 2012) also suggested that the gross morphology of microbial deposits is related to the interaction between the sediment supply, topography and substrate gradient (Fig. 3 and Fig. 12).

The microstructure and texture of microbialites are interpreted to have a microbial origin (i.e. bacterial, mostly cyanobacterial). The alternation of dark grey, dolomicrite laminae with ochre light-coloured, dolospar/dolomicrospar laminae is explained by the combination of different processes. The thicker light-coloured layers probably formed through the trapping and binding processes of silt-sized carbonate sediment by microbial communities that triggered the precipitation of $CaCO_3$. Calcite precipitation mediated by microbial activity probably induced the lithification of these laminae (Burne & Moore, 1987; Pentecost, 1991; Chafetz & Buczynski, 1992). The thinner, dark layers could represent the result of bacterial activity in microbial mats during periods of sediment stasis and dominant microbial accretion (Chafetz & Buczynski, 1992; Reid *et al*., 1995; Reid *et al.* 2000). This type of lamination may thus reflect diverse environmentally-induced processes that affect the microbial accretion pattern. The absence of coarse-grained sediment attached to laminae and the fact that they are partially dolomitised

make it difficult to assess the contribution of the different microbial processes. Although physical CO_2-degassing may account for much carbonate precipitation in some depositional settings (i.e., in shallow and agitated water contexts), the abundant and diverse calcified microbial filaments (Fig. 6c) together with the occurrence of numerous calcimicrobial bodies (Fig. 6d and e) suggest that biologically induced precipitation of carbonate by microbes could play a major role in the accretion and early lithification of these microbialites (Visscher et al., 2000; Dupraz and Visscher, 2005).

6.1.2. Ooidal-peloidal stromatolites

These microbialites formed during the RST-1 and TST-2. In contrast to stromatolites s.s., ooidal-peloidal stromatolites grew in variable water energy conditions and in settings where sediment supply (allochems) was involved in their formation. During periods of higher- energy conditions, ooids and peloids accumulated under the influence of hydraulic currents and waves. By contrast, during periods of lower energy conditions, the cessation of ooid and peloid accumulation leads to the proliferation of muddy micritic and micropeloidal intervals. The association of these microbialites with wavy, ripple and herringbone lamination is consistent with a deposition in a subtidal subenvironment subjected to intermittent water energy conditions (Fig. 3). The formation of aggregate grains took place under a strong influence of microbes, which may have been effective in binding and cementing the grains. Similarly in the Bahamas, grapestone grains are produced by the cementation of recrystallised ooids bound by 'algae' and encrusting foraminifera in marine environments (Winland and Matthews, 1974). According to these authors, the formation of these grains is enhanced by a high rate of water circulation, turbulence and low sedimentation rates. Purdy (1963) highlighted the biogenic influence ('algal filaments and cells') in the origin of intergranular cements, and later Macintyre et al., (2000) envisaged grapestones as a possible example of welded grains formed by the endolithic activity of cyanobacteria.

Moreover, the abundance of structureless, round dolomicrite grains (bahamite peloids) in the grainy intervals points to micritization caused by biological activity. Monty (1967) reported that the grains changed to cryptocrystalline carbonate because of 'algal' boring in Andros Island. In the Exuma Cay stromatolites, microboring and micritization of some oolite layers are produced by endolithic cyanobacteria (Reid et al., 1995; Macintyre et al., 2000) and their effects extend well below the densely microbored surface. Bahamite peloids have also been documented in an Upper Turonian stromatolite bed

of the Northern Iberian Ranges (Rodríguez-Martínez et al., 2011). They occur irregularly in the agglutinated parts and are interpreted to have been biologically modified by the former processes.

The Triassic ooidal-peloidal stromatolites (referred to as 'coarse-agglutinated stromatolites' by Riding 1991; 2000) display common micritization processes and fusion of grains, indicating that microbes participated actively in the formation of these deposits. The well-developed dolomicritic layers, the abundant microbial filaments and the peloidal dolomicrite textures are consistent with a microbially influenced carbonate precipitation. During periods of low sedimentation rates or hiatus, the micritic layers were colonized by borers and endolithic organisms (possibly sponges and benthic macrofauna), producing mm-scale borings. As for the ooidal layers, trapping and binding of coated grains (ooids and grapestones) by cyanobacteria and microbial secreted substances (e.g., EPS) occurred during periods of active deposition. However, some scattered ooids trapped within the micritic intervals revealed no evidence of micritization. This fact lends support to the idea that peloidal textures undergo early lithification contributing to the assimilation of exotic grains to calcified mats.

6.1.3. Thrombolites

These microbialites formed exclusively during the RST1 and occupied the middle and outer ramp settings (Fig. 4). Mega- and macrostructural geometries of thrombolite deposits (biostromes and bioherms) are controlled by the creation of accommodation space due to the participation of the la Riba fault (Mercedes-Martín et al., 2013a). In the Prades domain, thrombolites commonly nucleated on a substrate of peloidal and skeletal wackestone to packstone, whereas in the Baix-Ebre Priorat domain they grew above burrowed skeletal mudstone to packstone levels. The thrombolite growth was conditioned by the nature of the mesoclotted texture, the presence of specific microbial components, and the type of sediment that formed the matrix and the cavity-filling processes. The shape and arrangement of the Dmm show that incrustation and lateral accretion were the commonest growth mechanisms, forming a rigid and continuous framework above surfaces.There is no evidence in support of the trapping and binding of allochems within mesoclots. Thus, the framework of thrombolites (Dmm) is due to calcification of several types of microorganisms (calcimicrobes, cyanobacteria and coccoid-dominated microbial communities). As suggested by Webb (1987), the encrustation, breakage and transport of these components could have provided a possible mechanism of dispersion and re-colonization during periods of higher water fluxes. The presence of finning-upward grading and some bioclasts within the Mm and

Ipm points to deposition from suspended sediment which filled preexisting interspaces. In spite of the reworking and winnowing of allochems inside interspaces or cavities, an early lithification of the clotted microbial structures and calcimicrobes is postulated in these thrombolites. The accumulation of internal sediment-bearing allochemical grains (intraclasts, peloids and bioclasts; Ipm) is also common in several thrombolite reefs (Kennard, 1986; Webb, 1987, Kahle, 2001, Pratt and Haidl, 2008); these components may have originated by biochemical or physico-chemical processes, disintegration of organisms or to a combination of any of these processes (Kahle, 2001). As a consequence, the transport and reworking of these components into the cavities depend on an energetic flow. For this reason, a shallow subtidal subenvironment influenced by periods of storms and strong currents is associated with the formation of the Ladinian thrombolites.

Furthermore, the development of the marine cements played a crucial role in the upbuilding and cohesiveness of the thrombolites. In fact, the presence of abundant botryoidal cement-filled primary interstices within or around the components (calcimicrobes, microbial crusts, cryptic filaments and *Tubiphytes*-like forms) suggests that cementation occurred simultaneously with the microbial growth (Macintyre, 1984; Aitken and Narbonne, 1989; Kah and Grotzinger, 1992; Chow and George, 2004). Moreover, the megascale morphological diversity depicted by Type 1 and Type 2 thrombolites (Mercedes-Martín et al., 2013a) suggests that thrombolites were capable of accreting rapidly to keep up with changing environmental conditions (owing to the increase in accommodation space and water depth). Calvet & Tucker (1995) attributed the thrombolites to the cores of 'mud mounds'. These authors noted that thrombolitic facies evolved vertically through the 'mud mound' into an upper carbonate terminal complex composed of coral-reef builders accumulated in shallow water settings (facies F14 of Mercedes-Martín et al., 2013a). Tucker et al., (1995) recognised marine botryoidal and fibrous cements associated with the coral-reef facies and attributed their origin to the pumping of sea water through this facies during early diagenesis. Coral-reef facies are in turn capped by carbonate gravel and dasycladal rubble units (facies F15 and F16 of Mercedes-Martín et al., 2013a).

The mesoclotted texture of thrombolites is characterised by different types of microbial products which are recognised by their textures. The microbial nature of the mesoclots is demonstrated by their growth form showing accretionary, binding, and encrusting growth textures. Thus, the microbial communities that contributed to thrombolite accretion are: calcified biofilms, individual calcimicrobes, coccoid-dominated bacterial forms, or the juxtaposition of any of these components.

539 Thin micropeloidal and dense calcified biofilms were described in the Ladinian thrombolites and are
540 often associated with *Tubiphytes* group microproblematica (see Senowbari-Daryan, 2013) and
541 *Archaeolithoporella*-like cryptic forms. The latter organism formed veneers and thin crusts accompanied
542 by syndepositional botryoidal and fibrous marine cements during the Paleozoic (Sano et al., 1990; Shen et
543 al., 2012). Encrustation by these microorganisms was essential for the accretion of Ladinian thrombolites
544 as well. Microproblematica forms and syndepositional cements acted as framework stabilizers.
545 Calcimicrobes are less represented in the Ladinian thrombolites and occur as *Cayeuxia*, *Garwoodia*-like
546 and as other cryptic forms (porostromate microbes), favouring microbialite construction. Moreover,
547 spherical cluster aggregates of closely stacked clotted dolomicrite and peloids (80 to 100 μm in width) are
548 floating within microdolosparite to dolosparite marine cement. Although the origin of this types of
549 aggregates could be multiple, the cluster arrangement and morphology and the surrounding cement is
550 interpreted as products of *in situ* organic decay of coccoid bacterial colonies during an early diagenetic
551 stage (Chafetz, 1986; Riding and Tomás, 2006).
552 The presence of authigenic barite cements in thrombolites may indicate the presence of hydrothermal
553 fluids, which also may have participated in the formation of microbial components and botryoidal-fibrous
554 marine cements. In addition, hydrothermal mineralizations are known in the region (lead-zinc deposits
555 and small-scale mining). Thus, a physico-chemical mechanism should be considered for the origin of
556 cements and microbial textures, as was summarised by Monty (1995) for mud-mounds associated to
557 faults and seeps. Furthermore, the internal cavities of the thrombolites (Fig. 9a to c) are regarded as
558 originated by corrosion processes related to hydrothermal fluids (Esteban et al., 2009).
559
560 6.2. Microbialite co-occurrence and juxtaposition
561 The analysis of facies architecture and sequence stratigraphy suggest that microbialites grew
562 contemporaneously in different subenvironments of the same carbonate ramp or in close relationship in
563 the same setting above time-equivalent stratigraphic zones within the RST1 (Fig. 12a). Indeed, the
564 stromatolites s.s. and ooidal-peloidal stromatolites grew concomitantly as related facies within the same
565 depositional subenvironment throughout the TST2 (Fig. 3 and Fig. 12b). The palaeoenvironmental and
566 palaeoecological implications of these relations are discussed below.
567
568 6.2.1. Co-occurrence of stromatolites s.s., ooidal-peloidal stromatolites and thrombolites in the RST1

569 The coeval occurrence of these microbialites took place within the RST1 (Fig. 12a). Some
570 environmental factors played a key role in the development of specific microbialites and other factors
571 combined to promote their co-existence.
572
573 [Fig. 12. full page width]
574
575 Microbial biomass thrive in response to hypersalinity, high evaporation rates and restricted water
576 exchange by eliminating many competitors (Browne et al., 2000) and ensuring a low-diversity of
577 eukaryote species, as in Shark Bay, Australia (Playford and Cockbain, 1976; Jahnert and Collins, 2012).
578 Similarly, these conditions prevailed and enhanced proliferation of the Ladinian stromatolites s.s., which
579 developed in an enclosed hypersaline embayment in the inner ramp. Furthermore, the sediment movement
580 has been regarded as a critical factor restricting or eliminating biotic communities responsible for the
581 disruption of microbial mats at several sites in the Bahamas (Steneck et al., 1993; Reid et al., 1995;
582 Golubic and Browne, 1996). Likewise, the ooidal-peloidal stromatolites of the RST1 developed under
583 shallow subtidal conditions proliferating under alternating periods of high sediment mobility with periods
584 of microbial calcification. Furthermore, the possible predominance of microbial communities, which
585 effectively triggers rapid syndepositional lithification, was probably responsible for ooidal-peloidal
586 stromatolite accretion. The interplay between biological and oceanographic conditions could probably
587 favour carbonate precipitation, as has been suggested for the Bahamian stromatolites (Whittle et al.,
588 1993). Finally, thrombolites grew in shallow subtidal open environments, within the photic zone as
589 indicated by the presence of calcimicrobes. Their microtextures show a strong heterogeneity and are
590 formed by different microbial communities and components (calcimicrobes, coccoid cyanobacteria,
591 sponges and marine cements). The proliferation of thrombolites is ascribed to the interplay of several
592 biological and chemical-induced mechanisms which are thought to have acted sequentially or
593 simultaneously. However, further research is required to better understand the vertical evolution of
594 thrombolite facies, their textural variability and corrosion/ cementation processes.
595 Moreover, the typology of the underlying substrate has been considered a requirement for the
596 initiation and development of thrombolites (Kennard, 1994; Lehrmann 1999; Emmerich et al., 2005) and
597 stromatolites (Reid et al., 1995; 2003; Andres and Reid, 2006). In fact, all the Ladinian microbialites
598 nucleated over a unloose substrate composed of ooidal and/or peloidal to skeletal deposits.

On the other hand, many types of microbes/benthic microorganisms (filamentous and coccoid bacteria, among others) commonly colonize shallow marine environments but are absent in the settings subjected to intense bioturbation (Browne et al., 2000). Thus, metazoan competition (fauna that feed microbes) has been interpreted to be an important factor in limiting microbe biomass, mat cohesion and continuity (Garret, 1970; Neumann et al., 1970; Macintyre et al., 1996; Riding and Liang, 2005). Accordingly, the Lowermost Ladinian of the Catalan Basin is characterised by a impoverished invertebrate macrofauna and low-diversity ichnofossil assemblages (facies F7 of Mercedes-Martín et al., 2013a) reflecting a period of restricted marine conditions (Jordi M. Gibert, pers. comm.). These conditions were instrumental in reducing microbial competitors and in enhancing the overall microbial production during the entire Ladinian. As a result, the concomitant co-occurrence of diverse microbialites could be, at least partially, due to an unusual oceanographic event or specific biogeochemical conditions which substantially reduced microbial feeders.

6.2.2. Juxtaposition of stromatolites s.s and ooidal-peloidal stromatolites in the TST2

During the TST2, stromatolites s.s. and ooidal-peloidal stromatolites managed to grow in mutual association in the same subenvironment (internal fore-shoal, Fig. 3 and Fig. 12b), giving rise to a set of microbialites which became progressively more adapted to trap and bind coarse-grained particles into their mats. The juxtaposition of laminae couplets (type A → B → C couplets) reveals that the preferential microbial processes changed through time. Type A couplets (Fig. 6a, b) first developed in microbialites which accreted by calcite precipitation mainly induced by microbial activity. Trapping and binding processes, together with micritization and less common fusion of grains, were crucial in the formation of Type B couplets (Fig. 8a). In turn, Type C couplets (Fig. 8c, d and e) occurred as the last stage of microbialite colonization with common micritization, fused grains, endolithic borings, grapestone formation and early cementation. Microbially secreted mats and trapping and binding processes are also involved in microbialite construction. The variations in the stromatolitic laminae suggest that the local environmental variations and the specific sedimentary dynamics favoured their growth. Microbialites characterised by Type A couplets are thought to develop in upper intertidal settings; Type B couplets are associated with lower intertidal-shallow subtidal settings, whereas Type C couplets are formed under shallow subtidal conditions. Fourth-order sea-level fluctuations, which conditioned the water depth (subtidal or intertidal influence), the degree of water energy by waves and currents, and the type of

629 available sediment and accumulation rate, ultimately controlled the microbial processes and textures and,
630 thus, the microbialite types.

631 An example of juxtaposition of clotted with coarse-grained textures in microbialites can be found in
632 the Neoproterozoic of Southern California. Harwood and Sumner (2011) accounted for composite
633 microbialites whose clotted (thrombolitic) and laminated (stromatolitic) structures intermingled on a sub-
634 centimeter scale in the same peritidal environment. These authors attributed the co-occurrence of this
635 textural variability to simultaneous growth of morphologically different microbial communities rather
636 than to a change of the local sedimentary dynamics. In this case, the predominance of microbial clots
637 associated with discontinuous and deformed laminae, and also clotted textures interlayered with
638 laminated textures strongly support their assumption. However, the intermittent occurrence of coarse-
639 grained sediment (ooids, peloids and grapestones) within Ladinian microbialites supports the view that
640 their origin was closely linked to extrinsic factors (small changes in accommodation space and sediment
641 supply) although a vertical change of microbial communities may also be expected.

642

643 6.3. Comparison with ancient and modern examples

644 The Ladinian stromatolites s.s. resemble the well-known example of Hamelin Pool in Western
645 Australia. The hypersaline embayment of Shark Bay (Logan & Cebulski, 1970; Logan *et al.* 1974; Jahnert
646 and Collins, 2012) exhibits stromatolitic units in abnormal salinities as a consequence of high evaporation
647 rates and the presence of physical barriers that impede water circulation (Faure Sill). A difference
648 regarding the macrostructure of the stromatolites is observed in the Ladinian forms. Whereas the most
649 common shallow subtidal to intertidal stromatolites in Shark Bay occur as a variety of single columnar
650 and head-shaped buildups, the Ladinian stromatolites s.s. occur as tabular bodies (Type 1) which are
651 dominant over domal forms (Type 2). However, Shark Bay domal and columnar forms are preferentially
652 located in headlands (steep gradients of 4m/ 100m) rather than embayments (steep gradients of 30-50 cm/
653 1000m). This reflects that higher substrate gradients favour growth of high-relief domal microbial
654 deposits rather than tabular-pavement deposits (Jahnert and Collins, 2012). The Ladinian forms bear a
655 striking resemblance to the Santa Pola stromatolites (Miocene), formed in shallow, mostly intertidal
656 conditions (Feldmann and McKenzie, 1997). Giant domal and columnar stromatolites developed adjacent
657 to tabular and sheet-like stromatolites in areas with little sand deposition and low-energy environments
658 during sea level highstands. These dolomitic stromatolites have been interpreted to accrete in high saline

settings. In the case of the Miocene of Mallorca, Arenas and Pomar (2010) attributed the change of stratiform/small domal stromatolites to large domes as a result of increasing accommodation space and bathymetric changes. On the other hand, Shark Bay intertidal microbialites include thrombolitic clotted texture (pustular mats, Logan et al., 1974; Jahnert and Collins, 2012) and also laminated structures (smooth mats, Logan et al., 1974). In the two cases, the occurrence of sand-size peloids, ooids, skeletal fragments and detrital quartz facilitates the trapping and binding of particles and the construction of laminoid fenestral grainy texture by precipitation of cements (Logan et al., 1974). These textures are different from those reported in the Ladinian stromatolites s.s. basically because the Triassic ones were further removed from sediment supply and skeletal contribution and hence less affected by intense storms and waves. Thus, the possible silt-sized trapping and binding together with microbial calcification processes gave rise to well defined laminae in Ladinian stromatolites.

Ooidal-peloidal stromatolites closely resemble some ancient marine examples. Stromatolites composed of Type B couplets are very similar to the Bahamian examples (Reid et al., 1995, 2000; Feldmann and McKenzie, 1998; Macintyre et al., 2000). Both types are composed of well sorted ooids and peloids and very thin lithified layers corresponding to dolomicritic horizons. Evidence of micritization and rare fused grains that are cemented and truncated at point-contacts suggests a close petrographic similarity. Although specific microbial filaments are not evident in the Ladinian examples, a similar scarcity in calcified remains is observed in the Bahamian microbialites, probably because they are also subtidal in origin (Reid et al., 1995). Micro-boring and micro-filling processes together with truncation and minor fusion of grains have also been described in oolitic microbial laminites in the Miocene of Mallorca (Arenas & Pomar, 2010). The Ladinian ooidal-peloidal stromatolites are also very similar to those of the Miocene of Mallorca as regards their external morphology (Arenas & Pomar, 2010) with dominant stratiform disposition rather than columnar or individual domal buildups as reported in the Bahamian counterparts (Dravis, 1983; Dill et al, 1986; Andres and Reid, 2006). On the other hand, stromatolites constituted by type C couplets are similar to those reported by Chow and George (2004) in the Famenian of the Canning Basin. There, fenestral clotted and wavy laminated textures (both of microbial origin) are interbedded with graded laminated fabrics (ooid-intraclastic grainstone accumulation). According to these authors, complex interaction between microbial calcification/cementation, sediment trapping and binding processes combined with environmental factors produced the juxtaposition of these microfabrics in the same microbialite. Similarly, an Upper Turonian

689 stromatolite bed in the Northern Iberian Ranges recorded a comparable textural heterogeneity in its upper
690 portion where layers of clotted to peloidal texture are interbedded with layers of bahamite peloid texture
691 of equal or smaller thickness. Bahamite peloids are interpreted as biologically modified grains.
692 On the other hand, 'thrombolitic' reefs in the Dolomites (Bosellini, 1986) are composed of microbial
693 and biogenic crusts (Harris, 1993, 1994) which contribute to the enhancement of the rigidity and stability
694 of the reef structures (Flügel and Senowbari-Daryan, 2001). In Latemar (Dolomites), the *Tubiphytes*-
695 microproblematica bindstone assemblage is the most important faunal association and is located in the
696 reef crest, whereas *Tubiphytes multisiphonatus* thrombolites are abundant in the back-reef margin *sensu*
697 Emmerich et al., (2005) or the margin to slope transition according to Marangon et al., (2011). Similarly,
698 in the Marmolada platform, Blendinger (1986) recorded the presence of *Tubiphytes* organisms and
699 porostromate microbes in the reef facies. In the Northern Calcareous Alps (Austria), *Tubiphytes* and
700 sphinctozoans constituted the most widespread reef-building organisms in the Ladinian to Carnian
701 Wetterstein platforms, acting as framebuilders and bafflers on upper slopes and platform margins. These
702 organisms are frequently associated with incrusters (Rüffer and Zamparelli, 1997). Although the term
703 'thrombolite' has not been extensively used in some Ladinian basins of the Dolomites and the Alps, their
704 components (microbes, encrusters and syndepositional cements) acted as framebuilders and played an
705 important part in lithification processes (Blendinger, 1994; Russo et al., 2000; Senowbari-Daryan, 2013).
706
707 6.4. The hydrothermal influence in the formation of microbial and non-microbial components.
708 One of the most striking features of Ladinian reef thrombolites of the western Tethys is the
709 abundance of botryoidal and isopachous fibrous marine cements. Generally speaking, the Middle Triassic
710 of the Dolomites region corresponds to a period of platforms that grew under an episode of extremely
711 high subsidence, giving rise to the preferential development of isolated carbonate platforms or atoll-like
712 buildups (Bosellini, 1984; Blendinger, 1994; Preto et al., 2012 and references therein). As a rule, these
713 systems are characterised by flat-topped platform transitions and steep-fronted carbonate slopes
714 dominated by microbialites and early marine cements (Blendinger, 1986, 1994; Harris, 1993, 1994;
715 Marangon et al., 2011 among others). The Marmolada platform contains an average of 20% of early-
716 marine cements (isopachous and radiaxial fibrous) according to Russo et al., (2000) or 37% according to
717 Blendinger (1994); the Sella massif is made up an average of 37% of early marine cements (fibrous
718 cements in the form of botryoids, Keim and Schlager, 2001) and the Latemar platform is composed of an

719 average of 34% of cements (isopachous radiaxial fibrous and botryoidal, Marangon et al., 2011). Bearing
720 in mind the limitations of estimating these data, an important observation is inferred from these figures. In
721 these examples, early-marine cements are volumetrically the most abundant component together with
722 microbialite fabrics (stromatolitic, thrombolitic textures, and biofilms). The Ladinian thrombolites of the
723 Catalan Basin are not an exception. Despite having been accreted in fault-block carbonate ramp profiles,
724 they are also composed of at least 40% of botryoidal and fibrous cements, and microbialites as its Italian-
725 Alpine counterparts. Moreover, there is a widespread agreement in attributing these cements to the marine
726 early-diagenetic stage and to being made originally of aragonite (Blendinger, 1994; Harris, 1993; 1994;
727 Tucker and Marshall, 2004; Seeling et al., 2005; Marangon et al., 2012). However, the genesis of these
728 cements is still a matter of intense debate. An interesting revision of the controls on pervasive marine
729 cementation associated with deep slope settings is provided by Van Der Kooij, et al., (2010). In addition
730 to the factors discussed by Grotzinger and Knoll (1995), Webb (1996), Seeling et al., (2005) and Van Der
731 Kooij at al., (2010) another physico-chemical factor should be taken into account: the hydrothermal fluids
732 originated from thermal anomalies associated with volcanic and magmatic activity. In fact, during the
733 Middle and Late Triassic, volcanic activity has been reported in the Triassic rifting phase in the Catalan
734 Basin (Calvet et at., 1990; Salas and Casas, 1993) and in the Dolomites, Northen Italy (Doglioni, 1987).
735 A common mechanism of carbonate precipitation is degassing of oversaturated carbonate waters flowing
736 from marine hydrothermal vents or hot springs (Chafetz and Folk, 1984; Renaut and Jones, 2000).
737 Furthermore, botryoidal cements associated with seep carbonates are common in many ancient cases
738 (Campbell et al, 2002; Canet et al., 2003; Gómez-Pérez, 2003). Although the hypothesis of methane
739 seepage cannot be tested with confidence in the Catalan Basin, hydrocarbon-oil shows are recorded in
740 basinal black-shales of Ladinian age in commercial oil wells of the Maestrat Basin (Salas et al., 2001).
741 The main Rock Eval and geochemical parameters of this source rock are: a) equivalent vitrinite from
742 steranes: 0.85% Ro, b) pyrolysis Tmax: 440ºC, c) burial temperature: 138º C.

743 A prolonged hydrothermal circulation can be maintained through a persistent faulting and fracturing
744 which favours fluid flow, and is consistent with the geodynamic context of the Middle Triassic
745 (Ladinian). Moreover, the fact that pervasive cementation is commonly associated with the La Riba fault
746 strongly supports the hypothesis of fault-induced fluid flow for corrosion cementation. Authigenic barite
747 cements in thrombolites are also an evidence for hydrothermal vent fluid. Neither stromatolites s.s, nor
748 ooidal-peloidal stromatolites provides evidence of such a degree and type of cementation.

749 At this stage, some questions may be raised: What is the microbial and non-microbial contribution in
750 thrombolite formation? Did bacteria play a key role in mineral precipitation? Were bacteria merely
751 encased in essentially abiotic precipitates? or Are lacustrine and marine microbial and non-microbial
752 processes and products so different?
753 Several ancient marine examples record the (inorganic?) precipitation of large hemispheroidal
754 masses of composite aragonite botryoid fans concurrently with microbial textures in cold seeps and
755 hydrothermal vents (Savard et al., 1996; Peckman et al., 1999; Aharon, 2000; Peckman et al, 2001).
756 Moreover, a general perception supports the view that microbially mediated precipitates can subsequently
757 serve as sites for inorganic crystal nucleation under supersaturated fluids (Renaut and Jones, 2000,
758 Gómez-Pérez, 2003).
759 Controversies about the biotic and abiotic contribution of carbonate precipitates in travertine or hot
760 springs are not new (Chafetz and Folk, 1984; Ford and Pedley, 1996; Renaut and Jones, 2000). Similarly,
761 the presence of pervasive cementation associated with microbialites in marine settings warrants further
762 investigation. Fault-related hydrothermal processes, which are very common in lacustrine settings, may
763 have exerted a significant influence in marine microbial and non-microbial products during the Ladinian.
764 However, other abiotic factors should also be considered to account for the anomalous predominance of
765 cements in the Ladinian basins of the western Tethys, as occurs in the Late Permian (Grotzinger and
766 Knoll, 1995). Accordingly, the palaeogeographic configuration of the fault-block carbonate ramps of the
767 Catalan Basin may have limited the oceanic bottom circulation, producing protracted anoxic marine
768 conditions which could have been inherited from the Lower Triassic (Wignall and Twitchett, 1996; Grice
769 et al., 2005).
770
771 **7. Conclusions**
772 A comprehensive study of microbialite facies was performed in the Ladinian (Middle Triassic) of the
773 Catalan Basin (NE Spain) for the first time. The following conclusions may be drawn:
774 1) Three types of microbialites (stromatolites s.s., ooidal-peloidal stromatolites and thrombolites) were
775 recognised in accordance with their external features, internal textures and microbial and non-microbial
776 processes.
777 2) Stromatolite s.s. textures are formed by the combination of silt-sized trapping and binding processes
778 and microbially mediated precipitation. Ooidal-peloidal stromatolites are composed of grainy layers

779 dominated by trapping and binding of coated grains together with fused grains and micritization, and
780 muddy layers dominated by microbially secreted mats with evidence of boring and endolithic processes.
781 Thrombolites developed through accretionary, binding and encrusting processes (microbially mediated)
782 and pervasive cementation processes (physico-chemically mediated).
783 3) Stromatolites s.s. are deposited in an intertidal environment, in an enclosed hypersaline embayment to
784 tidal flat, resembling those of Shark Bay (Australia). Ooidal-peloidal stromatolites accumulated in an
785 internal fore-shoal, in normal marine, shallow-water environment, above fair-weather wave base, under
786 moderate to high energy conditions. These microbialites bear a striking resemblance to those in the
787 Bahamas. Thrombolites are deposited below fair-weather wave base, a shallow subtidal normal marine
788 environment, under low to moderate energy conditions and probably within the photic zone. The faunal
789 and textural attributes are similar to those in coeval settings as in the Dolomites (Italy-Alps).
790 4) The growth of stromatolites s.s. was conditioned by the limited occurrence of strong waves, tidal
791 currents together with a restricted supply of coarse sediment. Hypersaline conditions favoured their
792 development and the increasing accommodation accounts for their mega- and macrostructural transition
793 (planar to domal morphologies). Ooidal-peloidal stromatolite growth was influenced by the combination
794 of high-energy periods (high sediment input and trapping and binding processes) with low-energy periods
795 (low sediment input and microbial precipitation processes) characterised by high rates of cementation and
796 rapid lithification which enhanced the growth. Thrombolite growth was controlled by incrustation and
797 lateral accretion processes. The distribution and architecture of syn-sedimentary botryoidal-fibrous
798 cements played a crucial role in its upbuilding and cohesiveness.
799 5) Co-occurrence of the three types of microbialites in the RST1 may be explained by the occurrence of
800 unusual oceanographic conditions (hypersalinity, widespread anoxia?) which produced a substantial
801 reduction of the microbial feeders. Juxtaposition of stromatolites s.s. and ooidal-peloidal stromatolites
802 during the TST2 of T-R Sequence 2 was governed by fourth-order sea-level cyclicity, conditioning the
803 bathymetry, the hydraulic energy, the type of sediment and the accumulation rates which controlled the
804 type of microbial community and processes.
805 6) The abundance of botryoidal and isopachous fibrous marine cements, corrosions and microbial textures
806 in thrombolites could be ascribed to fault-controlled circulation of hydrothermal fluids during the Triassic
807 rifting. These supersaturated fluids could have induced the inorganic crystal nucleation of cements on

808 previous microbially mediated precipitates (biofilms). Similar processes could have taken place in coeval
809 basins in the western Tethys (Dolomites region).
810 7) Our results reveal that a) different types of microbial communities coexist and microbial processes act
811 together in the same subenvironment, b) some of these microbial and non-microbial processes may
812 operate regardless of the sedimentary environment, and c) microbial and non-microbial processes may act
813 simultaneously to build the microbialite framework.
814 8) The Ladinian microbial depositional models of the Catalan Basin show an interesting diversity and
815 coexistence of microbialites within a well-constrained sequence stratigraphic framework. Furthermore,
816 these patterns can be successfully used as conceptual models to better understand the relationship
817 between microbial and non-microbial textures and can be applied as integrated analogues of Shark Bay
818 (Australia), the Exuma Cays (Bahamas) and the Dolomites (Italy-Alps).
819
820 **Acknowledgements**
821 We are also indebted to Mateu Esteban for fruitful debates during the development of this project, and to
822 G. v. K. for revising the English of the manuscript. We gratefully acknowledge Repsol Exploración, S.A,
823 and the Spanish government's I+D+i research project CGL2008-04916, the Consolider-Ingenio 2010
824 programme under CSD 2006-0004 'Topo-Iberia' and the Grup Consolidat de Recerca 'Geologia
825 Sedimentària' (2009SGR-1451), for funding.
826
827 **References**
828
829 Aharon, P., 2000. Microbial processes and products fueled by hydrocarbons at submarine seeps. In:
830 Riding, R., Awramik, S. M. (Eds.). Microbial sediments. Springer-Verlag, Heilderberg.
831
832 Aitken, J. D., 1967. Classification and environmental significance of crytalgal limestones and dolomites,
833 with illustrations from the Cambrian and Ordovician of south western Alberta. Jour. Sed. Petrol., 37,
834 1163-1178.
835
836 Aitken, J. D., Narbonne, G. M., 1989. Two occurrences of Precambrian thrombolites from the Mackenzie
837 Mountains, Northwestern Canada. Palaios, 4, 384-388.

838

839 Alwood, A. C., Walter, M. R., Burch, I. W., Kamber, B. S., 2007. 3.43 billion-year-old stromatolite reef
840 from the Pilbara Craton of Western Australia: ecosystem-scale insights to early life on Earth. Precambrian
841 Research, 148, 198-227.

842

843 Andres, M. S., Reid, R. P., 2006. Growth morphologies of modern marine stromatolites: a case study
844 from Highborne Cay, Bahamas. Sedimen. Geol., 185, 319-328.

845

846 Arenas, C., Pomar, L., 2010. Microbial deposits in upper Miocene carbonates, Mallorca, Spain.
847 Palaeogeo., Palaeoclimat., Palaeoecol., 297, 465-485.

848

849 Armella, C., 1994. Thrombolitic-stromatolitic cycles of the Cambro-Ordovician boundary sequence,
850 Precordillera Oriental Basin, Western Argentina. In: Phanerozoic Stromatolites II. (Ed by J. Bertrand-
851 Sarfati & C.L.V Monty), pp. 421-441, Kluver.

852

853 Awramik, S. M., Buchheim, H. P., 2012. The quest for microbialite analogs to the South Atlantic Pre-Salt
854 carbonate hydrocarbon reservoirs of Africa and South America. HGS International Dinner Meeting talk.
855 URL: http://www.hgs.org/node/4875

856

857 Blendinger, W., 1986. Isolated stationary carbonate platforms: the Middle Triassic (Ladinian) of the
858 Marmolada area, Dolomites, Italy. Sedimentology 33, 159-183.

859

860 Blendinger, W., 1994. The carbonate factory of Middle Triassic buildups in the Dolomites, Italy: a
861 quantitative analysis. Sedimentology, 41, 1147-1159.

862

863 Bosellini, A., 1984. Progradation geometries of carbonate platforms: examplesfrom the Triassic of the
864 Dolomites, Northen Italy. Sedimentology, 31, 1-24.

865

866 Browne, K. M., Golubic, S., Seong-Joo, L., 2000. Shallow marine microbial carbonate deposits. In:
867 Riding, R., Awramik, S. M. (Eds.). Microbial sediments. Springer-Verlag, Heilderberg.

868

869 Burne, R.V., Moore, L. S., 1987. Microbialites; organosedimentary deposits of benthic microbial
870 communities. Palaios, 2, 241-254.
871
872 Calvet, F., Ramon, X., 1987. Estratigrafía, sedimentología y diagenesis del Muschelkalk inferior de los
873 Catalánides. Cuad. Geol. Iber., 11, 141-169.
874
875 Calvet, F., Tucker, M. E., 1995. Mud-mound with reefal caps in the upper Muschelkalk (Triassic), eastern
876 Spain. Spec. Publs. Int. Assoc. Sediment. 23, 311-333.
877
878 Calvet, F., Tucker, M. E., Henton, J. M., 1990. Middle Triassic carbonate ramp systems in the Catalan
879 Basin, northeast Spain: facies, systems tracts, sequences and controls. Spec. Publs. Int. Assoc. Sediment.
880 9, 79-108.
881
882 Campbell, K.A., Farmer, J.D., Des Marais D., 2002. Ancient hydrocarbon seeps from the Mesozoic
883 convergent margin of California; carbonate geochemistry, fluids and palaeoenvironments. Geofluids, 2,
884 63–94.
885
886 Canet, C., Prol-Ledesma, R. M., Melgarejo, J-C., Reyes, A., 2003. Methane-related carbonates formed at
887 submarine hydrothermal springs: a new setting for microbially-derived carbonates?. Marine Geology,
888 199, 245-261.
889
890 Chafetz, H. S., 1986. Marine peloids: a product of bacterially induced precipitation of calcite. J. Sedim.
891 Petrol., 56, 812-817.
892
893 Chafetz, H. S., Buczynski, C.,1992. Bacterially induced lithification of microbial mats. Palaios, 7, 277-
894 293.
895
896 Chafetz, H. S., Folk, R. L., 1984. Travertines: depositional morphology and bacterially constructed
897 constituents. J. Sed. Research, 54, 289-316.

Chow, N., George, A. D., 2004. Tepee-shaped agglutinated microbialites: an example from a Famenian carbonate platform on the Lennard Shelf, northen Canning Basin, Western Australia. Sedimentology, 51, 253-265.

Dill, R. F., Shinn, E. A., Jones, A. T., Kelly, K., Steinen, R. P., 1986. Giant subtidal stromatolites forming in normal salinity water. Nature, 324, 55-58.

Doglioni, C. 1987. Tectonics of the Dolomites. J. Struct. Geol., 9, 181-193.

Dorobek, S., Piccoli, L., Coffey, B., Adams, A., 2012. Carbonate rock-forming processes in the Pre-Salt "sag" successions of Campos Basin, off-shore Brazil: evidence for seasonal, dominantly abiotic carbonate precipitation, substrate controls, and broader geologic implications. AAPG Search and Discovery Article. AAPG Hedberg Conference, Microbial Carbonate Reservoir Charaterization, Houston, Texas.

Dravis, J. J, 1983. Hardened subtidal stromatolites, Bahamas. Science, 219, 385-386.

Dupraz, C., Reid, P. R, Braissant, O., Decho, A. W, Norman, R. S., Visscher, P. T., 2009. Processes of carbonate precipitation in modern microbial mats. Earth-Science Reviews, 96, 141-162.

Eckman, J.E., Andres, M.S., Marinelli, R.L., Bowlin, E., Reid, R.P., Aspden, R.J., Paterson, D. M., 2008. Wave and sediment dynamics along a shallow subtidal sandy beach inhabited by modern stromatolites. Geobiology 6, 21–32.

Esteban, M., Budai, T., Juhász, E., Lapointe, P., 2009. Alteration of Triassic carbonates in the Buda Mountains – a hydrothermal model. Central European Geology, 52, 1-29.

Emmerich, A., Zamparelli, V., Bechstädt, T., Zühlke, R., 2005. The reefal margin and slope of a Middle Triassic carbonate platform: the Latemar (Dolomites, Italy). Facies, 50, 573-614.

928 Fagundes de Rezende, M., Pope, M. C., 2013. Importance of microbial texture for the porosity
929 characterization in microbial carbonates. Microbial carbonates in space and time: implications for global
930 exploration and production. The Geological Society, London.
931
932 Feldmann, M., McKenzie, J. A., 1997. Messinian stromatolite-thrombolite associations, Santa Pola, SE
933 Spain: an analogue for the Paleozoic? Sedimentology, 44, 893-914.
934
935 Feldmann, M., McKenzie, J. A., 1998. Stromatolite-thrombolite associations in a modern environment,
936 Lee Stocking Island, Bahamas. Palaios, 13, 201-212.
937
938 Flügel, E, Senowbari-Daryan, B., 2001. Triassic reefs of the Tethys. In: The history and sedimentology of
939 ancient reef systems. (Ed. by G. Stanley), Topics in Geobiology, 17, 217-249.
940
941 Flügel, E., 2004. Microfacies of carbonate rocks. Analysis, interpretation and application. Springer-
942 Verlag Berlin Heildelberg.
943
944 Ford, T. D., Pedley, H. M., 1996. A review of tufa and travertine deposits of the world. Earth-Science
945 Reviews, 41, 117-175.
946
947 Franks, J, Stolz, J. F., 2009. Flat laminated microbial mat communities. Earth-Science Reviews, 96 (3),
948 163-172.
949
950 García-Senz, J., Salas, R., 2011. Sedimentary response to continental rifting in Iberia. Abstracts, 28th IAS
951 Meeting of Sedimentology, Zaragoza, Spain (Eds. B. Bádenas, M. Aurell and A. M. Alonso-Zarza). p. 37.
952
953 Garrett, P., 1970. Phanerozoic stromatolites: noncompetitive ecologic restriction by grazing and
954 burrowing animals. Science, 169, 171-173.
955
956 Golubic, S., Browne, K. M., 1996. Schizothrix gebeleinii sp.nov. builds subtidal stromatolites, Lee
957 Stocking Island, Bahamas. Algol Stud., 83, 273-290.

Gómez-Pérez, I., 2003. An Early Jurassic deep-water stromatolitic bioherm related to possible methane seepage (Los Molles Formation, Neuquén, Argentina). Palaeogeography, Palaeoclimatology, Palaeoecology, 201, 21-49.

Grice, K, Cao, C, Love, G. D., Böttcher, M. E., Twitchett, R. J., Grosjean, E., Summons, R. E, Turgeon, S. C., Dunning, W., Jin, Y., 2005. Photic zone euxinia during the Permian-Triassic superanoxic event. Science, 307, 706-709.

Grotzinger, J. P., Knoll, A. H., 1995. Anomalous carbonate precipitates: is the Precambrian the key to the Permian? Palaios, 10, 578-596.

Grotzinger, J. P., Knoll, A. H., 1999. Stromatolites in Precambrian carbonates: evolutionary mileposts or environmental dipsticks? Annual Reviews Earth and Planetary Sciences, 27, 313-358.

Harris, M. T., 1993. Reef fabrics, biotic crusts and syndepositional cements of the Latemar reef margin (Middle Triassic), northern Italy. Sedimentology, 40, 383-401.

Harris, M. T., 1994. The foreslope and toe-of-slope facies of the Middle Triassic Latemar buildup (Dolomites, Northen Italy). J. Sed. Research,64, 132-145.

Harris, M. T., Ellis, J., Purkis, S. J., 2013. Assessing the extent of carbonate deposition in early rift settings. AAPG Bulletin, 97, 27-60.

Harwood, C. L., Sumner, D.Y., 2011. Microbialites of the Neoproterozoic Beck Spring Dolomite, Southern California. Sedimentology, 58, 1648-1673.

Hillgärtner, H., Dupraz, C., Hug, W., 2001. Microbially induced cementation of carbonate sands: are micritic meniscus cements good indicators of vadose diagenesis? Sedimentology, 48, 117-131.

988 Hoffman, P. F., 1974. Shallow and deeper stromatolites in the Lower Proterozoic platform-to-basin facies
989 change, Great Slave Lake, Canada. AAPG Bulletin, 58, 856-867.
990
991 Jahnert, R., Collins, L. B., 2011. Significance of subtidal microbial deposits in Shark Bay, Australia. Mar.
992 Geol., 286, 106-111.
993
994 Jahnert, R., Collins, L. B., 2012. Characteristics, distribution and morphogenesis of subtidal microbial
995 systems in Shark Bay, Australia. Mar. Geol., 303, 115-136.
996
997 Jahnert, R., Collins, L. B., 2013. Controls on microbial activity and tidal flat evolution in Shark Bay,
998 Western Australia. Sedimentology, 60 (4), 1071-1099.
999
1000 Kah, L. C., Grotzinger, J. P., 1992. Early Proterozoic (1.9 Ga) thrombolites of the Rocknest Formation,
1001 Nortwest Territories, Canada. Palaios, 7, 305-315.
1002
1003 Kahle, C. F., 2001. Biosedimentology of a Silurian thrombolite reef with meter-scale growth framework
1004 cavities. Journal of Sed. Res., 71 (3), 410-422.
1005
1006 Keim, L., Schlager, W., 2001. Quantitative compositional analysis of a Triassic carbonate platform
1007 (Southern Alps, Italy). Sedimentary Geology, 139, 261-283.
1008
1009 Kennard, J. M., 1994. Thrombolites and stromatolites within shale-carbonate cycles, Middle-Late
1010 Cambrian Shannon Formation, Amadeus Basin, Central Australia. In: Sarfati, J. B-S., Monty, C. L. V.,
1011 (Eds.) Phanerozoic stromatolites II. Kluver.
1012
1013 Kennard, J. M., James, N. P., 1986. Thrombolites and stromatolites: two distinct types of microbial
1014 structures. Palaios, 1, 492-503.
1015
1016 Lehrmann, D. J., 1999. Early Triassic calcimicrobial mounds and biostromes of the Nanpanjiang basin,
1017 south China. Geology, 27, 359-362.

Logan, B. W., Cebulski, D. E., 1970. Sedimentary environments of Shark Bay, Western Australia. In: Logan, B. W., Davies, G. R., Read J. F., Cebulski, D. E., (Eds.). Carbonate sedimentation and environments, Shark Bay, Western Australia. AAPG Memoir, 13, 1-37.

Logan, B. W., Hoffman, P., Gebelein, C. D., 1974. Algal mats, cryptalgal fabrics, and structures, Hamelin Pool, Western Australia. In: Logan,, B. W., Read, J. F., Hagan, G. M., Hoffman, P., Brown, R. G., Woods P. J., Gebelein, C. (Eds.) Evolution and diagenesis of Quaternary carbonate sequences, Shark Bay, Western Australia AAPG Memoir, 22, 140-194.

Logan, B.W., Rezaki, R., Ginsburg, R. W., 1964. Classification and environmental significance of algal stromatolites. Jour. Geol., 72, 68-83.

Macintyre, I. G., Prufert-Bebout, L., Reid., R. P., 2000. The role of endolithic cyanobacteria in the formation of lithified laminae in Bahama stromatolites. Sedimentology, 47, 915-921.

Macintyre, I. G., Reid, R. P., Steneck, R. S., 1996. Growth history of stromatolites in a Holocene fringing reef, Stocking Island, Bahamas. J. Sed. Research, 66, 231-242.

Marangon, A., Gattolin, G., Della Porta, G., Preto, N., 2011. The Latemar: A flat-topped, steep fronted platform dominated by microbialites and synsedimentary cements. Sed. Geol., 240, 97-114.

Mercedes-Martín R., Salas R., Arenas C., 2013a. Facies heterogeneity and depositional models of a Ladinian (Middle Triassic) microbial-dominated carbonate ramp system (Catalan Coastal Ranges, NE Spain). Journal of Marine and Petroleum Geology, 46, 107-128.

Mercedes-Martín R., Salas R., Arenas C., 2013b. Microbial-dominated carbonate platforms during the Ladinian rifting: sequence stratigraphy and evolution of accommodation in a fault-controlled setting (Catalan Coastal Ranges, NE Spain). Basin Research, 25, 1-28.

1048 Monty C. L. V., 1967. Distribution and structure of Recent stromatolitic algal mats, eastern Andros
1049 Island, Bahamas. Ann. Soc. Géol. Belg., 90, 55-100.
1050
1051 Monty, C. L. V., 1976. The origin and development of cryptalgal fabrics. In: Walter M. R. (Ed.).
1052 Stromatolites. Developments in Sedimentology, 20, 193-249. Elsevier, Amsterdam.
1053
1054 Mutti M., Hallock, P., 2003. Carbonate systems along nutrient and temperature gradients: some
1055 sedimentological and geochemical constraints. Int. J. Earth. Sci (Geol. Rundsch), 92, 465-475.
1056
1057 Pentecost, A., 1991. Calcification processes in algae and cyanobacteria. In: Riding, R. (Ed.). Calcareous
1058 algae and stromatolites, Springer-Verlag, Berlin.
1059
1060 Planavsky, N., Ginsburg, R. N., 2009. Taphonomy of modern marine Bahamian microbialites. Palaios,
1061 24, 5-17.
1062
1063 Playford, P. E., Cockbain, A. E., 1976. Modern algal stromatolites at Hamelin Pool, a hypersaline barred
1064 basin in Shark Bay, Western Australia. In: Walter M. R. (Ed.). Stromatolites. Developments in
1065 Sedimentology, 20, 193-249. Elsevier, Amsterdam.
1066
1067 Pratt, B. R., 1995. The origin, biota and evolution of deep-water mud-mounds. In: Monty C.L.V.,
1068 Bosence, D.W. J., Bridges, P. H., Pratt, B. R. (Eds.). Carbonate mud-mounds: their origin and evolution.
1069 Intern. Assoc. Sediment., Spec. Publ., 23, 49-123.
1070
1071 Pratt, B. R., Haidl, F. M., 2008. Microbial pach reefs in Upper Ordovician Red River strata, Williston
1072 Basin, Saskatchewan: signal of heating in a deteriorating epeiric sea. In: Pratt, B. R., Holmden, C. (Eds.).
1073 Dynamics of epeiric seas. Spec. Pap. Geol. Assoc. Can. 48, 303-340.
1074
1075 Preto, N., Franceschi, M., Gattolin, G., Massironi, M., Riva, A., Gramigna, P., Bertoldi, L., Nardon, S.,
1076 2011. The Latemar: a Middle Triassic polygonal fault-block platform controlled by synsedimentary
1077 tectonics. Sedimentary Geology, 234, 1-18.

Purdy, E. G., 1963. Recent calcium carbonate facies on the Great Bahama Bank. 1. Petrography and reaction groups. J. Geol., 71, 334-355.

Reid, R. P., James, N. P., Macintyre, I. G., Dupraz, C. P., Burne, R. V., 2003. Shark Bay stromatolites: microfabrics and reinterpretation of origins. Facies, 49, 299-324.

Reid, R. P., Macintyre, I. G., Steneck, R. S. A., Browne, K. M., Miller, T. E., 1995. Stromatolites in the Exuma Cays, Bahamas: uncommonly common. Facies, 33, 1-18.

Reid, R.P., Visscher, P. T., Decho, A.W., Stolz, J. F., Bebout, B. M., Dupraz, C., Macintyre, I. G., Paerl, H. W., Pinckney, J. L., Prufert-Bebout, L., Steppe, T. F., D. J. Desmarals., 2000. The role of microbes in accretion, lamination and early lithification of modern marine stromatolites. Nature, 406, 989-992.

Renaut, R. W., Jones, B., 2000. Microbial precipitates around continental hot Springs and geysers. In: Riding, R., Awramik, S. M. (Eds.). Microbial sediments. Springer-Verlag, Heilderberg.

Riding, R. 1991. Classification of microbial carbonates. In: Riding, R. (Ed.). Calcareous algae and stromatolites. Springer-Verlag, Berlin.

Riding, R., 2000. Microbial carbonates: the geological record of calcified bacterial-algal mats and biofilms. Sedimentology, 47 (Suppl.), 179-214.

Riding, R., 2002. Biofilm architecture of Phanerozoic cryptic carbonate marine veneers. Geology, 30, 21-34.

Riding, R., 2011. Microbialites, stromatolites and thrombolites. In: Reitner., J. and V. Thiel (eds), Encyclopedia of Geobiology, Encyclopedia of Earth Science Series, Springer, Heidelberg, pp. 635-654.

Riding, R. E, Awramik, S. M., 2000. Microbial sediments. Springer-Verlag Berlin Heildelberg.

Riding, R., Braga, J. C., Martín, J. M., 1991. Oolite stromatolites and thrombolites, Miocene, Spain: analogues of Recent giant Bahamian examples. Sedimen. Geol., 71, 121-127.

Riding R., Liang, L., 2005. Geobiology of microbial carbonates: metazoan and seawater saturation state influences on secular trends during the Phanerozoic. Palaeogeography, Palaeoclimatology, Palaeoecology, 219, 101-115.

Riding, R. Tomás, S., 2006. Stromatolite reef crusts, Early Cretaceous, Spain: bacterial origin of in situ-precipitated peloid microspar? Sedimentology, 53, 23-34.

Rodríguez-Martínez, M., Reitner, J., Mas, R., 2011. Micro-framework reconstruction from peloidal-dominated mud mounds (Viséan, SW Spain). Facies, 56, 139-156.

Rüffer, T., Zamparelli, V., 1997. Facies and biota of Anisian to Carnian carbonate platforms in the Northern Calcareous Alps (Tyrol and Bavaria). Facies, 37, 115-136.

Russo, F., Mastandrea, A., Stefani, M., Neri, C., 2000. Carbonate facies dominated by syndepositional cements: a key component of Middle Triassic platforms. The Marmolada case history (Dolomites, Italy). Facies, 42, 211-226.

Russo, F., Neri, C., Mastandrea, A., Baracca, A., 1997. The mud mound nature of the Cassian platform margins of the Dolomites. A case history: the Cipit boulders from Punta Grohmann (Sasso Piatto Massif, Northern Italy). Facies., 36, 25–36.

Salas R., Guimera J., Mas R., Martin-Closas C., Melendez A., Alonso A., 2001. Evolution of the Mesozoic Central Iberian Rift System and its Cainozoic inversion (Iberian chain). In: Ziegler, P.A., Cavazza, W., Robertson, A.H.F., Crasquin-Soleau, S. (Eds.). Peri-Tethys memoir 6: Peri-Tethyan Rift/Wrechn Basins and Passive Margins. Mém. Mus. Hist. Nat. 186, 145–185.

1138 Sano, H., Horibo, K., Kumamoto, Y., 1990. *Tubiphytes-Archaeolithoporella-Girvanella* reefal facies in
1139 Permian buildups, Mino terrane, central Japan. Sed. Geol., 68, 293-306.
1140
1141 Savard, M. M., Beauchamp, B., Veizer, J., 1996. Significance of aragonite cements around Cretaceous
1142 marine methane seeps. J. Sed. Research, 66, 430-438.
1143 Seeling, M., Emmerich, A., Bechtädt, T., Zühlke, R., 2005. Accomodation/ sedimentantion development
1144 and massive early marine cementation: Latemar vs. Concarena (Middle/ Upper Triassic, Southen Alps).
1145 Sed. Geol., 175, 439-457.
1146
1147 Senowbari-Daryan, B., 2013. Tubiphytes Maslov, 1956 and description of similar organisms from
1148 Triassic reefs of the Tethys. Facies, 59, 75-112.
1149
1150 Shapiro, R. S., 2000. A comment on the systematic confusion of thrombolites. Palaios, 15, 166-169.
1151
1152 Sharp, I., Verwer, K., Ferreira, H., Lapponi, F., Snidero, M., Machado, V., Holtar, E., Swart, R., Marsh,
1153 J., Gindre, L., Puigdefagregas, C, Fejerkov, M., 2013. Pre- and Post-Salt Non-Marine Carbonates of the
1154 Namibe Basin, Angola. Microbial carbonates in Space and Time: implications for global exploration and
1155 production. The Geological Society, London.
1156
1157 Shen, J-W, Yang, H-J., Qing, H., Zhang, L-J., Yang, H-Q., 2012. Calcimicrobes and microbialites in
1158 lagoonal sediments from Mississippian Midale Beds, Williston Basin, southeastern, Saskatchewan,
1159 Canada. Int. J. Earth Sci. (Geol. Rundsch), 101, 109-127.
1160
1161 Steneck, R. S., Miller, T. E., Reid, R. P., Macintyre, I. G., 1993. Ecological factors controlling the
1162 distribution and abundance of intertidal stromatolites, Stocking Island, Bahamas. Geol. Soc. America,
1163 Abstract 25/6.
1164
1165 Sumner, D. Y., 2000. Microbial versus environmental influences on the morphology of late Archean
1166 fenestrated microbialites. In: Riding, R., Awramik, S. M. (Eds.). Microbial sediments. Springer-Verlag,
1167 Heilderberg.

Tonietto, S. N., Shane, E. K., Ahr, W. M., Pope, M. C., 2012. Pore type characterization and petrophysical properties on microbial carbonate reservoirs. AAPG Search and Discovery Article. AAPG Hedberg Conference, Microbial Carbonate Reservoir Charaterization, Houston, Texas.

Tucker M. E., Marshall J., 2004. Diagenesis and geochemistry of Upper Muschelkalk (Triassic) buildups and associated facies in Catalonia (NE Spain): a paper dedicated to Francesc Calvet. Geol. Act., 4, 257-269.

Tucker, M. E., Wright, V. P., 1990. Carbonate sedimentology. 482 pp. Blackwell Science Ltd.

Van der Kooij, B., Immenhauser, A., Steuber, T., Bahamonde Rionda, J. R., Meríno Tomé, O. 2010. Controlling factors of volumetrically important marine carbonate cementation in deep slope settings. Sedimentology, 57, 1491-1525.

Vargas H., Gaspar-Escribano J.M., López-Gómez J., Van Wees J-D., Cloetingh S., De La Horra R., Arche, A., 2009. A comparison of the Iberian and Ebro Basins during the Permian and Triassic, Eastern Spain: A quantitative subsidence modelling approach. Tectonophysics, 474, 160-183.

Virgili C., Sopeña A., Ramon A., Arche A., Hernando, A., 1983. El relleno posthercínico y el comienzo de la sedimentación Mesozoica. Libr. Jub. Jos. María Rios, Mad., 2, 25-36.

Webb, G. E., 2006. Was Phanerozoic reef history controlled by the distribution of non-enzymatically secreted reef carbonates (microbial carbonate and biologically induced cement)? Sedimentology, 43, 947-971.

Webb, G. E., 1987. Late Mississippian thrombolite bioherms from the Pitkin Formation of northern Arkansas. Geol. Soc. America Bull., 99, 686-698.

Whittle, G. L., Kendall, C.G. St. C, Dill, R. F. Rouch, L., 1993. Carbonate cement fabrics displayed: a traverse across the margin of the Bahamas Platform near Lee Stocking Island in Exuma Cays. Mar. Geology, 110, 213-243.

Wignall, P. B., Twitchett, R., J., 1996. Oceanic anoxia and the end Permian mass extinction. Science, 272, 1155-1158.

Winlaw, H. D., Matthews, R. K., 1974. Origin and significance of grapestone, Bahamas Islands. J. Sediment. Petrol., 44, 921-927.

Wright, P., 2013. To be or not to be, microbial: does it matter? Microbial carbonates in Space and Time: implications for global exploration and production. The Geological Society, London.

Ziegler, P. A., 1982). Triassic rifts and facies patterns in Western and Central Europe. Geolog. Runds. 71, 747-772.

Figure1

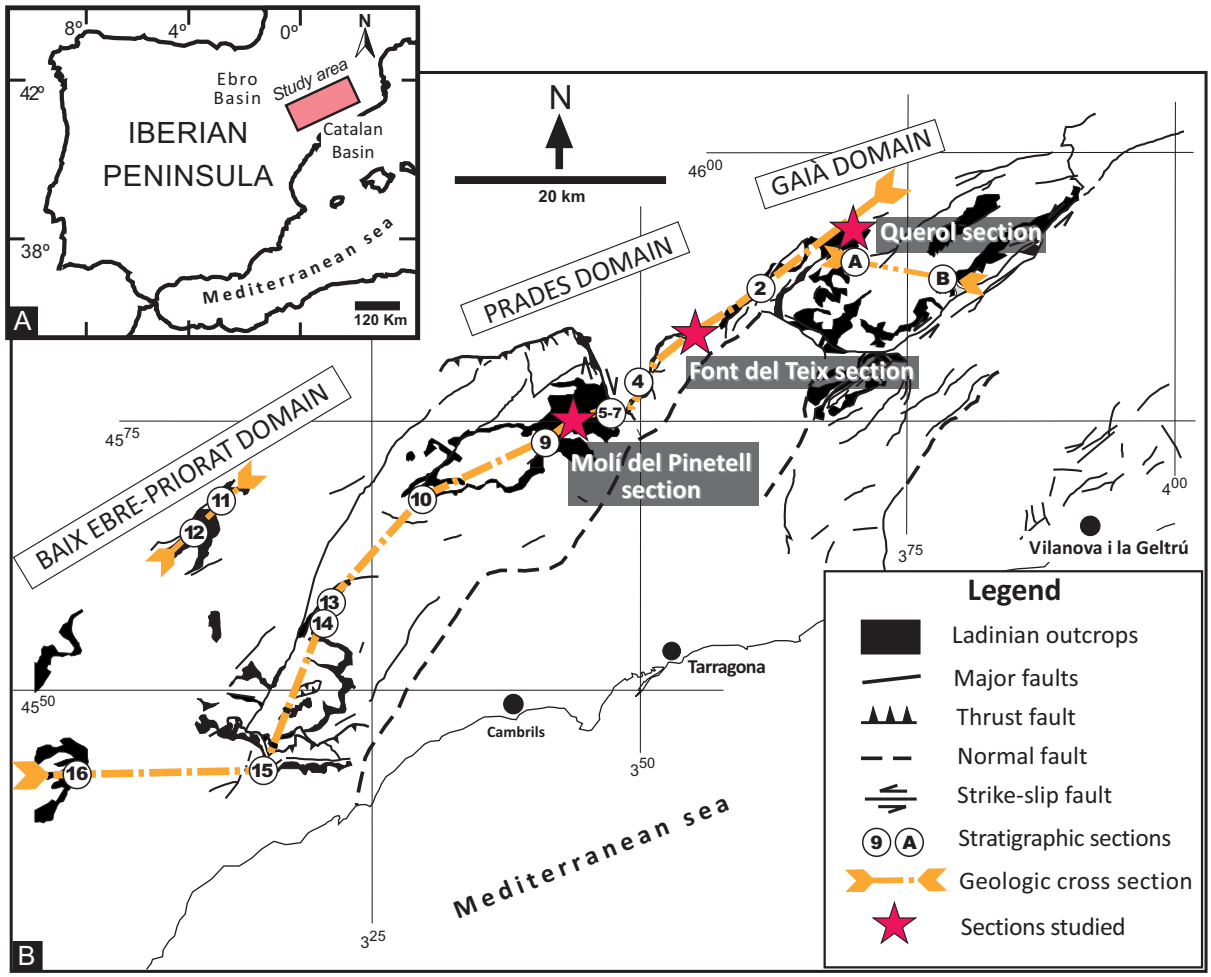
A
8º
4º
0º
N
42º
Ebro Basin
Study area
IBERIAN PENINSULA
Catalan Basin
38º
Mediterranean sea
120 Km
B
N
20 km
46 00
GAIÀ DOMAIN
PRADES DOMAIN
BAIX EBRE-PRIORAT DOMAIN
Querol section
Font del Teix section
Molí del Pinetell section
45 75
45 50
4 00
3 75
3 50
3 25
Vilanova i la Geltrú
Tarragona
Cambrils
Mediterranean sea
Legend
Ladinian outcrops
Major faults
Thrust fault
Normal fault
Strike-slip fault
Stratigraphic sections
Geologic cross section
Sections studied

Figure 2

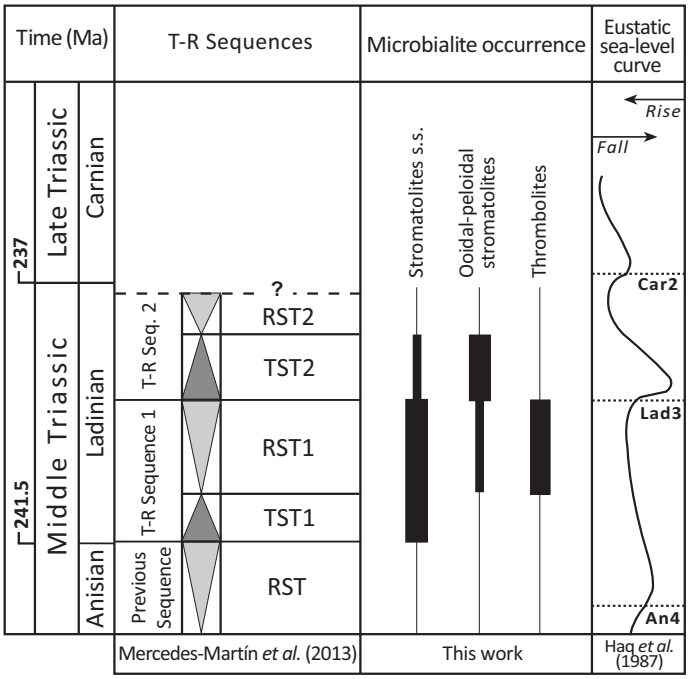
Time (Ma)
T-R Sequences
Microbialite occurrence
Eustatic sea-level curve
Late Triassic
Middle Triassic
Carnian
Ladinian
Anisian
237
241.5
?
RST2
TST2
RST1
TST1
RST
T-R Seq. 2
T-R Sequence 1
Previous Sequence
Stromatolites s.s.
Ooidal-peloidal stromatolites
Thrombolites
Rise
Fall
Car2
Lad3
An4
Mercedes-Martín et al. (2013)
This work
Haq et al. (1987)

Figure 3

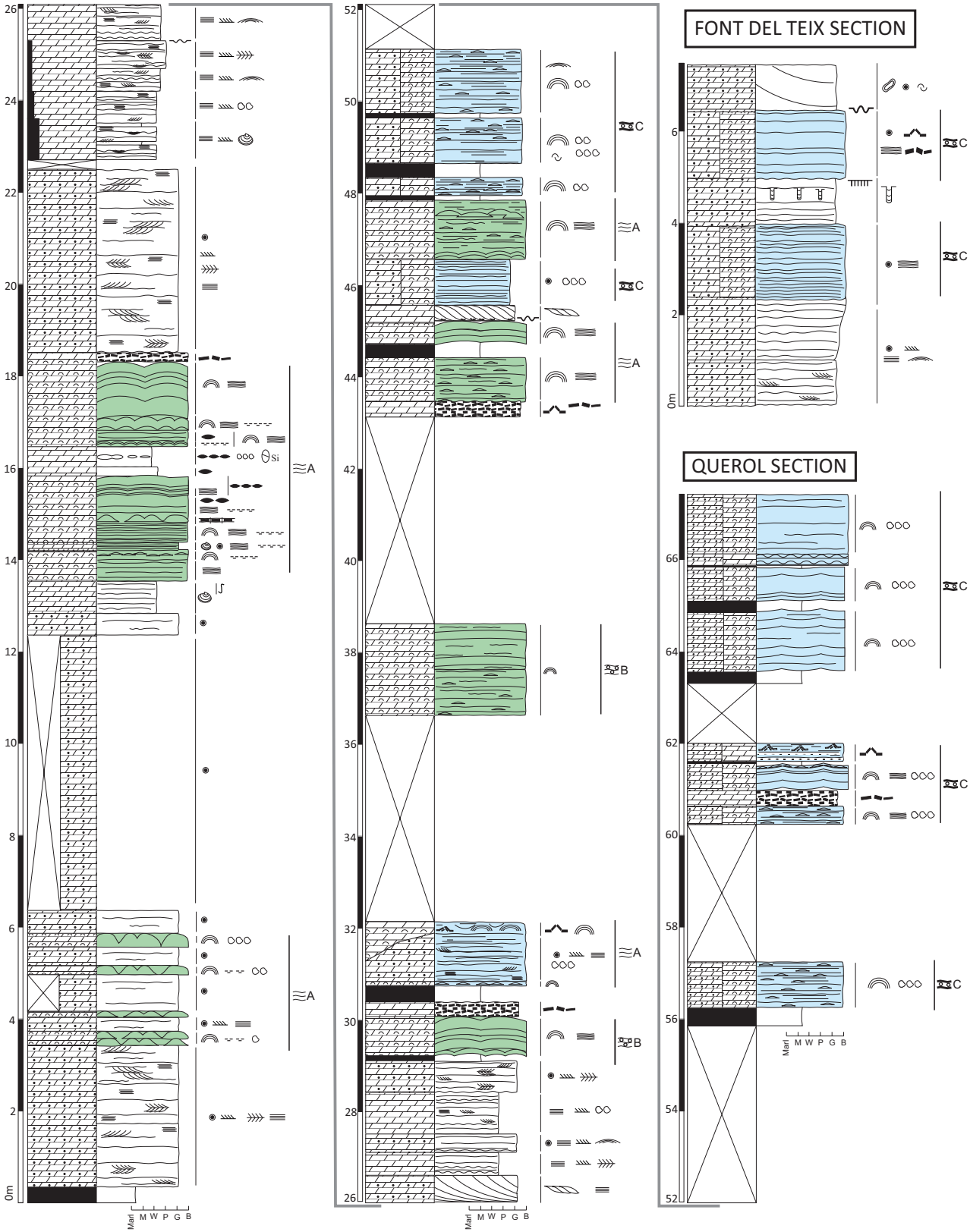
FONT DEL TEIX SECTION
QUEROL SECTION
Marl M W P G B
A
B
C
Si
0m
2
4
6
10
12
14
16
18
20
22
24
26
28
30
32
34
36
38
40
42
44
46
48
50
52
54
56
58
60
62
64
66

Figure 4

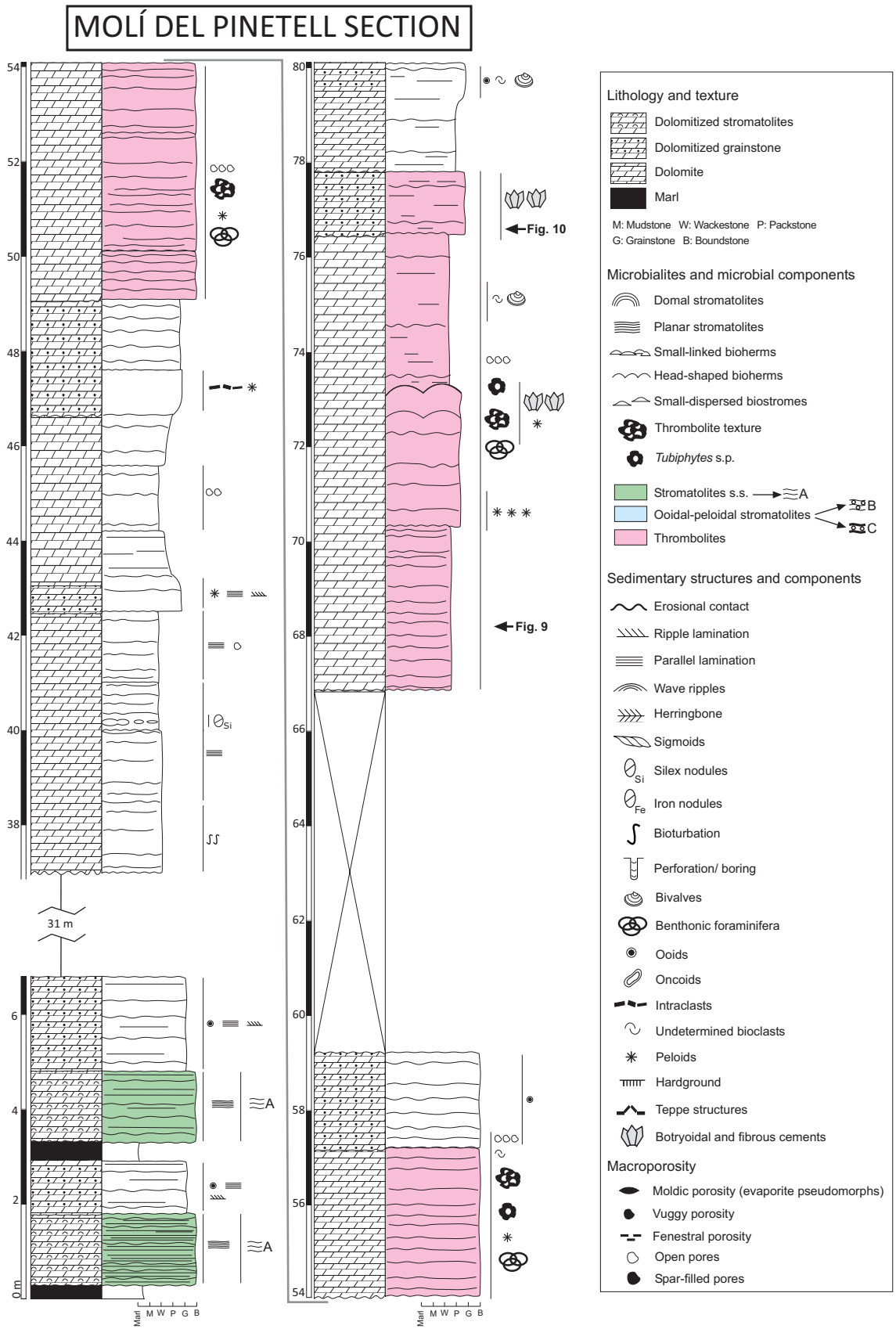
MOLÍ DEL PINETELL SECTION
31 m
Fig. 10
Fig. 9
Marl M W P G B
Lithology and texture
Dolomitized stromatolites
Dolomitized grainstone
Dolomite
Marl
M: Mudstone W: Wackestone P: Packstone
G: Grainstone B: Boundstone
Microbialites and microbial components
Domal stromatolites
Planar stromatolites
Small-linked bioherms
Head-shaped bioherms
Small-dispersed biostromes
Thrombolite texture
Tubiphytes s.p.
Stromatolites s.s.
Ooidal-peloidal stromatolites
Thrombolites
Sedimentary structures and components
Erosional contact
Ripple lamination
Parallel lamination
Wave ripples
Herringbone
Sigmoids
Silex nodules
Iron nodules
Bioturbation
Perforation/ boring
Bivalves
Benthonic foraminifera
Ooids
Oncoids
Intraclasts
Undetermined bioclasts
Peloids
Hardground
Teppe structures
Botryoidal and fibrous cements
Macroporosity
Moldic porosity (evaporite pseudomorphs)
Vuggy porosity
Fenestral porosity
Open pores
Spar-filled pores

Figure 5

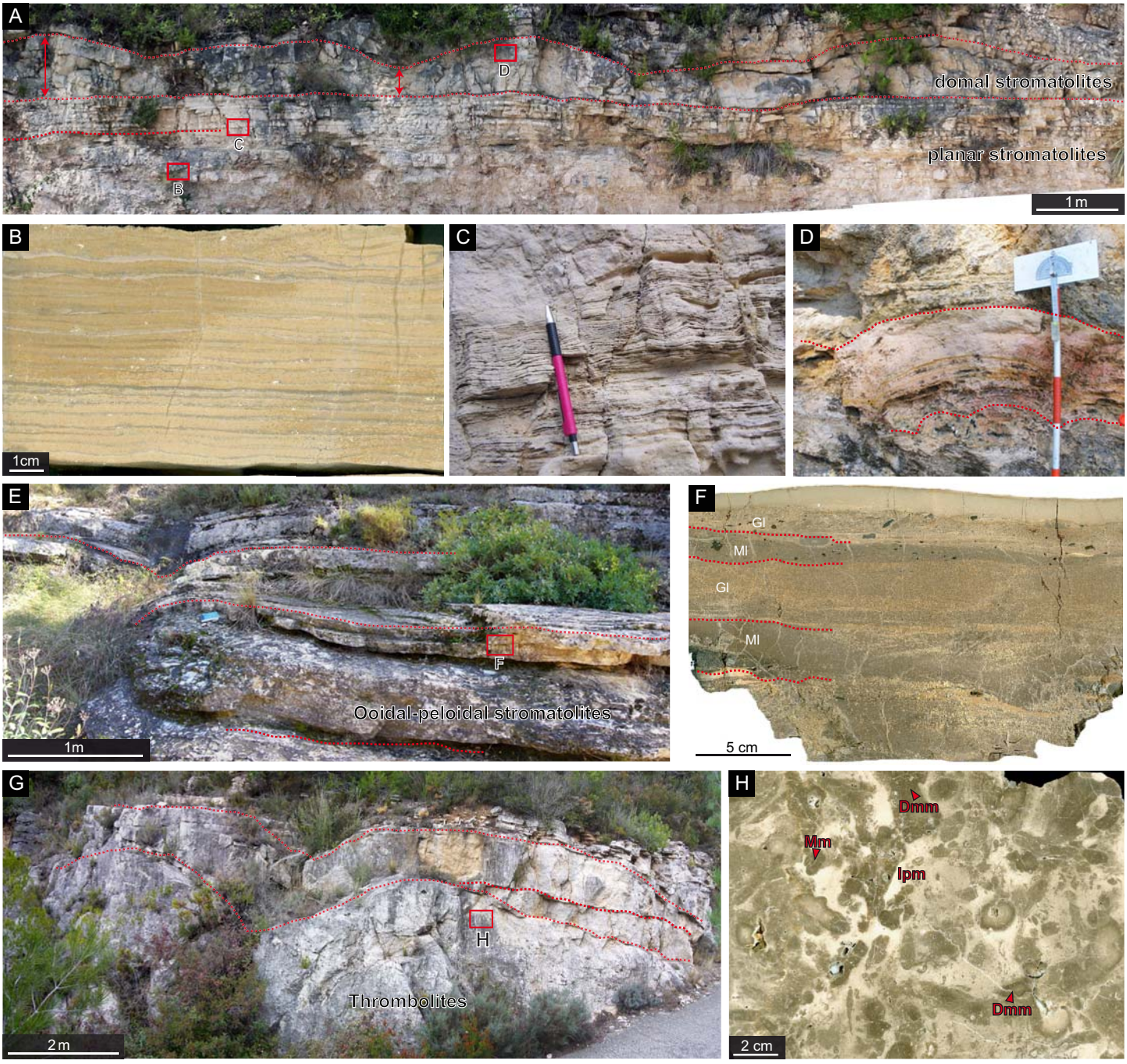
A
D
C
B
domal stromatolites
planar stromatolites
1 m
B
1cm
C
D
E
F
Ooidal-peloidal stromatolites
1m
F
GI
MI
GI
MI
5 cm
G
H
Thrombolites
2 m
H
Dmm
Mm
lpm
Dmm
2 cm

Figure 6

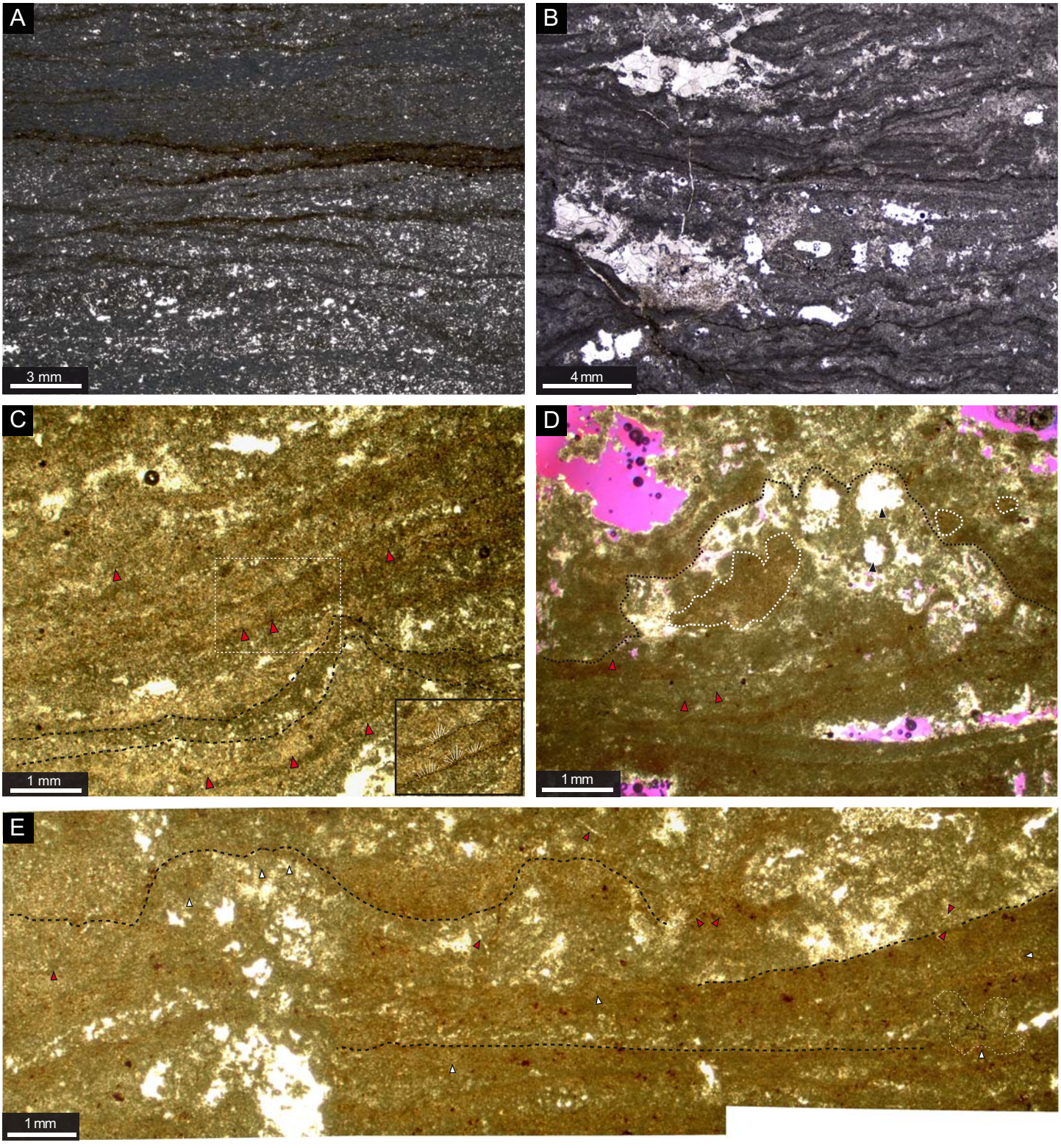

Figure 7

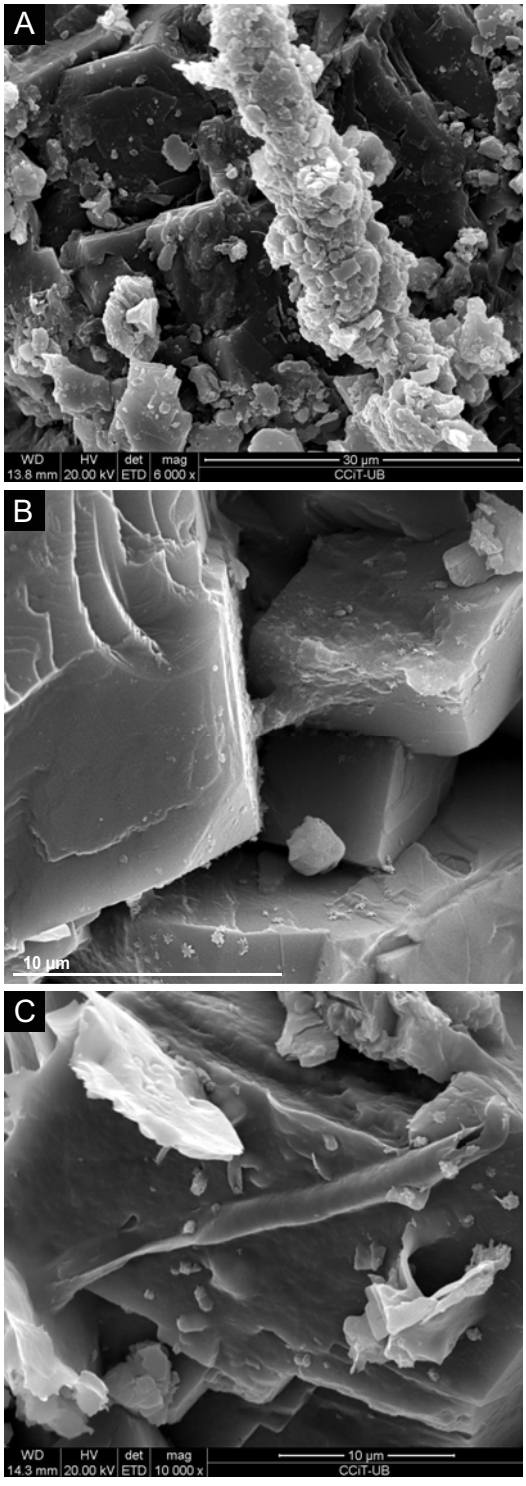
A
WD
13.8 mm
HV
20.00 kV
det
ETD
mag
6 000 x
30 µm
CCiT-UB
B
10 µm
C
WD
14.3 mm
HV
20.00 kV
det
ETD
mag
10 000 x
10 µm
CCiT-UB

Figure 8a

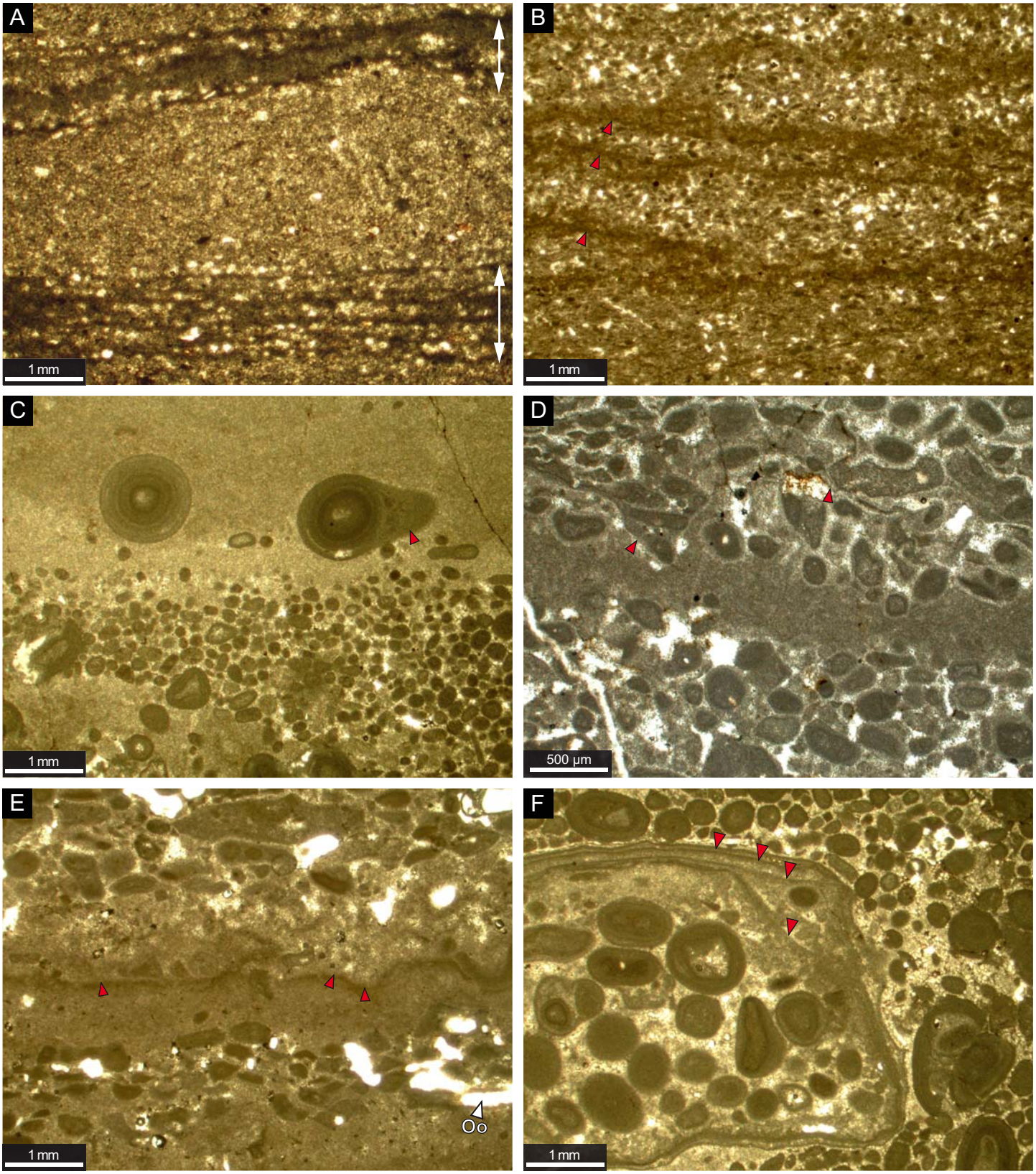

Figure 8b

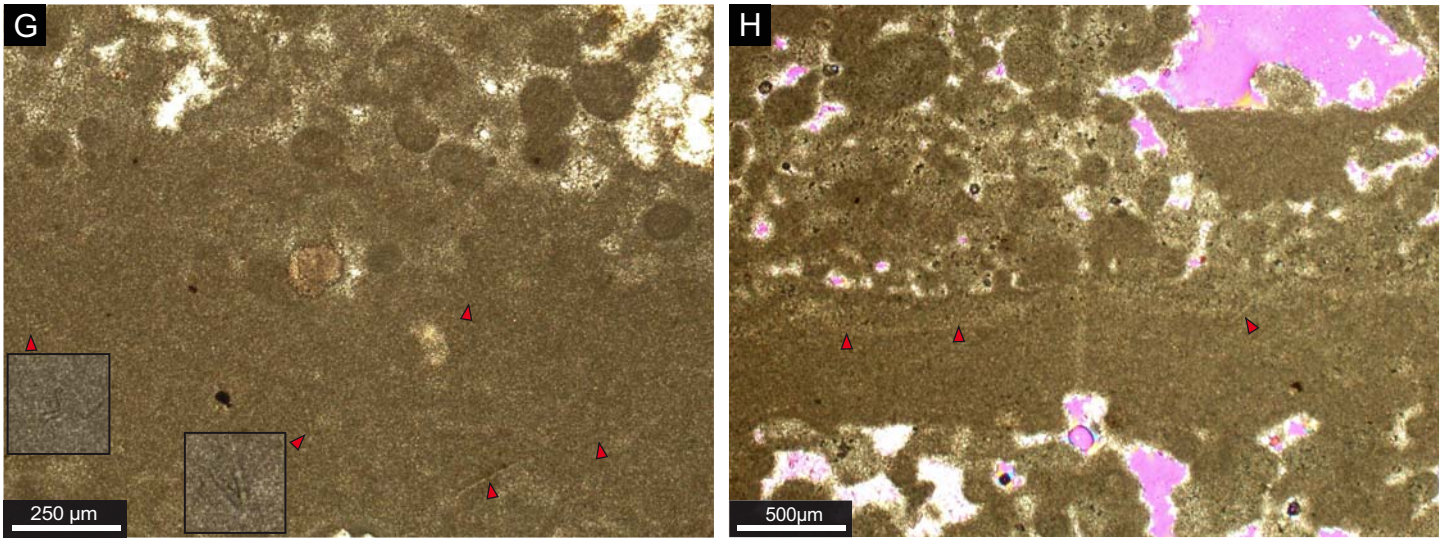

Figure 9

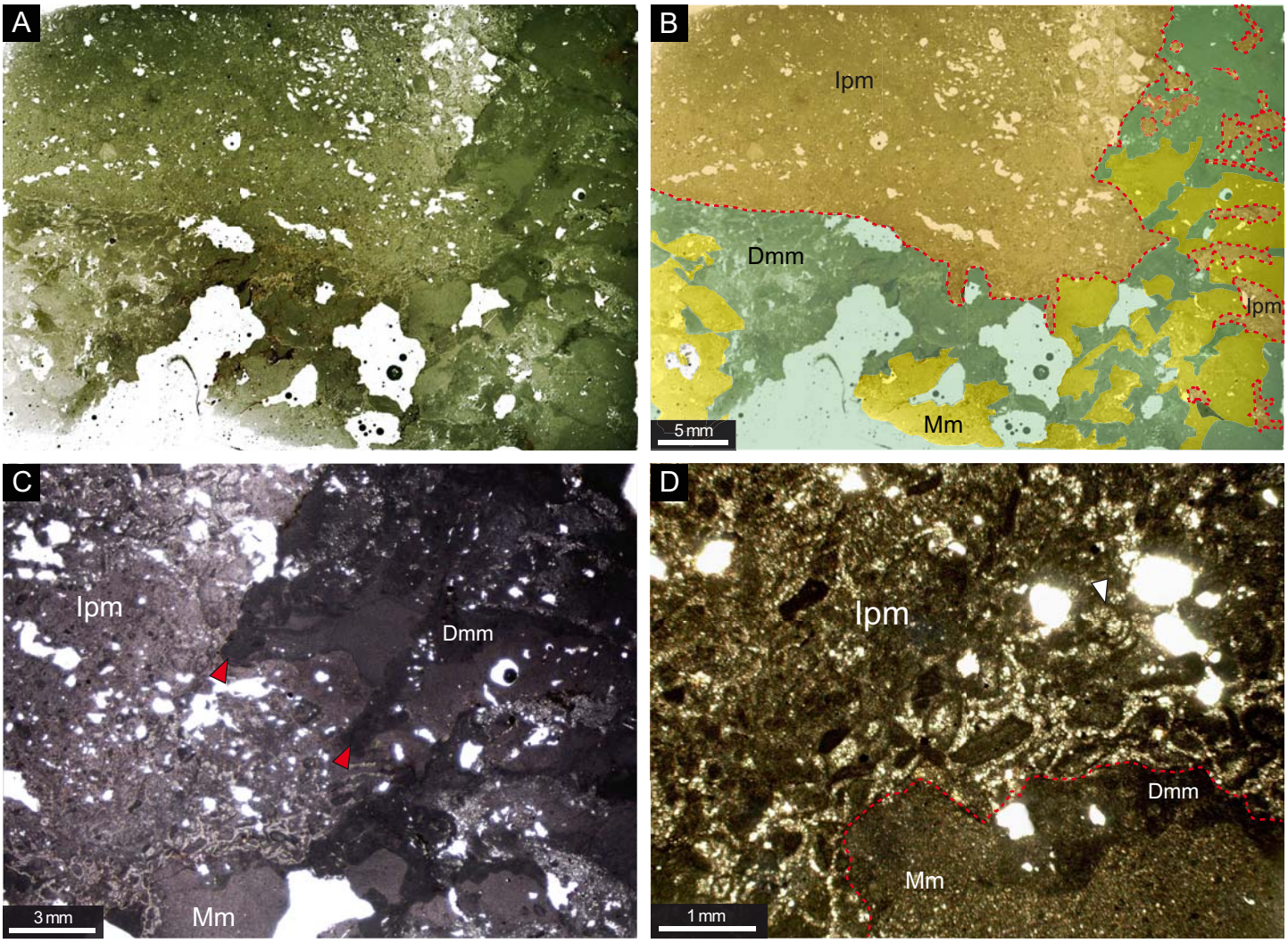

Figure 10

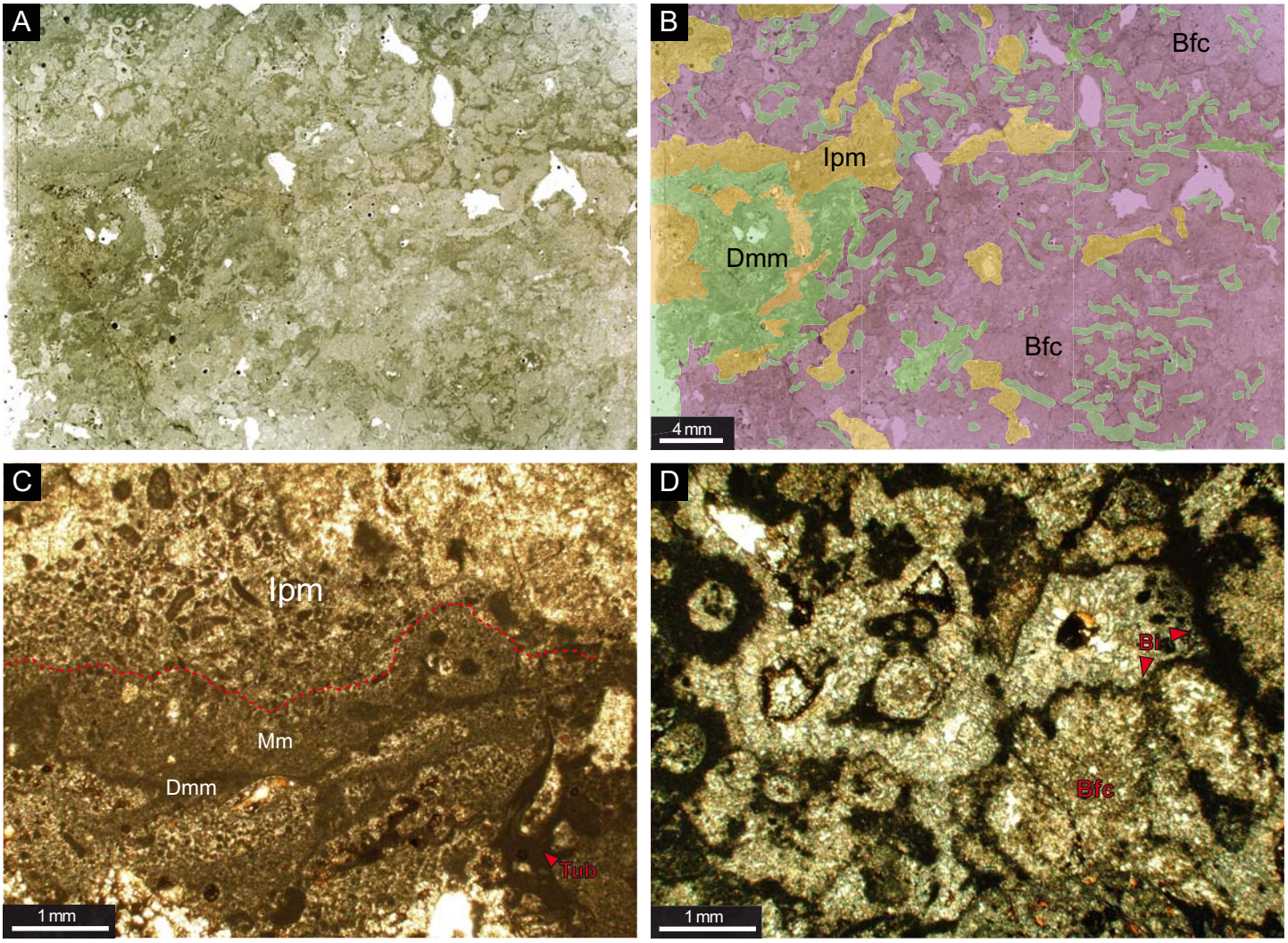

Figure 11

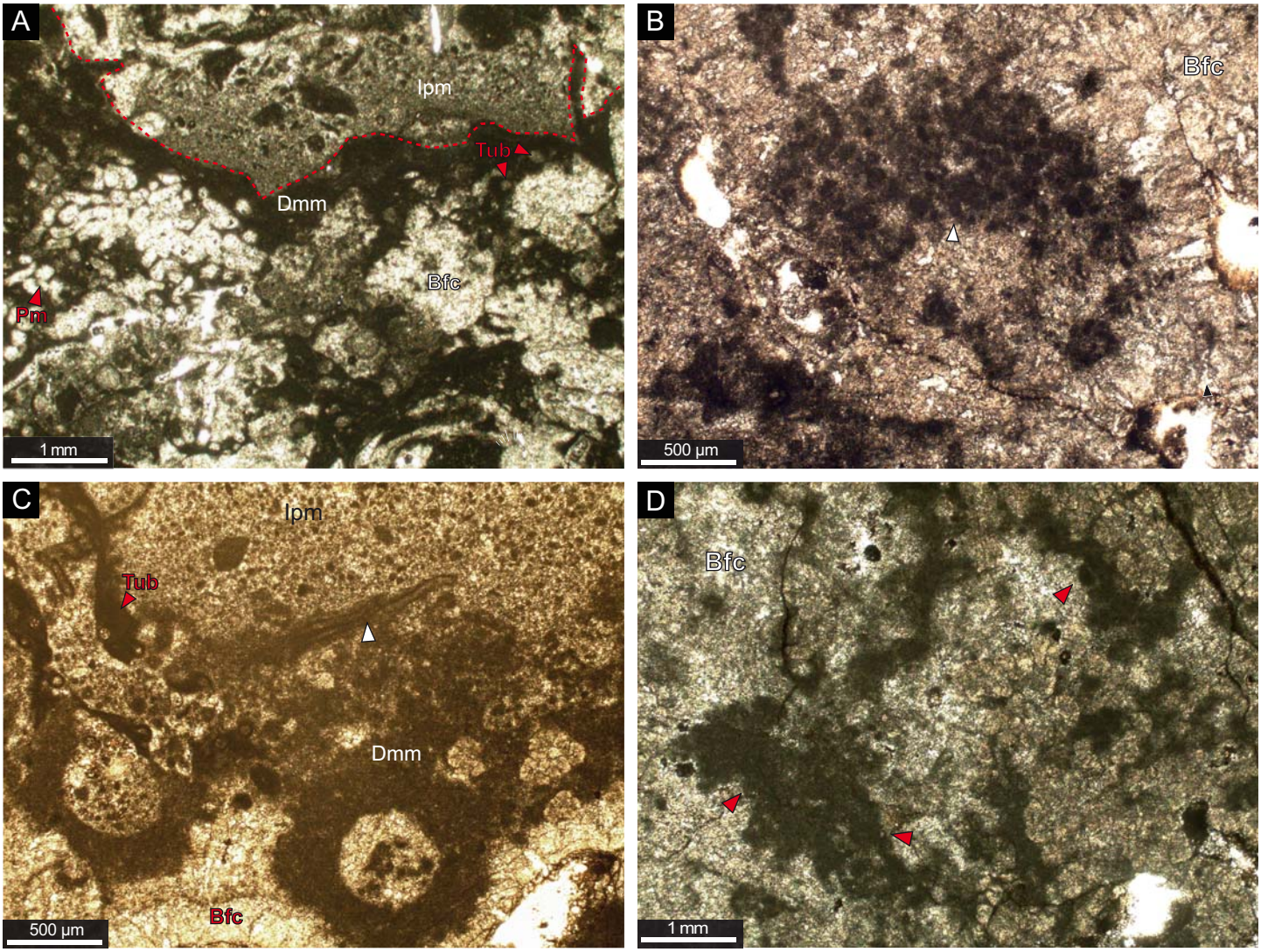
A
lpm
Tub
Dmm
Bfc
Pm
1 mm
B
Bfc
500 µm
C
lpm
Tub
Dmm
Bfc
500 µm
D
Bfc
1 mm

Figure 12

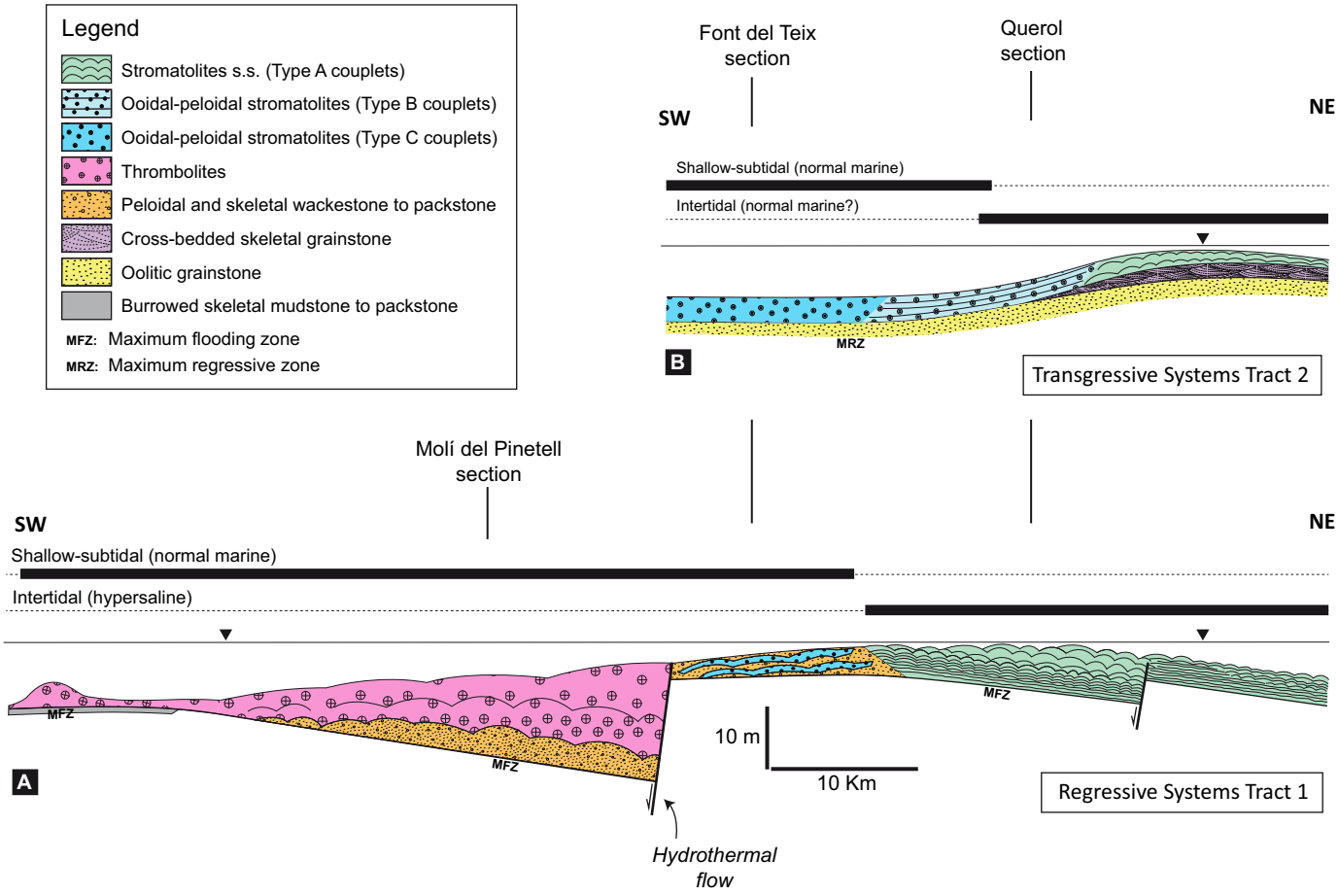
Legend
Stromatolites s.s. (Type A couplets)
Ooidal-peloidal stromatolites (Type B couplets)
Ooidal-peloidal stromatolites (Type C couplets)
Thrombolites
Peloidal and skeletal wackestone to packstone
Cross-bedded skeletal grainstone
Oolitic grainstone
Burrowed skeletal mudstone to packstone
MFZ: Maximum flooding zone
MRZ: Maximum regressive zone
Font del Teix section
Querol section
SW
NE
Shallow-subtidal (normal marine)
Intertidal (normal marine?)
MRZ
B
Transgressive Systems Tract 2
Molí del Pinetell section
SW
NE
Shallow-subtidal (normal marine)
Intertidal (hypersaline)
MFZ
MFZ
MFZ
10 m
10 Km
A
Regressive Systems Tract 1
Hydrothermal flow

Table 1
Click here to download Table: Table 1..doc

MICROBIALITE TYPE	MICROBIALITE SUBTYPE	GEOMETRY AND DIMENSIONS	TEXTURE AND LAMINATION	MICROBIAL REMAINS
Stromatolites s.s.	Type 1: Stratiform	Tabular, rarely dome-shaped Thickness: up to 5 m Width: - Lateral extent: at least 30 Km Rare small dome-shaped bodies (up to 15 cm high and 20 cm wide) and low synoptic relief bodies with a conical profile (up to 2 cm high and 5 cm wide)	Alternation of thicker dark and thinner light dolomicrite and dolosparite layers (Type A couplets) Light laminae: peloidal dolomicrite, microdolospar and dolospar (500 to 1500 µm thick) Dark laminae: dense dolomicrite, mostly peloidal, clotted and cloudy (100 to 250 µm thick) Composite intervals composed of several dark laminae (2 to 4 mm thick)	Light laminae: Domed structures (convex-upward bodies) with filamentous dolomicrite bodies subperpendicular to the domes Isolated fan-like, filament-bearing dolomicrite bodies subperpendicular to the lamination Dark laminae: Subperpendicular, isolated micrite filamentous bodies Calcimicrobial bodies (*Cayeuxia*-like forms)
	Type 2: Domal	Head-shaped, domed buildups commonly linked laterally Thickness: up to 2 m Width: 6 m Lateral extent: at least 20 Km Rare small, isolated spaced intermingled domes (up to 10 cm high and 15 cm wide)		

TABLE 1

Table 2
Click here to download Table: Table 2..doc

MICROBIALITE TYPE	GEOMETRY AND DIMENSIONS	TEXTURE AND LAMINATION	MICROBIAL REMAINS
Ooidal-peloidal stromatolites	Stratiform and low-relief hemielliptical buildups. Thickness: up to 3 m Width: - Lateral extent: at least 40 Km	Alternation of oolitic grainstone layers with micrite layers (both dolomitised) *Oolitic layers*: smooth, planar to slightly wavy (sub-millimeter to a 5 cm thick) *Micritic layers*: tabular to wavy (few µm to 2 cm thick) Type B couplets: micritic layers with several µm thick Type C couplets: micritic layers exceeding 1mm thick Light laminae: peloidal dolomicrite, microdolospar and dolospar (500 to 1500 µm thick) Dark laminae: dense dolomicrite, mostly peloidal, clotted and cloudy (100 to 250 µm thick) Composite intervals composed of several dark laminae (2 to 4 mm thick)	Light laminae: Domed structures (convex-upward bodies) with filamentous dolomicrite bodies subperpendicular to the domes Isolated fan-like, filament-bearing dolomicrite bodies subperpendicular to the lamination Dark laminae: Subperpendicular, isolated micrite filamentous bodies Calcimicrobial bodies (*Cayeuxia*-like forms)

TABLE 2

Table 3
Click here to download Table: Table 3..doc

MICROBIALITE TYPE	MICROBIALITE SUBTYPE	GEOMETRY AND DIMENSIONS	TEXTURE AND MICROBIAL REMAINS
Thrombolites	Type 1: Stratiform	Extensive flat-relief biostromes Thickness: average of 40 m Width: - Lateral extent: at least 45 Km	<u>Dense micritic mesoclots</u> (Dmm): dark-coloured, massive and dense microcrystalline masses. 1) Micropeloidal to peloidal cloudy dolomicritic veneers (biofilms) 2) Calcified microfossils (*Garwoodia*, *Cayeuxia*-like porostromate calcimicrobes, *Tubiphytes, Koivaella?, Isnella?* or *Tubiphytes*-like, 3) Isolated and dispersed micropeloidal bodies (e.g. coccoid bacteria bushes and micropeloidal clusters) 4) Isolated sponges (*Solenolmia manon manon)* <u>Micritic matrix</u> (Mm): homogeneous and structureless light mudstone. <u>Intraclastic-peloidal masses</u> (Ipm): Interframework cavities filled with intraclastic and peloidal wackestone. <u>Botryoidal and fibrous cements</u> (Bfc): cavity-filling early marine cements (botryoidal and fibrous).
	Type 2: Mud mound	Head-shaped, domed buildups commonly linked laterally Thickness: average of 40 m Width: 50-100m Lateral extent: at least 45 Km	

TABLE 3

FIGURE CAPTIONS

Fig. 1. (a) Location of the study area in the Catalan Basin area. (b) Geological map of the Catalan Basin showing the Ladinian rocks and the geological transect studied (modified from Mercedes-Martín *et al*. 2013a).

Fig. 2. Types of microbialites in the Ladinian of the Catalan Basin and their sequence stratigraphic context. Thinner lines correspond to less abundant content of microbialites. Absolute ages from Gradstein *et al.* (2012) and short-term eustatic curve from Haq *et al.* (1987).

Fig. 3. Querol and Font del Teix stratigraphic sections (see Fig. 1 for location of the sections and Fig. 4 for a detailed legend).

Fig. 4. Molí del Pinetell stratigraphic section (see Fig. 1 for location of the section). Note that Figure 9 and 10 are referred in the section.

Fig. 5. Outcrop and polished slab photographs of microbialites. (a) Outcrop photomosaic of the stromatolites s.s. showing the juxtaposition of Type 1 stratiform morphologies and Type 2 domal morphologies. (b) Polished slab of stratiform stromatolites displaying an alternation of flat and continuous, dark and light dolomite layers. (c) Outcrop example of stratiform stromatolites showing undulate and wavy laminae. (d) Small stromatolitic dome constituted by continuous laminae and fenestral macroporosity. (e) Outcrop example of ooidal-peloidal stromatolites characterised by low-relief hemielliptical buildups. (f) Polished slab detail from the previous outcrop, displaying an alternation of grainstone intervals (GI) with micritic intervals (MI). Note some intraclasts at the top. (g) Photograph of the thrombolites in Molí del Pinetell section. Note the mounded geometry. (h) Polished slab detail of the previous outcrop, displaying the clotted textures characterizing the thrombolites (Ipm: intraclastic-peloidal masses; Mm: micritic matrix and Dmm: dense micritic mesoclots). Pencil is 15 cm long.

Fig. 6. Photomicrographs of stromatolites s.s. displaying the Type A couplets. (a) Alternation of dark and light dolomicrite layers Note the parallel stacking of laminae which are commonly wavy to ondulate. (b) Alternation of dark and light dolomicritic layers with wrinkled and ondulate profiles. Note

the presence of small domes (left side) and occluded fenestral and ancient vuggy porosity filled by dolospar. (c) Detail of a dome formed by alternation of laminae. The light laminae encompass small domed structures (convex-upward bodies) that contain filamentous bodies subperpendicular to the domes (red arrows). (d) Detail of a dome constituted by calcimicrobial bodies (*Cayeuxia*-like forms in white dashed circles) and mouldic occluded porosity associated to them (black arrows). Note the filamentous bodies (red arrows) embedded in lighter laminae and the interlaminar pores (lower part) corresponding to decayed microbial mats. (e) Photomosaic depicting two small domes constituted by microbial filamentous remains (red arrows) and busk-like calcimicrobial bodies (white arrows and white dashed circle). Pink and open pores are due to weathering and thin-section artifacts.

Fig.7. SEM photomicrographs corresponding to stromatolites s.s. (a) Large filamentous body that probably corresponds to calcified cyanobacteria. (b) Small filament linking dolomite crystals and extending as a thin film in its base. (c) Small filamentous remain attached to a dolomite crystal

Fig. 8. Photomicrographs of stromatolites s.s. and ooidal-peloidal stromatolites. (a) Composite intervals in stromatolites s.s (Type A couplets), consisting of several dark laminae (arrows) of several mm thick alternating with light laminae of peloidal dolomicrite. (b) Type B couplets of ooidal-peloidal stromatolites. An alternation of smooth grainstone layers with tabular to wavy several μm-thick micritic layers, in arrows. (c) Type C couplets of ooidal-peloidal stromatolites. Some ooids are embedded in the micritic layers and develop a micritic envelop (arrow). (d) Type C couplets of ooidal-peloidal stromatolites. Some micritic intervals show evidence of erosion with micro-scours filled with ooids (arrows) and thin ferruginous crusts on top. Note that the coated grains are commonly micritized. (e) Microbial filamentous remains (arrows) are commonly rooted in the dark, massive to peloidal dolomicrite laminae. Oomouldic porosity is common (Oo). Some grapestones are observed on top. (f) Thin, dark dolomicrospar laminae and light peloidal to micropeloidal cloudy dolomicrite envelops (arrows) constitute the aggregate grains in ooidal-peloidal stromatolites. Grains are often micritized. (g) Microbial filamentous remains (arrows) are observed in the dolomicritic intervals and they are attached to the dark, massive to peloidal dolomicrite laminae. (h) Complex network of chaotic and subperpendicular to subparallel microbial filaments (arrows) in micritic layers. Pink and open pores are due to weathering and thin-section artifacts.

Fig. 9. Photomicrographs of thrombolites. Ipm = Intraclastic-peloidal masses; Dmm = Dense micritic mesoclots; Mm = Micritic matrix. (a) Thrombolitic texture in thin-section. (b) Thin-section mapping of components identified in (a). Note that Ipm is filling the interframework cavities generated by corrosion processes (dashed line). Dmm is composed by dark-coloured, massive and dense microcrystalline masses, rounded, amoeboid and arborescent in shape. Mm is composed of a structureless light mudstone representing the internal sediment. (c) Detail of the previous thin section. Note the Dmm (red arrows) is made up micropeloidal to peloidal cloudy dolomicritic masses. A small intraclastic layer is observed on the bottom of the Ipm filling. (d) Detail of the previous thin section. Evidence of neomorphic microsdoloparite to dolosparite replacing the dolomicritic matrix around intraclasts is observed in the centre of the image. Corrosion surface (dashed line) affecting Mm and Dmm. Open pores correspond to weathering effects and thin-section artifacts.

Fig. 10. Photomicrographs of thrombolites. Ipm = Intraclastic-peloidal masses; Dmm = Dense micritic mesoclots; Mm = Micritic matrix; Bfc = botryoidal and fibrous cements. (a) Thrombolitic texture in thin-section. (b) Thin-section mapping of components identified in (a). Note that Bfc is the most abundant component. (c) Dmm occurs in form of micropeloidal to peloidal cloudy dolomicritic veneers. Subsequent interframework cavities are filled with Mm and Ipm. Note the presence of *Tubiphytes* sp. (Tub).(d) Bfc showing fan-shaped botryoidal cements encrusted by biofilms (Bi) which grew synchronously. Open pores correspond to weathering effects and thin-section artifacts

Fig. 11. Photomicrographs of microbial remains in thrombolites. Ipm = Intraclastic-peloidal masses; Dmm = Dense micritic mesoclots; Bfc = botryoidal and fibrous cements; Tub = *Tubiphytes*. (a) Porostromate microbes (Pm) grew concomitantly with biofilms and Tub. Bfc are encrusted by biofilms and filling the interspaces between Dmm and Ipm. (b) Coccoid bacteria bushes and micropeloidal clusters (white arrow) are often embedded in Bfc. (c) Imp occurs in the interframework cavities around Dmm. Small Tub and *Isnella?* microfossils (white arrow) have been observed. Bfc are filling the pore spaces. (d) Arborescent, micropeloidal masses resembling coccoid bacteria (red arrows) are embedded in Bfc. Open pores correspond to weathering effects and thin-section artifacts.

Fig. 12. Microbial depositional profile displaying the occurrence of microbialites within a sequence stratigraphic context. See Fig. 1 for section location. (a) Regressive Systems Tract 1. Profile displaying the concomitant occurrence of stromatolites s.s., ooidal-peloidal stromatolites and thrombolites occupying different facies belts in a fault-block ramp. Note that thrombolites developed only in the hanging-wall block and probably associated with hydrothermal fluids related to of La Riba fault. Besides, stromatolites s.s., ooidal-peloidal stromatolites developed in the foot-wall block. (b) Transgressive Systems Tract 2. Profile showing the co-occurrence of stromatolites s.s. and ooidal-peloidal stromatolites. Note that these microbialites are developed only in the inner part of the fault-block ramp.

Grup de Geologia Sedimentària

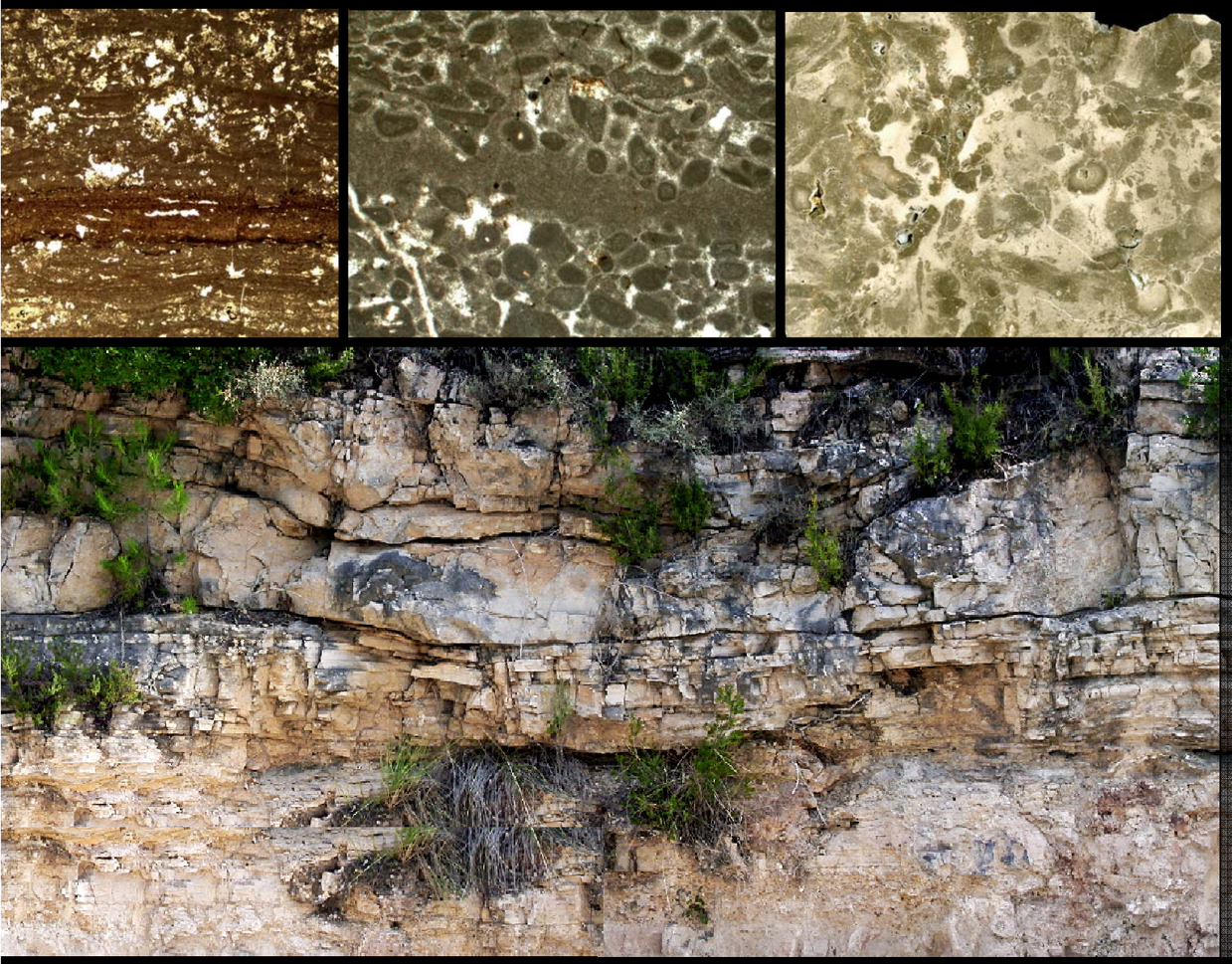

Septiembre 2013

Estudio de carbonatos microbiales en afloramiento como análogos de la caracterización y modelización de reservorios de hidrocarburos

Ramón Mercedes Martín

Universitat de Barcelona

REPSOL

Facultat de Geologia
Departament de Geoquímica, Petrologia i Prospecció Geològica
Programa de Doctorat en "Ciències de la Terra"
Universitat de Barcelona

Estudio de carbonatos microbiales en afloramiento como análogos de la caracterización y modelización de reservorios de hidrocarburos

Ramón Mercedes Martín

Tesis Doctoral dirigida por

Dr. Ramon Salas

Dra. Concha Arenas Abad